DISSERTATION

DETECTION AND QUANTIFICATION OF SUB-MICROMOLAR CONCENTRATIONS OF AQUEOUS ANIONS USING INFRARED SPECTROSCOPY AND MASS SPECTROMETRY

Submitted by

Gretchen N. Hebert

Department of Chemistry

In partial fulfillment of the requirements

For the Degree of Doctor of Philosophy

Colorado State University

Fort Collins, Colorado

Spring, 2004

COLORADO STATE UNIVERSITY

January 22, 2004

WE HEREBY RECOMMEND THAT THE DISSERTATION PREPARED UNDER OUR SUPERVISION BY GRETCHEN N. HEBERT ENTITLED *DETECTION AND QUANTIFICATION OF LOW CONCENTRATIONS OF AQUEOUS ANIONS USING INFRARED SPECTROSCOPY AND MASS SPECTROMETRY* BE ACCEPTED AS FULLFILING IN PART REQUIREMENTS FOR THE DEGREE OF DOCTOR OF PHILOSOPHY.

Committee on Graduate Work

Ellen Fisher

Gary E. Maciel

Debbie C. Crans

Kenneth F. Reardon

Advisor Steven H. Strauss

Department Head Anthony K. Rappe

ABSTRACT OF DISSERTATION

DETECTION AND QUANTIFICATION OF SUB-MICROMOLAR CONCENTRATIONS OF AQUEOUS ANIONS USING INFRARED SPECTROSCOPY AND MASS SPECTROMETRY

Two different techniques, electrospray ionization mass spectrometry (ESIMS) and attenuated total reflectance Fourier transform infrared (ATR-FTIR) spectroscopy, were used for the detection and quantification of low concentrations of aqueous anions. Some of these anions, including perfluoroalkanesulfonates ($PFAS^-$), perchlorate, phosphonates, and cyanide, are of interest given that they may cause human health problems and/or persist in the environment. Two ESIMS methods, standard addition and direct-injection, are presented for the quantification of aqueous $PFAS^-$ anions, specifically perfluoro-*n*-octanesulfonate ($PFOS^-$). A concentration of 0.6 ± 0.1 μM $PFOS^-$ was quantified in groundwater from a well at a fire-training area at Wurtsmith Air Force Base (WAFB), Oscoda, MI using the method of standard additions. Using the direct-injection method, detection down to 6 nM $PFOS^-$ was successful and linear calibration curves were determined ranging from 0.01 to 5 μM $PFOS^-$. The direct-injection method was used to quantify $PFAS^-$ anions in the groundwater from wells at WAFB. The concentrations of $PFAS^-$ anions determined using the standard addition method were the same to within experimental error as those determined using the direct-injection method. It is probable that the observed $PFAS^-$ anions were components of some of the fire-fighting materials, including aqueous film-forming foams (AFFFs), used at this site until 1993. Concentrations of $PFAS^-$ anions up to 0.6 μM were found in the groundwater despite a minimum of five years since active fire-fighting activity ceased at WAFB. This is the first reported example of the persistence of $PFAS^-$ anions in groundwater over a period of several years.

A new ATR-FTIR method was developed for the detection and identification of sub-micromolar concentrations of aqueous polyatomic anions. The technique involves coating the surface of an ATR crystal with a thin-film coating of an organometallic ion-exchange extractant, which enabled anion detection limits to be lowered up to 23,000-fold below those achieved using the same commercially available ATR-FTIR spectrometer with an uncoated ATR crystal. A four-coordinate nickel (II) complex was used as a ligand-exchange reagent to detect cyanide. All of the other anions were detected using the nitrate or the chloride salt of a tetraalkylated ferrocenium cation. Detection limits for perchlorate, chlorate, trifluoromethanesulfonate, perfluoro-*n*-butanesulfonate, perfluoro-*n*-octanesulfonate, pinacolylmethylphosphonate, and cyanide were 0.03, 0.2, 0.05, 0.07, 0.06, 0.7, and 0.09 μM, respectively, using coated ATR crystals. Detection limits were defined as the concentration for which the signal-to-noise ratio was $\geq 3 \pm 1$ for a 10-minute analysis time. Linear calibration curves based on d(absorbance)/d*t*, which is related to the rate of anion exchange, were established in the 0.04–30 μM range. Several complex matrixes, including synthetic tap water, simulated seawater, and hydroponic fertilizers, were examined. Using the method of standard additions, trace quantities of perchlorate were detected in some hydroponic nitrate fertilizers where the nitrate to perchlorate concentration ratios were as high as 9,000. The concentrations of perchlorate detected in these fertilizers were the same within experimental error as those determined by three other techniques performed in three different laboratories. This simple ATR-FTIR detection/quantification method afforded good reproducibility with relatively fast (10-minute) detection times.

Gretchen N. Hebert
Chemistry Department
Colorado State University
Fort Collins, CO 80523
Spring 2004

ACKNOWLEDGMENTS

I would like to thank all of the members of the Strauss Research Group, both past and present, for your support and assistance as my colleagues and friends. Specifically, I would like to acknowledge Dr. Matthew Odom, Dr. Brady Clapsaddle, and Dr. Stephanie Bowman for helping me along the way with many aspects of my research. I thank my advisor, Dr. Steven H. Strauss, for his friendship, which, along with his wisdom, guidance, and patience helped train me to become a successful scientist. I would also like to thank Mr. Don Dick for his help with mass spectrometry. Special thanks goes out to my parents for their support and enthusiastic encouragement over the many years of my education. Finally, I would like to thank my husband, Tim, for his constant support, understanding, and encouragement. Your positive affirmations helped drive this achievement to completion.

Table of Contents

List of Tables

List of Figures

Chapter 1

Introduction: Detection Limits

Introduction

Detection, identification and quantification of aqueous anions such as perfluoroalkanesulfonates, perchlorate, phosphonates, and cyanide are of interest given that they can cause problems to human health and persist in the environment. In the following chapters detection limits will be determined for these and other anions using two separate instrumental methods, electrospray ionization mass spectrometry (ESIMS) and attenuated total reflectance (ATR) FTIR. To fully appreciate these methods it is necessary to define the limit of detection (LOD). The standard definition of an LOD is the analyte concentration for which the signal-to-noise ratio (*SNR*) is three. Since *SNR*s have experimental errors associated with them, the LOD can only be determined within certain error limits. In this work, the LOD is defined as the analyte concentration for which the $SNR \geq 3 \pm x$ and $x \leq 1$, where x is the estimated standard deviation of the *SNR*. All *SNR*s reported are averages of three or more trials at that concentration. This definition was used for determining all LODs using both the ATR-FTIR and ESIMS methods.

Determination of limits of detection (LODs). The definition of the LOD as the analyte concentration that gives a signal intensity three times higher than the intensity of the noise can be ambiguous, especially for IR spectra. Consider the IR spectrum of aqueous 1 mM $LiClO_4$ shown in Figure 1.1 (2,500 scans, 8 cm^{-1} resolution). The perchlorate ν(ClO) signal at ca. 1108 cm^{-1} is obvious and by visual inspection is

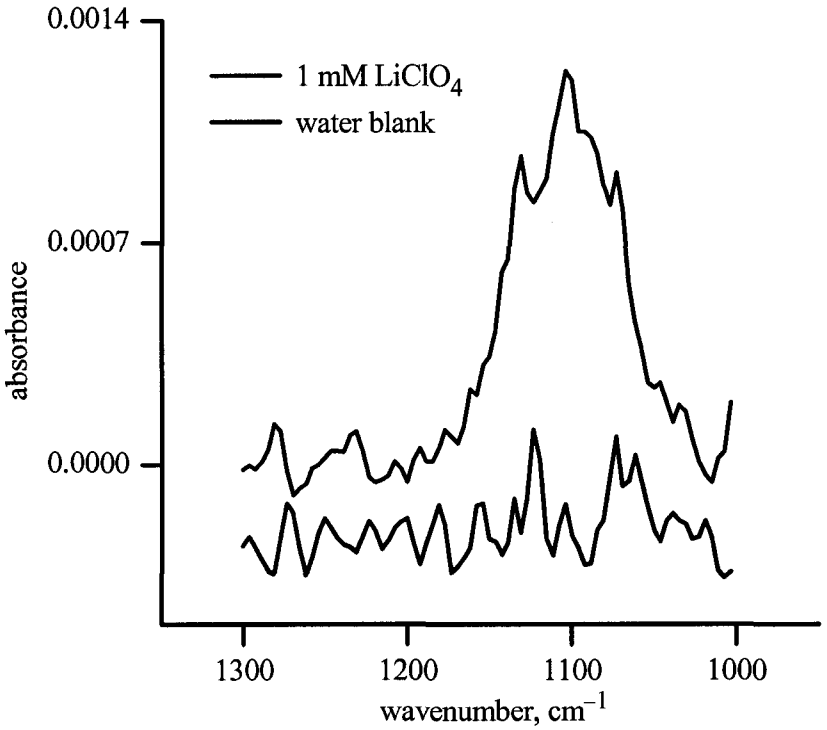

Figure 1.1. ATR-FTIR spectra of 1 mM aqueous $LiClO_4$ and a distilled, deionized water blank. Both spectra were collected over fifteen minutes (2,500 scans, 8 cm^{-1} resolution). The peak position and *SNR* for the $LiClO_4$ spectrum were determined to be 1108 cm^{-1} and 8, respectively.

most likely greater than three times the intensity of the noise. However, the peak position (accurate to ±4 cm^{-1} at 8 cm^{-1} resolution), the absorbance at that position, and the noise in the vicinity of that position need to be determined from the experimental data for the *SNR* to be calculated. It should be clear that the peak position and absorbance become increasingly difficult to measure as the concentration of analyte is lowered and the true LOD is approached.

To address these issues, the LOD literature was consulted. Reported definitions of LOD vary widely and have been heavily disputed.[1-13] These papers culminated in the publication of an IUPAC resolution in 1978 that attempted to standardize procedures for determining LODs.[3,8] The IUPAC defined the LOD as the concentration, c_L, derived from the smallest signal, x_L, that can be detected with reasonable certainty. The quantity x_L is defined by Equation 1.1, in which x_b is the mean of the signal intensity

$$x_L = x_b + ks_b \tag{1.1}$$

from the blanks, s_b is the standard deviation of these blank signal intensities, and k is a numerical factor corresponding to a specific confidence level. The quantity x_b should be determined from blanks that do not intentionally contain the analyte and otherwise have the same composition as the sample to be analyzed. The concentration, c_L, is a function of x_L, as shown in Equation 1.2, where m is the slope of a calibration curve of analyte

$$c_L = (x_L - x_b)/m \tag{1.2}$$

signal, x, versus concentration, c. Substituting Equation 1.1 into Equation 1.2 results in Equation 1.3, which defines the LOD.

$$c_L = ks_b/m \tag{1.3}$$

This approach is only valid if m is well-defined and has a very small error associated with it *and* if the intercept of the calibration curve is essentially zero. The value $k = 3$ defines a confidence level of 99.6% for the quantity x_L (see Equation 1.1) and has been generally accepted.[2-7] Values of x_b and s_b should be experimentally determined from a sufficiently large number of blanks ($\geq$20). Several examples of this method of determining LODs will be shown in Chapter 3 after the determination of calibration curves has been discussed.

As an alternative, the IUPAC suggested that s_b can be determined from a single measurement when using techniques that involve counting statistics. This simplification can be used with FTIR spectroscopy, since a typical spectrum is the result of multiple scans (e.g., either 64, 1,660, 2,500, or 5,000 co-added scans per spectrum in our experiments). Several authors have defined s_b to be equal to the root-mean-square of the noise (N_{RMS}) from a blank spectrum.[1,13-15] This assumes that the noise in the spectrum is essentially white noise (i.e., random noise with no drift). Since white noise follows a normal probability error distribution, it can be used to define the standard deviation.[1] If N_{RMS} is substituted into Equation 1.1 for s_b then Equation 1.4 results when $k = 3$. When

$$x_L - x_b = 3N_{RMS} \tag{1.4}$$

a typical sample FTIR spectrum is collected, the signal from the blank, x_b, is ratioed out as the background so the measured signal, S, from the sample spectrum of an analyte can be defined as shown in Equation 1.5. Substituting Equation 1.5 into Equation 1.4 gives

$$S = x_L - x_b \tag{1.5}$$

$S = 3N_{RMS}$, leading to the familiar definition that the LOD is the concentration for which $S/N_{RMS} = 3$. It should be noted that N_{RMS} is typically calculated using software that

accompanies a spectroscopic instrument. This software first squares all the signal values within a designated range resulting in all the values being positive. The square root of the average of these positive values is then calculated giving the root-mean-square of the selected data.[16] The N_{RMS} can also be approximated manually as 1/5 of the peak-to-peak noise.[1,13-15,17]

The definition of LOD can now be applied to the spectrum of 1 mM aqueous $LiClO_4$ shown in Figure 1.1. Using least-squares fitting in the graphing/analysis software Origin®, the peak was fit to a Gaussian using Equation 1.6, in which m is the

$$y = mx + y_0 + \left(\frac{A}{w(\pi/2)^{1/2}}\right) \exp\left(-2\left(\frac{x-x_c}{w}\right)^2\right) \tag{1.6}$$

slope of the linear baseline, y_0 is the y-intercept of the baseline, A is the integrated area under the peak, w is the peak width at half maximum, and x_c is the x value with the highest absorbance. An iterative approach was used to minimize the calculated residuals. Good fits resulted in residual plots with a slope close to zero. A fairly good Gaussian fit to the 1 mM $LiClO_4$ spectrum was achieved, as shown in Figure 1.2. A plot of the residuals, offset for clarity, is also shown.

In order to obtain the true intensity (absorbance) of the peak, the baseline from the Gaussian fit ($y = -1.8275 \times 10^{-7}x + 0.00016$) was subtracted from both the least-squares fit and from the spectrum. The resulting curves are shown in Figure 1.3. Using this baseline-adjusted spectrum, the peak position, 1108 cm^{-1} and the signal at that position, 1.14×10^{-3}, were determined.

Deciding on the proper wavenumber region over which the noise of an IR spectrum should be measured (the noise window) is also problematic. In the older literature, the noise on either side of a peak was averaged. This assumes, however, that one can determine where the peak "ends" and the baseline "begins", and this is difficult at

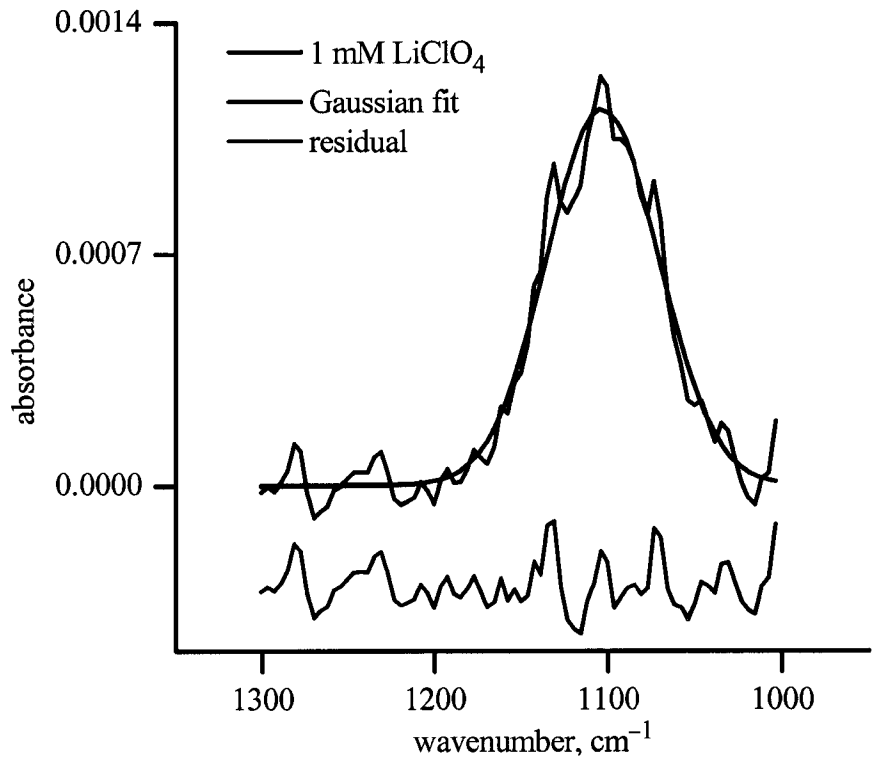

Figure 1.2. ATR-FTIR spectrum (2,500 scans, 8 cm^{-1} resolution) of 1 mM aqueous $LiClO_4$ fitted to a Gaussian curve. A plot of the residuals of the fit is shown, offset, in red.

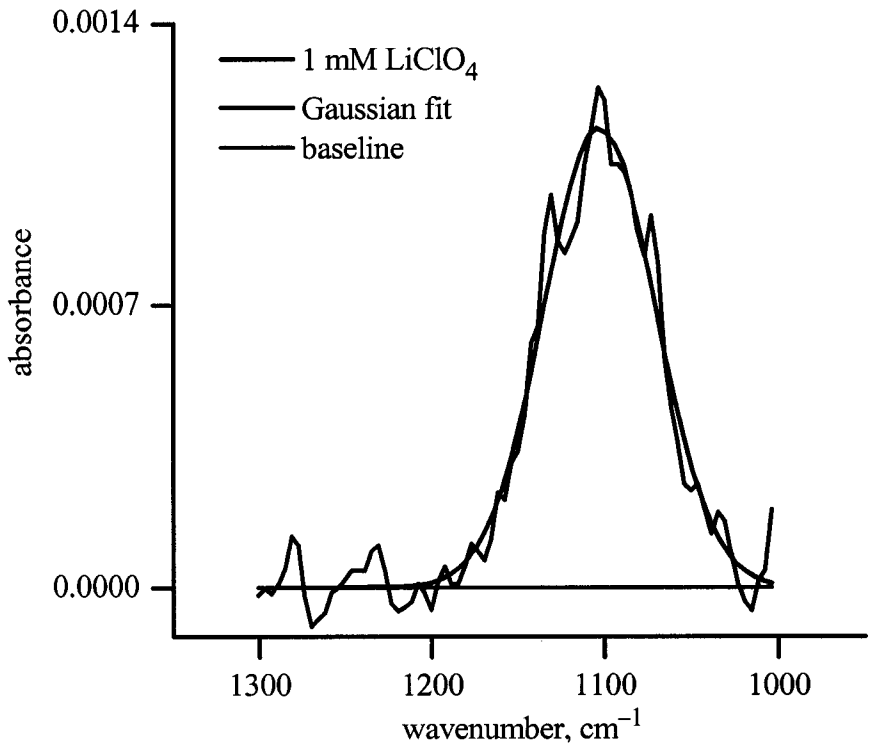

Figure 1.3. ATR-FTIR spectrum of 1 mM aqueous $LiClO_4$ and its Gaussian fit after subtraction of a baseline ($y = -1.8275 \times 10^{-7}x + 0.00016$) to yield a horizontal baseline ($y = 0$).

concentrations approaching the LOD. In addition, what wavenumber regions of baseline on either side of the peak should be used? ±20 cm^{-1}? ±50 cm^{-1}? or ±100 cm^{-1}?

For the ATR-FTIR LOD experiments presented in this work, the noise window was chosen as follows. The spectrum of a high concentration of analyte was recorded. The noise window for LOD spectra was chosen so that it was centered at the peak maximum in the high-concentration spectrum and included those wavenumbers on either side of the peak position where the peak intensity was 1% or greater of the peak maximum. This window, which was determined from three spectra similar to that in Figure 1.3 to be 198 cm^{-1} (1200–1002 cm^{-1}), was used as the noise window for all ClO_4^- trials using the same conditions. It was subsequently determined for several of the anions that the corresponding noise window was frequently within ±20 cm^{-1} of the window defined in the same manner but using the fitted spectra instead of high-concentration spectra.

The N_{RMS} for each LOD experiment was calculated from at least 10 blank spectra over this window using the root-mean-square noise function in the IR software (ReactIR, Applied Systems Inc., Millersville, MD) that operates the particular spectrometer used in our study. In the case of aqueous ClO_4^-, N_{RMS} over the range 1200–1002 cm^{-1} was $1.5(2) \times 10^{-4}$. Control experiments confirmed that N_{RMS} is approximately equal to 1/5 of the peak-to-peak noise over a given spectral window, as previously reported in the literature.[13-15]

With the signal intensity (1.14×10^{-3}) and noise ($1.5(2) \times 10^{-4}$) determined, the *SNR* for the peak shown in Figure 1.3 was determined to be 8. The average *SNR* for 1 mM ClO_4^- was 7 ± 1 (4 trials). Thus, 1 mM was determined to be above the LOD for ClO_4^- for this particular spectrometer, ATR probe material, and set of spectral acquisition parameters. To determine the LOD for ClO_4^-, lower concentrations were examined until the average *SNR* was 3 ± 1.

The process just described for determining a *SNR* becomes more complex for analytes that have multiple IR bands in the region of interest. For example, the FTIR spectrum (64 scans, 8 cm^{-1} resolution) shown in Figure 1.4 was taken using a diamond ATR crystal coated with a thin-film of the ion-exchange extractant 1,1′,3,3′-tetrakis(2-methyl-2-nonyl)ferrocenium chloride (DEC^+Cl^-) after 30 minutes in contact with 1 mM aqueous pinacolylmethylphosphonate ($C_7H_{16}PO_3^-$; $PMPA^-$). Under these conditions, the coating has become saturated with the analyte and is essentially $DEC^+PMPA^-(s)$. Experimental details for this type of analysis will be discussed in Chapters 3 and 4, whereas here only the determination of the *SNR* for a complex IR spectrum will be discussed. In Figure 1.4, at least six major peaks are present, not counting the small bands at 1116 and 934 cm^{-1}. In general, for analytes with more than one band in their IR spectrum, the most intense peak was used for all analyses that gave the smallest error (fewest interfering bands from water, the coating, and itself).

The $DEC^+PMPA^-(s)$ spectrum was least-squares fitted to a combination of seven Gaussian peaks, all but one of which overlap each other, as shown in Figure 1.5. Contrary to what was done to fit the perchlorate peaks, an integer baseline (i.e., y_0 = constant) was used for simplicity. The integer baseline ($y_0 = 4.36 \times 10^{-3}$) was subtracted from both the combined fit and the $DEC^+PMPA^-(s)$ spectrum resulting in a new baseline ($y_0 = 0$) as shown in Figure 1.6. Using this baseline-adjusted spectrum, the signal was measured from the absorbance of the most intense peak ($S = 0.1060$ at 1046 cm^{-1} for this case). The noise value of $1.9(2) \times 10^{-4}$ was calculated from 18 blank spectra over the noise window, which ranged from 1212 to 926 cm^{-1}. The *SNR* was calculated to be 560 for 1 mM aqueous $PMPA^-$ in contact with the DEC^+Cl^--coated diamond ATR crystal after 30 minutes. Thus, 1 mM was determined to be above the LOD for $PMPA^-$ for this particular spectrometer, ATR probe, and set of spectral acquisition parameters. In the cases where anions had multiple IR bands, such as $PMPA^-$, the *SNR* was calculated for all of the major peaks.

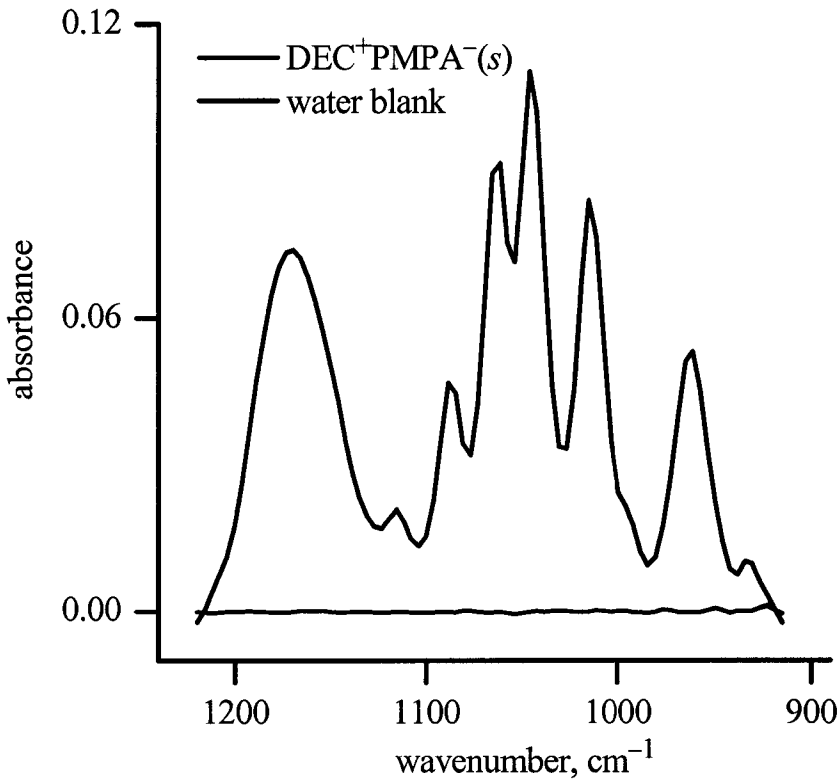

Figure 1.4. ATR-FTIR spectra (64 scans and 8 cm^{-1} resolution) of the DEC^+Cl^--coated diamond ATR crystal immersed in DI water (blank) and after 30 minutes in contact with a 1 mM aqueous solution of $PMPA^-$, which results in a coating that is essentially DEC^+PMPA^-.

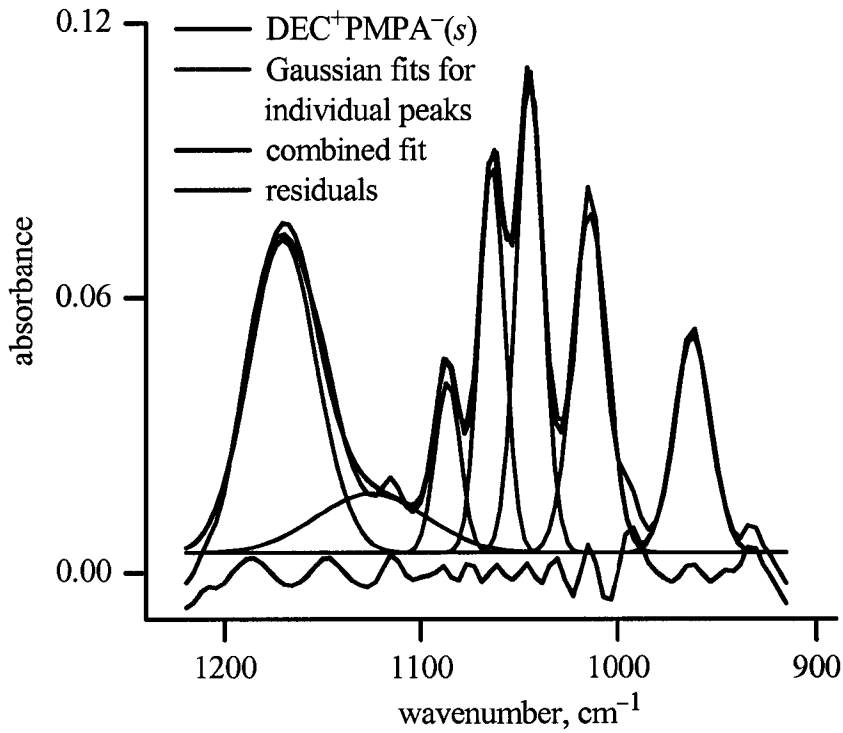

Figure 1.5. ATR-FTIR spectrum of the $DEC^{+}PMPA^{-}(s)$ coating on the diamond ATR crystal. The seven Gaussian fits to each of the seven individual peaks are shown and were combined into one overall fit of the spectrum with a baseline of $y_0 = 4.36 \times 10^{-3}$. A plot of the residuals, offset for clarity, is shown in green.

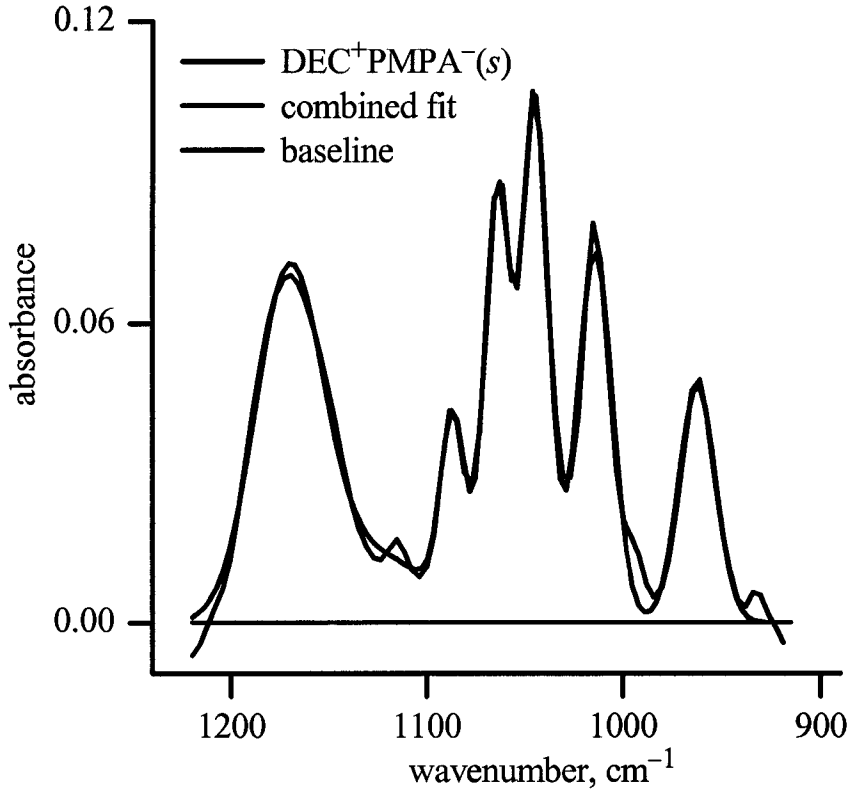

Figure 1.6. ATR-FTIR spectrum of $DEC^{+}PMPA^{-}(s)$ coating on the diamond ATR crystal. The spectrum was fit to a combination of seven Gaussian curves, and a baseline of $y_0 = 4.36 \times 10^{-3}$ was subtracted from both the spectrum and the combined Gaussian fit.

Williams and Salin reported another method for calculating the *SNR* to find the LOD in a "blankless experiment" (i.e., in an experiment where a single sample spectrum is collected and no blank spectrum is recorded).[7] In such cases, the noise can be calculated from the average of the N_{RMS} measurements taken inside a 21 point window on either side of the analyte peak (this would be ca. 81 cm^{-1} on our instrument at 8 cm^{-1} resolution). This method assumes that there are no signal features in the windows on either side of the analyte peak. Since blanks are available for all of the analyses presented here, this method was not used.

Scope of the Dissertation

In the following chapters detection limits for various aqueous anions determined using two different techniques, mass spectrometry and infrared spectroscopy, will be described in detail. Chapter 2 describes the detection and quantification of perfluorooctanesulfonate ($C_8F_{17}SO_3^-$; $PFOS^-$) in aqueous solutions using negative ion ESIMS. Two methods (standard addition and direct-injection) were applied to the quantification of perfluoroalkanesulfonates with perfluoroalkyl chains ranging in length from four to eight carbon atoms. Detection down to an LOD of 6 nM $PFOS^-$ was achieved for both distilled deionized water and untreated groundwater. Linear calibration curves were determined ranging from 0.01 to 5 μM $PFOS^-$. This work has been published, and copies of these papers are attached as appendixes to this dissertation.[18,19]

Chapter 3 describes the development of an ATR-FTIR method that allows for the detection of aqueous anions at concentrations less than 1 μM in 10 minutes. The technique involves coating the surface of an ATR crystal with a thin-film of a salt of the ion-exchange extractant 1,1′,3,3′-tetrakis(2-methyl-2-nonyl)ferricenium (DEC^+X^-; where X^- is NO_3^- or Cl^-), which increased the sensitivity up to 23,000-fold over the commercially available ATR FTIR spectrometer. Calibration curves that are linear over at least one order of magnitude are presented for ClO_4^-, $PMPA^-$, and $PFOS^-$. This

method has also been applied to the detection of ClO_4^- in commercial hydroponic fertilizers containing high concentrations of NO_3^-, which demonstrates the high selectivity of $DEC^+NO_3^-$ for the more weakly hydrated anion ClO_4^-. The majority of this work has been published in *Analytical Chemistry*,[20] while some has been published in two earlier reports.[21,22] Reprints of these papers are attached as appendixes to this dissertation.

Finally, Chapter 4 details a similar ATR-FTIR method that uses the compound 1,3-bis(diphenylphosphino)propanedichloronickel(II) ($NiCl_2$(dppp)) to coat the surface of the ATR crystals. Aqueous cyanide can then be detected following a Cl^-/CN^- ligand exchange with $NiCl_2$(dppp). The LOD for CN^- was found to be 0.09 μM for a 10-minute analysis. A linear calibration curve was generated ranging from 0.1 to 10.0 μM CN^-. Preliminary studies were done using more complex matrixes, which show the selective extraction and detection of CN^- even in the presence of 100,000 times as much Cl^-.

References

1. Parsons, M. L. *J. Chem. Educ.* **1969**, *46*, 290–292.
2. Kaiser, H. *Anal. Chem.* **1970**, *42*, 26A–59A.
3. *Spectrochim. Acta B* **1978**, *33B*, 241–245.
4. Boumans, P. W. J. M. *Spectrochim. Acta B* **1978**, *33B*, 625–634.
5. *Anal. Chem.* **1980**, *52*, 2242–2249.
6. Long, G. L.; Winefordner, J. D. *Anal. Chem.* **1983**, *55*, 712A–724A.
7. Williams, T. W.; Salin, E. D. *Anal. Chem.* **1988**, *60*, 725–727.
8. *Spectrochim. Acta B* **1978**, *33B*, 248–265.
9. Winefordner, J. D.; McCarthy, W. J.; St. John, P. A. *J. Chem. Educ.* **1967**, *44*, 80–83.
10. McCarthy, W. J. In *Advances in Analytical Chemistry and Instrumentation*; Reilley, C. N., McLafferty, F. N., Eds.; Wiley-Interscience: New York, 1971, pp 493–518.
11. Glaser, J. A.; Foerst, D. L.; McKee, G. D.; Quave, S. A.; Budde, W. L. *Environ. Sci. Technol.* **1981**, *15*, 1426–1435.
12. Faber, K.; Lorber, A.; Kowalski, B. R. *J. Chemom.* **1997**, *11*, 419–461.
13. St. John, P. A.; McCarthy, W. J.; Winefordner, J. D. *Anal. Chem.* **1967**, *39*, 1495–1497.
14. Parsons, M. L.; Winefordner, J. D. *Appl. Spectrosc.* **1967**, *21*, 368–374.
15. Ingle, J. D., Jr. *Anal. Chem.* **1975**, *47*, 1217–1221.
16. Malmstadt, H. V.; Enke, C. G.; Crouch, S. R.; Horlick, G. *Electronic Measurements for Scientists*; W. A. Benjamin: Reading, MA, 1974.
17. Griffiths, P. R.; de Haseth, J. *Fourier Transform Infrared Spectrometry*; John Wiley & Sons: New York, 1986.
18. Hebert, G. N.; Odom, M. A.; Craig, P. S.; Dick, D. L.; Strauss, S. H. *J. Environ. Monit.* **2002**, *4*, 90–95.

19. Moody, C. A.; Hebert, G. N.; Strauss, S. H.; Field, J. A. *J. Environ. Monit.* **2003**, *5*, 341–345.

20. Hebert, G. N.; Odom, M. A.; Bowman, S. C.; Strauss, S. H. *Anal. Chem.* **2004**, *76*, 781–787.

21. Strauss, S. H.; Odom, M. A.; Hebert, G. N.; Clapsaddle, B. J. *J. Am. Water Works Assoc.* **2002**, *94*, 109–115.

22. Collette, T. W.; Williams, T. L.; Urbansky, E. T.; Magnuson, M. L.; Hebert, G. N.; Strauss, S. H. *Analyst* **2003**, *128*, 88–97.

Chapter 2

Detection and Quantification of Perfluoroalkanesulfonates Using ESIMS

Introduction

In March 1999 we started a collaboration with researchers at Oregon State University who were interested in the detection and quantification of perfluorocarboxylates in groundwater. They detected perfluorocarboxylates in groundwater at Wurtsmith Air Force Base (WAFB), Oscoda, MI, where aqueous film-forming foams (AFFFs) are known to have been used for fire-fighting practice,[1,2] despite the fact that perfluorocarboxylates are not listed on the MSDS sheet of at least one commonly used AFFF formulation.[3] Salts of perfluoroalkanesulfonates ($PFAS^-$), specifically, perfluorooctanesulfonate ($PFOS^-$), have been used for many years in commercial products such as AFFFs, and Scotch Guard® fabric treatments.[3-5] As a result, our collaborators requested a method be developed for the detection and quantification of $PFAS^-$ in groundwater at WAFB. Since no method for the detection of low concentrations of $PFOS^-$ had been reported at that time, a new method was developed using electrospray ionization mass spectrometry (ESIMS). Most of the work included in this chapter has been reported in two recent publications.[6,7]

Perfluorooctanesulfonate ($C_8F_{17}SO_3^-$; $PFOS^-$). Some perfluorinated surfactant anions, including perfluoro-*n*-octanesulfonate, have recently become pollutants of concern.[2,4,5,8-16] The properties, synthesis, production, applications, toxicity, analysis, occurrence, and techniques for treatment of $PFOS^-$ have been reviewed.[8] Salts of $PFOS^-$

are known to cause significant toxic effects, including mortality, in cynomolgus monkeys (oral doses of 0.75 mg kg^{-1} day^{-1}),[17] rabbits (oral doses of 3.75 mg kg^{-1} day^{-1}),[18] rats (oral doses of 1.6 mg kg^{-1} day^{-1}),[15] mice (oral does of 20 mg kg^{-1} day^{-1}),[19,20] green algae, macrophyte, and invertebrates (exposure to ca. 200 μM),[21] and zooplankton (exposure to 20 μM).[22] Other biological effects of $PFOS^-$ exposure have also been reported.[23-34] The growing evidence that $PFOS^-$ is toxic to higher organisms is noteworthy because it has been found in the tissues of many animals around the globe, including white rabbits in New Zealand, eagles near the Baltic Sea, various birds in Italy, Korea, Japan, and the southeastern United States, polar bears in Alaska, river otters in Washington and Oregon, seals in the arctic regions of Canada and Norway, penguins in Antarctica, fish in the Pacific Ocean, Mediterranean Sea, Belgian North Sea, and Lake Michigan, and oysters in the Gulf of Mexico and Chesapeake Bay.[35-45] It is clear from this list that $PFOS^-$ is distributed globally in the environment.

Furthermore, 31 human serum and/or liver samples from nonoccupationally exposed humans were found to contain $PFOS^-$ up to 0.12 μM.[46] Sixty-five human serum samples obtained from four different U.S. biological supply companies had $PFOS^-$ concentrations ranging from 0.014 to 0.16 μM.[47] These concentrations are significantly less than the $PFOS^-$ concentrations up to 26 μM that have been found in serum of fluorochemical plant employees in Alabama and Belgium.[48,49] Whole blood from Japanese individuals showed the presence of 0.004–0.04 μM $PFOS^-$, which is significantly lower than that tested to date in the United States.[50] The widespread presence and persistence of $PFOS^-$ in the environment as well as the discovery of its toxicity prompted the 3M Company to discontinue its production in 2000[9,14] and for the EPA to regulate its production and use in the United States in 2002.[5]

Salts of $PFOS^-$ were used for years in many consumer and industrial formulations, including fabric treatments, anti-static agents, paper coatings approved for food contact, shampoos, corrosion inhibitors, insecticides, and AFFFs.[4,5] AFFFs, some of

which contain perfluoroalkanesulfonates[3] including $PFOS^-$,[6] have proven to be effective at extinguishing liquid-fuel fires and are widely and routinely used by civilian and U.S. military fire-fighters.[51-53] Historically, effluents from AFFF fire-fighting activities were neither impounded nor pre-treated prior to discharge to wastewater treatment systems or to the environment. Such releases may have been responsible for the presence of $PFOS^-$ in specific, localized environments in the past.

The $PFOS^-$ anion, like many other perfluorinated chemical species, is very stable.[54] It is resistant to thermal degradation and chemical attack in aqueous solution. In addition, $PFOS^-$ is not metabolized by some pseudomonads.[55] Its resistance to degradation in wastewater treatment systems causes excessive foaming that inhibits nitrification.[56] Perfluorinated surfactants were detected in surface water near Toronto, Canada downstream from an accidental spill site five months after the release.[57,58] In addition, $PFOS^-$ concentrations as high as 0.28 nM were detected in the Tennessee River 45 miles (72 km) downstream of a fluorochemical manufacturing facility in Decatur, AL (this value is significantly higher than the ca. 0.06 nM concentrations found upstream of the facility).[59] Recently, several studies have been performed that report very low concentrations of $PFOS^-$ (i.e., 0.4 pM to 0.3 nM) in Japanese surface water (both coastal seawater and several rivers).[60] Levels of $PFOS^-$ barely above the detection limit (i.e., 0.2 pM to 0.1 nM) have been reported in Japanese drinking water.[61] Although there are fluorochemical plants located in Japan, none of these are known to manufacture $PFAS^-$, therefore the findings of $PFOS^-$ in water is probably due to environmental contamination from general uses.[50]

At the time that the research reported in this chapter was started, no methods had been developed for the detection of low concentrations $PFOS^-$ in water. Thus, an ESIMS method with limits of detection (LODs) for $PFOS^-$ and perfluorobutanesulfonate ($C_4F_9SO_3^-$; $PFBS^-$) in water of 0.01 μM was developed.[6] However, during the preparation of our *Journal of Environmental Monitoring* manuscript, Hansen et al. and

Moody et al. both reported ESIMS methods for the detection of $PFOS^-$.[47,57] Since then, several other authors have reported MS methods with LODs for $PFOS^-$ ranging from 0.2 pM to 0.01 μM.[58-60,62] These will be discussed in detail later.

Quantitative ESIMS. Electrospray was first used as an ionization method in 1968 by Dole et al. for macromolecules.[63,64] In 1984, the use of electrospray ionization was first combined with mass spectrometry.[65-68] Since then, there has been a dramatic increase in literature on ESIMS,[69,70] which has been overviewed in a compilation edited by Cole.[71] Electrospray has become a common soft ionization method for mass spectrometry with large molecules.[72-74] ESIMS is a very sensitive method well known for its ability to identify ions with little to no fragmentation of the parent ion.[71] Mann has gone into great detail on several aspects of ESIMS (e.g., liquid flow rate, drying gas flow rate, analyte concentration, and analyte mass) that affect its ability to be used in a quantitative manner.[75]

Several studies have been performed using ESIMS as a method of quantification including one by Tang and Kebarle who built several types of calibration curves for heroin and other alkaloids which resulted from their proposed theory that relates ion intensity and analyte concentration. They also looked at the effects of electrolyte concentration and the use of an internal standard on the analyte ion intensity.[76] In 1994, Agnes and Horlick developed the method of comparing the ratios of the analyte signal to the signal from a constant amount of internal standard to create linear calibration curves for the examination of a mixture of metal ions.[77] Capitalizing on this internal standard method, Selby et al. were able to quantify alkaloids from multicomponent mixtures.[78] Halides and halogenic atoms including perchlorate were quantified by Barnett and Horlick with detection limits as low as 5 nM. They examined these ions individually and as constituents of more complex mixtures such as mouthwash.[79] Clewell et al. directly detected perchlorate ions in drinking water as well as in groundwater that contained low levels of dissolved solids with a detection limit of 3.8 nM.[80] Perchlorate has also been

quantified by forming stable association complexes with tetraalkylammonium cations and minimally nucleophilic, sterically hindered organic bases by Urbansky et al., who found the LOD for these complexes to be 0.1 μM.[81]

Electrospray mass spectrometry was also tested for its ability to quantify degradation products of tributylphosphate in aqueous nitrate solutions.[82] Hind et al. developed a method for quantitation of the series of quaternary ammonium surfactant compounds. The use of appropriate internal standards allowed them to study the effects of chain length.[83] Calibration curves with linear response from 10 fmol to 7.5 pmol of various sulfonamides were demonstrated by Purves et al.[84] Quantitation of the kinetically labile species $Sr(EDTA)^{2-}$ in complex, multicomponent systems was shown by Wang and Agnes.[85]

In addition to these examples, ESIMS has found a wide variety of applications in the fields of biochemistry and medicine. Polyphosphoinositides in a complex matrix of polar lipids have been quantified with a detection limit in the low pM range by Michelsen et al.[86] Guther et al. reported the quantification of glycolipid C, a glycosylphosphatidylinositol intermediate.[87] Quantitative analysis of individual phospholipid molecular species from sub-picomole amounts of human erythrocyte plasma membrane phospholipids was reported by Han and Gross.[88] Carver et al. used ESIMS to determine changes in the phosphorylation of the bovine α-crystallin subunits with age.[89] Bile acid concentrations in blood spots from infants, used to detect cholestatic hepatobiliary disorders in neonates, were also quantified.[90] The drug WEB 2086 was quantified using ESIMS by Subbanagounder et al.[91] The amount of *S*-nitrosated hemoglobin was quantified by Bonaventura et al.[92] Ofori-Acquah et al. were able to quantify γ-globulin in blood, which is found in patients with fetal hemoglobin and sickle cell anaemia.[93] Jorgensen et al. rapidly quantified mixtures of vancomycin-group antibiotics and their bacterial cell-wall receptors allowing the identification of subtle differences in binding constants.[94] Opiod peptides extracted from a biological matrix

were quantified by Dass et al. as well as methionine enkephalin and β-endorphin extracted from a human pituary gland.[95] As can be seen from this brief history of quantitative ESIMS, the method has been used with a wide variety of matrixes and has successfully quantified very small concentrations of analyte molecules.

ESIMS general instrumentation. The basic setup of an electrospray ionization mass spectrometer is shown below in Figure 2.1.[70,96] Several authors have provided good descriptions of the general method.[70,71,73,96,97] First, the liquid sample is introduced through the electrospray capillary in the presence of a high electric field. The field at the capillary tip charges the surface of the emerging liquid, which is dispersed by Coulombic forces into a fine spray of charged droplets. These droplets are drawn into a desolvating capillary by the electric field. While the charged droplets migrate through the desolvating capillary, evaporation of the solvent decreases the diameter of each droplet. This results in an increase in charge density on the droplet surface until the point at which the Coulombic repulsion is approximately equal to the surface tension. This equivalence is referred to as the Rayleigh limit, and is when the droplet becomes very unstable. This instability causes a Coulomb explosion or droplet fission to occur, which ultimately results in the formation of gas-phase ions. Next, a series of skimmer cones and ion optics are used to transport these anions into the mass analyzer. Each set of skimmers gradually decreases the pressure of each part of the vacuum chamber, while an electrical bias is used to focus the ion beam. Various types of mass analyzers can be used including single or multiple quadrupoles, or a time-of-flight tube.

Wurtsmith Air Force Base site description and characterization. Wurtsmith Air Force Base (WAFB), which was decommissioned in 1993, is located in northeastern Michigan as shown in Figure 2.2. Beginning in 1952, Fire-Training Area Two (FTA-02) at WAFB was used to train U.S. military personnel in fire-fighting procedures. Training exercises consisted of flooding a concrete pad with flammable liquids, igniting the fluids, and extinguishing the fire with fire-fighting agents including AFFF.[3] Prior to the

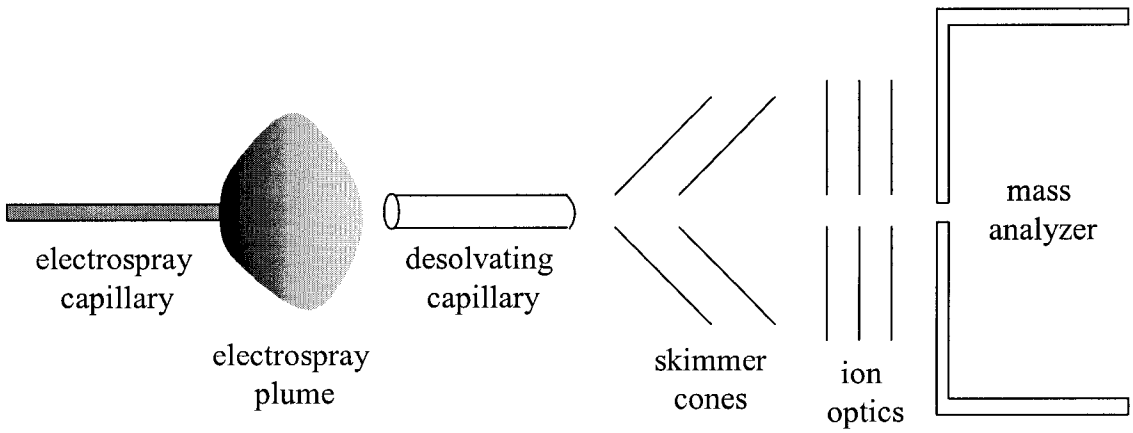

Figure 2.1. Basic instrumental setup of an electrospray ionization mass spectrometer. Sample is introduced at the left of the diagram through the electrospray capillary and the target ions are detected in the mass analyzer.

Figure 2.2. Map showing the location of Wurtsmith Air Force Base (WAFB), Oscoda, Michigan in relationship to the surrounding states and Canada.

construction of a concrete pad and an oil/water separator, fuel was dumped directly onto wet ground and ignited for each fire-training exercise.[98] Although, the pad was the central location of recent fire-training activity, AFFF and other fire-extinguishing materials may have been used to extinguish fires in other areas at FTA-02.[99]

The soil and groundwater at WAFB in the area around FTA-02 have been studied in detail.[98-105] The aquifer at WAFB is composed of alternating eolian sands and glacial outwash material that is highly permeable and exhibits hydraulic conductivities on the order of 30 m day^{-1}.[99,102,104] The water table is located between 5 and 8 m below the land surface. Aquifer solids are composed of greater than 85% quartz minerals, with organic carbon and inorganic carbon contents below 0.1% and approximately 6.0%, respectively.[99,102] Flow in the sand and gravel upper aquifer is generally eastward towards Lake Van Etten and south-southeast to the Au Sable River discharge areas at average rates of 0.1 to 0.3 m day^{-1}.[99,101,104] The direction of groundwater flow at WAFB does not change significantly from season to season.[104]

A contaminant plume at FTA-02 was previously defined in several studies by examining groundwater from the numerous wells around the fire-training area for volatile organic compounds and specific conductance. The generally accepted plume boundary was approximated by specific conductance values greater than 250 μS cm^{-1}.[98-100] Specific conductances of groundwater collected from 68 wells ranged from 110 to 3,170 μS cm^{-1}, with the highest values measured near the fire-training pad area.[7] The pH of the groundwater samples varied from 5.5 to 8.6.[7] Benzene, toluene, ethylbenzene, and xylenes were found in the groundwater at concentrations ranging from 10 to 2,000 μg L^{-1}.[99,100] The groundwater at FTA-02 was found to contain non-volatile total organic carbon (TOC) ranging from 1 mg L^{-1} (LOD) to 225 mg L^{-1}.[7] In addition to non-aqueous phase liquids,[101] a discontinuous 0.1-m thick layer of a black, tar-like substance occurs 0.3 to 0.9 m below the surface up to 50 m downgradient from the fire-training pad.[98] Anionic surfactant concentrations ranging from 1 to 25 μM[7] were also found in the

groundwater which was tested using a standard method for methylene blue active substances.[106]

In this chapter, two simple mass-spectral methods for the quantitative determination of individual $PFAS^-$ anions, ranging from four to eight carbon atoms, in groundwater and other homogeneous aqueous samples are reported. The use of the direct-injection method will be described for the detection of $PFOS^-$ and the related surfactant $C_6F_{13}SO_3^-$ ($PFHxS^-$) in Michigan groundwater. This groundwater was originally contaminated with untreated AFFF wastewater at the former Wurtsmith Air Force base, Oscoda, MI. A similar ESIMS method using standard additions will also be described for quantification of $PFAS^-$ in complex matrixes including an AFFF concentrate. Small concentrations of $PFOS^-$ were even detected in Kimwipes® which are commonly used in the laboratory.

Experimental Section

Standards and reagents. Sodium dodecylsulfate (Na(DDS), Sigma (St. Louis, MO), >99%) was dried under vacuum at 25 °C for 24 hours and was stored in a helium-filled glovebox prior to use. Two perfluoroalkylcarboxylic acids, $C_{11}F_{23}CO_2H$ and $C_5F_{11}CO_2H$ (Aldrich, Milwaukee, WI), were used as received. Acetonitrile (HPLC grade. Fisher, Fairlawn, NJ) was used as received. Distilled water was purified and deionized to an initial resistivity of 18 MΩ cm (Barnstead NanoPure, Dubuque, IA). The solid buffer Na_2HPO_4/KH_2PO_4 was used as received (pHydrion buffer; Micro Essential Lab, Inc., Brooklyn, NY). Sodium sulfate (Na_2SO_4) was used as received (Aldrich, Milwaukee, WI). Kimwipes® (Kimberly-Clark, Roswell, GA) and Bounce® (Outdoor fresh scent, Proctor & Gamble, Cincinnati, OH) were obtained commercially and used without alteration.

The AFFF formulation FC-203CF LIGHT WATER Brand Aqueous Film Forming Foam® (3M Company, St. Paul, MN) was used as received. The MSDS sheet

for this formulation lists the components as water (70%), 2-(2-butoxyethoxy)ethanol (20%), two alkylsulfate salts (5%), amphoteric fluoroalkylamide derivative (3%), five perfluoroalkanesulfonate salts (1%), triethanolamine (1%), and methyl-1H-benzotriazole (0.1%).[3]

Potassium perfluorooctanesulfonate, K(PFOS), was synthesized from perfluorooctylsulfonyl fluoride (3M Company, St. Paul, MN) by adding it to aqueous potassium hydroxide (Fisher, Fairlawn, NJ). The white crystalline compound K(PFOS) was the major product from this reaction, while perfluoroalkanesulfonates with other chain lengths (perfluoroheptane- and perfluorohexanesulfonate) were also present in small amounts. Five recrystallizations from hot water were carried out to take advantage of the lower solubility of K(PFOS) in cold water compared to $PFAS^-$ salts with shorter chain lengths. In addition to different chain lengths of the $PFAS^-$ anions, commercial perfluoroalkylsulfonyl fluoride products are known to contain ca. 70% linear and ca. 30% branched isomers.[107] An impurity, *iso*-perfluorooctanesulfonate, can seen in the ^{19}F NMR spectrum in Figure 2.3. The purity of K(PFOS) was determined to be >99% by ESIMS and by ^{19}F NMR spectroscopy. A yield of 65% was achieved based on perfluorooctylsulfonyl fluoride. Purified K(PFOS) was dried under vacuum and stored in a helium-filled glovebox. The synthesis of potassium perfluorobutanesulfonate, K(PFBS), from perfluorobutylsulfonyl fluoride (3M Company, St. Paul, MN) and potassium hydroxide was the same in every respect except that the higher solubility of this salt in water resulted in a much lower yield of purified material (30% based on perfluorobutylsulfonyl fluoride).

Water samples from the Ohio River and Cincinnati tap water were donated by E. T. Urbansky of the U.S. Environmental Protection Agency in high-density polyethylene bottles. Horsetooth Reservoir water (Fort Collins, CO) was collected in December 2001 in high-density polyethylene bottles.

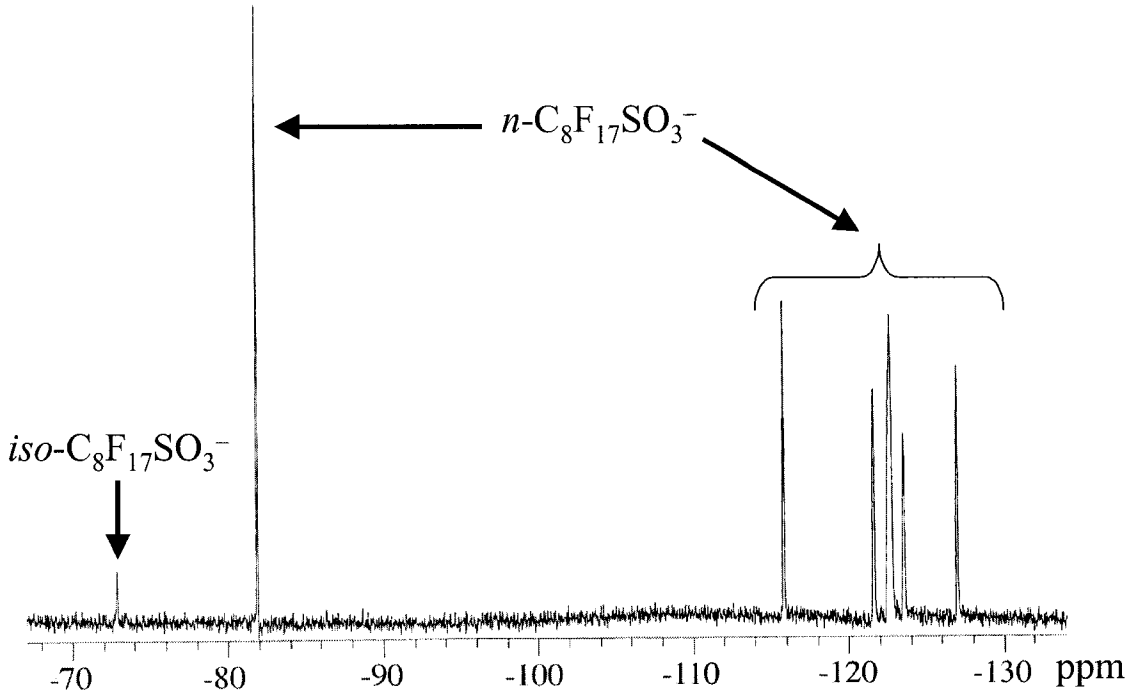

Figure 2.3. Fluorine-19 NMR spectrum of K(PFOS) dissolved in acetonitrile-d_3 was recorded using a Varian Inova-300 spectrometer at 25 °C. The ^{19}F frequency was 282 MHz and the chemical shift was referenced to an external $CFCl_3$ standard (δ 0.0). Peaks for $PFOS^-$ were located at δ –81.9 (triplet (t), 3F), –115.9 (multiplet (m), 4F), –121.6 (m, 2F), –122.6 (m, 4F), –123.6 (m, 2F), –126.9 (t, 2F).

WAFB groundwater collection. Groundwater samples were collected from 19 monitoring wells at FTA-02 as shown in Figure 2.4. The position of the wells relative to the plume boundary are illustrated using the previously reported well designations.[98-100,102-104] Monitoring wells with the identifier FT (fire-training) denote iron-cased 10-cm inner diameter wells with 1 to 2 m stainless steel screened intervals located 3 to 6 m below the water table.[104] Wells with ML notations describe multilevel wells constructed from 2.5-cm inner diameter PVC casing with 0.3-m screened intervals that are vertically spaced from 0.5 to 2 m.[102] More detailed descriptions of these wells have been reported in the literature.[98-100,102-104] Groundwater samples from the ML wells were collected in November 1998 and samples from the FT wells were collected in June 1999. Because the wells at FTA-02 were sampled several months apart, the groundwater velocity (0.1 to 0.3 m day^{-1})[99,101,104] was used to calculate travel distance over that elapsed time period. The small distance the water traveled between collection dates (ca. 20 m) indicates that combining the data from the two different sampling times should not affect interpretation of the data. All samples were collected in high-density polypropylene bottles shipped on ice without preservation and stored at 25 °C prior to analysis.[7]

Instrumentation. Both a Fisons VG Quattro (Beverly, MA) single quadrupole mass spectrometer and a Finnigan LCQ Duo (San Jose, CA) mass spectrometer were used to collect the ESIMS data. Instrumental parameters are compared in Table 2.1. Samples (ca. 100 μL) were introduced into both instruments by continuous infusion from a 500 μL syringe. The syringe used to inject the samples was washed three times between each sample with 1:1 (v:v) acetonitrile to water. A single spectrum was the average of 25 scans. The instrument was calibrated monthly with a standard containing 2 μg mL^{-1} NaI and 0.05 μg mL^{-1} CsI in a 1:1 (v:v) water to isopropanol solution.

Standard-addition experiments were conducted using only the Finnigan LCQ Duo instrument. All other experiments were performed using both instruments. Results were similar for both instruments with the exception that the Fisons instrument had slightly

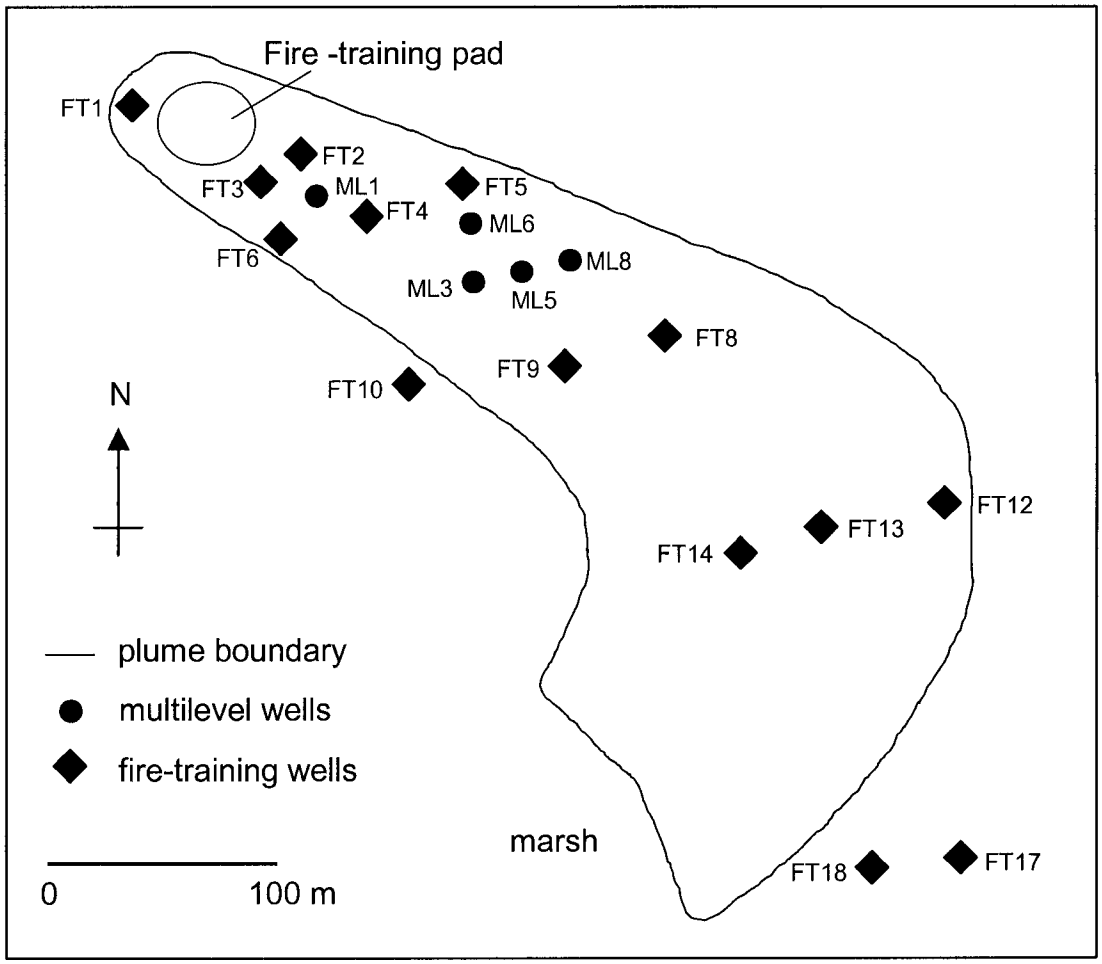

Figure 2.4. Map showing the FTA-02 groundwater plume at retired Wurtsmith Air Force Base (WAFB), Oscoda, MI. Groundwater was collected from two types of wells, fire-training (FT) wells and multilevel (ML) wells.

Table 2.1. Comparison of instrumental parameters for the Finnigan LCQ Duo and the Fisons VG Quattro mass spectrometers

Finnigan LCQ Duo		Fisons VG Quattro	
spray voltage[a]	–3.5 kV	capillary voltage	–2.9 kV
capillary voltage	–39 V	cone voltage	– 30 V
capillary temperature	200 °C	source temperature	75 °C
infusion rate	5 μL min^{-1}	flow injection rate	4 μL min^{-1}

[a] Different names have been given to the same components by the two companies.

lower detection limits but also had higher relative errors. The Fisons mass spectrometer had an LOD of 6 nM $PFOS^-$ while the Finnigan mass spectrometer had an LOD of 10 nM $PFOS^-$. Several experiments were specifically performed to compare the two spectrometers. A set of two standards containing low and high $PFOS^-$ concentrations was prepared with four replicates each. The first standard contained 0.5 μM $PFOS^-$ (*m/z* 499) and 0.5 μM DDS^- (*m/z* 265) in 1:1 (v:v) acetonitrile:water and had a ratio of ESIMS intensities, I(499)/I(265), of 3.9 ± 0.9 (Fisons) and 4.8 ± 0.4 (Finnigan). The second standard contained 5 μM $PFOS^-$ and 0.5 μM DDS^- in 1:1 (v:v) acetonitrile:water and had values of I(499)/I(265) of 26 ± 4 (Fisons) and 33 ± 3 (Finnigan). In both cases, the ratios of intensities were the same within the error of each spectrometer. In addition, log-log calibration plots, I(499)/I(265) versus concentrations, were made using each spectrometer. The slopes of the plots were 0.98 ± 0.07 (Fisons) and 0.93 ± 0.04 (Finnigan).

The pH was measured using an Orion meter (Boston, MA) with a Corning® pH electrode (Corning, NY). The conductivity was measured with a Yellow Springs conductivity probe and meter (Yellow Springs, OH). NMR spectra were recorded using a Varian VXR (Palo Alto, CA) 300 MHz spectrometer.

ESIMS sample preparation. In general, three to five replicates of each sample (groundwater or standard) were analyzed and the Q test was used to eliminate spurious data. All experimental values are reported with ±1σ. Blanks containing only 1:1 (v:v) acetonitrile:water were run after the replicates of each sample to insure that there was no carry-over between samples. Due to the sensitivity of ESIMS peak intensities to minor changes in experimental conditions, a strict experimental procedure was followed when preparing and analyzing all samples. A 1:1 (v:v) acetonitrile to water solvent matrix was used for all of the ESIMS samples. This matrix was used due to the inefficient ionization of the anions during the electrospray process using pure water. Figure 2.5 shows a comparison of a 100% water matrix (neat) and a 1:1 (v:v) acetonitrile to water matrix of a

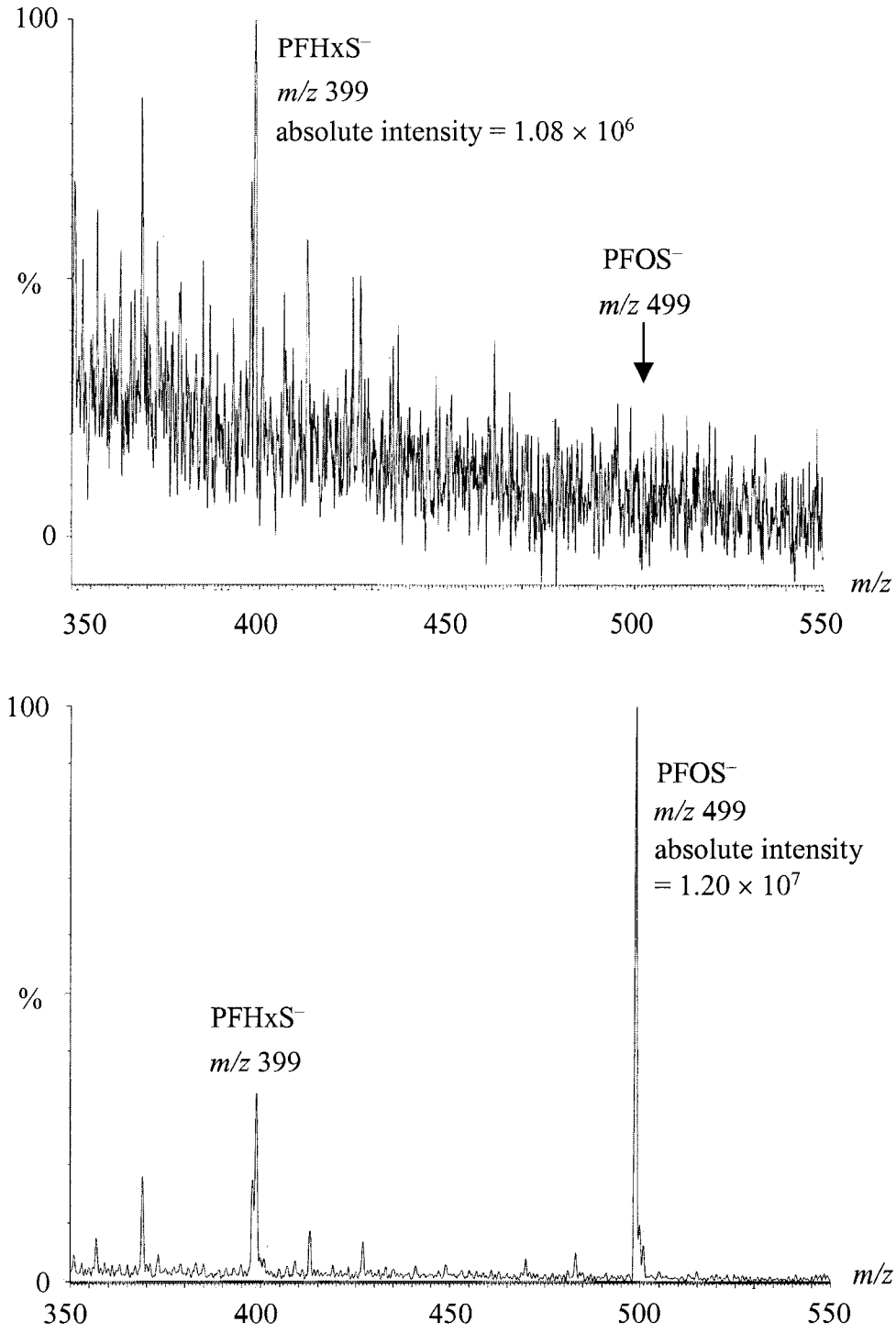

Figure 2.5. The top ESIMS spectrum is of a neat groundwater sample that was not diluted. The bottom spectrum is of the same groundwater sample, but it was diluted 2.5-fold so that the sample is in a 1:1 (v:v) acetonitrile:water matrix.

single groundwater sample. Note the increase of $PFAS^-$ peak heights at *m/z* 499 and *m/z* 399 and the decrease in noise by adding acetonitrile to the matrix. Increasing the amount of acetonitrile to 4:1 (v:v) acetonitrile to water gave the highest peak intensities when testing standard solutions. This effect is probably due to the different volatilities of acetonitrile and water (the normal boiling point of acetonitrile is 82 °C). As the volatility of the solvent increases, more sample is introduced into the electrospray chamber. Accordingly, the most intense peaks were observed for the solvent mixture with the highest acetonitrile to water ratio. However, most of the groundwater samples examined contained such low concentrations of $PFAS^-$ anions that they were diluted as little as possible. A 4:1 (v:v) acetonitrile to water matrix would require more dilution of the groundwater samples so a compromise was made by using the 1:1 (v:v) acetonitrile to water matrix. With a 2.5-fold dilution using the 1:1 (v:v) acetonitrile to water matrix, the spectrum in Figure 2.5 shows peaks that are more than an order of magnitude larger than the neat sample.

All samples were prepared using gas-tight syringes that were calibrated by weighing a specific volume of water using a mass balance that was accurate to ±0.0001 g. The 500, 50, and 10 μL syringes had 0.04%, 0.6%, and 1.0% relative errors, respectively, for a series of three replicates each. It is assumed that if the balance was more accurate at lower weights, the 10 μL syringe would have less error. The syringes were rinsed with 1:1 (v:v) acetonitrile:water at least five times after each use and conditioned by rinsing three times with each new sample before an aliquot of the sample was withdrawn for analysis.

Groundwater samples were centrifuged for 15 min at 5,000 rpm to separate any fine particulate that cannot be injected into the ESIMS instrument. The samples were not filtered since this might result in some loss of analyte by adsorption onto the filter. A single groundwater sample, analyzed by the method of standard-additions,[6] was prepared as follows. A series of 200-μL aliquots of the centrifuged groundwater supernatant was

treated with appropriate volumes of a 10 μM solution of $PFOS^-$ in 1:1 (v:v) acetonitrile:water. The samples were then diluted with 200 μL of acetonitrile and 25 μL of a 10 μM DDS^- solution in 1:1 (v:v) acetonitrile:water. The diluted sample was then diluted further with a sufficient amount of 1:1 (v:v) acetonitrile:water so that the final volume was 500 μL. This sample preparation process resulted in a 2.5-fold dilution of the original groundwater sample. This series of standard addition samples contained 0.25 to 1.0 μM added $PFOS^-$.

All of the groundwater samples were analyzed by the more simple direct-injection ESIMS method (defined as the method that requires only dilution and addition of DDS^-, the internal standard, prior to analysis).[7] This greatly reduced both the sample preparation time and the number of samples to be analyzed. After centrifugation, an aliquot of each sample was spiked with 0.5 μM DDS^- as the internal standard. Five replicate samples of each groundwater sample were analyzed. The concentration of $PFHxS^-$ in the samples was also determined using the DDS^- internal standard. Concentrations of $PFOS^-$ and $PFHxS^-$ were determined by comparison with a calibration graph. The samples used to generate the calibration curve for the direct-injection method were prepared as above except that deionized water was used instead of the groundwater supernatant. Much larger volumes (e.g., 10 mL) of these samples were prepared, but the dilution factors were the same. Calibration graph standards contained 0.5 μM DDS^- and from 0.01 to 5.0 μM $PFOS^-$.

All samples were prepared using glass laboratory equipment, since it was not known whether $PFAS^-$ anions might adhere differently to different materials and thus interfere with our analyses. It was previously reported that perfluorinated carboxylates and other surfactants may bind to glass surfaces.[47,108] To investigate this possibility, 10-mL samples containing equal concentrations of K(PFOS) and K(PFBS) were analyzed before and after being rolled for 20 minutes and left still for 24 hours in 1 L Pyrex and high-density polypropylene bottles. As can be seen by the mass spectral intensities of

$PFOS^-$ and $PFBS^-$ ratioed to DDS^- in Table 2.2, samples that were rolled in either plastic or glass did not differ from the control samples. Additionally, water from one of the wells at WAFB was collected in both plastic and glass containers and then tested for $PFAS^-$ anions using the ESIMS method to look for a difference between the bottle types. The concentrations found for both $PFOS^-$ and $PFHxS^-$ were the same for both sample containers to within experimental error. This indicates that, at these concentrations, there was no preferential adhesion of either $PFOS^-$ or $PFHxS^-$ to plastic containers. Even though it appears that there was no preferential adhesion of the analytes to either glass or plastic, glass apparatus was used for all experiments. All glassware was thoroughly cleaned with hot soapy water, rinsed with hot tap water and distilled deionized water, and air dried between each use.

Results and Discussion

Internal standard choice. Dodecylsulfate (DDS^-) was used as an internal standard for all ESIMS samples to allow for the quantification of $PFAS^-$ anions. In general, it is important that an ESIMS internal standard has properties similar to the analyte, so that both species will tend to form ions under the same set of instrumental conditions. Several researchers have used an isotopically labeled form (e.g., a perdeuterated or polydeuterated isotopomer) of their analyte as their internal standard, but that was not possible for perfluorinated compounds.[71,97,109] By keeping the internal standard similar in structure and mass, it should have a similar sensitivity coefficient to the analyte. The sensitivity coefficient is a constant that is related to the efficiency of an analyte to form individual molecular ions in the electrospray source.[71,97] The ratio of anion peak intensities is equal to the ratio of sensitivity coefficients when the concentrations of the anions are equal.[71,97]

Samples were analyzed containing equal concentrations of $PFOS^-$ and DDS^- to compare their sensitivity coefficients. The two different ESIMS peak intensities for the

Table 2.2. Ratio of mass spectral intensities of $PFOS^-$ (*m/z* 499) and $PFBS^-$ (*m/z* 299) to DDS^- (*m/z* 265) compared after contact with glass and plastic for 24 hours

	I(499)/I(265)[a]	I(299)/I(265)[b]
control[c]	0.76 ± 0.6	0.60 ± 0.06
glass[d]	0.83 ± 0.06	0.69 ± 0.05
plastic[e]	0.74 ± 0.07	0.6 ± 0.1

[a] Ratio of the intensity of the $PFOS^-$ (*m/z* 499) peak to the intensity of the DDS^- (*m/z* 265) peak. [b] Ratio of the intensity of the $PFBS^-$ (*m/z* 299) peak to the intensity of the DDS^- (*m/z* 265) peak. [c] Control samples were made directly from stock solutions and transferred only once to glass scintillation vials. [d] Glass samples were made from stock solutions and transferred to 1 L Pyrex volumetric flasks that were rolled for 20 minutes and let sit for 24 hours. [e] Plastic samples were made from stock solutions and transferred to 1 L high-density polypropylene bottles that were rolled for 20 minutes and let sit for 24 hours.

same concentration of $PFOS^-$ and DDS^- indicates they have different sensitivity coefficients. However, the ratio of these intensities, I(499)/I(265), was relatively constant (to within experimental error) for samples containing equal concentrations of $PFOS^-$ and DDS^- ranging from 0.01 to 50 μM, as shown in Figure 2.6. This makes DDS^- an appropriate internal standard for the quantification of $PFOS^-$. The validity of DDS^- as an internal standard should be evaluated for each new matrix.

To determine if DDS^- is appropriate for use with $PFHxS^-$ and other $PFAS^-$ anions, it was necessary to obtain pure samples of each surfactant salt. Since such a sample of $PFHxS^-$ was not available commercially, it was assumed that $PFHxS^-$ will behave similarly to $PFOS^-$ in the electrospray source. Some evidence that chain length can slightly effect the ionization efficiency of the electrospray source for quaternary ammonium compounds has been presented.[83] To examine this further, a series of experiments were done to determine the relative sensitivity coefficients of $PFOS^-$ and $PFBS^-$. Figure 2.7 shows that at equal concentrations over the range 0.01 to 1.00 μM, the sensitivity coefficients for the two perfluorinated anions $PFOS^-$ and $PFBS^-$ were found to be the same within experimental error. Also note that the intensity ratios I(299)/I(265) were the same within error as the intensity ratios I(499)/I(265) displayed in Figure 2.6 at the equivalent concentrations. Based on these observations, we assume that the sensitivity coefficients of $PFPnS^-$ ($C_5F_{11}SO_3^-$), $PFHxS^-$, and $PFHpS^-$ ($C_7F_{15}SO_3^-$) are also equal to that of $PFOS^-$ and $PFBS^-$ over equimolar concentration ranges.

Method of standard additions. Two methods (standard addition and direct-injection) of determining unknown concentrations of $PFOS^-$ (and therefore unknown concentrations of $PFBS^-$, $PFPnS^-$, $PFHxS^-$, and $PFHpS^-$) were investigated. A single groundwater sample from the former Wurtsmith Air Force base near Oscoda, MI will serve to exemplify the first method. The method of standard additions takes into account variations in the composition of different groundwater samples (i.e., the method employs matrix matching).[110] The groundwater sample, labeled FT3, consisted of a clear, colorless

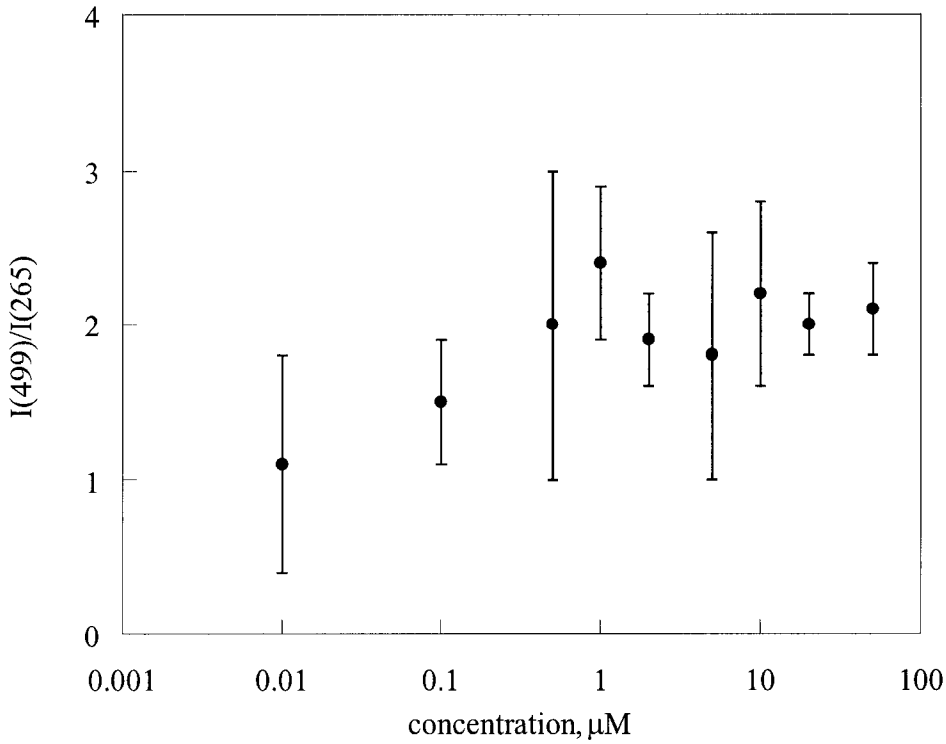

Figure 2.6. The ratio of the intensity of the $PFOS^-$ (*m/z* 499) peak to the intensity of the DDS^- (*m/z* 265) peak when the concentrations of $PFOS^-$ and DDS^- are equal. Error bars represent $\pm 1\sigma$.

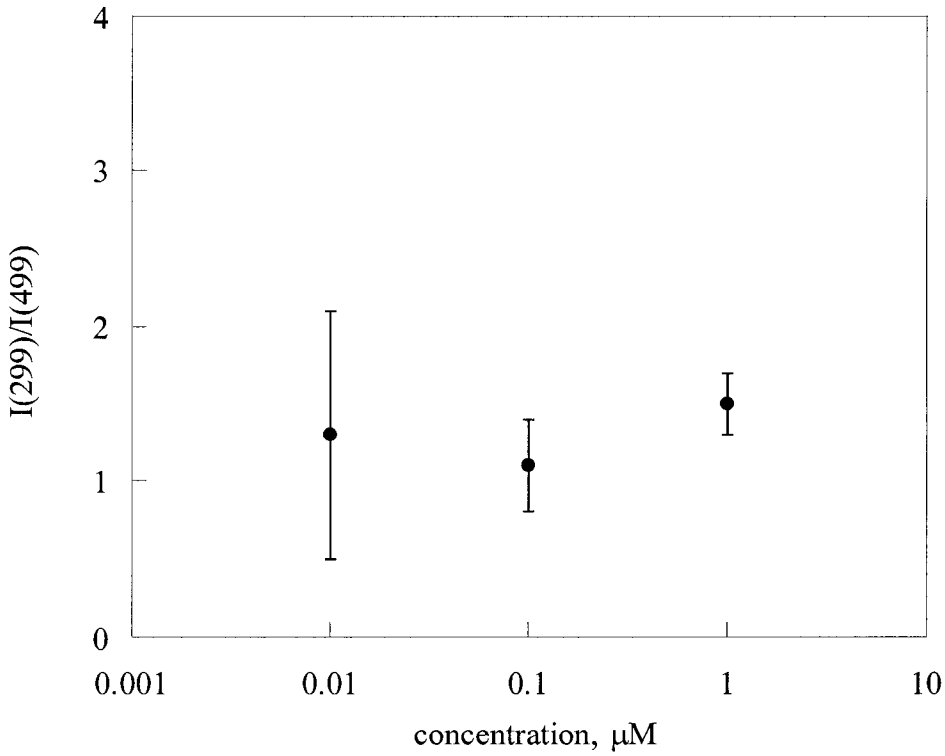

Figure 2.7. The ratio of the intensity of the $PFOS^-$ (*m/z* 499) peak to the intensity of the $PFBS^-$ (*m/z* 299) peak when the concentrations of $PFOS^-$ and $PFBS^-$ are equal. Error bars represent $\pm 1\sigma$.

supernatant and a small amount of solid particles. The pH and specific conductivity of the supernatant were 6.2 and 736 μS cm^{-1}, respectively. Standard-addition samples were prepared at four different concentrations with four replicates at each of concentration. Along with four replicates of FT3 that did not contain added $PFOS^-$, the spiked samples were examined by ESIMS (Finnigan) after each was made to be 0.5 μM DDS^- in 1:1 (v:v) acetonitrile:water.

A plot of I(499)/I(265) vs. the concentration of added $PFOS^-$ is shown in Figure 2.8 (each data point is the average of four replicates). The absolute value of the *x*-axis intercept of a linear least-squares fit to the data, 0.24 ± 0.04 μM, represents the experimentally determined concentration of $PFOS^-$ in the diluted groundwater sample. The concentration of $PFOS^-$ in undiluted FT3 groundwater is 2.5 times that value, 0.6 ± 0.1 μM (17% relative error) using the Finnigan ESIMS instrument.

No peaks were detected in the ESIMS spectra of these samples for other $PFAS^-$ anions with three, four, five, or seven carbon atoms. However, there was a detectable peak corresponding to $PFHxS^-$ (*m/z* 399). A separate standard-addition experiment was not possible since neither $PFHxS^-$ nor its sulfonyl fluoride precursor are commercially available. Based on the assumption that the sensitivity coefficients of $PFOS^-$ and $PFHxS^-$ are equal, the concentration of $PFHxS^-$ present was determined by comparing the intensity ratio I(499)/I(265) of the sample with no added $PFOS^-$ with the intensity ratio I(399)/I(265). The result of this data analysis is that the concentration of $PFHxS^-$ in undiluted FT3 groundwater is 0.4 ± 0.1 μM. Therefore, the $PFOS^-$ to $PFHxS^-$ molar ratio is 1.5 ± 0.5.

Direct-injection method. In some situations, the standard-addition method may be more time consuming than desired for a quick estimate of unknown concentrations of $PFAS^-$ anions. To explore the possibility of a direct measurement (i.e., after addition of DDS^- but with no added $PFOS^-$), the following experiments were performed. A series of twenty aqueous samples (four replicates of five different concentrations) that contained

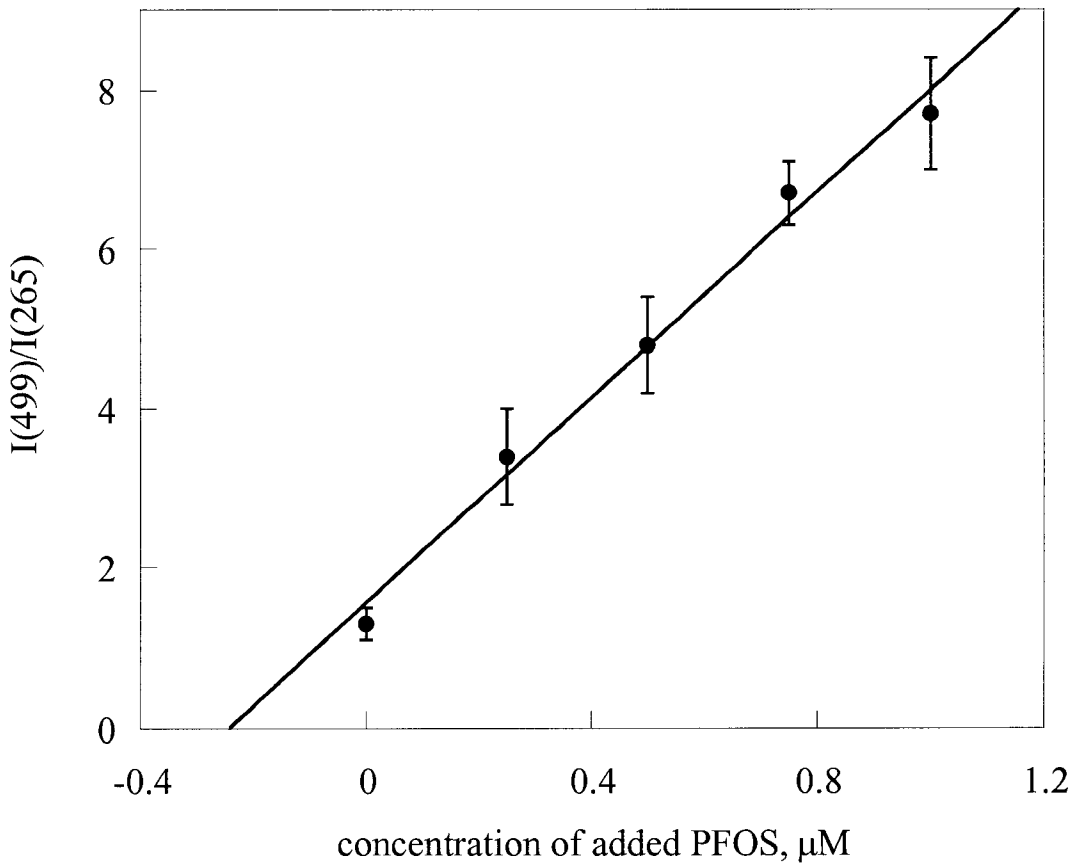

Figure 2.8. A plot of the mass-spectral intensity ratio I(499)/I(265) vs. concentration of $PFOS^-$ added to groundwater sample FT3 (collected at Wurtsmith Air Force Base, Oscoda, MI) that was diluted 2.5 times with 1:1 (v:v) acetonitrile:water and contained 0.5 μM DDS^-. The equation for the least squares linear fit is $y = 6.4(4)x + 1.6(2)$ with a correlation coefficient of 0.99. Error bars represent $\pm 1\sigma$ for an average of four replicates. The absolute value of the x-axis intercept, 0.24 ± 0.04 μM, represents the experimentally determined concentration of $PFOS^-$ in the diluted groundwater sample. The concentration of $PFOS^-$ in undiluted FT3 groundwater is 2.5 times that value, 0.6 ± 0.1 μM.

0.5 μM DDS^- and that varied in concentration of 0.05 to 5 μM $PFOS^-$ were prepared for injection into the Finnigan ESIMS. A log-log plot of I(499)/I(265) vs. the $PFOS^-$ concentration with a linear least-squares slope of 0.93 ± 0.04 and a correlation coefficient of 0.996 is shown in Figure 2.9. Each point on the Finnigan ESIMS calibration graph has a relative standard error ranging from 6 to 14%. The detection limit (as defined in Chapter 1: signal-to-noise ratio, *SNR*, greater than three) and the quantification limit (*SNR* greater than five) for $PFOS^-$ using the Finnigan ESIMS are 10 nM and 50 nM, respectively.

A similar calibration curve was prepared using the Fisons ESIMS with samples containing 0.5 μM DDS^- and varied in concentration of $PFOS^-$ from 0.01 to 5 μM. A log-log plot of I(499)/I(265) vs. the $PFOS^-$ concentration with a linear least-squares slope of 0.98 ± 0.07 and a correlation coefficient of 0.97 is shown in Figure 2.10. Each point on the Fisons ESIMS calibration graph has a relative standard error ranging from 8 to 50% from the average of at least five trials at each concentration. The detection and quantification limits for $PFOS^-$ using the Fisons ESIMS are 6 nM and 10 nM, respectively. Under the assumption that $PFHxS^-$ has the same sensitivity coefficient as $PFOS^-$, the same calibration curve equation was used to calculate the concentration of $PFHxS^-$.

Analysis of groundwater samples using direct-injection. The FT3 groundwater sample was analyzed using the direct-injection method with the Finnigan ESIMS. Samples were prepared (four replicates each) with a 2.5-fold dilution factor and with 0.5 μM DDS^- added as a standard. Using the Finnigan ESIMS calibration curve, the concentration of $PFOS^-$ in the FT3 groundwater sample was determined to be 0.48 ± 0.08 μM (cf., 0.6 ± 0.1 μM $PFOS^-$ by the standard-addition method). The concentration of $PFHxS^-$ in the FT3 groundwater sample was also calculated using the calibration curve equation for $PFOS^-$. The concentration of $PFHxS^-$ was determined to be 0.33 ± 0.03 μM (cf., 0.4 ± 0.1 μM $PFHxS^-$ by the standard-addition method). Note that the concentrations

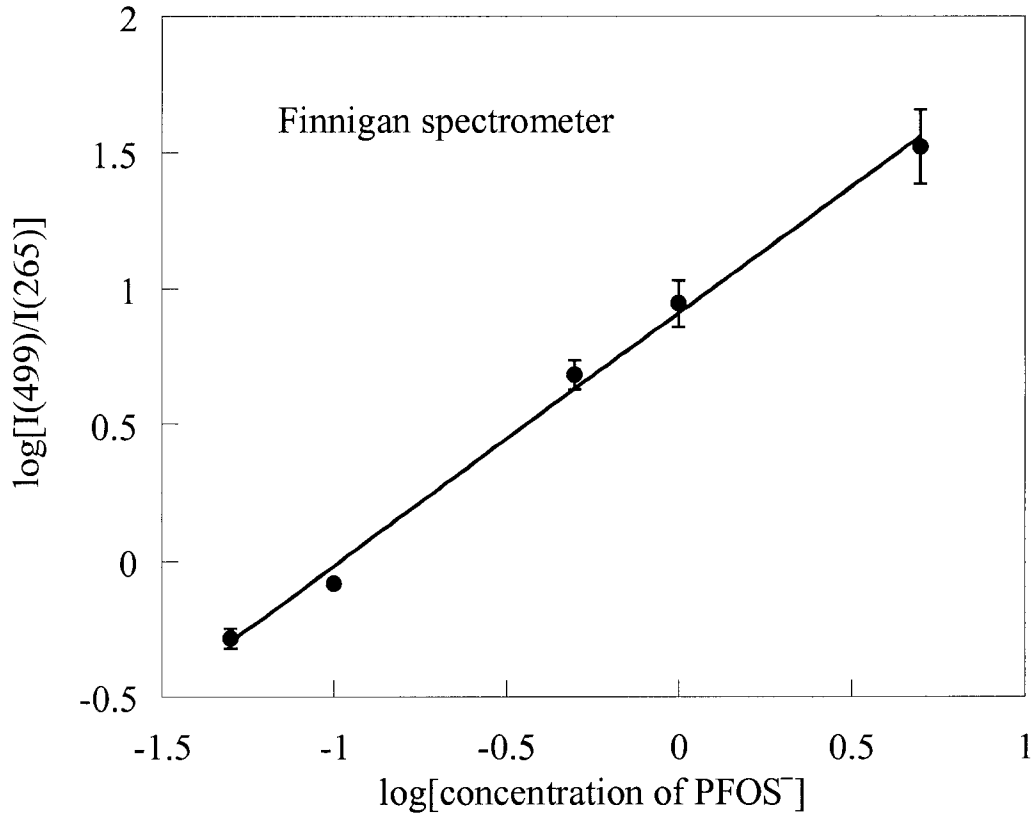

Figure 2.9. A log-log plot of the mass-spectral intensity ratio I(499)/I(265) vs. concentration of $PFOS^-$ for a series of five standards ranging from 0.05 to 5.0 μM (four replicates at each concentration) using the Finnigan spectrometer. Each standard contained 0.5 μM DDS^- in 1:1 (v:v) acetonitrile:water. The correlation coefficient for this calibration graph is 0.996 and the slope is 0.93 ± 0.04. For some points, the error bars (±1σ) are smaller than the size of the points on the graph.

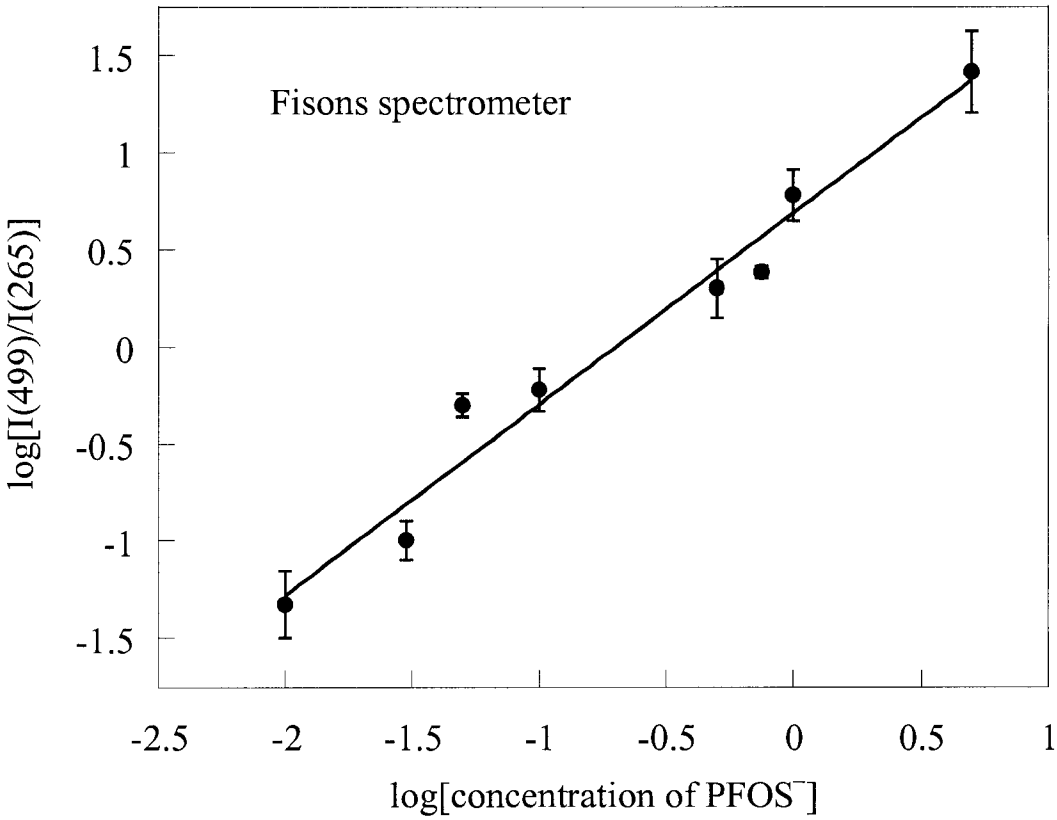

Figure 2.10. A log-log plot of the mass-spectral intensity ratio I(499)/I(265) vs. concentration of $PFOS^-$ for a series of five standards ranging from 0.01 to 5.0 μM (four replicates at each concentration) using the Fisons spectrometer. Each standard contained 0.5 μM DDS^- in 1:1 (v:v) acetonitrile:water. The correlation coefficient for this calibration graph is 0.97 and the slope is 0.98 ± 0.07. For some points the error bars (±1σ) are smaller than the point.

found for the groundwater sample FT3 using the standard addition method were the same as those using the direct-injection method calculated from the Finnigan ESIMS calibration graph. This suggests that the WAFB groundwater matrix did not seem to affect the ionization process for $PFAS^-$ anions.

The concentrations of $PFOS^-$ and $PFHxS^-$ in the groundwater from 19 wells at WAFB listed in Table 2.3 were determined by the direct-injection method using the Fisons ESIMS calibration curve. The Fisons ESIMS instrument was used for the analysis of these groundwater samples even though it has higher relative error than the Finnigan spectrometer since the Finnigan ESIMS instrument was not purchased until after the analysis of the groundwater samples was virtually complete. The concentrations of $PFOS^-$ in WAFB groundwater ranged from 0.01 to 0.30 μM and the concentrations of $PFHxS^-$ ranged from 0.02 to 0.30 μM. Groundwater from all of the wells contained measurable concentrations of $PFOS^-$. Measurable concentrations of $PFHxS^-$ were detected in 17 of the 19 wells. The errors in $PFOS^-$ and $PFHxS^-$ concentrations listed in Table 2.3 ranged from ca. 3% for the higher concentrations to ca. 50% near the detection limit. Table 2.3 also lists the distance of each of the wells from the fire-training pad. The location of each well relative to the fire-training pad was depicted in Figure 2.5.

The concentrations of $PFOS^-$ and $PFHxS^-$ seem to be somewhat related. Generally, if one was present at high concentrations in the groundwater from a given well the other was also present at high concentrations. In addition to $PFOS^-$ and $PFHxS^-$, some AFFF formulations are know to contain relatively small amounts of at least three other $PFAS^-$ anions, $PFBS^-$, $PFPnS^-$, and $PFHpS^-$.[6] However, these $PFAS^-$ homologues were not observed in any of the groundwater samples that were analyzed.

The $PFOS^-$ and $PFHxS^-$ concentrations from ten geographically representative wells are mapped in Figure 2.11. The highest concentration of $PFAS^-$ anions was observed in groundwater collected near the fire-training pad. Groundwater collected from wells located downgradient from the pad had lower concentrations. Figure 2.11 also

Table 2.3. Concentrations of perfluoroalkanesulfonates measured in the groundwater at FTA-02 at Wurtsmith Air Force Base

well	approximate distance from pad, m	$PFOS^-$, μM[a]	$PFHxS^-$, μM[a]
FT1	–46[b]	0.017(8)	0.090(5)
FT2	17	0.036(4)	0.30(6)
FT3	18	0.28(3)	0.258(9)
ML1	37	0.30(9)	0.17(5)
FT4	53	0.017(4)	nd[c]
FT6	60	0.018(7)	nd
FT5	61	0.031(6)	0.044(7)
ML5	110	0.052(8)	0.21(3)
ML3	114	0.22(2)	0.16(4)
ML6	114	0.042(6)	0.20(2)
ML8	121	0.029(9)	0.09(1)
FT10	175	0.013(5)	0.02(1)
FT8	183	0.017(8)	0.09(3)
FT9	183	0.09(3)	0.11(2)
FT12	305	0.015(3)	0.060(5)
FT13	305	0.06(1)	0.065(9)
FT14	305	0.039(7)	0.07(1)
FT18	518	0.06(3)	0.08(1)
FT17	540	0.010(1)	0.023(3)

[a] Errors shown in parentheses are ±1σ and were calculated from five replicate analyses.

[b] Well FT1 is located upgradient from the fire-training pad. [c] nd = not detected.

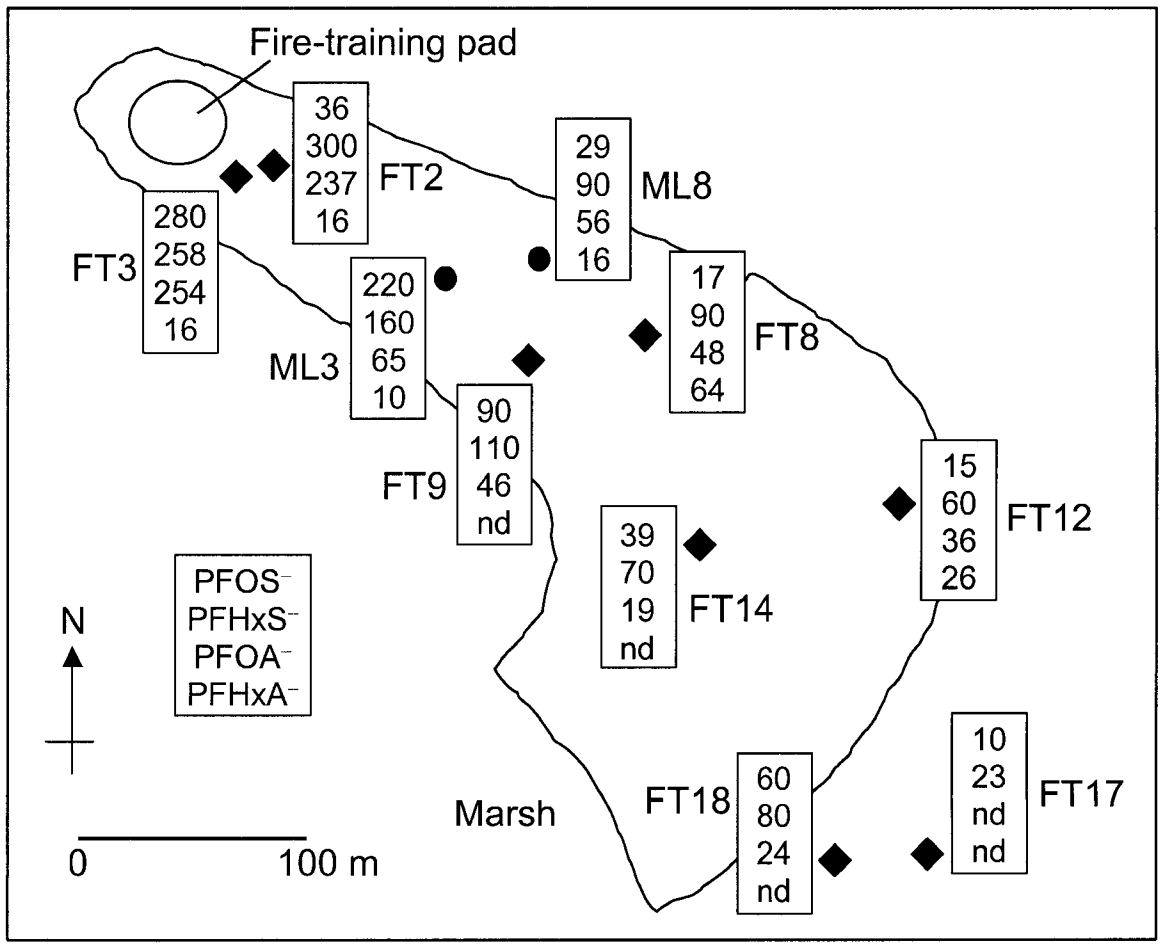

Figure 2.11. Map showing the concentration of perfluorinated surfactants in the FTA-02 groundwater plume at retired Wurtsmith Air Force Base (WAFB), Oscoda, MI. Groundwater samples from the indicated wells (diamonds and circles) were analyzed for perfluorooctanesulfonate ($PFOS^-$), perfluorohexanesulfonate ($PFHxS^-$), perfluorooctanoate ($PFOA^-$), and perfluorohexanoate ($PFHxA^-$). The boxes next to each well list the concentrations of the four analytes, in the order shown in the legend, in nM (nd = not detected).

displays the concentrations of two perfluorocarboxylates, perfluorooctanoate ($C_7F_{15}COO^-$, $PFOA^-$) and perfluorohexanoate ($C_5F_{11}COO^-$, $PFHxA^-$) that were determined after being derivatized to their methyl esters by Dr. Cheryl Moody Bartel and Dr. Jennifer Field using electron impact gas chromatography-mass spectrometry.[7] In general the total concentration of $PFAS^-$ anions was larger than the total concentration of perfluorocarboxylates. The ratios of total mass of perfluoroalkanesulfonates to total mass of perfluorocarboxylates varied from 0.95 to 5.4.

Groundwater from a background well located at WAFB, but not at FTA-02, contained no detectable perfluorocarboxylates (i.e., <7 nM), indicating that the occurrence of perfluorocarboxylates in groundwater downgradient from the fire-training pad at FTA-02 are likely the result of AFFF applications and discharge during fire-training exercises.[7] The water from this background well was not available to be tested in our lab for $PFAS^-$ anions. However, since there were no detectable perfluorocarboxylates, it is also possible that there were no $PFAS^-$ anions present above their LODs. The presence of $PFAS^-$ anions in groundwater up to 500 m downgradient of the fire-training pad may indicate that this class of anionic surfactants migrates in the sub-surface environment. One important consideration for anionic perfluorinated surfactant transport is the organic content of soil. For example, Sullivan and Mabury determined that soil partition coefficients for $PFAS^-$ anions increased with perfluorinated chain length and were linearly related to organic carbon content and sorption.[111] Since there are several other factors that may affect the concentrations of $PFAS^-$ anions in the WAFB groundwater including groundwater flow rates, soil type, distance of the well from the fire-training pad, and sampling depth, more research would be required to fully investigate the factors that govern the transport behavior of perfluorinated surfactants.

Several reports of $PFAS^-$ in surface waters have recently been published and reviewed.[8,58-61] In general, most of the reported concentrations of $PFAS^-$ anions are significantly lower than the amount detected in the groundwater at WAFB. Very low

concentrations of $PFOS^-$ (0.4 pM–0.3 nM) have been quantified in Japanese surface water (coastal seawater and several rivers).[60] Even lower concentrations of $PFOS^-$ (0.2 pM–0.1 nM) have been reported in drinking water in Japan.[61] Surface water collected from the Tennessee River near a fluorochemical manufacturing site contained concentrations of $PFOS^-$ (0.03–0.29 nM).[59] All of these reported concentrations of $PFOS^-$ are significantly lower than groundwater concentrations at WAFB FTA-02 (0.01–0.30 μM). Higher concentrations of $PFOS^-$, up to ca. 2 μM, were found in surface water downstream from an accidental spill of fire-fighting foam into the Etobicoke Creek, Toronto, ON.[58] These observed concentrations are closer to the concentrations of $PFAS^-$ found in the groundwater at WAFB FTA-02.

Comparison to literature methods. The direct-injection method has an LOD of 10 nM and a linear calibration range of 50 to 5000 nM $PFOS^-$. While these data were being prepared for publication (our manuscript was submitted in September 2001),[6] a February 2001 report by Hansen et al. with LODs of 3.4 and 17 nM $PFOS^-$ extracted from blood serum and whole liver tissue, respectively.[47] Due to the complex nature of these matrixes, their method required (i) extraction of $PFOS^-$ (and the other fluorochemical anions) into an organic solvent using an ion-pairing reagent, (ii) evaporation of the solvent and reconstitution in another solvent, (iii) HPLC separation of the anions on a Betasil C_{18} column, and (iv) atmospheric pressure ESIMS/MS (the tandem technique was necessary because of possible biological interferants).[47] Hansen's linear calibration range of 10 to 2000 nM $PFOS^-$, is nearly the same as the linear calibration range for the direct-injection method presented here.[47] A few months after our direct-injection paper was published in January 2002,[6] another article was published by Hansen et al. reporting a similar method for detection of $PFOS^-$ in surface water with a much lower LOD of 0.01 nM.[59] Hansen's new method involved preconcentration of the samples by solid phase extraction, HPLC separation on using a C_8 column, and detection by atmospheric pressure ESIMS.[59]

Again prior to the submission of our manuscript containing our ESIMS method in September 2001, a former collaborator (Moody) published in May 2001 two additional methods for the detection of aqueous $PFOS^-$, LC-ESIMS/MS and ^{19}F NMR.[57] Their LC-ESIMS/MS method also involved a preconcentration step using solid phase extraction to give an LOD of 0.03 nM $PFOS^-$ and a linear calibration range of 1.7 to 420 nM.[57] However, the ^{19}F NMR method described has a much higher $PFOS^-$ LOD (20 nM).[57] Importantly, the two methods reported by Moody et al. gave quantitative results for $PFOS^-$ in surface water that were significantly different from each other, presumably because of the presence of other surfactants that yield ^{19}F NMR spectra similar to that of $PFAS^-$ anions.[57]

In 2003, Takino et al. reported an LOD of 0.01 nM $PFOS^-$ in river water using a complex series of LC separation steps with atmospheric pressure photoionization MS detection.[62] After a separation using turbulent flow chromatography, $PFOS^-$ was back-flushed onto a reversed-phase LC column. They report a linear calibration curve over the concentration range 0.02–200 nM $PFOS^-$.[62] Although this method is purported to be useable as an automated, on-line detection scheme for aqueous $PFOS^-$, a rather complex experimental setup is required.

Most recently, Saito et al. reported an LC-ESIMS method with an LOD for $PFOS^-$ (0.0002 nM) that is significantly lower than any other mass spectral method reported to date.[60] However, several sample pretreatment and preconcentration steps were necessary including solid phase extraction, filtering, and a preconcentration column.[60] Even with these preconcentration steps, quantification was only possible over the concentration range of 0.2–200 nM $PFOS^-$, which is similar to that reported by Takino et al.[60] Specifically, this method consisted of passing a 1-L sample through two different filters prior to preconcentration using a Presep-C Agri column with a very low flow rate (10 mL min^{-1}). A 10 μL aliquot of the concentrated sample was then injected into an LC-ESIMS and $PFOS^-$ was detected by selected ion monitoring of the *m/z* 499 peak.

Analysis of each LC-ESIMS sample required ca. 20 minutes, not including the time required for the filtering and preconcentration steps, or rinsing the LC-ESIMS instrument between samples.[60]

All of these methods required at least one sample preparation step which resulted in relatively long analysis times. The trade-off can be clearly seen: a more complex, time-consuming method will yield a lower LOD while our more simple direct-injection ESIMS method yielded a higher LOD than most of the other methods in the literature.

Detection of perfluorocarboxylate anions. It was possible to detect perfluorocarboxylate anions, specifically, perfluorooctanoate ($C_7F_{15}CO_2^-$, *m/z* 413) and perfluorohexanoate ($C_5F_{11}CO_2^-$, *m/z* 313) by ESIMS in most of 19 groundwater samples collected from WAFB. Quantification by ESIMS was not possible, however, due to fragmentation during ionization. It was proposed that they undergo decarboxylation to a perfluoroalkyl intermediate during a gas phase reaction similar to the one below.[112] Both

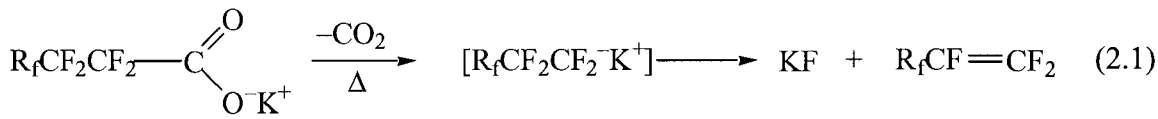

$$R_fCF_2CF_2{-}C(=O)O^-K^+ \xrightarrow[\Delta]{-CO_2} [R_fCF_2CF_2^-K^+] \longrightarrow KF + R_fCF{=}CF_2 \quad (2.1)$$

the perfluorocarboxylate anions and the final product of their decomposition, perfluoroolefins, are known to be toxic.[113-117] This type of fragmentation has been corroborated by ESIMS spectra of two commercially available, perfluorocarboxylate anions, perfluorooctanoate and perfluorododecanoate shown in Figures 2.12 and 2.13. Each spectrum exhibits two peaks separated by 44 mass units. In Figure 2.12, the *m/z* 413 and *m/z* 369 peaks correspond to $C_7F_{15}CO_2^-$ and $C_7F_{15}^-$, respectively. In Figure 2.13, the *m/z* 613 and *m/z* 569 peaks correspond to $C_{11}F_{23}CO_2^-$ and $C_{11}F_{23}^-$, respectively. Although ESIMS is a soft ionization technique that does not normally cause fragmentation, these control experiments with relatively pure samples suggest that decarboxylation fragments do form under the instrumental conditions used in this study.

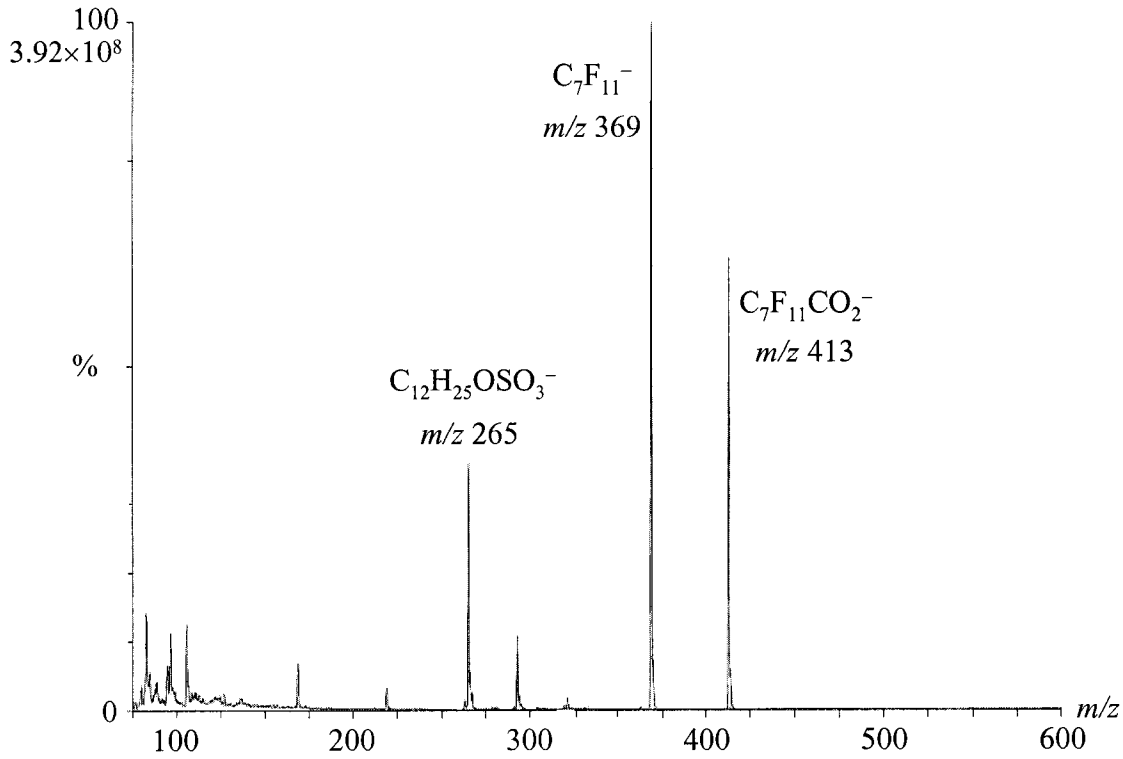

Figure 2.12. ESIMS spectrum of perfluorooctanoate ($C_7F_{11}CO_2^-$, *m/z* 413) in a 1:1 (v:v) acetonitrile:water solution. A fragment of this surfactant can be seen at *m/z* 369 ($C_7F_{11}^-$). This sample also contained DDS^- (*m/z* 265) as an internal standard.

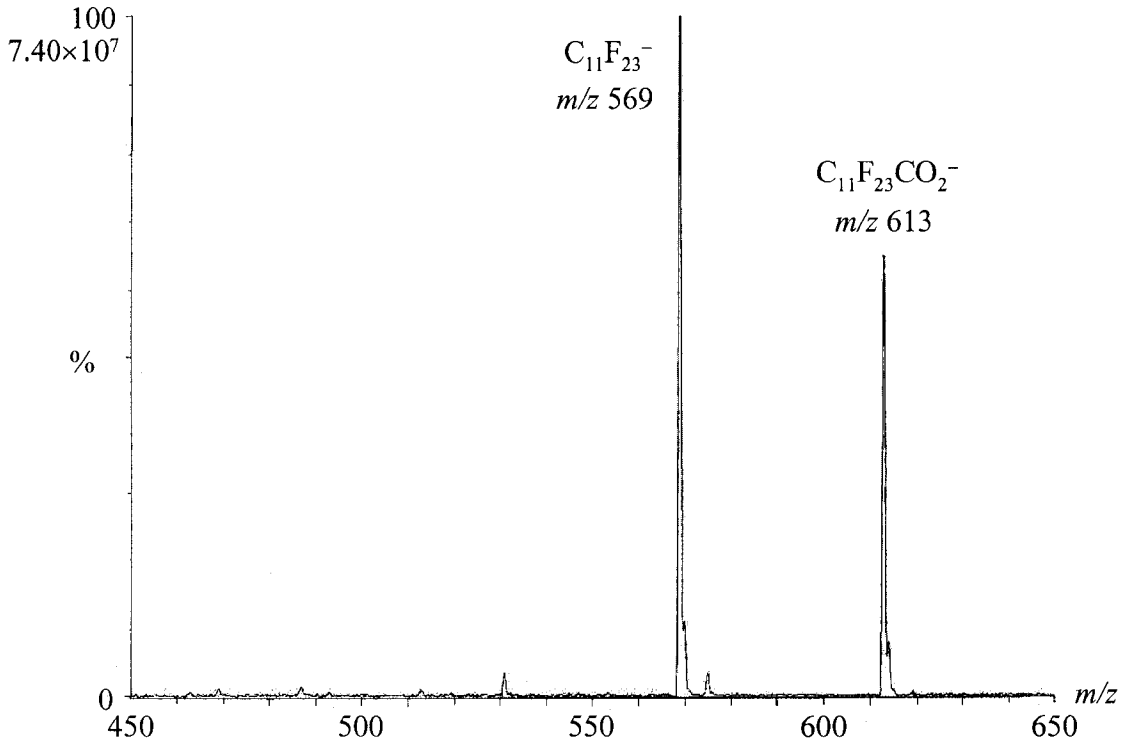

Figure 2.13. ESIMS spectrum of perfluorododecanoate ($C_{11}F_{23}CO_2^-$, *m/z* 613) in a 1:1 (v:v) acetonitrile:water solution. A fragment of this surfactant can be seen at *m/z* 569 ($C_{11}F_{23}^-$).

Analysis of an AFFF concentrate. One formulation of AFFF, FC-203CF LIGHT WATER Brand Aqueous Film Forming Foam®, was analyzed by ESIMS for the quantitative determination of $PFAS^-$ anions and qualitative determination of perfluorocarboxylate anions. Four samples were prepared by diluting the AFFF concentrate with a solution of 1:1 (v:v) acetonitrile:water to a 40,000-fold final dilution and also contained 0.5 μM DDS^- as an internal standard. Note that in a parallel experiment for which DDS^- was not added, no ESIMS peak was observed at *m/z* 265. Therefore, since DDS^- or another species with *m/z* 265 is not present in this formulation of AFFF, DDS^- is an appropriate internal standard. An ESIMS spectrum of the dilute AFFF is shown in Figure 2.14. The characteristic peaks of six $PFAS^-$ anions can be seen at *m/z* 249 ($C_3F_7SO_3^-$), 299 ($C_4F_9SO_3^-$), 349 ($C_5F_{11}SO_3^-$), 399 ($C_6F_{13}SO_3^-$), 449 ($C_7F_{15}SO_3^-$), and 499 ($C_8F_{17}SO_3^-$). However, only five $PFAS^-$ anions are listed in the MSDS sheet for this formulation of AFFF.[3] Two alkylsulfate salts are listed on the MSDS sheet and their peaks can be seen at *m/z* 209 ($C_8H_{17}SO_4^-$) and 237 ($C_{10}H_{21}SO_4^-$).[3] Peaks are also present for $C_7F_{15}CO_2^-$ (*m/z* 413) and $C_5F_{11}CO_2^-$ (*m/z* 313) as well as for their $C_7F_{15}^-$ and $C_5F_{11}^-$ fragments at *m/z* 369 and 269, respectively. Therefore, perfluorocarboxylate anions are present in at least one formulation of AFFF even though they are not listed in either the patent or the MSDS sheet.[3,118]

Concentrations of the $PFAS^-$ anions present in this formulation of AFFF were determined using a modified version of the method of standard additions. Four samples were prepared by adding 0.5 μM $PFOS^-$, $PFBS^-$, and DDS^- to the 40,000-fold diluted AFFF. Four additional samples were prepared by adding only 0.5 μM DDS^- to the dilute AFFF. The concentrations of $PFOS^-$ (17 ± 3 mM) and $PFBS^-$ (1.9 ± 0.3 mM) in the AFFF concentrate were determined by comparing the intensity ratios of the unspiked AFFF samples to the samples containing the known concentrations of the three standards. The concentrations of the other four $PFAS^-$ anions were determined by comparing the intensity ratios of the unspiked samples and concentrations of both $PFOS^-$ and $PFBS^-$ to

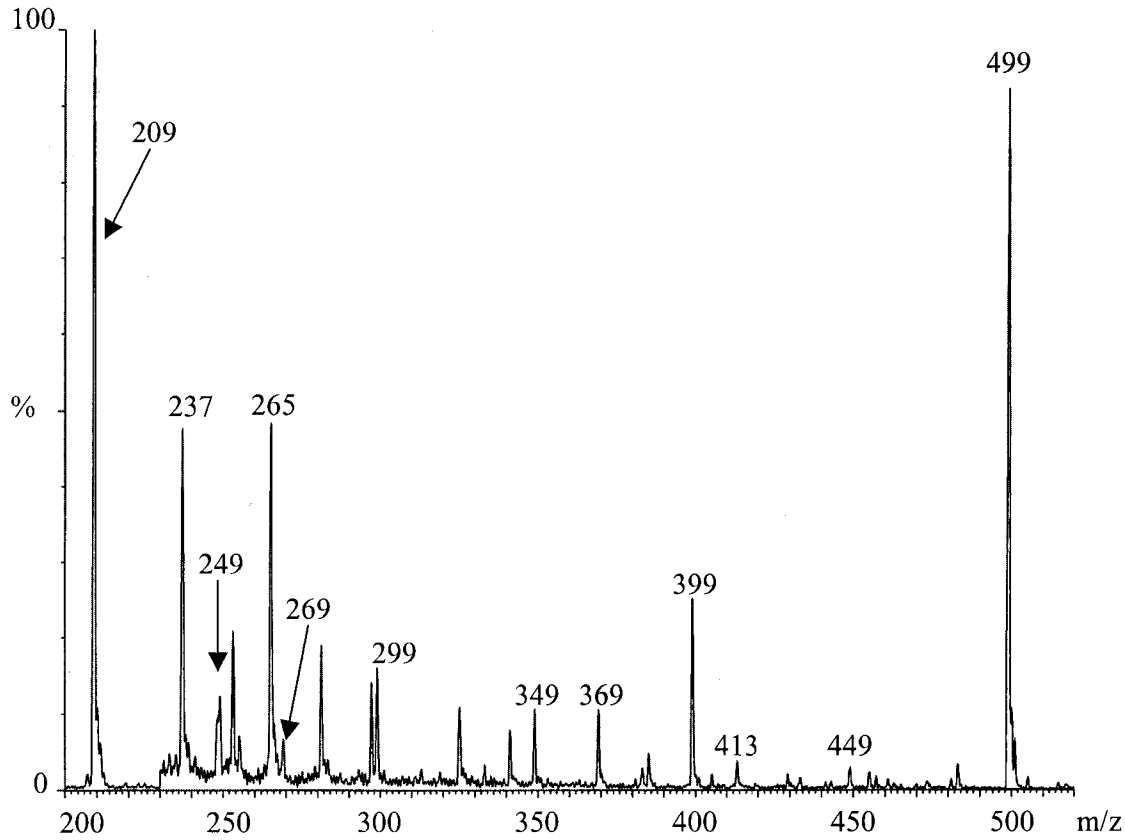

Figure 2.14. ESIMS spectrum of one formulation of AFFF, FC203-LIGHTWATER. The commercial concentrate was diluted 40,000 times with 1:1 (v:v) acetonitrile:water and contained with 0.5 μM DDS^- (*m/z* 265). The vertical scale from *m/z* 230–520 has been expanded eight times. The peaks at *m/z* 249, 299, 349, 399, 449, 499 are assigned to the perfluoropropane-, perfluorobutane-, perfluoropentane-, perfluorohexane-, perfluoroheptane-, and perfluorooctanesulfonate anions, respectively. The peaks at *m/z* 209 and 237 are assigned to $C_8H_{17}SO_4^-$ and $C_{10}H_{21}SO_4^-$, respectively. The peaks at *m/z* 413, 369, 313, and 269 are assigned to $C_7F_{15}CO_2^-$, $C_7F_{15}^-$, $C_5F_{11}CO_2^-$, and $C_5F_{11}^-$, respectively.

the intensity ratios of the $PFAS^-$ anion of unknown concentrations. This method gives concentration ranges of 1.1–2.8 mM for $C_3F_7SO_3^-$, 0.9–2.5 mM for $C_5F_{11}SO_3^-$, 2.0–5.4 mM for $C_6F_{13}SO_3^-$, and 0.3–0.7 mM for $C_7F_{15}SO_3^-$.

Testing other water matrixes. Several experiments were performed to explore the effects of the water matrix on the intensity ratio I(499)/I(265). Three natural water matrixes, Horsetooth Reservoir (Fort Collins, CO), Cincinnati tap water, and Ohio River water, were tested using a modified standard-addition method. Spectra for all three matrixes with no added $PFOS^-$ or DDS^- exhibited no peak for either anion. Samples (four replicates each) were made from each matrix to contain 0.5 μM DDS^- and two different concentrations of $PFOS^-$ (0.1 and 0.5 μM). The ESIMS intensity ratios I(499)/I(265) for these standard additions are listed in Table 2.4. Both Cincinnati tap water and water from the Ohio River had significantly different values of I(499)/I(265) compared to the standards. The intensity ratios of Horsetooth Reservoir water were very close to the expected intensity ratio for the 0.1 μM $PFOS^-$ sample and it had the same intensity ratio for the 0.5 μM $PFOS^-$ sample, indicating that this matrix had the least effect on the ionization efficiency of the standards within the spectrometer. Therefore, the direct-injection method can be used with the Horsetooth Reservoir water samples. However, the variation of the intensity ratios of Cincinnati tap water and Ohio River water shows that these matrixes are significantly different from distilled deionized water and therefore, the method of standard additions must be used for quantification. Each new matrix should be tested as described here to determine the proper method of quantification.

Testing Kimwipes® and Bounce® for $PFOS^-$. It is commonly known that $PFAS^-$ anions, including $PFOS^-$, have been used in the manufacturing of various commercially available products for its anti-static properties.[5] Out of scientific curiosity, it was decided to test two products, Kimwipes® (Kimberly-Clark) and Bounce® (Proctor & Gamble), that are known for their anti-static applications. A single sheet of each

Table 2.4. Comparison of the ESIMS intensity ratio I(499)/I(265) of standards with the I(499)/I(265) ratio of natural water samples spiked with 0.5 μM DDS^- and two different $PFOS^-$ concentrations[a]

	0.1 μM $PFOS^-$	0.5 μM $PFOS^-$
standards	1.0 ± 0.1	4.7 ± 0.7
Horsetooth Reservoir water[b]	1.3 ± 0.1	5.4 ± 0.2
Cincinnati tap water[c]	1.9 ± 0.3	9 ± 2
Ohio River water[c]	1.9 ± 0.2	7 ± 1

[a] Data are reported with ±1σ. [b] Samples collected from Horsetooth Reservoir, Fort Collins, CO [c] Samples provided by E. T. Urbansky of the U.S. Environmental Protection Agency.

product was placed in a beaker of water (ca. 80 mL) and stirred for 20 hours. The utmost care was taken to prevent any contamination of these samples with $PFOS^-$ by conducting the entire experiment in a laboratory room known to have no intentional contact with salts of $PFOS^-$ and using new or acid washed equipment for all sample preparation steps. Analysis by ESIMS with 0.5 μM DDS^- as the internal standard (1:1 (v:v) acetonitrile:water solutions) yielded no detectable $PFOS^-$ peak from the Bounce® extract. However, a $PFOS^-$ peak that was ca. three times the noise was observed from the Kimwipe® extract. Control samples revealed no peak intensity at *m/z* 265 for either product, making DDS^- an appropriate internal standard. Since $PFOS^-$ was observed in the Kimwipe® water extract, a second extraction following the above procedure was done using 1:1 (v:v) acetonitrile:water as the extraction solvent instead of pure water. This resulted in an even larger peak at *m/z* 499 which presumably corresponds to the presence of $PFOS^-$ in this particular box of Kimwipes®. The small concentration of $PFOS^-$ found in Kimwipes® could have contributed to the error in the $PFOS^-$ measurements since prior to this discovery, Kimwipes® were routinely used to dry the syringe tip prior to injection into the ESIMS instruments. It might be possible to develop a more efficient scheme for the extraction of $PFOS^-$ from Kimwipes®, but this was not the focus of these experiments. It was simply desired to detect $PFOS^-$ as a proof of the concept that some commercially available products may contain, or could in the past have contained, $PFOS^-$. The presence of $PFOS^-$ in commercial products, without being listed on product labels and therefore without the public's knowledge, could have contributed to the current presence of $PFOS^-$ in human blood.[47]

Reproducibility. The reproducibility of the direct-injection ESIMS method was tested using standard solutions that were performed with each set of samples. By analyzing the same standard solutions over many different days, the instrumental conditions were recorded and any differences in the peak intensities observed from the standard solutions helped explain changes in the peak intensities observed from sample

solutions. The four standard solutions contained (i) 10 μM DDS^- and $PFOS^-$, (ii) 1 μM DDS^- and $PFOS^-$, (iii) 1 μM DDS^-, and (iv) 0.5 μM DDS^- in 1:1 (v:v) acetonitrile to water solutions. The average ratios I(499)/I(265) are reported in Table 2.5. Over a three month period the ratio of $PFOS^-$ to DDS^-, I(499)/I(265), had 20%, 11%, 13% and 50% relative standard deviation for the four standard solutions respectively. The high error for the 0.5 μM DDS^- solution is due mostly to the intensity at *m/z* 499 ($PFOS^-$), which was occasionally slightly above background levels. Even though all equipment that contacted $PFOS^-$ solutions was rinsed thoroughly, it is possible that residual $PFOS^-$ from the injection syringe or the ESIMS instrument caused the higher variation of this ratio.

Ionic strength effects. The ionic strength of the 19 groundwater samples from WAFB that were analyzed for $PFAS^-$ anions ranged from 116 to 736 μS cm^{-1}. To determine if this range of ionic strengths had an effect on the intensity ratio I(499)/I(265), the ionic strength of standard solutions was varied from 1.4 to 742 μS cm^{-1}. The ESIMS spectra of a series of four aqueous samples (three replicates each) that were 0.1 μM $PFOS^-$ and 0.5 μM DDS^- and varied in specific conductivity from 1.4 to 742 μS cm^{-1} by addition of Na_2SO_4 were recorded (the 1.4 μS cm^{-1}-samples had no added Na_2SO_4). The values of I(499)/I(265) varied randomly from 0.18 to 0.36. This indicates that a change in specific conductivity over the range found in the WAFB groundwater samples will result in concentrations of $PFOS^-$ determined by the direct-injection method that are reliable only to within a factor of two.

pH effects. The pH of the 19 groundwater samples from WAFB that were analyzed for $PFAS^-$ anions ranged from 5.5 to 8.1. To determine if this range of pHs had an effect on the intensity ratio I(499)/I(265), the pH of standard solutions was varied from 6 to 8 with constant ionic strength. The ESIMS spectra of a series of three standard samples (three replicates each) that were 0.1 μM $PFOS^-$ and 0.5 μM DDS^- and varied in pH from 6–8 were recorded. The pH was adjusted with Na_2HPO_4/KH_2PO_4 buffer. The values of I(499)/I(265) varied randomly from 0.36 to 0.60, indicating that changes in pH

Table 2.5. Reproducibility of the intensity ratio I(499)/I(265) for four standard solutions

standards	number of trials	I(499)/I(265)[a]	RSD[b]
10 μM $PFOS^-$ + DDS^-	11	2.5 ± 0.5	20%
1 μM $PFOS^-$ + DDS^-	6	2.7 ± 0.3	11%
1 μM DDS^-	5	0.045 ± 0.006	13%
0.5 μM DDS^-	8	0.006 ± 0.003	50%

[a] Average values with the error given as ±1σ. [b] RSD = relative standard deviation.

over the range found in the WAFB groundwater samples will result in concentrations of $PFOS^-$ determined by the direct-injection method are reliable only to within a factor of two over this pH range.

A second study was done to examine the effects of pH when using higher concentrations of $PFOS^-$. A series of standards containing 25 μM $PFOS^-$ and 1 μM DDS^- at four different pH's (6, 7, 8, and 10) were made using the Na_2HPO_4/KH_2PO_4 buffer with constant ion strength. As can be seen from Figure 2.15, there is no adverse effect of pH on the values of I(499)/I(265) between pH 6 and 8. At more basic pH's the I(499)/I(265) values decrease somewhat, which could be a result of the increased ionic strength of the sample. Therefore, over the pH range found in the WAFB groundwater samples (pH 5.5–8.1), $PFOS^-$ concentrations can be reliably determined.

Conclusions

Two methods for the quantification of $PFAS^-$ anions in aqueous solution have been presented in this chapter. These methods allow for the identification and quantification of individual $PFAS^-$ anions (i.e., $PFOS^-$, $PFHxS^-$) instead of the total (collective) concentration of all $PFAS^-$ anions present in solution. A tandem mass spectrometry method was not investigated; however, fragmentation experiments could be useful when evaluating samples from sources where $PFAS^-$ anions could be confused with other anions present in solution. The direct-injection method has an LOD of 10 nM and a linear calibration range of 0.05 to 5 μM for $PFOS^-$. The LOD for $PFOS^-$ using this direct-injection ESIMS method is higher than most of the other recent methods reported in the literature except for an ^{19}F NMR method that had an LOD of 20 nM.[57] However, all of the other ESIMS methods with lower LODs required the use of at least one preconcentration step as well as at least one separation step prior to MS detection.[47,57-60,62]

It is concluded that the method of standard additions presented here should be used to quantify $PFOS^-$ in aqueous solutions. The direct-injection method can be used

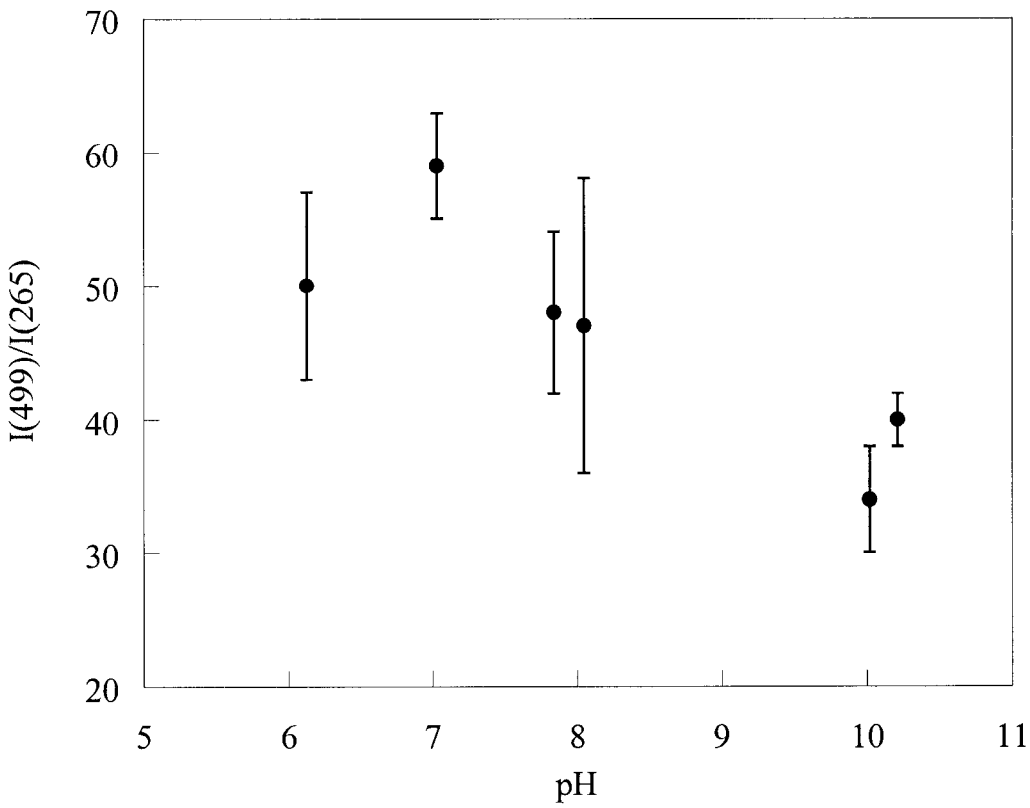

Figure 2.15. Effect of pH on the intensity ratio I(499)/I(265) for standard solutions containing 25 μM $PFOS^-$ and 1 μM DDS^- at a constant ionic strength. The pH 6-samples contained no added buffer. Error bars represent ±1σ.

when the matrix involved is less complex or when a faster determination of $PFOS^-$ concentration is required. The method of direct-injection was used to detect and quantify $PFAS^-$ anions in Michigan groundwater. Concentrations of $PFAS^-$ anions up to 0.3 μM were found in the groundwater at FTA-02 despite a minimum of 5 years since active fire-fighting activity occurred at WAFB. It is believed that the observed $PFAS^-$ anions were components of some of the fire-fighting materials used at this site until 1993 when fire-fighting activity ceased. Given that the groundwater velocity is 0.1 to 0.3 m day^{-1},[99,100,104] and assuming that the source of $PFAS^-$ anions was the fire-training pad, it can be estimated that the perfluorinated surfactants found in groundwater ca. 500 m from the fire-training pad have been in the groundwater environment for a minimum of 5 years and potentially for as long as 15 years. The observation of $PFAS^-$ and perfluorocarboxylates in WAFB groundwater indicates that the compounds are resistant to degradation under the prevailing groundwater conditions at this site.

References

1. Moody, C. A.; Field, J. A. *Environ. Sci. Technol.* **1999**, *33*, 2800–2806.
2. Moody, C. A.; Field, J. A. *Environ. Sci. Technol.* **2000**, *34*, 3864–3870.
3. "Material Safety Data Sheet for FC-203CF Light Water AFFF 3%," 3M Company: Saint Paul, MN, 1999.
4. *Fed. Regist.* **2000**, *65*, 62319–62333.
5. *Fed. Regist.* **2002**, *67*, 11008–11030.
6. Hebert, G. N.; Odom, M. A.; Craig, P. S.; Dick, D. L.; Strauss, S. H. *J. Environ. Monit.* **2002**, *4*, 90–95.
7. Moody, C. A.; Hebert, G. N.; Strauss, S. H.; Field, J. A. *J. Environ. Monit.* **2003**, *5*, 341–345.
8. Schultz, M. M.; Barofsky, D. F.; Field, J. A. *Environ. Eng. Sci.* **2003**, *20*, 487–501.
9. Brown, D.; Mayer, C. E. *The Washington Post*, May 17, 2000, p A1.
10. Key, B. D.; Howell, R. D.; Criddle, C. S. *Environ. Sci. Technol.* **1997**, *31*, 2445–2454.
11. Purdy, R. Proceedings of the Society of Environmental Toxicology and Chemistry Conference, Nashville, TN, 2000, PMP124, p 160.
12. Renner, R. *Environ. Sci. Technol.* **2001**, *35*, 154A–160A.
13. Renner, R. *Sci. Am.* **2001**, *March 17*, 18.
14. Tullo, A. *Chem. Eng. News* **2000**, *May 22*, 9–10.
15. Tullo, A. *Chem. Eng. News* **2000**, *May 29*, 12–13.
16. Wood, A.; Clarin, W. *Chem. Week* **2000**, *May 24*, 9.
17. Seacat, A. M.; Thomford, P. J.; Hansen, K. J.; Olsen, G. W.; Case, M. T.; Butenhoff, J. L. *Toxicol. Sci.* **2002**, *68*, 249–264.
18. Case, M. T.; York, R. G.; Christian, M. S. *Int. J. Toxicol.* **2001**, *20*, 101–109.

19. Thibodeaux, J. R.; Hanson, R. G.; Rogers, J. M.; Grey, B. E.; Barbee, B. D.; Richards, J. H.; Butenhoff, J. L.; Stevenson, L. A.; Lau, C. *Toxicol. Sci.* **2003**, *74*, 369–381.

20. Lau, C.; Thibodeaux, J. R.; Hanson, R. G.; Rogers, J. M.; Grey, B. E.; Stanton, M. E.; Butenhoff, J. L.; Stevenson, L. A. *Toxicol. Sci.* **2003**, *74*, 382–392.

21. Boudreau, T. M.; Sibley, P. K.; Mabury, S. A.; Muir, D. G. C.; Solomon, K. R. *Arch. Environ. Contam. Toxicol.* **2003**, *44*, 307–313.

22. Sanderson, H.; Boudreau, T. M.; Mabury, S. A.; Cheong, W.-J.; Solomon, K. R. *Environ. Toxicol. Chem.* **2002**, *21*, 1490–1496.

23. Berthiaume, J.; Wallace, K. B. *Toxicol. Lett.* **2002**, *129*, 23–32.

24. Derbel, M.; Hosokawa, M.; Satoh, T. *Biol. Pharm. Bull.* **1996**, *19*, 765–767.

25. Ikeda, T.; Fukuda, K.; Mori, I.; Enomoto, M.; Komai, T.; Suga, T. In *Peroxisomes in Biology and Medicine*; Fahimi, H. D., Sies, H., Eds.; Springer-Verlag: Berlin, 1987, pp 304–308.

26. Sohlenius, A.-K.; Eriksson, A. M.; Hogstrom, C.; Kimland, M.; DePierre, J. W. *Pharmacol. Toxicol.* **1993**, *72*, 90–93.

27. Starkov, A. A.; Wallace, K. B. *Toxicol. Sci.* **2002**, *66*, 244–252.

28. Leubker, D. J.; Hansen, K. J.; Bass, N. M.; Butenhoff, J. L.; Seacat, A. M. *Toxicology* **2002**, *176*, 175–185.

29. Haughom, B.; Spydevold, O. *Biochim. Biophys. Acta* **1992**, *1128*, 65–72.

30. Boudreau, T. M.; Janutka, R.; Solomon, K. R.; Sibley, P. K.; Muir, D. C. G.; Mabury, S. A. Proceedings of the Society of Environmental Toxicology and Chemistry Conference, Nashville, TN, 2000, 348, p 77.

31. Boudreau, T. M.; Janutka, R.; Solomon, K. R.; Sibley, P. K.; Muir, D. C. G.; Mabury, S. A. Proceedings of the Society of Environmental Toxicology and Chemistry Conference, Madrid, Spain, 2001, M/MF144, p 129.

32. Seacat, A. M.; Thomford, P. J.; Hansen, K. J.; Clemen, L. A.; Eldridge, S. R.; Elcombe, C. R.; Butenhoff, J. L. *Toxicology* **2003**, *183*, 117–131.

33. Hoff, P. T.; Van Dongen, W.; Esmans, E. L.; Blust, R.; De Coen, W. M. *Aquat. Toxicol.* **2003**, *62*, 349–359.

34. Hu, W. y.; Jones, P. D.; De Coen, W.; King, L.; Franker, P.; Newsted, J.; Giesy, J. P. *Comp. Biochem. Physiol., C* **2003**, *135*, 77–88.

35. Kannan, K.; Choi, J.-W.; Iseki, N.; Senthilkumar, K.; Kim, D. H.; Masunaga, S.; Giesy, J. P. *Chemosphere* **2002**, *49*, 225–231.

36. Kannan, K.; Newsted, J.; Halbrook, R. S.; Giesy, J. P. *Environ. Sci. Technol.* **2002**, *36*, 2566–2571.

37. Kannan, K.; Corsolini, S.; Falandysz, J.; Oehme, G.; Focardi, S.; Giesy, J. P. *Environ. Sci. Technol.* **2002**, *36*, 3210–3216.

38. Kannan, K.; Hansen, K. J.; Wade, T. L.; Giesy, J. P. *Arch. Environ. Contam. Toxicol.* **2002**, *42*, 313–318.

39. Kannan, K.; Franson, J. C.; Bowerman, W. W.; Hansen, K. J.; Jones, P. D.; Giesy, J. P. *Environ. Sci. Technol.* **2001**, *35*, 3065–3070.

40. Kannan, K.; Koistinen, J.; Beckmen, K.; Evans, T.; Gorzelany, J. F.; Hansen, K. J.; Jones, P. D.; Helle, E.; Nyman, M.; Giesy, J. P. *Environ. Sci. Technol.* **2001**, *35*, 1593–1598.

41. Giesy, J. P.; Kannan, K. *Environ. Sci. Technol.* **2001**, *35*, 1339–1342.

42. Hoff, P. T.; Van de Vijver, K.; Van Dongen, W.; Esmans, E. L.; Blust, R.; De Coen, W. M. *Environ. Toxicol. Chem.* **2003**, *22*, 608–614.

43. Taniyasu, S.; Kannan, K.; Horii, Y.; Hanari, N.; Yamashita, N. *Environ. Sci. Technol.* **2003**, *37*, 2634–2639.

44. Taniyasu, S.; Kannan, K.; Horii, Y.; Yamashita, N. *Organohalogen Compd.* **2002**, *59*, 311–314.

45. Kannan, K.; Giesy, J. P. *Organohalogen Compd.* **2002**, *59*, 267–270.

46. Olsen, G. W.; Hansen, K. J.; Stevenson, L. A.; Burris, J. M.; Mandel, J. H. *Environ. Sci. Technol.* **2003**, *37*, 888–891.

47. Hansen, K. J.; Clemen, L. A.; Ellefson, M. E.; Johnson, H. O. *Environ. Sci. Technol.* **2001**, *35*, 766–770.

48. Olsen, G. W.; Burris, J. M.; Mandel, J. H.; Zobel, L. R. *J. Occup. Environ. Med.* **1999**, *41*, 799–806.

49. Olsen, G. W.; Burris, J. M.; Burlew, M. M.; Mandel, J. H. *J. Occup. Environ. Med.* **2003**, *45*, 260–270.

50. Masunaga, S.; Kannan, K.; Doi, R.; Nakanishi, J.; Giesy, J. P. *Organohalogen Compd.* **2002**, *59*, 319–322.

51. Howell, R. D.; Tucker, E. E. *Am. Environ. Lab* **1996**, *12*, 10–11.

52. Darwin, R. L.; Ottman, R. E.; Norman, E. C.; Gott, J. E.; Hanauska, C. P. *Natl. Fire Protect. Assoc.* **1995**, 67–73.

53. Chan, D. B.; Chian, E. S. K. *Environ. Prog.* **1986**, *5*, 104–109.

54. Kissa, E. *Fluorinated Surfactants: Synthesis, Properties, and Applications*; Marcel Dekker: New York, 1994.

55. Key, B. D.; Howell, R. D.; Criddle, C. S. *Environ. Sci. Technol.* **1998**, *32*, 2283–2287.

56. Erten-Unal, M.; Schafran, G. C.; Paranjape, S.; Williams, F.; Cotnoir, D.; Kirk, D. *Proceedings of the National Conference on Environmental Engineering* **1998**, *98*, 494–499.

57. Moody, C. A.; Kwan, W. C.; Martin, J. W.; Muir, D. C. G.; Mabury, S. A. *Anal. Chem.* **2001**, *73*, 2200–2206.

58. Moody, C. A.; Martin, J. W.; Kwan, W. C.; Muir, D. C. G.; Mabury, S. A. *Environ. Sci. Technol.* **2002**, *36*, 545–551.

59. Hansen, K. J.; Johnson, H. O.; Eldridge, J. S.; Butenhoff, J. L.; Dick, L. A. *Environ. Sci. Technol.* **2002**, *36*, 1681–1685.

60. Saito, N.; Sasaki, K.; Nakatome, K.; Harada, K.; Yoshinaga, T.; Koizumi, A. *Arch. Environ. Contam. Toxicol.* **2003**, *45*, 149–158.

61. Harada, K.; Saito, N.; Sasaki, K.; Inoue, K.; Koizumi, A. *Bull. Environ. Contam. Toxicol.* **2003**, *71*, 31–36.

62. Takino, M.; Daishima, S.; Nakahara, T. *Rapid Commun. Mass Spectrom.* **2003**, *17*, 383–390.

63. Dole, M.; Mack, L. L.; Hines, R. L.; Mobley, R. C.; Ferguson, L. D.; Alice, M. B. *J. Chem. Phys.* **1968**, *49*, 2240–2249.

64. Mack, L. L.; Kralic, P.; Rehude, A.; Dole, M. *J. Chem. Phys.* **1970**, *52*, 4977–4986.

65. Yamashita, M.; Fenn, J. B. *J. Phys. Chem.* **1984**, *88*, 4451–4459.

66. Yamashita, M.; Fenn, J. B. *J. Phys. Chem.* **1984**, *88*, 4671–4675.

67. Aleksandrov, M. L.; Gall, L. N.; Krasnov, V. N.; Nikolaev, V. I.; Pavlenko, V. A.; Shkurov, V. A. *Dokl. Akad. Nauk* **1984**, *277*, 379–383.

68. Aleksandrov, M. L.; Gall, L. N.; Krasnov, V. N.; Nikolaev, V. I.; Pavlenko, V. A.; Shkurov, V. A.; Baram, G. I.; Gracher, M. A.; Knorre, V. D.; Kusner, Y. S. *Bioorg. Khim.* **1984**, *10*, 710–712.

69. Braun, T.; Zsindely, S. *Trends Anal. Chem.* **1992**, *11*, 307–309.

70. Hofstadler, S. A.; Bakhtiar, R.; Smith, R. D. *J. Chem. Educ.* **1996**, *73*, A82–A88.

71. Cole, R. B. *Electrospray Ionization Mass Spectrometry: Fundamentals, Instrumentation, and Applications*; John Wiley and Sons: New York, 1997.

72. McCloskey, J. A.; Crain, P. F. *Int. J. Mass Spectrom. Ion Processes* **1992**, *118/119*, 593–615.

73. Smith, R. D.; Loo, J. A.; Edmonds, C. G.; Barinaga, C. J.; Udseth, H. R. *Anal. Chem.* **1990**, *62*, 882–899.

74. Smith, R. D.; Loo, J. A.; Loo, R. R. O.; Busman, M.; Udseth, H. R. *Mass Spectrom. Rev.* **1991**, *10*, 359–451.

75. Mann, M. Quantitative Aspects of Electrospray Mass Spectrometry. Ph.D. Dissertation, Yale University, New Haven, CT, 1989.

76. Tang, L.; Kebarle, P. *Anal. Chem.* **1993**, *65*, 3654–3668.

77. Agnes, G. R.; Horlick, G. *Appl. Spectrosc.* **1994**, *48*, 649–654.

78. Selby, D. S.; Guilhaus, M.; Murby, J.; Wells, R. J. *J. Mass Spectrom.* **1998**, *33*, 1232–1236.

79. Barnett, D. A.; Horlick, G. *J. Anal. At. Spectrom.* **1997**, *12*, 497–501.

80. Clewell, R.; Tsui, D. T. Proceedings of the American Chemical Society, 1999, 39, pp 71–74.

81. Urbansky, E. T.; Magnuson, M. L.; Freeman, D.; Jelks, C. *J. Anal. At. Spectrom.* **1999**, *14*, 1861–1866.

82. Lamouroux, C.; Virelizier, H.; Moulin, C.; Tabet, J. C.; Kankowski, C. K. *Anal. Chem.* **2000**, *72*, 1191–1186.

83. Hind, A. R.; Bhargava, S. K.; Cullis, P. G. *Anal. Chim. Acta* **1998**, *377*, 39–45.

84. Purves, R. W.; Gabryelski, W.; Li, L. *Rapid Commun. Mass Spectrom.* **1998**, *12*, 695–700.

85. Wang, H.; Agnes, G. R. *Anal. Chem.* **1999**, *71*, 3785–3792.

86. Michelsen, P.; Jergil, B.; Odham, G. *Rapid Commun. Mass Spectrom.* **1995**, *9*, 1109–1114.

87. Guther, M. L. S.; Treumann, A.; Ferguson, M. A. J. *Mol. Biochem. Parasitol.* **1996**, *77*, 137–145.

88. Han, X.; Gross, R. W. *Proc. Natl. Acad. Sci. U.S.A.* **1994**, *91*, 10635–10639.

89. Carver, J. A.; Nicholls, K. A.; Aquilina, J. A.; Truscott, R. J. W. *Exp. Eye Res.* **1996**, *63*, 639–647.

90. Mills, K. A.; Mushtaq, I.; Johnson, A. W.; Whitfield, P. D.; Clayton, P. T. *Pediatr. Res.* **1998**, *43*, 361–368.

91. Subbanagounder, G.; Leitinger, N.; Shih, P. T.; Faull, K. F.; Berliner, J. A. *Circ. Res.* **1999**, *85*, 311–318.

92. Bonaventura, C.; Ferruzzi, G.; Tesh, S.; Stevens, R. D. *J. Biol. Chem.* **1999**, *274*, 24742–24748.

93. Ofori-Acquah, S. F.; Green, B. N.; Wild, B. J.; Lalloz, M. R. A.; Layton, D. M. *Int. J. Mol. Med.* **1998**, *2*, 451–453.

94. Jorgensen, T. J. D.; Staroske, T.; Roepstorff, P.; Williams, D. H.; Heck, A. J. R. *J. Chem. Soc., Perkin Trans. 2* **1999**, 1859–1863.

95. Dass, C.; Kusmierz, J. J.; Desiderio, D. M.; Jarvis, S. A.; Green, B. N. *J. Am. Soc. Mass Spectrom.* **1991**, *2*, 149–156.

96. Fenn, J. B.; Mann, M.; Meng, C. K.; Wong, S. F. *Science* **1989**, *246*, 64–71.

97. Kebarle, P.; Tang, L. *Anal. Chem.* **1993**, *65*, 972A–986A.

98. "Phase II - Confirmation/Quantification Stage 2: Wurtsmith Air Force Base, MI, Investigation of Soil and Groundwater Contamination at Selected Sites, Vol. I," United States Geological Survey: Lansing, MI, 1995.

99. Barcelona, M. J. Proceedings of the Symposium on Natural Attenuation of Chlorinated Organics in Groundwater, Dallas, TX, September 1996, pp 98–103.

100. "Phase II - Confirmation/Quantification Stage 1: Wurtsmith Air Force Base, MI: Investigations of Groundwater and Soil Contamination at Selected Sites," United States Geological Survey: Lansing, MI, 1991.

101. Bermejo, J. L.; Sauck, W. A.; Atekwana, E. A. *Ground Water Monit. Rem.* **1997**, 131–137.

102. Chapelle, F. H.; Haack, S. K.; Adriaens, P.; Henry, M. A.; Bradley, P. M. *Environ. Sci. Technol.* **1996**, *30*, 3565–3569.

103. Dojka, M. A.; Hugenholtz, P.; Haack, S. K.; Pace, N. R. *Appl. Environ. Microbiol.* **1998**, *64*, 3869–3877.

104. Gillespie, J. L. "Installation Restoration Program Phase II - Confirmation/Quantification Stage 2," United States Geological Survey: Lansing, MI, 1990.

105. McGuire, J. T.; Long, D. T.; Klug, M. J.; Haack, S. K.; Hyndman, D. W. *Environ. Sci. Technol.* **2002**, *36*, 2693–2700.

106. APHA-AWWA-WPCF, Ed. *Standard Methods for the Examination of Water and Wastewater*; 20th ed.; American Public Health Association: Washington DC, 1998, pp 5-47–5-49.

107. Giesy, J. P.; Kannan, K. *Environ. Sci. Technol.* **2002**, *36*, 146A–152A.

108. Belisle, J.; Hagen, D. F. *Anal. Biochem.* **1980**, *101*, 369–376.

109. Webb, K. S.; Baker, P. B.; Cassells, N. P.; Francis, J. M.; Johnston, D. E.; Lancaster, S. L.; Minty, P. S.; Reed, G. D.; White, S. A. *J. Forensic Sci.* **1996**, *41*, 938–946.

110. Harris, D. C. *Quantitative Chemical Analysis*; 4th ed.; W. H. Freeman: New York, 1995.

111. Sullivan, R. C.; Mabury, S. A. Proceedings of the Society of Environmental Toxicology and Chemistry Conference, Baltimore, MD, 2001, PM278, p 193.

112. Podol'skii, A. V.; Khonina, T. G.; Filyakova, T. I.; Kachalkova, M. I.; Kodess, M. I. *Izv. Akad. Nauk, Ser. Khim.* **1991**, 1977–1979.

113. Reo, N. V.; Goecke, C. M.; Narayanan, L.; Jarnot, B. M. *Toxicol. Appl. Pharmacol.* **1994**, *124*, 165–173.

114. Goecke, C. M.; Jarnot, B. M.; Reo, N. V. *Chem. Res. Toxicol.* **1992**, *5*, 512–519.

115. Clayton, J. W., Jr. *Fluorine Chem. Rev.* **1967**, *1*, 197–252.

116. Ohmori, K.; Kudo, N.; Katayama, K.; Kawashima, Y. *Toxicology* **2003**, *184*, 135–140.

117. Witzmann, F. A.; Parker, D. N.; Jarnot, B. M. *Toxicol. Lett.* **1994**, *71*, 271–277.

118. Alm, R.; Stern, R. M. U.S. Patent 5,085,786, 1992.

Chapter 3

ATR-FTIR Detection and Quantification of Low Concentrations of Aqueous Polyatomic Anions

Introduction

An ongoing need exists to detect and quantify anionic pollutants such as perchlorate, chlorate, perfluoroalkanesulfonates, and phosphonates at low concentrations in aqueous media given that they can cause problems to human health and persist in the environment. The following is a brief description of each anion and (i) why its presence in the environment causes concern or why it is a good model for other anionic pollutants, (ii) its common uses and possible routes for its introduction into the environment, and (iii) the limits set by the U.S. Environmental Protection Agency (EPA) for its presence in drinking water. The detection and quantification of these anions will be demonstrated using an attenuated total reflectance (ATR) FTIR spectroscopy method.

Perchlorate (ClO_4^-). Beginning in the late 1990's, perchlorate was identified as a contaminant in some natural waterways that are used extensively for recreation, drinking, and crop irrigation.[1] It is a known pollutant in the drinking water of several western states including Utah, California, Arizona, and Nevada,[2,3] and there have been confirmed releases of perchlorate in at least 20 states within the United States.[4] Recently, the contamination of the Colorado River with perchlorate was the subject of a cover story article in *Chemical & Engineering News* that described the widespread use of this perchlorate-tainted water for drinking and irrigation.[3] Concern over perchlorate arises

from its ability to interfere with the function of the thyroid gland, which can affect metabolism and development.[5,6]

Perchlorate contamination can be attributed primarily to the defense and aerospace industries and to military operations,[7,8] where salts of perchlorate are used as oxidants in munitions and solid fuels for rockets. In addition to many other smaller scale uses of perchlorate, it is also used on a large scale as a component of automobile air bag inflators.[9] The only reported natural occurrence of perchlorate is in nitrate-bearing ores, called caliche, that are located predominantly in Chile.[10] These ores are mined, and $NaNO_3$ (Chile saltpeter) is refined and sold as a finished fertilizer product (N-P-K grade 16-0-0, i.e., 16% N, 0% P_2O_5, 0% K_2O by mass). Fertilizer products derived from Chilean ores were widely used many decades ago, and the finished 16-0-0 fertilizer product was consistently found to contain perchlorate just below the level of 2,000 mg kg^{-1}.[11,12]. However, their use has diminished to less than 0.2% of current U.S. fertilizer consumption[11] as a result of the low cost of synthetically produced nitrogen sources. Additionally, the only current vendor for this material has recently modified the caliche refinement process in order to reduce the level of perchlorate to less than 100 mg kg^{-1}.[13] The EPA recently released the most comprehensive survey to date on the presence or absence of perchlorate in fertilizers and related materials.[13] Perchlorate was not found in any of the approximately 50 tested materials except for the few known to originate from Chile saltpeter. Because of these reasons, nitrate fertilizers are not generally seen as a major source of perchlorate in the environment.[12-15]

Following the detection of perchlorate at 0.18 μM or higher in a variety of lakes, rivers and groundwater sources in the southwestern United States,[2] the state of California set drinking water action limits for perchlorate at 0.04 μM.[16] The EPA added perchlorate to the Contaminant Candidate List for drinking water in 1998[17] and to the Unregulated Contaminant Monitoring Regulation list in 1999.[18] Based on the EPA's latest risk

assessment draft, which proposed a reference dose of 0.03 μg/kg-day for ClO_4^-,[4] a concentration near 0.01 μM in drinking water is presumed to be safe.[2]

Chlorate (ClO_3^-). Although the oxoanion chlorate is related to perchlorate, it is much less of an environmental concern since it is readily biodegraded by microorganisms under anaerobic conditions.[19] It has been shown that there is no tendency for chlorate to accumulate or bioconcentrate in organisms, and it is not magnified in the food chain.[20] Human toxicity has been shown only in extreme cases of suicidal ingestion of more than 100 g sodium chlorate.[20]

Sodium chlorate is most commonly used as a non-selective herbicide that is considered toxic to all green plant parts. It is also used as part of various industrial processes and as a component of match heads.[20] The use of chlorine dioxide for purification of drinking water results in the production of chlorate as a disinfection byproduct.[21] Although there is no chlorate-specific EPA guideline for disinfection byproducts, the EPA recommends that the total concentration of chlorine dioxide, chlorate, and chlorite be kept below 14 μM (1 mg L^{-1} as Cl_2).[22]

Perfluorooctanesulfonate ($C_8F_{17}SO_3^-$; PFOS$^-$). Some perfluorinated surfactant anions, including perfluoro-*n*-octanesulfonate have recently become pollutants of concern.[23-34] The properties, synthesis, production, applications, toxicity, analysis, occurrence, and techniques for treatment of $PFOS^-$ has been reviewed.[23] Details on the toxicity, occurrence, and regulation of $PFOS^-$ were discussed in Chapter 2.

Pinacolylmethylphosphonate ($C_7H_{16}PO_3^-$; PMPA$^-$). Use of chemical and biological weapons in warfare is not new. As early as 1000 BC, the Chinese used arsenic smoke in warfare. During World War I, the German army, and eventually all combatants, used various chemical warfare agents.[35,36] The use of chemical and biological weapons, along with their development, production, and stockpiling, was banned at the Chemical Warfare Convention that was ratified by the U.S. in 1997. One chemical warfare agent of current concern, Soman (GD), which is shown in Equation 3.1, is part of the

organophosphorous class of nerve agents. In aqueous solution, Soman undergoes rapid hydrolysis to $PMPA^-$.[37,38] Although $PMPA^-$ itself is not toxic, identifying $PMPA^-$ in

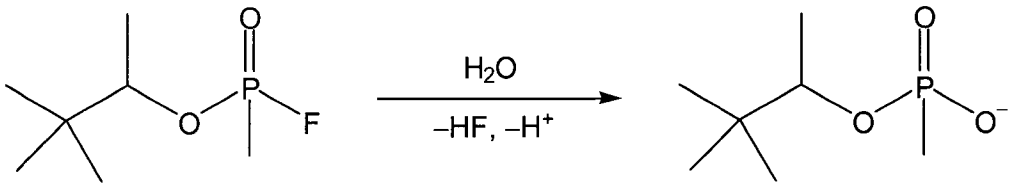

Soman $PMPA^-$ (3.1)

water would indicate the possible manufacture and/or release of Soman in the vicinity of, or upstream of, the point of sampling. The detection of $PMPA^-$ as well as the hydrolysis products of other organophosphorus nerve agents in aqueous media is an important challenge to the U.S. Department of Defense. As of 1995, the military-recommended guidelines for Soman in drinking water based on the consumption of 15 L day^{-1} and 5 L day^{-1}, are 11 and 34 nM, respectively.[36]

A redox recyclable extractant. As is evident from the foregoing discussion, the detection of these contaminant anions at low concentrations is an important area of research. Historically, much research has been done on the separation and recovery of ionic pollutants from aqueous media.[39-45] Anion extraction has been commonly carried out using anion-exchange resins that contain polymerized quaternary ammonium or pyridinium salts with exchangeable anions.[39-42] More recently, extractants consisting of organometallic complexes were developed by the Strauss Research Group to address the need for a new approach for the extraction and recovery of pollutant ions.[46-53] A class of tetraalkylated ferrocenium salts was developed for use in liquid-liquid extractions as well as for use as an extractant on solid supports. One such salt, 1,1′,3,3′-tetrakis(2-methyl-2-hexyl)ferrocenium nitrate ($HEP^+NO_3^-$), shown below, has been used for the efficient extraction and recovery of weakly hydrated anions from water.[46-51] These experiments followed the general redox-recyclable extraction and recovery (R^2ER) process shown in

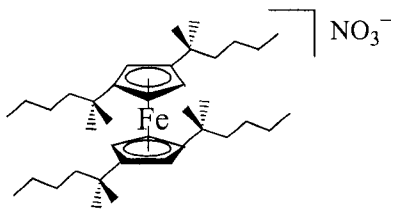

$HEP^{+}NO_3^{-}$

Figure 3.1. The organometallic complex in its active, oxidized (cationic), form is ion paired with an exchangeable anion, NO_3^-, and is able to selectively extract anions from aqueous media with hydration energies lower than that of NO_3^-. In its active form, $HEP^{+}NO_3^-$ is green in color, while in its reduced (neutral), inactive form, HEP is orange in color. This color change gives a useful visual indication of the redox state of the extractant. These ferrocenium salts have been shown to (i) be highly selective for the target anion, (ii) have high capacities, (iii) undergo rapid ion-exchange, (iv) be recyclable and to be stable with respect to over-oxidation or over-reduction, (v) allow for recovery of the target anion in a minimal volume of secondary waste and (vi) be hydrophobic/lipophilic enough to prevent being lost to the aqueous phase.[46-52]

Recently, $HEP^{+}NO_3^-$ was adsorbed to polymeric substrates to yield redox-recyclable materials that were used in ion-exchange chromatography extraction experiments.[47] These materials were used for the selective extraction of perrhenate (ReO_4^-) and $PFOS^-$ from aqueous media. Even after prolonged exposure to aqueous solutions, $HEP^{+}NO_3^-$ was not observed to desorb from the surface of the solid-support (polymer beads). Extraction and recovery of $PFOS^-$ using a proprietary technique resulted in 88–100% recovery of $PFOS^-$ as its solid potassium salt.[47] The recovery of $PFOS^-$ in a relatively pure, crystalline form represents the greatest possible reduction in secondary waste volume. In fact, depending on its purity, the recovered K(PFOS) could be recycled.

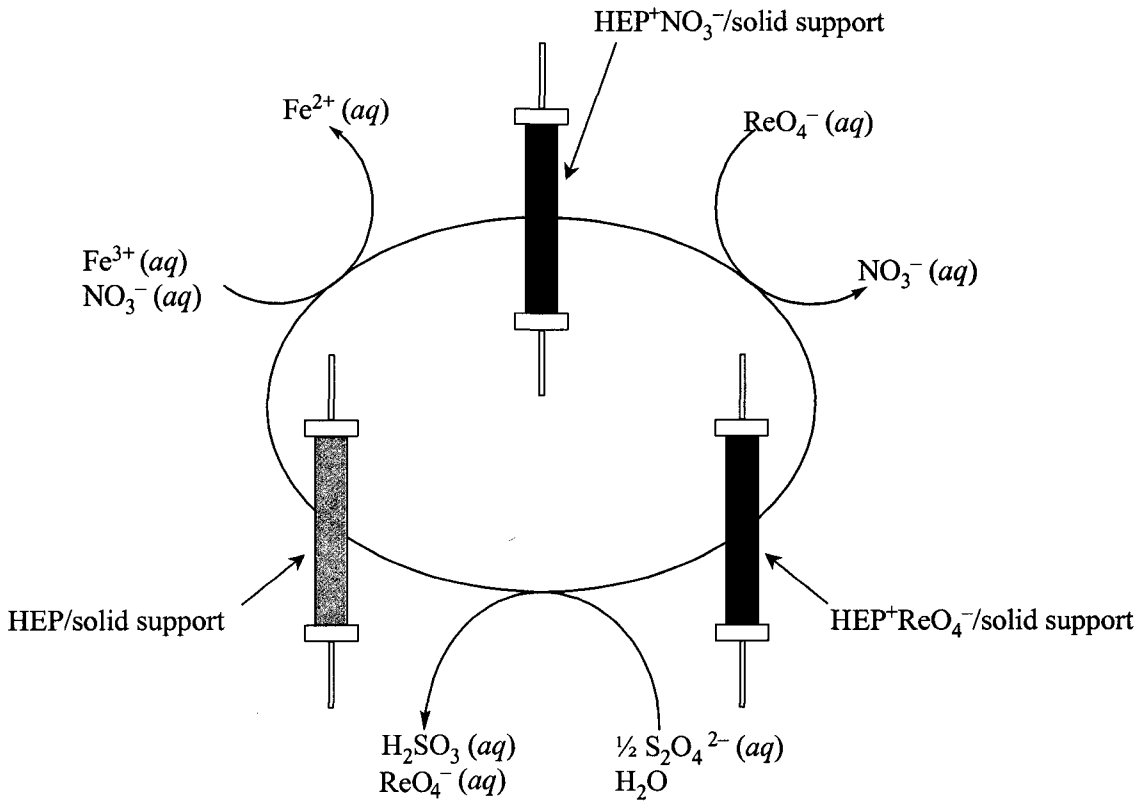

Figure 3.1. The R^2ER cycle for the extraction and recovery of the perrhenate anion (ReO_4^-) using $HEP^+NO_3^-$ on a solid support in an ion-exchange chromatography process. Aqueous sodium dithionite ($Na_2S_2O_4$) was used as the reduction (deactivation) and recovery reagent, while acidic aqueous ferric nitrate, $Fe(NO_3)_3$, was used as the reoxidation (reactivation) reagent. The colors of the deactivated (orange) and reactivated (green) complexes are shown. This figure is reprinted with permission from Dr. Matthew Odom.[47]

Selectivity of R^2ER extractants. The compound $HEP^+NO_3^-$ is only one of a number of selective, ferrocene-based, water-insoluble, organometallic ion-exchange compounds that have been synthesized by the Strauss group.[46] The compound most relevant to the work described in this dissertation is 1,1′,3,3′-tetrakis(2-methyl-2-nonyl)ferrocenium nitrate ($DEC^+NO_3^-$), shown below. The large size of the DEC^+

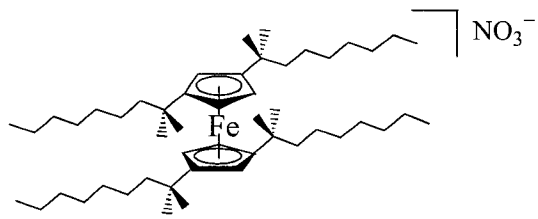

$DEC^+NO_3^-$

cation takes advantage of one of the two dominant factors that control anion-exchange selectivity, the solvation environment and size bias. These two factors have been discussed in an important review by Moyer and Bonnesen.[54]

A simple model generalizing the liquid-liquid anion-exchange process is shown in Figure 3.2. The cationic extractant, R^+, is ion paired with NO_3^- and is dissolved in the organic solvent. When the aqueous solution containing ClO_4^- is contacted with the organic phase, ClO_4^- partitions into the organic phase and NO_3^- partitions into the aqueous phase. This equilibrium is shown below in Equation 3.2. The net driving force

$$ClO_4^-\,(aq) + R^+NO_3^-\,(org) \rightleftharpoons NO_3^-\,(aq) + R^+ClO_4^-\,(org) \qquad (3.2)$$

for this anion-exchange is the difference in standard Gibbs free energies of transfer ($\Delta\Delta G°_{tr}$) for the two anions. This difference refers to the process of transferring an ion from water into the gas phase and resolvating it in a water-saturated solvent containing R^+. As shown in Equation 3.3, $\Delta\Delta G°_{tr}$ is the sum of three terms, the differences in hydration energies ($\Delta\Delta G°_{hyd}$) and solvation energies ($\Delta\Delta G°_{solv}$) of the two anions and

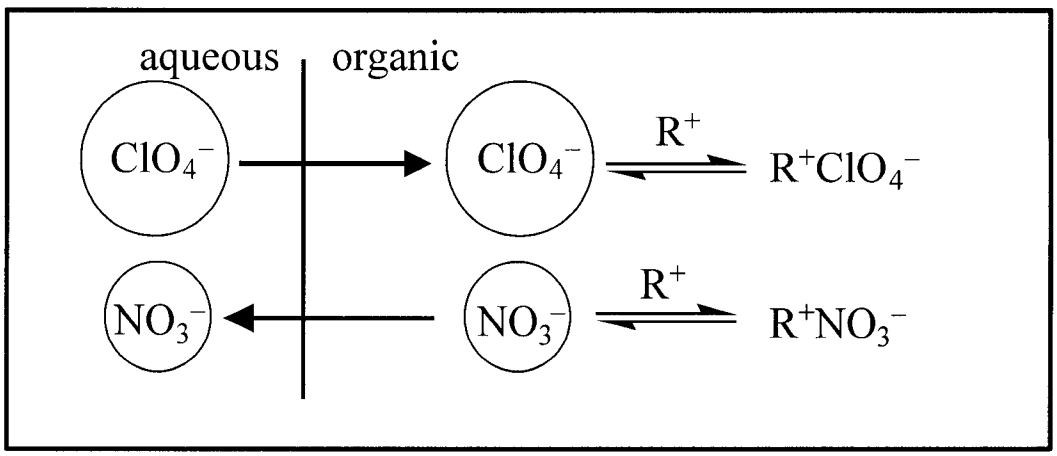

Figure 3.2. A model representing the liquid-liquid anion exchange of ClO_4^- for NO_3^-. The species R^+ represents a lipophilic cation soluble in organic solvents.

the difference in the ion-pair energies ($\Delta\Delta G°_{ion\text{-}pair}$) for the ion pairs in the non-aqueous solvent. In this model, it is assumed that ion pairing in the aqueous phase is negligible.

$$\Delta\Delta G°_{tr} \approx \Delta\Delta G°_{hyd} + \Delta\Delta G°_{solv} + \Delta\Delta G°_{ion\text{-}pair} \quad (3.3)$$

The overall $\Delta G°$ for the process in Equation 3.2 is shown by the following series of equations.

$$R^+NO_3^-\,(org) \rightleftharpoons R^+\,(org) + NO_3^-\,(org) \qquad -\Delta G°_{ion\text{-}pair(NO_3^-)} \quad (3.4)$$

$$NO_3^-\,(org) \rightleftharpoons NO_3^-\,(g) \qquad -\Delta G°_{solv(NO_3^-)} \quad (3.5)$$

$$NO_3^-\,(g) \rightleftharpoons NO_3^-\,(aq) \qquad \Delta G°_{hyd(NO_3^-)} \quad (3.6)$$

$$ClO_4^-\,(aq) \rightleftharpoons ClO_4^-\,(g) \qquad -\Delta G°_{hyd(ClO_4^-)} \quad (3.7)$$

$$ClO_4^-\,(g) \rightleftharpoons ClO_4^-\,(org) \qquad \Delta G°_{solv(ClO_4^-)} \quad (3.8)$$

$$R^+\,(org) + ClO_4^-\,(org) \rightleftharpoons R^+ClO_4^-\,(org) \qquad \Delta G°_{ion\text{-}pair(ClO_4^-)} \quad (3.9)$$

Since the hydration energies of ClO_4^- and NO_3^- are –259 and –314 kcal mol^{-1},[54] respectively, the overall difference in hydration energies ($\Delta\Delta G°_{hyd}$) is –55 kcal mol^{-1}, which indicates a favorable process. In order to take advantage of this favorable difference in hydration energies, $\Delta\Delta G°_{solv}$ and $\Delta\Delta G°_{ion\text{-}pair}$ must be minimized. The $\Delta\Delta G°_{solv}$ term can be minimized by using a solvent with a low dielectric constant, preferably less than 10. The $\Delta\Delta G°_{ion\text{-}pair}$ term can be minimized by using an organic solvent with a high dielectric constant or alternatively by using a large extractant cation.

The reduction of $\Delta\Delta G^{\circ}_{\text{ion-pair}}$ by using a large cation is possible since ion pairing energies are inversely proportional to the sum of the radii of the ions. Since both $\Delta\Delta G^{\circ}_{\text{solv}}$ and $\Delta\Delta G^{\circ}_{\text{ion-pair}}$ are dependent on the dielectric constant of the organic solvent, it is clear that a compromise must be reached. These factors are summarized in the modified Born equation for $\Delta\Delta G^{\circ}_{\text{tr}}$, shown in Equation 3.10, where B is a

$$\Delta\Delta G^{\circ}_{\text{tr}}(\text{kJ/mol}) = B\left\{\frac{1}{\varepsilon_S}\left[\left(\frac{1}{r_X}-\frac{1}{r_Y}\right)+2\left(\frac{1}{r_Y+r_R}-\frac{1}{r_X+r_R}\right)\right]+\frac{1}{\varepsilon_W}\left(\frac{1}{r_Y}-\frac{1}{r_X}\right)\right\} \qquad (3.10)$$

temperature independent constant equal to –69.47 kJ nm mol^{-1}, r_Y and r_X are the radii of the respective anions, r_R is the radius of the cation, ϵ_W is the dielectric constant of water, and ϵ_S is the dielectric constant of the solvent. There is an inverse relationship between $\Delta\Delta G^{\circ}_{\text{tr}}$ and the radii of the anions, as may be expected from the dependence of $\Delta\Delta G^{\circ}_{\text{hyd}}$ on anion size. From Equation 3.10 it can be seen that as r_R approaches infinity, the term containing r_R approaches zero. Thus, a very large cation results in $\Delta\Delta G^{\circ}_{\text{tr}}$ being dependent only on the dielectric constant of the organic solvent and the anion radii ($\Delta\Delta G^{\circ}_{\text{hyd}}$). In this case, an organic solvent with a lower dielectric solvent can be used without compromising selectivity. From this discussion, the advantage of the larger size of DEC^+ relative to HEP^+ or smaller ferrocenium cations (e.g., 1,1′,3,3′-tetra-*t*-butyl ferrocenium) is evident. The NO_3^- and Cl^- salts of the cationic extractant DEC^+ were successfully used as part of an ATR-FTIR detection method for the target anions mentioned above.

ATR-FTIR general instrumentation. In the past, Fourier transform infrared spectroscopy has not been viewed as a useful method for the detection of trace amounts of analytes in water matrixes.[55] This is due to the intense OH stretching and bending bands that extend over large regions of the IR spectrum. With the development of

attenuated total internal reflectance (ATR) FTIR spectroscopy, this problem has been mitigated to some extent. ATR-FTIR is a versatile technique that allows for the analysis of solid and liquid, organic and aqueous, IR active compounds.

When using ATR-FTIR, the material to be analyzed is in contact with a crystal with a high refractive index through which the beam of infrared radiation is transmitted. In general, as the IR beam passes from the more dense crystal to the less dense sample with which it is in contact, it is partially reflected and partially refracted. This surface interaction can be described using Snell's law, where θ_1 is the angle between the incident

$$\frac{\sin\theta_1}{\sin\theta_2} = \frac{n_2}{n_1} \tag{3.11}$$

radiation and the normal to the interface, θ_2 is the angle of the refracted beam relative to the normal, and n_1 and n_2 are the refractive indexes of the dense material (the ATR crystal) and the sample, respectively.[56] This relationship is shown in Figure 3.3. As the angle of the incident beam is increased (away from the normal), less light is refracted and more light is reflected within the crystal until a critical angle is reached. At or beyond the critical angle, θ_c, all of the light is internally reflected, a condition known as total internal reflection. The refractive indexes of the materials at the interface are related to θ_c by Equation 3.12.[57]

$$\sin\theta_c = \frac{n_2}{n_1} \tag{3.12}$$

For the trapezoidal ATR crystal shown in Figure 3.4, the IR beam enters the crystal at one of the beveled edges, is totally reflected inside the crystal (in this case five times) by the two parallel crystal faces, and exits the crystal at the other beveled edge. The sensing of the sample occurs at the crystal/sample interface when the incident and reflected radiation interact to form a standing wave. This wave, which is generally

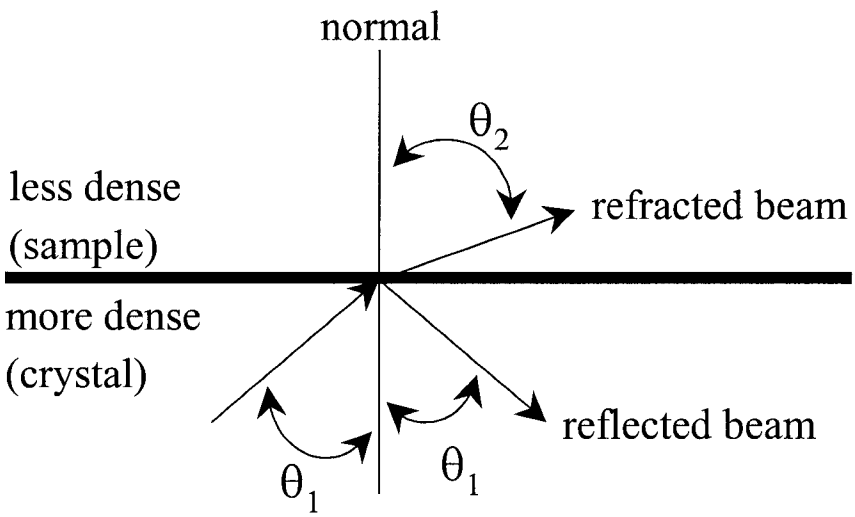

Figure 3.3. Radiation passes at some angle θ_1 from a more dense medium to a less dense medium. Some portion of this radiation is reflected at an angle equal to the incident angle, θ_1, and some is refracted at a larger angle, θ_2, found using Snell's law.

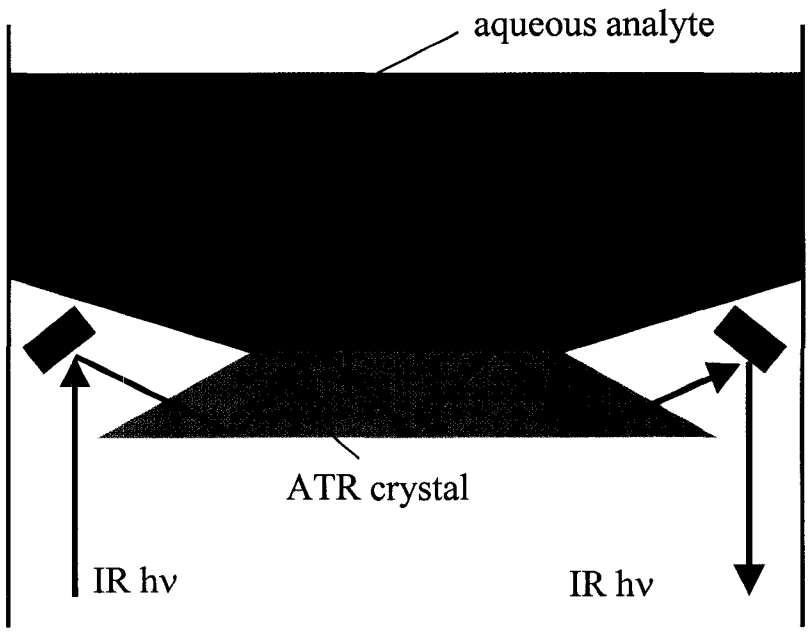

Figure 3.4. Interaction of a totally internally reflected IR beam within an ATR crystal and the IR-active aqueous analyte that will attenuate the beam.

referred to as the evanescent wave, penetrates into the less dense medium and exponentially decays in intensity according to Equation 3.13 and as seen in Figure 3.5 (I is the intensity of the evanescent wave at a distance z from the surface, I_0 is the initial

$$I = I_0 e^{-z/d_p} \tag{3.13}$$

intensity, and d_p is the penetration depth of the evanescent wave, defined below).[57] From Equation 3.13, it can be calculated that the evanescent wave intensity when z is equal to d_p is 37% of the original intensity at the interface. The theory behind this phenomenon, which occurs with infrared, ultraviolet, and visible radiation, involves complex solutions to Maxwell's equations.[57] The distance d_p that the evanescent wave penetrates into the less dense medium, which is important for sensing, can be calculated using Equation 3.14, where ν is the wavenumber of the radiation, θ is the angle of incidence of the light

$$d_p = \frac{1}{2\pi\nu\sqrt{n_1^2 \sin\theta - n_2^2}} \tag{3.14}$$

beam at the interface, and n_1 and n_2 are the refractive indexes of the ATR crystal and the sample, respectively.[58]

The evanescent wave penetrates into the rarer medium beyond the two parallel ATR crystal faces. This radiation can be absorbed by any IR active molecules, which causes an attenuation of the beam's intensity. There is an evanescent wave generated at each point of reflection with the potential for energy to be absorbed. Therefore, the greater the number of reflections in the crystal, the more IR radiation is adsorbed by the sample and the lower the detection limit for a given analyte. A large number of internal reflections is especially important for dilute liquid samples. Although ATR crystals that allow only a single reflection are commonly used with many ATR-FTIR spectrometer, the ATR crystals used in this chapter have 18 or 30 reflections. It is also important that

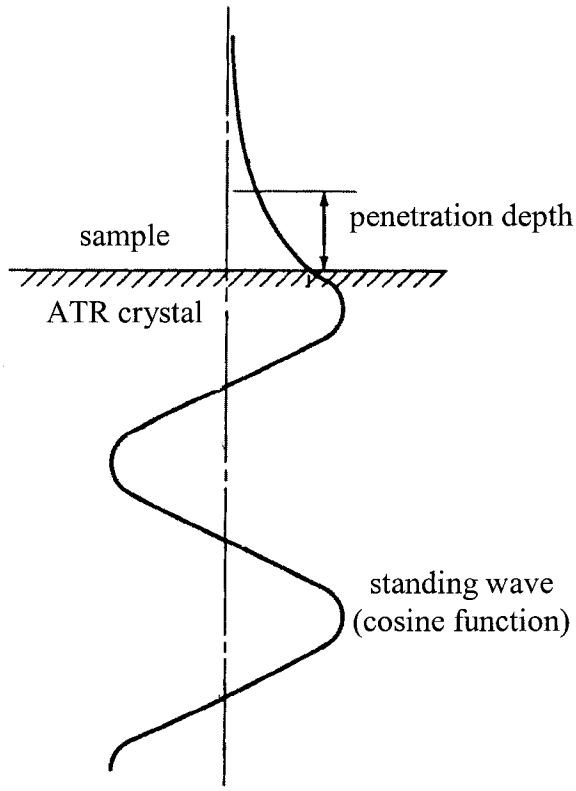

Figure 3.5. An evanescent wave within the ATR crystal that decays exponentially in the less dense sample medium.

the IR beam passes through a non-IR active gas or vacuum on its way to and from the detector to avoid unintentional attenuation of the beam. In our system, this is minimized by purging the chamber with dry nitrogen gas.

Using our ATR-FTIR spectrometer with either silicon or diamond ATR crystals, an evanescent wave is generated at the surface of the ATR crystal that extends from 0.15 to 1.75 μm (depending on wavenumber and the index of refraction of the material) beyond the surface. Several other ATR crystal materials have been commonly used for ATR-FTIR, including zinc selenide (ZnSe), and Ge. An ATR crystal material is generally chosen for its physical properties, refractive index, and the wavenumber region over which there is good transmission. Regardless of ATR crystal material, the evanescent wave only extends a short distance beyond the surface of the crystal, which reduces the amount of IR radiation absorbed by water compared to transmission IR and therefore generally allows for the detection of aqueous analytes at millimolar concentrations.

Coated ATR crystals. The sensitivity of the ATR-FTIR spectrometer can be enhanced by concentrating the analyte in the region probed by the evanescent wave. In this work, this was accomplished by coating the ATR crystal with a thin layer of the water-insoluble, organometallic extractant DEC^+X^-, where X^- is NO_3^- or Cl^-. Using this ion-exchange extractant, monoanionic analytes were concentrated in the coating on the ATR crystal surface as shown in Figure 3.6. Using the $DEC^+NO_3^-$-coated ATR crystal resulted in limits of detection (LODs) in the low micromolar range, which have been reported in a paper recently published in *Analytical Chemistry* which can be found in Appendix F.[59]

The spectra in Figure 3.7 show the progress of the ion-exchange reaction of aqueous ClO_4^- with a thin-film coating of $DEC^+NO_3^-$ on an ATR crystal as described in Equation 3.15. Notice that the ν(NO) band decreases and the ν(ClO) band increases as

$$DEC^+NO_3^-(s) + ClO_4^-(aq) \rightleftharpoons DEC^+ClO_4^-(s) + NO_3^-(aq) \qquad (3.15)$$

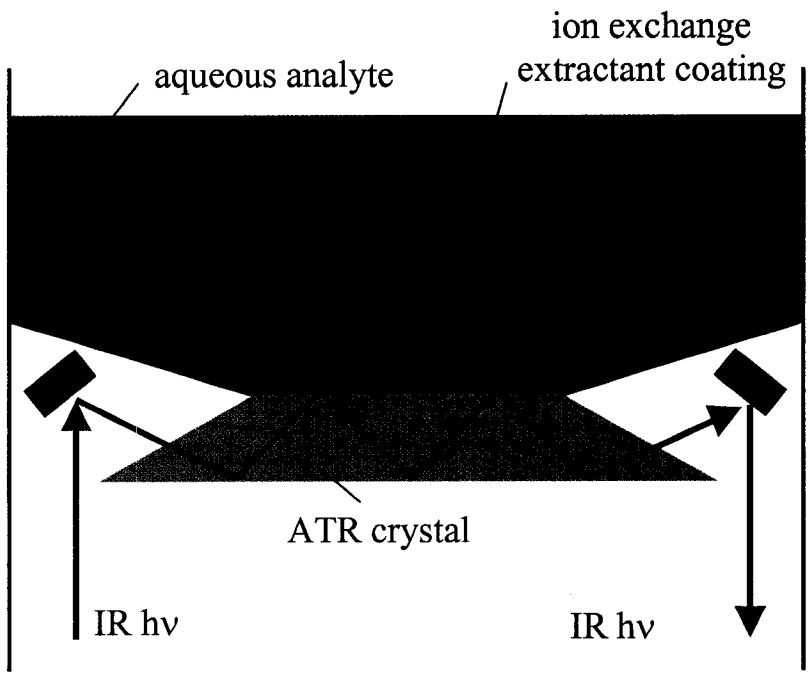

Figure 3.6. Diagram of a thin-film coating of the extractant $DEC^{+}NO_3^{-}$ on an ATR crystal that concentrates the aqueous analyte in the region sensed by the evanescent wave, thus enhancing the sensitivity of the ATR-FTIR for IR-active aqueous analytes.

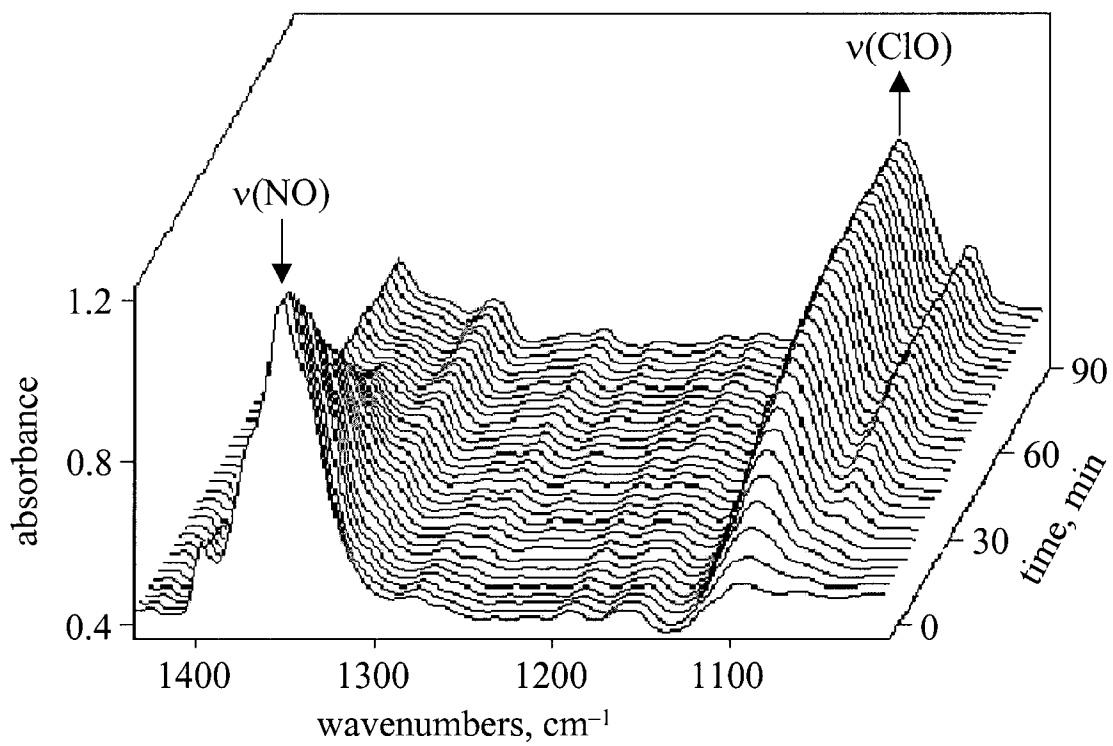

Figure 3.7. ATR-FTIR detection of 5 μM ClO_4^- (100 mL water) using the silicon ATR probe which was coated by evaporation of 20 μL of a 1 mM dichloromethane solution of $DEC^+NO_3^-$. Spectra (64 co-added scans; 30 s collection time) were recorded every minute for 90 minutes. The decrease of the ν(NO) band at ca. 1350 cm^{-1} (due to the original $DEC^+NO_3^-$ coating) to the baseline is concurrent with the increase of the ν(ClO) band at ca. 1096 cm^{-1} (due to the presence of $DEC^+ClO_4^-$ in the coating).

the NO_3^- in the coating is replaced with ClO_4^-. Similar spectra were recorded for aqueous solutions of all of the anions studied in this chapter.

The ion exchange is driven by the difference in hydration energies of the NO_3^- and ClO_4^- anions, which is larger than the difference in lattice energies of the ATR coatings $DEC^+NO_3^-$ and $DEC^+ClO_4^-$ because the DEC^+ cation is very large.[54] Ion-exchange reactions involving similar anions have been shown to be selective for the most weakly hydrated anion present in solution.[48,51] Therefore, given a mixture of anions present in solution, only the most weakly hydrated anion should generally be detected by the extractant-coated ATR probe *at equilibrium*. Note that this ion exchange is selective only for monoanions; multiply-charged anions such as SO_4^{2-} and PO_4^{3-} were not extracted using DEC^+Cl^- or $DEC^+NO_3^-$ because they have much larger hydration energies.

Some of the work described in this chapter has been previously reported by the Strauss Research Group in several manuscripts which can be found in Appendix F.[15,59,60] Also outlined in this chapter are general procedures for typical detection experiments. The generation of linear calibration curves for three different anions is reported. Several control experiments were done to examine the reproducibility, pH dependence, and temperature dependence of the method. Additionally, perchlorate was analyzed in the presence of several complex matrixes including high-nitrate, hydroponic fertilizers.

Experimental Section

Reagents. Lithium perchlorate (95%) and ammonium perchlorate (99.5%) were used as received from GFS Chemical (Columbus, OH). Sodium perchlorate (98%), sodium chlorate (99%), sodium nitrate (99.2%), potassium nitrate (99.2%), and dichloromethane (99.9%) were used as received from Fisher (Fairlawn, NJ). Pinacolylmethylphosphonic acid ($PMPA^-$, 97%) and lithium trifluoromethanesulfonate

(96%) were used as received from Aldrich (Milwaukee, WI). Potassium perchlorate (99%) was used as received from J. T. Baker Chemical (Phillipsburg, NJ).

The polyalkylated ferricenium salts 1,1′,3,3′-tetrakis(2-methyl-2-nonyl)ferricenium nitrate ($DEC^+NO_3^-$), DEC^+Cl^-, $DEC^+ClO_4^-$ and $DEC^+CB_{11}H_{12}^-$ were synthesized in our lab by literature methods.[51,61] The carborane cage salt $CsCB_{11}H_{12}$ was synthesized in our lab according to a literature method.[62] Potassium perfluoro-*n*-octanesulfonate (K(PFOS)) and potassium perfluoro-*n*-butanesulfonate (K(PFBS)) were synthesized from their respective sulfonyl fluorides with potassium hydroxide as described in the Experimental Section of Chapter 2.

Sample procurement and preparation of fertilizers. Seven hydroponic fertilizers (#1–5 solid, #6–7 liquid) were purchased at a retail store in Athens, GA, during March and May of 2000 by our EPA collaborators. A sample of the solid fertilizer Bulldog Soda (SQM North America Corporation) was also obtained commercially in January 2000. Bulldog Soda is a single-component fertilizer product consisting of sodium nitrate derived solely from Chilean caliche. The samples were mixed and divided as described by Collette et al.[15] One part was received for analysis by ATR-FTIR spectroscopy, a second part was retained in Athens, GA, for analysis by Raman spectroscopy, and a third part sent to Cincinnati, OH, for analysis by ion chromatography (IC) and complexation electrospray ionization mass spectrometry (cESIMS).[15] Extracts of these solid fertilizers were then prepared under somewhat different conditions at each laboratory as described by Collette et al., reflecting different instrument requirements.[15] In particular, the solid-to-water ratio for the extracts varied considerably depending on the demands of the various techniques. For ATR-FTIR analysis, the seven hydroponic fertilizer samples were dissolved in water to make 10 g L^{-1} stock solutions except for #4 for which a 3 g L^{-1} stock solution was made. A 10 g L^{-1} stock solution was made for the Bulldog Soda fertilizer.

Instrumentation. The pH was measured using an Orion meter (Boston, MA) with a Corning® pH electrode (Corning, NY). Electronic spectra were collected using a Lambda 40 UV-vis spectrometer (Perkin Elmer, Norwalk, CT). IR spectra were recorded using the ATR-FTIR spectrometer shown in Figure 3.8 (ReactIR™-1000, Applied Systems Inc., Millersville, MD), which was equipped with either a silicon (SiComp®) or diamond (DiComp®) ATR probe (Applied Systems Inc, Millersville, MD) and a liquid-nitrogen-cooled mercury cadmium telluride (MCT) detector. The spectral window was 4000 to 650 cm^{-1} with a nominal spectral resolution of 8 cm^{-1}. The electronic gain was 1 (SiComp® probe) or 2 (DiComp® probe). Happ-Ganzel apodization was used with no post-run spectral smoothing. The SiComp® probe, shown in Figure 3.9, consisted of a 30-bounce silicon ATR crystal mated to a ZnSe optical focusing element and was housed in a 5.2 cm long × 2.5 cm diameter cylindrical stainless-steel conduit. The DiComp® probe, also shown in Figure 3.9, consisted of a 18-bounce diamond ATR crystal mated to a ZnSe optical focusing element and housed in a 1.3 cm thick × 7.6 cm diameter stainless-steel DuraDisk™ (Applied Systems Inc., Millersville, MD). The wetted surface of both the silicon and diamond ATR crystals was a circular area 0.9 cm in diameter.

Procedure. All aqueous stock solutions were prepared in Class A volumetric glassware using distilled deionized (DI) water (Barnstead NANOpure, Dubuque, IA) that had an initial resistivity of 18 MΩ cm. All experiments were performed at 24 ± 1 °C (room temperature) unless otherwise noted. Aqueous stock solutions were made from the K^+, Li^+, NH_4^+, or Na^+ salts of each anion except for $PMPA^-$ where H(PMPA) was used. Since the pK_a of H(PMPA) is 2.4,[63,64] the concentration ratio $[PMPA^-]/[H(PMPA)]$ is ca. 400 when $[PMPA^-] + [H(PMPA)] = 10$ μM.

The general steps for ATR-FTIR analysis of an aqueous analyte are listed below for both the coated and uncoated ATR probes.

1. Cooling and purging the instrument. The optical compartment and conduits leading to the ATR probes were purged with gaseous N_2 for at least 15 minutes prior to

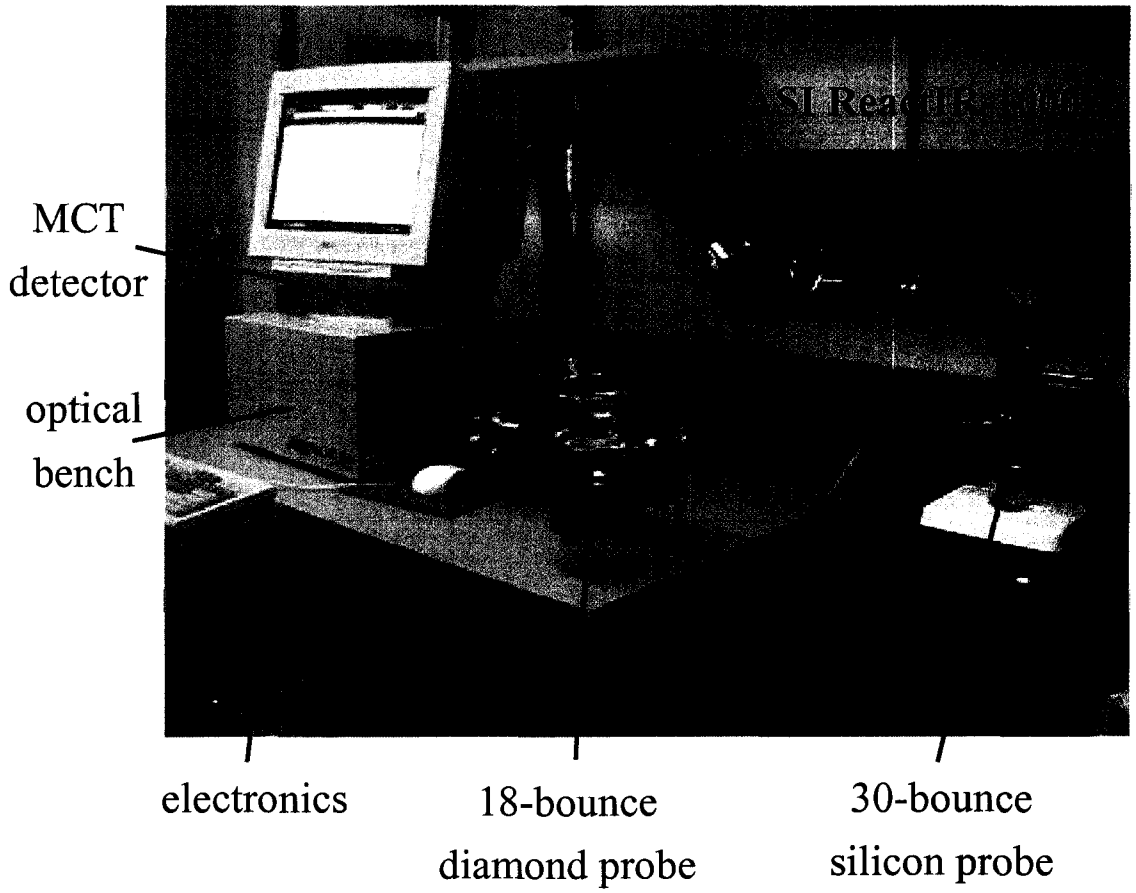

Figure 3.8. Photograph of the ASI ReactIR 1000 ATR-FTIR spectrometer used in this research.

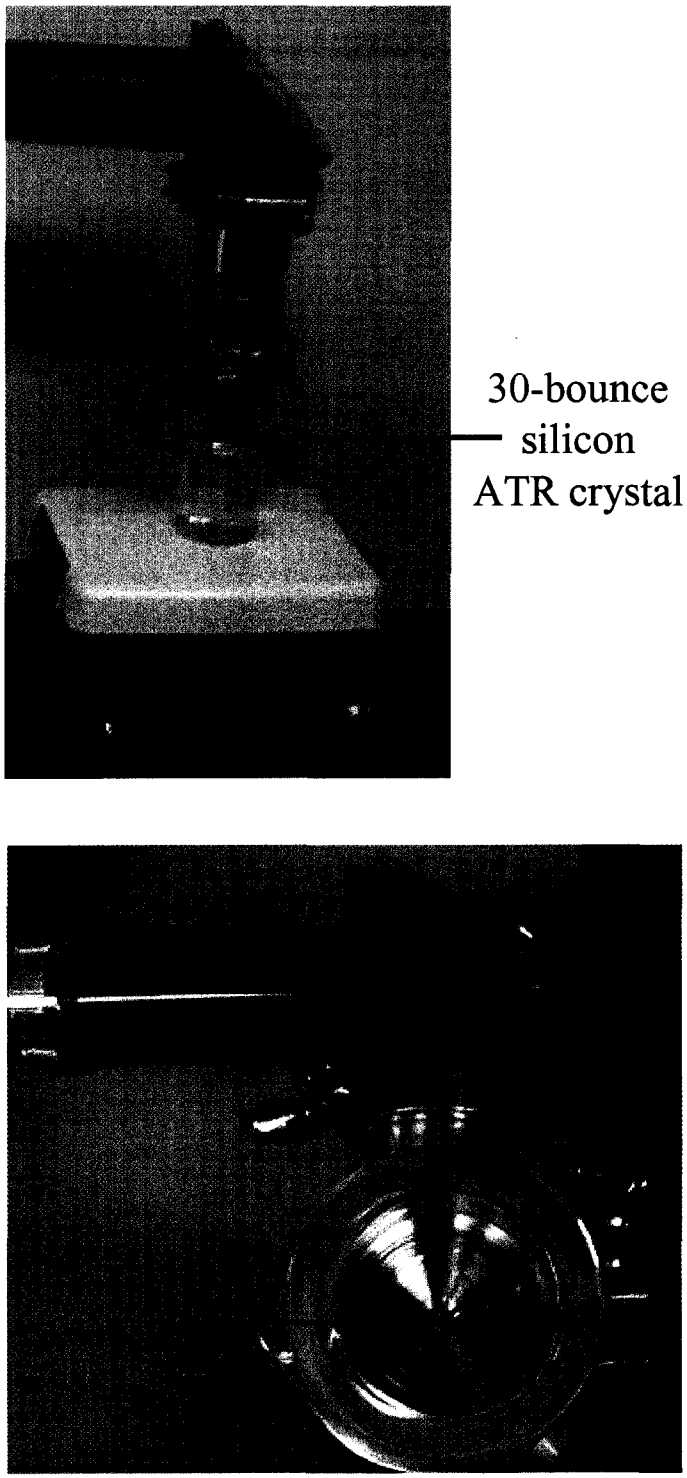

Figure 3.9. Photographs of the SiComp® and DiComp® ATR probes. The top picture shows a side view of the SiComp® ATR probe and the bottom diagram shows a top-down view of the DiComp® probe.

use and were purged continually during instrument use. The flow rate was set at ca. 3 mL min^{-1}. The MCT detector was cooled with liquid N_2. During periods of extended use, liquid N_2 has to be added to the detector Dewar every eight hours.

2. Cleaning the probe. The surface of the sensing element (silicon or diamond), as well as the metal support unit, was washed with water prior to each use. This was done by placing 1 mL of DI water on the upright portion of the probe and gently wiping it dry with a paper towel or cotton tipped applicator. After two water washes, the probe was cleaned using dichloromethane or acetone following the same procedure. Any particulate matter from the paper towels was removed with a minimal amount of pressurized air.

3a. Uncoated probe procedure. When using the silicon probe, it was placed in the inverted position, and immersed in a beaker of 100 mL DI water. Because of the recessed area where the silicon crystal is located, an air pocket was formed covering the surface of the crystal. The air bubble was removed by stirring the solution at a fast rate to create a vortex that pulled the bubble away from the crystal and removed it from the probe. As soon as the bubble was removed the stirring speed was returned to 200 rpm. When using the diamond probe, it was kept in the upright position and the molded beaker, which was clamped to the DuraDisk™, was then filled with 100 mL of DI water. For both probes, a bubble level was used to ensure a reproducible, rigorously horizontal surface of the ATR crystal. Each solution was stirred either with a magnetic stir bar and stir plate (silicon probe at ca. 200 rpm) or an overhead mechanical stirrer (diamond probe at ca. 60 rpm) and a background spectrum was collected. Some spectra were collected with 64 co-added scans, 8 cm^{-1} resolution, and a collection window ranging from 650–4000 cm^{-1} (ca. 30 s). Other experiments were performed by scanning continually for 10 minutes. These spectra consisted of 1,660 co-added scans (8 cm^{-1} resolution) and also had a collection window range of 650–4000 cm^{-1}.

After the background spectrum was collected, an aliquot (0.01–10 mL) of a concentrated stock solution was added to the DI water with stirring after the same volume

of water had been removed. Control experiments with colored dye showed that dispersion of the added aliquot occurred within 10 s for both probes. A sample spectrum was then collected and analyzed for any recognizable peaks.

3b. Coated probe procedure. First, the probe was placed in a position for analyzing 100 mL of water (the silicon probe was inverted, the diamond probe was upright) using the bubble level as above. A background spectrum (64 co-added scans, 8 cm^{-1} resolution, 650–4000 cm^{-1}) was then taken with only air in contact with the surface of the probe.

Next, the probe was positioned in an upright position using the bubble level. The exposed surface of the ATR crystal was treated with 20 ± 3 μL of a fresh (<1 week old) dichloromethane solution of DEC^+X^-. Since all DEC^+X^- extractant solutions were made using dichloromethane, the disposable plastic tip of a pipettor was conditioned by drawing up and releasing 20 μL of the extractant solution five times prior to depositing 20 μL of the solution on the crystal surface. This volume was chosen since most of the solution stays on the crystal surface instead of on the metal surrounding the crystal. Evaporation of the dichloromethane occurred within 30 s and left a dry thin-film coating on the surface of the ATR crystal. The probe was then returned to the level position at which the air background had been recorded, and a spectrum of the thin-film coating was collected. The coated ATR probe was used for a single analysis, after which the thin-film coating was removed by washing with acetone or dichloromethane. The bare ATR crystal was re-coated with a thin film of extractant for each subsequent analysis.

The absolute and relative absorbance of the observed IR bands from the initial spectrum of each coating was compared to previous coatings. For 46 coatings prepared from 20 μL of a 3 mM dichloromethane solution of $DEC^+NO_3^-$ on the silicon crystal, the absolute absorbances of the 2926 cm^{-1} ν(CH) band and the 1332 cm^{-1} ν(NO) band varied by only ±5% and ±6%, respectively. A table of these absorbance values, the ratio

of these two bands, and the average ratios with their associated standard deviations can be found in Appendix A.

ATR crystals were coated with $DEC^+NO_3^-$ for the analysis of all of the anions studied except $PMPA^-$. Apparently, $PMPA^-$ is more strongly hydrated than NO_3^- since it could not be extracted using $DEC^+NO_3^-$. Coating the diamond ATR crystal with DEC^+Cl^- enabled the extraction of $PMPA^-$ from aqueous solution as a result of the use of the more strongly hydrated anion, Cl^-, relative to NO_3^-.

Next, the coated ATR probe was immersed in 100 mL of DI water which was stirred (ca. 200 rpm for the silicon probe using a 3 cm magnetic stir bar, and ca. 75 rpm for the diamond probe using a top-stirrer). When using the inverted silicon probe, the air bubble formed by the recessed area around the crystal was removed by fast stirring as described above. The coating was allowed to equilibrate with water for 10 minutes, at which time a background spectrum was collected, while the coated probe was still immersed in the solution with constant stirring.

Immediately following the collection of the background spectrum, a sequence of spectra were collected every minute for an appropriate amount of time (usually 10–60 minutes). Between the collection of the first and second spectra (i.e., between 0 and 1 minute), an appropriate amount of an analyte stock solution (usually 0.01–10 mL) was added to the water with stirring to achieve the desired final analyte concentration. Note that prior to addition of the stock solution, that same volume of water was removed so that the total volume of the solution remained 100 mL. The solution was stirred continuously during the entire experiment.

Results and Discussion

The goal of this project was to demonstrate, despite popular belief to the contrary, that IR spectroscopy is a suitable analytical method for the detection and quantification of aqueous anionic pollutants such as perchlorate and perfluoro-*n*-octanesulfonate at sub-

micromolar concentrations. The justification for the prejudice against analytical IR spectroscopy for trace analysis can be seen by examining the LODs listed in Table 3.1, which are all in the low millimolar concentration range when using the uncoated ATR probes. In a preliminary communication, 60-minute LODs for ClO_4^- and $PFOS^-$ using the silicon probe with and without a thin-film coating of $DEC^+NO_3^-$ were reported by the Strauss Research Group.[60] In that paper, we also noted that the time necessary to reach a particular signal-to-noise ratio (*SNR*) decreased as the analyte concentration increased when using a coated ATR crystal. This suggested that analyte quantification might be possible by monitoring the initial rate of absorbance increase for a particular analyte IR band, which itself is a function of the rate of anion exchange between the coating and the aqueous sample.

Another goal was to develop a relatively simple IR methodology, one that could potentially be used by technicians in water-quality laboratories (and possibly in the field), not only by skilled spectroscopists or materials scientists. This led to the reliance on replaceable thin-film coatings that were molecular anion-exchangers, designed to be insoluble in water but soluble in organic solvents to make the coating and subsequent cleaning of the ATR crystal as simple as possible. Thus, any laboratory with an ATR-FTIR spectrometer would be able to use the methodology. ATR probes with permanent, reusable anion-exchange coatings might improve reproducibility but would involve more sophisticated polymer-casting or sol-gel techniques for their preparation and could be subject to fouling over time. Although the focus of this work is on non-permanent coatings, some initial experiments have been done exploring the possibility of recycling the ferrocene-based ion-exchange coating through a redox cycle which would allow a single coating to be used multiple times. This preliminary study will be discussed later.

10-Minute limits of detection (LODs). An objective of this study was to show how the sensitivity of a commercially-available ATR-FTIR spectrometer can be dramatically improved simply by applying a thin-film coating of an ion-exchange

Table 3.1. Ten-minute limits of detection (LODs) for aqueous anions determined by ATR-FTIR[a]

anion	uncoated probe[b]			ATR crystal	extractant coated probe[c]			LOD ratio[d]
	ν, cm^{-1}	LOD, mM	*SNR*(σ)		ν, cm^{-1}	LOD, μM	*SNR*(σ)	
ClO_4^-	1108	0.7	4(1)	Di[e]	1096	0.03	2.8(6)	23,000
ClO_4^-	1108	0.8	4.0(6)	Si[e]	1096	0.04	3.5(8)	20,000
ClO_3^-	973	1.0	4(1)	Di[e]	973	0.2	3.2(7)	5,000
ClO_3^-	992	2.0	3.0(7)	Si[e]	988	0.7	3.4(6)	2,860
$CF_3SO_3^-$	1258	0.3	3.7(7)	Si[f]	1266	0.05	2.9(5)	6,000
$PFBS^-$	1254	0.5	3.5(7)	Si[f]	1270	0.07	3.5(8)	7,140
$PFOS^-$	1243	0.01	4(1)	Si[f]	1270	0.06	3(1)	170
$PMPA^-$	1042	0.3	4(1)	Di[g]	1046	0.7	4(1)	430

[a] Abbreviations: *SNR*, signal-to-noise ratio; ν, IR spectral band monitored; $PFBS^-$, perfluoro-*n*-butanesulfonate; $PFOS^-$, perfluoro-*n*-octanesulfonate; $PMPA^-$, pinacolylmethylphosphonate. [b] Uncoated-probe LODs were determined from sample and background spectra (1,660 co-added scans each) collected over 10-minute intervals. [c] Extractant-coated-probe LODs were determined from sample and background spectra (64 co-added scans each). The sample spectrum was collected after a 10-minute period during which analyte/NO_3^- or analyte/Cl^- anion exchange took place. [d] Ratio of the uncoated probe LOD to the coated probe LOD. [e] The silicon (Si) or diamond (Di) ATR crystal was coated by evaporation of 20 μL of a 3 mM dichloromethane solution of $DEC^+NO_3^-$. [f] The ATR crystal was coated by evaporation of 20 μL of a 1 mM dichloromethane solution of $DEC^+NO_3^-$. [g] The ATR crystal was coated by evaporation of 20 μL of a 5 mM dichloromethane solution of DEC^+Cl^-.

material to the surface of the ATR crystal. It was not an objective to design a method that would give LODs lower than all other analytical methods. It should be acknowledged that more elaborate and time-consuming methods such as solid phase extraction coupled with LC-MS can achieve the orders-of-magnitude lower LOD of 0.0002 nM for aqueous $PFOS^-$ compared to the 60 nM 10-minute LOD determined using the $DEC^+NO_3^-$-coated silicon ATR-FTIR probe.[65] However, our 0.05 μM LOD for $CF_3SO_3^-$ using the $DEC^+NO_3^-$-coated silicon probe is lower than the lowest reported literature LOD of 150 μM using an ion selective electrode.[66]

The definition of an LOD is the analyte concentration for which $SNR \geq 3 \pm 1$ as described in detail in Chapter 1. For any Fourier-transform method, the *SNR* is dependent on the collection time. In principle, the *SNR* is proportional to the square root of the number of scans that are averaged. Therefore, an LOD determined by FTIR is not a fixed quantity because it is time dependent. ATR-FTIR LODs in this work are defined as $SNR \geq 3 \pm 1$ for a *10-minute* analysis. The choice of 10 minutes was arbitrary. In the case of ClO_4^-, 30-second and 30-minute LODs were also determined for comparison.

For a given analyte, the most meaningful comparison of the LOD for a coated silicon or diamond probe with the LOD for the same probe without the extractant coating would be one that involved equal *total* analysis times, not equal numbers of scans averaged. For a coated-probe LOD, the probe was allowed to undergo ion exchange with the aqueous analyte solution for 10 minutes followed by the collection of only 64 co-added scans. For an uncoated-probe LOD, the probe was immersed in the analyte solution and 1,660 co-added scans were collected over the 10-minute interval. The 10-minute LODs using both the coated an uncoated probes are listed in Table 3.1.

To determine the 10-minute LOD for ClO_4^- using the silicon probe, the series of concentrations listed in Table 3.2 were examined. For 0.8 mM ClO_4^-, the *SNR* was 4.0 ± 0.6 (average of 3 trials). For 0.7 mM ClO_4^-, the average *SNR* was 2.9 ± 0.7 (3 trials). Therefore, the 10-minute LOD for ClO_4^- using the uncoated silicon probe was

Table 3.2. Calculation of the 10-minute LOD for ClO_4^- using the uncoated silicon probe[a]

concentration, mM	ν ClO signal[b]	average signal (σ)[c]	average *SNR* ± error[d]
1	0.000833	0.0010(1)	7 ± 1
1	0.00111		
1	0.0011		
1	0.00114		
0.8[e]	**0.000652**	**0.00060(5)**	**4.0 ± 0.6**
0.8	**0.000529**		
0.8	**0.000631**		
0.7	0.000502	0.00044(8)	2.9 ± 0.7
0.7	0.000489		
0.7	0.000317		

[a] Each 10-minute spectrum was the result of 1,660 co-added scans. [b] Absorbance at 1108 cm^{-1}. [c] σ = standard deviation. [d] Signal-to-noise ratio (*SNR*) where the average noise = $1.5(2) \times 10^{-4}$ and the error was propagated from the signal and noise standard deviations. [e] The bold values are the LOD as listed in Table 3.1.

determined to be 0.8 mM (shown in bold in Table 3.2), and this is the value listed in Table 3.1. Similar tables for the determination of the 10-minute LODs using the uncoated ATR probes for ClO_4^-, ClO_3^-, $PFOS^-$, $PFBS^-$, $CF_3SO_3^-$, and $PMPA^-$ are given in Appendix B.

The same process was followed to determine the 10-minute coated-probe LODs as shown by the examination of progressively lower concentrations of $PMPA^-$ in Table 3.3. The LOD for $PMPA^-$ using the DEC^+Cl^--coated diamond probe was determined to be 0.7 μM (shown in bold in Table 3.3), and this is the value listed in Table 3.1. Similar tables for the determination of the 10-minute LODs using the coated ATR probes for ClO_4^-, ClO_3^-, $PFOS^-$, $PFBS^-$, and $CF_3SO_3^-$ are given in Appendix C.

An example of a 10-minute LOD spectrum of 0.7 μM $PMPA^-$ after 10 minutes in contact with the DEC^+Cl^--coated diamond probe is shown in Figure 3.10. The $PMPA^-$ peaks are still observable compared to the spectrum of a water blank (DI water in contact with the DEC^+Cl^--coated diamond probe). To better show the shape of the $PMPA^-$ bands, a spectrum of 1 mM $PMPA^-$ after 10 minutes in contact with the DEC^+Cl^--coated diamond probe is overlayed. There is very good agreement of the peak assignments between the higher and lower concentration spectra. For anions such as $PMPA^-$ with multiple IR bands, the *SNR* was calculated for all of the major peaks. The *SNR*s for the four major $PMPA^-$ peaks are listed in Table 3.4.

LODs decrease with coated ATR probe. The LODs of the ATR-FTIR instrument used in this study were greatly improved by coating the ATR crystals. For example, the 10-minute LOD for ClO_4^- using the $DEC^+NO_3^-$-coated silicon probe was lowered by a factor of 20,000 to 0.04 μM (the uncoated silicon-probe LOD is 0.8 mM). Using the $DEC^+NO_3^-$- or DEC^+Cl^--coated ATR probes, the LODs for all of the anions listed in Table 3.1 are in the sub-micromolar range. The increase in sensitivity of the coated ATR probes relative to the unmodified probes ranged from a factor of 170 for $PFOS^-$ to a factor of 23,000 for ClO_4^-.

Table 3.3. Calculation of the 10-minute LOD for $PMPA^-$ using the DEC^+Cl^--coated diamond probe[a]

concentration, μM	signal[b]	average signal (σ)[c]	average *SNR* ± error[d]
5	0.00392	0.00392(8)	21 ± 2
5	0.00383		
5	0.00401		
1	0.00119	0.00119(1)	6.2 ± 0.7
1	0.0012		
1	0.00118		
0.7	**0.000675**	**0.0008(2)**	**4 ± 1**
0.7	**0.001112**		
0.7	**0.000668**		
0.6	0.000259	0.00026(3)	1.4 ± 0.2
0.6	0.000224		
0.6	0.000308		

[a] Each trial was done using the diamond probe coated with 20 μL of a 5 mM dichloromethane solution of DEC^+Cl^-. [b] Absorbance at 1046 cm^{-1}. [c] σ = standard deviation. [d] Signal-to-noise ratio (*SNR*) where the average noise = $1.9(2) \times 10^{-4}$ and the error was propagated from the signal and noise standard deviations. [e] The bold values are the LOD as listed in Table 3.1.

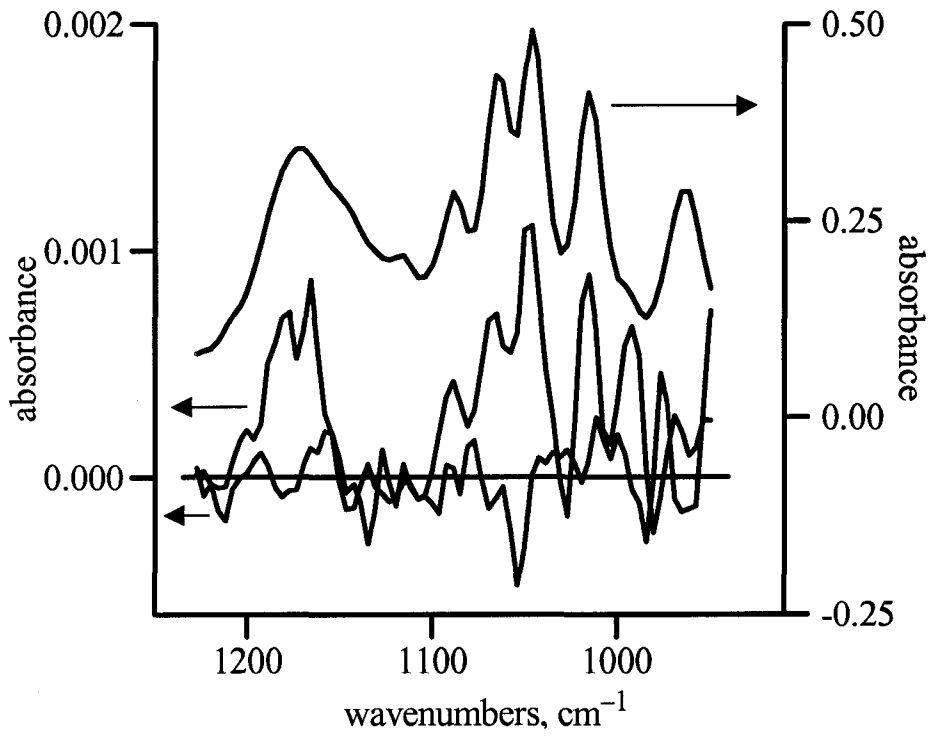

Figure 3.10. Spectra of 0.7 μM $PMPA^-$ (black) and 1 mM $PMPA^-$ (blue) after 10 minutes in contact with the DEC^+Cl^--coated diamond probe. A blank spectrum is shown in green, and the baseline ($y = 0$) in red. The absorbance scale on the left corresponds to the black and green spectra and the absorbance scale on the right corresponds to the blue spectrum.

Table 3.4. The signal-to-noise ratios (*SNR*s) for the major $PMPA^-$ peaks from the 10-minute detection of 0.7 μM $PMPA^-$ in contact with the DEC^+Cl^--coated diamond probe

ν, cm^{-1}	average *SNR* ± error[a]
1170	2.9 ± 0.5
1065	2.6 ± 0.6
1046[b]	4 ± 1
1015	3 ± 1

[a] The error was propagated from the standard deviations of the signal and noise values.

[b] The 1046 cm^{-1} peak was the peak used to determine the 10-minute LOD listed in Tables 3.1 and 3.3.

Using the unmodified ATR probes, the LODs for all of the anions listed in Table 3.1 are in the low millimolar range. Note that the 10-min LOD for $PFOS^-$ with the uncoated probe, 0.01 mM, is 30 to 50 times lower than the uncoated-probe LODs for the shorter-chain-length sulfonate anions $PFBS^-$ and $CF_3SO_3^-$. This could be due to the more intense ν(CF) bands of the longer perfluoroalkyl chain of $PFOS^-$, but this does not explain why the LODs for $PFBS^-$ and $CF_3SO_3^-$ are essentially the same.

Comparison of ATR-FTIR LODs with literature LODs. Although the goal of this study was not to determine LODs that were lower than all other known techniques, it is useful to compare our extractant-coated probe LODs for each anion to the best LOD from published methods. These results, along with some concentration limits for drinking water (target concentrations) set by the EPA (ClO_4^- and ClO_3^-)[16,22] and the U.S. military (Soman, which becomes $PMPA^-$ in aqueous solution)[36] are listed in Table 3.5. The 10-minute ATR-FTIR LODs listed are the same as those shown earlier in Table 3.1. With the exception of $CF_3SO_3^-$, all of the literature LODs are lower than the 10-minute ATR-FTIR LODs determined using the extractant-coated probes. Nevertheless, for both ClO_4^- and ClO_3^-, the 10-minute ATR-FTIR coated probe LODs are smaller than the target concentrations for those anions in drinking water. The literature methods for each anion will be briefly reviewed in the following paragraphs .

Perchlorate. The EPA has published a standard ion chromatography (IC) method for ClO_4^- that has an LOD of 5.3 nM and a linear response range of at least 0.04–4 μM.[67] This method consists of running a 1 mL sample through a guard column, then a Dionex AS16 4 mm separation column, then an anion suppressor column. Detection is with a conductivity meter.[67] IC is the most commonly used technique for ClO_4^- detection and a typical analysis takes approximately 20 minutes.[68-70] One disadvantage of IC is that high ionic strength matrixes may cause a shift in retention times. To alleviate this problem, samples must be pretreated with a second column, which can introduce impurities into the sample. Sample that contain high concentrations of Cl^-, SO_4^{2-}, or CO_3^{2-} may cause

Table 3.5. Comparison of 10-minute ATR-FTIR LODs with target concentrations and LODs reported in the literature for selected anions

anion[a]	target concentration, nM[b]	ATR-FTIR coated-probe LOD, nM	literature LOD, nM[ref]	best literature method
ClO_4^-	40	30[c]	5.3[67]	IC[f]
ClO_3^-	14,000	200[c]	20[71]	IC
$CF_3SO_3^-$	na	50[d]	150,000[66]	ISE[g]
$PFBS^-$	na	70[d]	ca. 10[72]	ESIMS[h]
$PFOS^-$	na	60[d]	0.0002[65]	LC-ESIMS
$PMPA^-$	11–34	700[e]	0.04[73]	MIP-fluorescence[i]

[a] $PFBS^-$ = perfluorobutanesulfonate; $PFOS^-$ = perfluorooctanesulfonate; $PMPA^-$ = pinacolylmethylphosphonate. [b] Target concentrations are limits set by the EPA (ClO_4^- and ClO_3^-)[16,22] or the U.S. military ($PMPA^-$)[36] for that anion in drinking water; na = not applicable, no limits have been set. [c] The diamond ATR crystal was coated by evaporation of 20 μL of a 3 mM dichloromethane solution of $DEC^+NO_3^-$. [d] The silicon ATR crystal was coated by evaporation of 20 μL of a 1 mM dichloromethane solution of $DEC^+NO_3^-$. [e] The diamond ATR crystal was coated by evaporation of 20 μL of a 5 mM dichloromethane solution of DEC^+Cl^-. [f] IC = ion chromatography. [g] ISE = ion selective electrode. [h] ESIMS = electrospray ionization mass spectrometry. [i] MIP = molecularly imprinted polymer with fluorescence detection.

the baseline to increase, and these weakly retained anions may tail into the ClO_4^- window.[67] Another disadvantage is chromatographic coelution, which occurs when other anions present in the matrix, such as iodide, have retention times similar to ClO_4^- and can result in false positive readings. Therefore, additional analytical methods are required to confirm the presence of perchlorate in complex matrixes.

Electrospray ionization mass spectrometry (ESIMS) can directly detect aqueous ClO_4^- (*m/z* 99). However, it is limited by interfering species formed in the electrospray source from ions native to groundwater that have the same molecular weight, such as $Br(H_2O)^-$ (*m/z* 99).[74,75] The basic ESIMS method yields a 50 nM LOD when using pure water.[75] Adding field asymmetric waveform ion mobility spectrometry (FAIMS) to ESIMS resulted in lowering the LOD to 1 nM.[76] A separate study showed that extraction of ClO_4^- with a cationic surfactant, followed by separation of the ion-pair to a different solvent, reduced the possibility of interferants and resulted in an LOD of 0.1 nM at the expense of adding several extra steps to the method.[74]

Several other analytical methods for the determination of perchlorate have been reported, including perchlorate ion-selective electrodes (ISE) that have LODs as low as 0.71 μM and give virtually instantaneous readings.[77] A lower LOD of 0.10 μM was reached when an ISE was coupled with capillary electrophoresis (CE) to separate out interfering ions such as nitrate.[7,77] Raman spectroscopy was used to detect perchlorate at 500 μM levels in fertilizers.[12] With suitable sample clean-up, some of these techniques have also been applied to the analysis of aqueous extracts of plants that absorb and accumulate perchlorate (e.g., salt cedar,[78] some fruits and vegetables,[12,79] and tobacco[80]).

Chlorate. The EPA has established an IC standard method for disinfection byproducts that has an LOD of 0.02 μM for chlorate.[71] A 225 μL sample is run through a guard column, Dionex AS9-HC 4 mm separation column, an eluent suppressor, and finally is detected with a conductivity meter. This method takes approximately 25 minutes if no additional pretreatment steps are needed. Three possible interferants include

(i) coelution, (ii) high ionic strength solutions that cause a shift to shorter retention times, and (iii) the possibility of neighboring peaks overlapping with the ClO_3^- peak. A linear calibration curve was made over the concentration range 0.06–6 μM for ClO_3^-.[71]

Perfluoroalkanesulfonates. Several ESIMS methods have been developed for the detection of $PFOS^-$ with LODs ranging from 0.2 pM to 0.01 μM.[65,72,81-83] All of these ESIMS techniques, with the exception of our direct-injection method described in Chapter 2, involve at least one preconcentration and one preseparation step prior to MS detection. Using our direct-injection ESIMS method, an LOD of ca. 0.01 μM $PFBS^-$ was determined.[72]

It is possible that some of these EISMS methods could also be suitable for the detection of low concentrations of other perfluoroalkanesulfonates, including $CF_3SO_3^-$ (triflate). Triflate has also been independently detected using a liquid membrane ISE with a LOD of 150 μM.[66] This technique involves taking a 2 mL aqueous sample and diluting it with 1 M sodium sulfate to 55 mL total volume. The liquid membrane electrode was made using a synthetically prepared ion-exchange compound $[Ni(bphen)_3][CF_3SO_3^-]_2$ (bphen = 4,7-diphenyl-1,10-phenanthroline) dissolved in 2-nitro-*p*-cymene and uses an Ag/AgCl reference electrode. Although this ISE has a response time of only two minutes, other ions present in the matrix, including ClO_4^- and MnO_4^-, are interferants and cause false positive readings. The liquid membrane ISE has a linear response range of 0.3–100 mM for triflate.[66]

Pinacolylmethylphosphonate. Jenkins et al. reported a europium-containing styrene composite molecularly imprinted polymer (MIP) that is selective for $PMPA^-$ with an LOD of 0.04 nM.[73] A luminescent europium complex with the chelating ligand 3,5-divinylmethylbenzoate is used as a crosslinker for inclusion of the europium center in a polymer matrix. This polymer was dip-coated onto optical fibers, which resulted in 15–20 μm thick layers of polymer per dip. The sensitivity of these coated fibers was greatly enhanced by using fibers with tapered ends which were obtained by manually pulling the

fiber ends. Contact of an optical fiber coated with the Eu/styrene MIP with an aqueous $PMPA^-$ solution causes the appearance of a new narrow luminescence band that is the result of $NO_3^-/PMPA^-$ ion exchange and concomitant coordination of $PMPA^-$ to Eu^{3+} ions in the copolymer. This method has a linear response ranging from 1.25 μM to 180 mM.[73] For a fiber coated with 60–80 μm of the Eu/styrene MIP, 80% of the maximum response was achieved in ca. eight minutes. One of the main limitations to this method is that it cannot be used with solutions with pH values less than 6, since this will remove any $PMPA^-$ from the polymer. Another limitation is the size and weight of the argon laser and power supply required to produce the luminescence of the coated fiber optic sensors. Several other methods have been reported in the open literature for the detection of $PMPA^-$ in aqueous solutions, including solid phase micro-extraction with GC/MS detection (LOD = 0.3 nM),[84] CE with UV detection (LOD = 10 nM),[85] CE with conductivity detection (LOD = 420 nM),[86] MIP solid phase extraction with CE detection (LOD = 560 nM),[87] and electrospray ion-mobility spectrometry (LODs = 6.7–7.3 μM).[88,89]

FTIR detection of aqueous analytes using coated ATR crystals. Several reviews on the detection of analytes in aqueous solution using ATR crystals coated with polymeric or sol-gel materials have been published.[90,91] Numerous studies have been reported on the detection of chlorinated hydrocarbons using ATR crystals coated with polymer films.[92-100] ATR crystals have also been coated with layers of polymeric or sol-gel materials and used to detect a variety of other neutral molecules in water including benzene, nitrobenzene, benzonitrile, pesticides, and proteins.[101-107] In addition to the use of ATR crystals, similar techniques have been developed using fiber-optic sensors.[108] As can be seen, numerous authors have studied analytical uses of ATR-FTIR spectroscopy, but there are only a handful of publications, listed in Table 3.6, that focus on coated ATR crystals for the quantification and/or detection of aqueous anions. In most cases, the ATR-FTIR spectrometer was used to examine the properties of the coating, not as an

Table 3.6. List of references for the detection of aqueous anions using coated ATR crystals

corresponding author[ref]	anion(s)	lowest reported concentration	ATR coating material(s)
Hug[109]	sulfate	1 μM	hematite
Blesa[110]	carboxylates	1 μM	TiO_2
Martin[111]	carboxylates	10 μM (LOD)	hematite
Elzinga[112]	sulfate	30 μM	goethite
Borda[113]	oxalate	50 μM	goethite
Peak[114]	borate	50 μM	hydrous ferric oxide
Hug[115]	arsenate	90 μM	ferrihydrite
Mizaikoff[116]	2,4-D[a]	210 μM (LOD)	MIPs[b]
McQuillan[117]	perchlorate, sulfate, thiosulfate	1 mM	Cr_2O_3
McQuillan[118]	carboxylates	1 mM	metal oxides
McQuillan[119]	carbonate	1 mM	ZrO_2 sol-gel
Schulthess[120]	carbonate	1 mM	goethite
Sheals[121]	*N*-phosphonomethylglycine	0.7 μmol/m^2	goethite
Kellner[122]	thiosulfate	100 mM	PVC-membrane

[a] 2,4-D = 2,4-dichlorophenoxyacetic acid. [b] MIPs, molecularly imprinted polymers.

anion sensor. As a result, all but two of the concentrations listed are the lowest concentration reported, not the LOD.

Many studies have been performed using ferric oxide of different levels of crystallinity to coat ATR crystals and then adsorb various anions from aqueous solutions. In two different studies, Hug reported the adsorption of low concentrations of sulfate by hematite (α-Fe_2O_3) that had been deposited on a ZnSe ATR crystal.[109,123] Hug also used a ferrihydrite-coated diamond ATR crystal to adsorb arsenite and arsenate from aqueous solution.[115] Martin studied the surface complexation of a range of carboxylates with hematite by ATR-FTIR.[111] Elzinga used goethite (α-FeOOH) to coat a ZnSe ATR crystal and monitored the adsorption of sulfate at the mineral-water interface.[112] Borda used Ge ATR crystals coated with thin-films of goethite to adsorb oxalate from aqueous solutions.[113] Schulthess studied aqueous carbonate anions by coating a ZnSe ATR crystal with a coating of goethite.[120] Peak used hydrous ferric oxide to coat ZnSe ATR crystals and observed the adsorption of $B(OH)_4^-$ from aqueous NaOH.[114] Sheals characterized the adsorption of *N*-phosphonomethylglycine (a component of some organophosphorus herbicides) on goethite-coated ATR crystals.[121]

Mizaikoff used a ZnSe ATR crystal coated with molecularly imprinting polymers (MIPs) to determine an LOD of 210 μM for the herbicide 2,4-dichlorophenoxyacetic acid (2,4-D).[116] Using a ZnSe ATR crystal coated with TiO_2, Blesa published IR spectra showing the detection of oxalic and salicylic acids in water at concentrations as low as 1 μM.[110] In a series of papers, McQuillan detailed ATR-FTIR studies of the adsorption of aqueous perchlorate, sulfate, thiosulfate, aliphatic carboxylates, and carbonate anions to a wide range of metal oxides (Cr_2O_3, TiO_2, ZrO_2, Al_2O_3, and Ta_2O_5) that were used to coat ZnSe ATR crystals.[117-119] Finally, in a different type of study, Kellner presented the results of monitoring the ion transport of thiosulfate through ion-selective PVC-membranes coated on Ge ATR crystals.[122]

Most literature studies that have used coated ATR crystals to detect aqueous anions examined concentrations that ranged from 1 μM to 100 mM, as seen in Table 3.6. The LOD for ClO_4^- using the $DEC^+NO_3^-$-coated diamond ATR probe, 0.03 μM, is four orders of magnitude lower than 1 mM aqueous ClO_4^- detected using Cr_2O_3-coated ZnSe ATR crystals.[117] In fairness, it should be noted that 1 mM was the concentration of ClO_4^- used for an experiment described in this reference; this concentration is not necessarily the LOD for the Cr_2O_3-coated ATR crystal. Of the studies listed in Table 3.6, only two studies have reported the detection of low micromolar concentrations of aqueous anions by ATR-FTIR using coated ATR crystals. In one study, 1 μM aqueous sulfate was detected using a ZnSe ATR crystal coated with Fe_2O_3.[109] In the other study, 1 μM aqueous carboxylate anions were detected with ZnSe ATR crystals coated with TiO_2.[110] These LODs are larger than the sub-micromolar ATR-FTIR LODs for most of the anions listed in Table 3.1.

Factors that affect the LOD. The silicon and diamond LODs for ClO_4^- and ClO_3^- listed in Table 3.1 show that the detection limit of the anion can depend on the material of the ATR crystal. This is mainly because the IR throughput of the silicon ATR crystal decreases more significantly below 1000 cm^{-1} than the throughput of the diamond crystal. Other minor factors might be the difference in evanescent wave penetration depths due to the differences in refractive indexes of diamond and silicon and the possibility of different coating morphologies on the different ATR crystals. The decreased throughput of the silicon ATR crystal results in an increase in noise below 1000 cm^{-1}, as shown over various wavenumber regions in Table 3.7. The noise is 2–6 times larger for the silicon probe when compared with the diamond probe over similar wavenumber regions. Because of this, the *SNR*s for analytes that have IR bands below 1000 cm^{-1}, such as ClO_3^-, are ca. four times smaller with the 30-bounce silicon probe than with the 18-bounce diamond probe for the same analyte concentration in spite of the greater number of internal reflections. The *SNR* of a spectrum of 10 μM $PMPA^-$ in

Table 3.7. Comparison of noise values over various wavenumber regions for silicon and diamond ATR crystals

anion	coated[a] or uncoated[b] probe	ATR crystal[c]	noise window, cm^{-1}	number of trials	average noise(σ)[d]	ratio of Si to Di noise
ClO_3^-	coated[e]	Di	1038–830	16	$6(1) \times 10^{-4}$	3
ClO_3^-	coated[e]	Si	1054–907	12	$1.8(3) \times 10^{-3}$	
ClO_3^-	uncoated	Di	1073–870	26	$1.3(2) \times 10^{-4}$	3.8
ClO_3^-	uncoated	Si	1080–864	31	$5.0(9) \times 10^{-4}$	
ClO_4^-	coated[e]	Di	1166–1023	11	$1.9(3) \times 10^{-4}$	3.2
ClO_4^-	coated[e]	Si	1166–1023	32	$6(1) \times 10^{-4}$	
ClO_4^-	uncoated	Di	1191–1011	24	$9(3) \times 10^{-5}$	1.7
ClO_4^-	uncoated	Si	1200–1002	20	$1.5(2) \times 10^{-4}$	
$PMPA^-$	coated[f]	Di	1212–926	18	$1.9(2) \times 10^{-4}$	6.3
$PMPA^-$	coated[f]	Si	1220–923	16	$1.2(2) \times 10^{-3}$	

[a] Each extractant-coated probe noise value was determined from a blank spectrum (64 co-added scans) of DI water in contact with the coated probe. [b] Each uncoated probe noise value was determined from a blank spectrum (1,660 co-added scans) of DI water collected over a 10-minute interval. [c] Silicon (Si) or diamond (Di) ATR crystal. [d] The noise is calculated as the root-mean-square noise using a blank spectrum, σ = standard deviation. [e] The ATR crystal was coated by evaporation of 20 µL of a 3 mM dichloromethane solution of $DEC^+NO_3^-$. [f] The ATR crystal was coated by evaporation of 20 µL of a 5 mM dichloromethane solution of DEC^+Cl^-.

contact with the DEC^+Cl^--coated silicon probe after 10-minutes, shown in Figure 3.11, is ca. four times smaller than that with the diamond probe. The inherently lower noise level of the diamond probe below 1000 cm^{-1} led to a significantly lower LOD for ClO_3^- relative to the silicon probe. Even ClO_4^-, with ν(ClO) centered ca. 1100 cm^{-1}, has a slightly lower LOD with the diamond probe than with the silicon probe.

Another factor affecting the LOD of a certain anion using ATR-FTIR is the molar absorptivity of the molecule. This property is intrinsic to each molecule and is related to the amount of radiation the molecule can absorb per mole. The molar absorptivity of a molecule is wavenumber dependent and is directly related to the absorbance through Beer's Law for traditional FTIR.[56] However, when using ATR, the relative absorbance is not equal at all wavenumbers.[57,58] Compared to transmission spectra, bands are relatively more intense at smaller wavenumbers in ATR spectra, even though the locations of the bands remains about the same. Because of this skewing of the absorbance spectrum, ATR-FTIR spectra are often converted to absorbance units from percent transmission using the Kramers-Kronig relationship, which minimizes these differences.[58] However, this algorithm was not used for experiments described in this chapter due to software limitations.

Differences in molar absorptivities between anions can cause some variations in the LODs. The most striking example from Table 3.1 is the uncoated silicon probe LOD for $PFOS^-$ (0.01 mM) compared to the much higher LOD for $CF_3SO_3^-$ (0.3 mM). Since the main peaks for $PFOS^-$ and $CF_3SO_3^-$ (1243 and 1258 cm^{-1}, respectively) are relatively close together, there should be very little ATR effect on the intensity of the peaks. One would expect similar absorbances for these two anions at equal concentrations *if* they have similar molar absorptivities. In this case, it can be assumed that they have very different molar absorptivities, as is shown by the following example. For 10-minute spectra (1,660 co-added scans) of 1 mM solutions of $PFOS^-$ and $CF_3SO_3^-$ in contact with the uncoated silicon probe, the absorbance at the peak maximum was

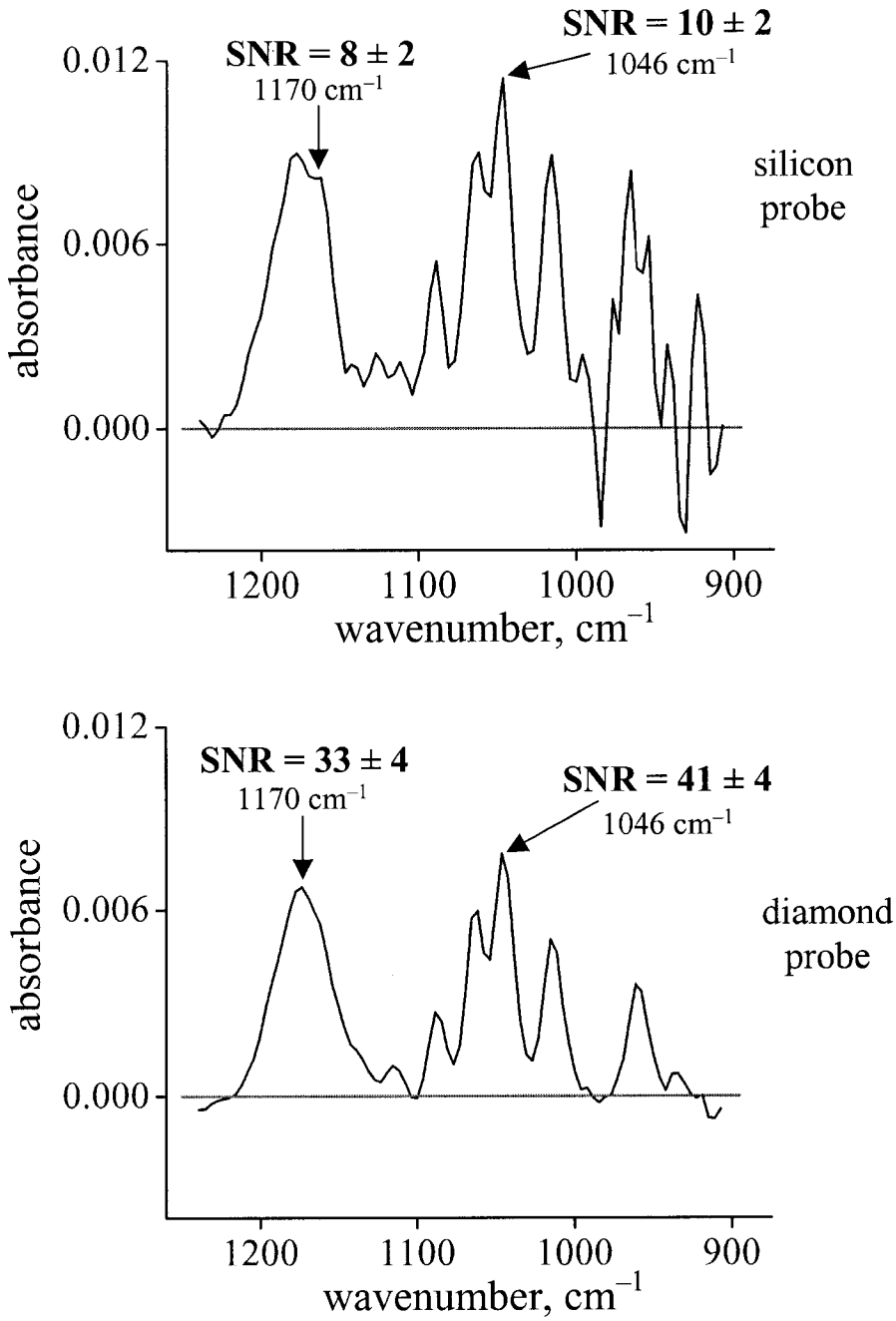

Figure 3.11. Spectra of 10 μM $PMPA^-$ after 10-minutes in contact with DEC^+Cl^--coated ATR crystals. The top spectrum was collected using the coated silicon ATR crystal and the bottom spectrum was collected using the coated diamond ATR crystal.

0.012(2) and 0.0014(1), respectively, where the standard deviation is given in parenthesis. The absorbance of the $PFOS^-$ band is ca. 10 times more intense than the $CF_3SO_3^-$ band. The larger molar absorptivity of $PFOS^-$ compared to $CF_3SO_3^-$ is probably a result of more C–F bonds in $PFOS^-$ which contribute to more intense ν(CF) bands. As a result, $PFOS^-$ has a much lower LOD than $CF_3SO_3^-$ when using the uncoated probe.

The LODs listed in Table 3.1 for the uncoated ATR probes could be improved somewhat by increasing the number of co-added scans that constitute a single spectrum. As the number of scans per spectrum is increased, the *SNR* increases with the square root of the number of scans being signal averaged.[55] For example, increasing the scanning time from 10 minutes (1,660 scans) to 30 minutes (5,000 scans) should increase the *SNR* by a factor of 1.74. The LODs for ClO_4^- using the unmodified silicon probe after analysis times of 10 and 30 minutes are 0.8 and 0.4 mM. To one significant figure, this two-fold decrease in LOD agrees well with theory. Although there is some advantage to collecting more scans per spectrum in order to further lower the LOD, this must be balanced with the increased amount of time required for the analysis. Furthermore, there is a point of diminishing returns: the 60-minute LOD (10,000 co-added scans) for ClO_4^- was not significantly different than the 30-minute LOD (5,000 co-added scans) even though it was expected to drop by a factor of 1.41. When spectra are being collected with large numbers of co-added scans, it is not uncommon for error to be introduced by the instability of the interferometer.[124] According to the manufacturer of our ATR-FTIR instrument, it becomes shot noise limited after ca. 1,000 co-added scans per spectrum. Therefore, even by collecting 10,000 co-added scans for a 60-minute spectrum, the noise will not decrease noticeably beyond the 5,000 co-added scans collected for a 30-minute spectrum. Conversely, decreasing the number of scans per spectrum to 64 (30 s collection time), results in a five-fold increase in the noise compared to a 10-minute spectrum (average noise for 64 scans = $7(1) \times 10^{-4}$). The 30-second LOD of 3 mM ClO_4^- is ca.

four time higher than the 10-minute LOD. Both the increase in the noise and LOD correlate well with the expected five-fold increases due to the smaller number of scans.

The LODs for anions using extractant-coated ATR probes can also be lowered by collecting spectra over a longer time, however, the mechanism for this lowering of the LOD is different than that for the uncoated-probe LODs. Instead of collecting more scans per spectrum, the ion exchange is allowed to proceed for a longer period of time and then a spectrum is collected. Until ion-exchange equilibrium is reached, lower LODs are possible at longer extraction times because the ion-exchange reaction is concentrating the analyte over time in the volume probed by the evanescent wave.

Figure 3.12 shows the detection of 1 μM ClO_4^- using the $DEC^+NO_3^-$-coated silicon probe over a 6 hour time period. The absorbance of the T_2 ν(ClO) perchlorate peak increased linearly for more than 60 minutes after ion-exchange was initiated. This can be seen more clearly by plotting the absorbance of the 1096 cm^{-1} peak versus time as seen in Figure 3.13. Since the absorbance of the analyte peak increased with time but the noise remained the same (because 64 co-added scans were collected regardless of the length of the anion-exchange time interval), the *SNR* was higher at longer extraction times. This resulted in a 30-minute LOD of 0.02 μM ClO_4^-, two times lower than the 10-minute LOD of 0.04 μM ClO_4^-. To one significant figure, the two-fold lowering of the 30-minute LOD is close to the expected three-fold decrease.

At longer extraction times (e.g., 60 minutes) the peak absorbance (signal) is still increasing linearly with time as can be seen in Figure 3.13. Note that at higher concentrations the absorbance versus time graph is linear for a shorter amount of time. One would expect the *SNR* to be higher at 60 minutes than at 10 or 30 minutes since the signal is still increasing, however, this assumes that the noise is constant. For the graph in Figure 3.13, the absorbance at 10 minutes is ca. 0.024 while the absorbance at 60 minutes is ca. 0.135. This is an increase by a factor of 5.6, which is approximately equal to the factor of 6 by which the time has increased. For the ClO_4^- noise window using the

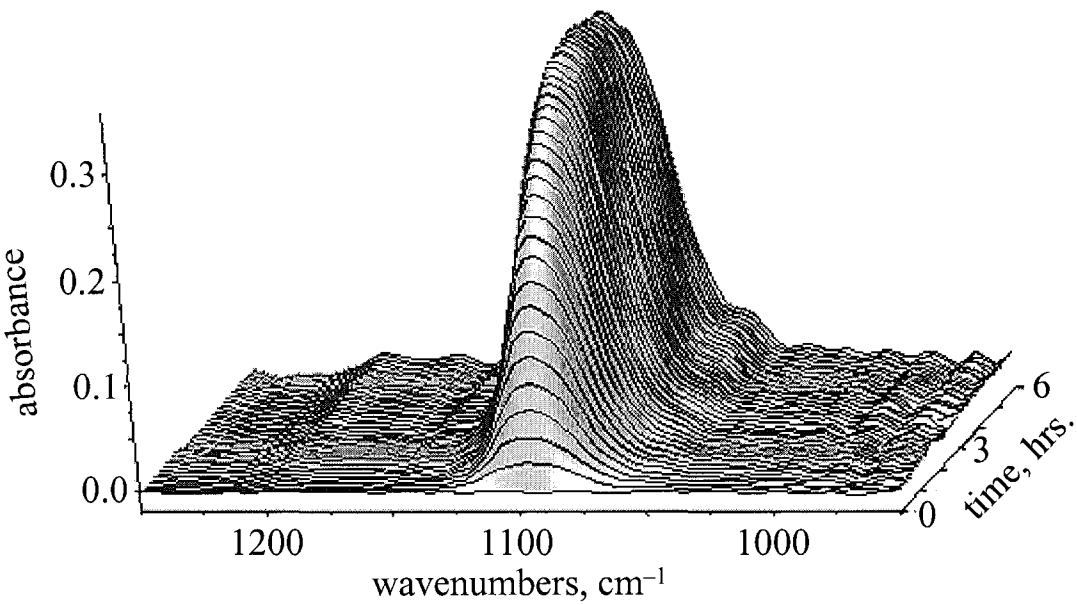

Figure 3.12. Detection of 1 μM ClO_4^- using the silicon probe which was coated by the evaporation of 20 μL of a 3 mM dichloromethane solution of $DEC^+NO_3^-$. Spectra (64 co-added scans) were recorded every minute for 6 hours. For clarity, only every 10^{th} spectrum is displayed.

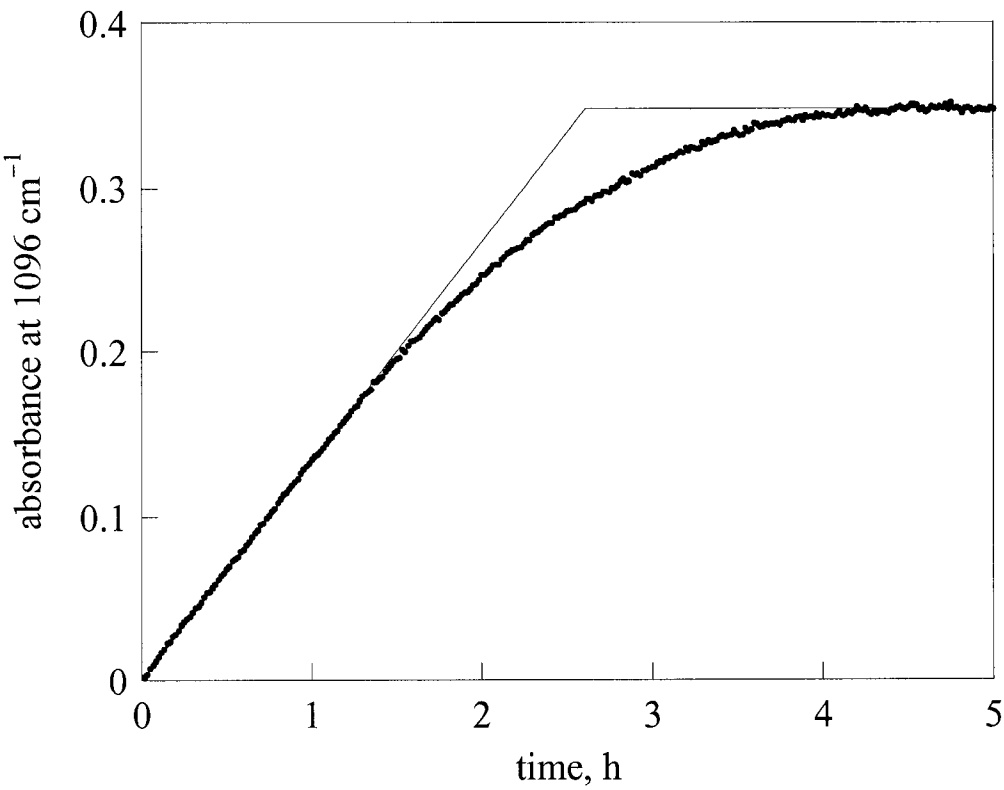

Figure 3.13. A plot of the absorbance of the ClO_4^- peak at 1096 cm^{-1} versus time from the detection of 1 μM ClO_4^- using the silicon probe coated with 20 μL of a 3 mM dichloromethane solution of $DEC^+NO_3^-$, as shown in Figure 3.12. The two arbitrary lines are used to show the linearity of the initial slope and the constant absorbance at long extraction times.

$DEC^+NO_3^-$-coated probe (1023–1166 cm^{-1}) the average noise remained the same within error for blank spectra collected after 1 and 10 minutes at $6(1) \times 10^{-4}$. However, the noise of the spectra after 30 minutes of DI water in contact with the $DEC^+NO_3^-$-coated probe increased slightly to 7.4×10^{-4} and doubled to 1.2×10^{-3} after 60 minutes. These noise values were calculated from spectra taken after the 1st, 10th, 30th, and 60th minute when the $DEC^+NO_3^-$-coated silicon probe was in contact with DI water with no added ClO_4^-. Since the noise is not the same at 60 minutes compared to 10 or 30 minutes, the *SNR* will not be directly proportional to time even though the signal intensity increases linearly over 60 minutes. Because of these factors, the point of diminishing returns has been reached for the length of time of extraction and thus the 30-minute LOD is not significantly different than the 60-minute LOD for ClO_4^-. The two-fold increase in extraction time (and thus signal) is offset by the two-fold increase in noise.

Calibration curves. The Beer-Lambert law can generally be used in spectroscopic experiments to produce linear calibration curves of absorbance versus analyte concentration. For example, a plot of absorbance at 1347 cm^{-1} ($\nu_{asym}(NO)$ for aqueous NO_3^-) versus $[NO_3^-]$ using the uncoated silicon probe, shown in Figure 3.14, is linear from 10 to 400 mM. An ATR-FTIR calibration curve for aqueous solutions of NO_3^- was described by Wilhite and Ellis in 1963, but the plot was not displayed.[125] Notably, Wilhite's NO_3^- calibration curve had nearly the same linear range (10–100 mM) as the one presented here.

Calibration curves based on final absorbance values are not possible with DEC^+X^--coated probes. This is because $DEC^+NO_3^-$ and DEC^+Cl^- are such selective extractants for weakly hydrated anions that the extractant coatings become completely or nearly completely saturated with the analyte anion at equilibrium, resulting in the same maximum or final absorbance value for a wide range of concentrations of a given analyte. This saturation of the DEC^+X^- coating results in a leveling off of the absorbance versus time plots at long times, as seen in Figure 3.13. A constant final absorbance value over a

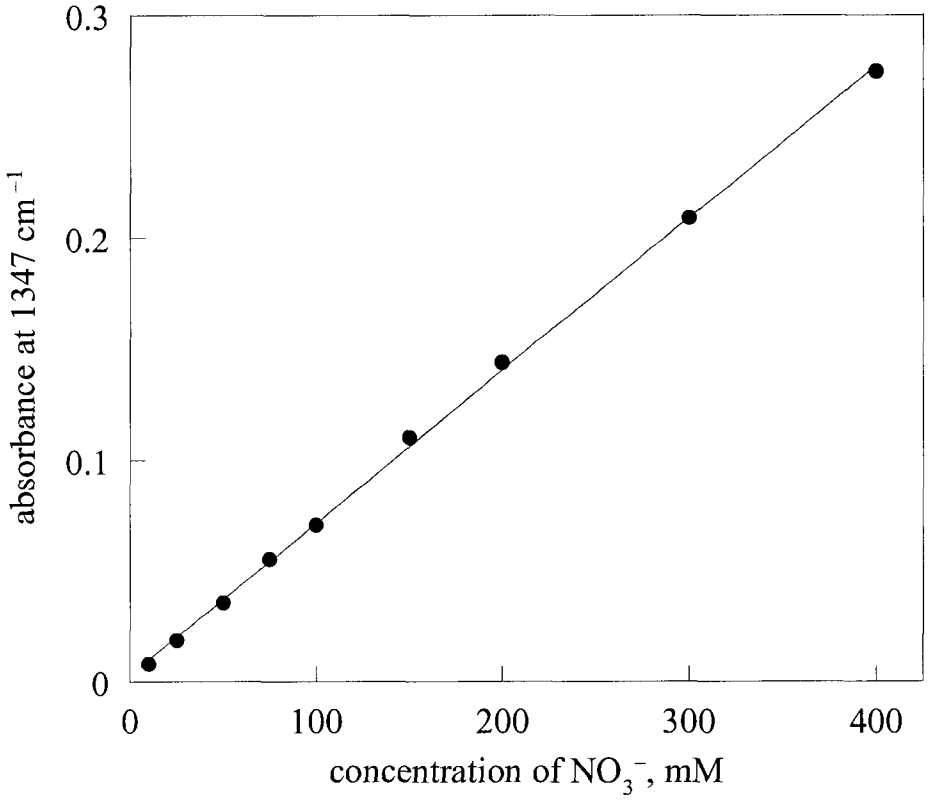

Figure 3.14. Calibration curve for aqueous nitrate (ν(NO) at 1347 cm^{-1} (7.42 μm)) using the uncoated silicon probe. A set of three spectra (64 co-added scans) were averaged for each concentration and the error bars ($\pm 1\sigma$) are smaller than the points. Wilhite and Ellis monitored the same band but reported its position as 7.46 μm (1340 cm^{-1}).[125] The equation for the least-squares linear fit is $y = 6.87(7) \times 10^{-4}x + 3(1) \times 10^{-3}$ with a correlation coefficient of 0.999.

range of analyte concentrations will occur as long as there is an excess amount of analyte present relative to the amount of extractant used to coat the ATR probe. The final absorbance of the ClO_4^- peak for solutions ranging in concentration from 5 to 30 μM in contact with the $DEC^+NO_3^-$-coated silicon probe was 0.26(2), as shown in Figure 3.15. However, since there were only 0.9 moles of ClO_4^- per mole of $DEC^+NO_3^-$ for the 0.15 μM solution, the final absorbance for that concentration was significantly less than the other final absorbance values.

Since the final absorbance value is not proportional to concentration, it cannot be used to create a linear calibration curve. However, it was found that a linear calibration curve based on ion-exchange kinetics could be constructed to determine unknown analyte concentrations. Looking again at Figure 3.13, the plot rises sharply at short times and exponentially approaches the final absorbance of 0.35 after several hours. There was a corresponding decrease in the $\nu_{asym}(NO)$ at 1347 cm^{-1}, and at equilibrium this band had completely disappeared. In general, the sharp rise at short times (i.e., the initial slope of the absorbance versus time curve, hereinafter referred to as dA/dt) was found to be constant for at least the first 10 to 30 minutes of the analysis for a given analyte concentration. More importantly, dA/dt was found to be directly proportional to analyte concentration up to a limiting concentration. For example, a plot of dA/dt versus $[ClO_4^-]$, shown in Figure 3.16 was linear from 0.04 to 1.0 μM. Recall that the LOD of aqueous ClO_4^- using the uncoated silicon probe is 800 μM. The use of initial dA/dt values instead of final absorbance values for quantification is a significant time advantage. The time necessary to determine a dA/dt value is only 10 minutes, whereas it can take hours to reach the final absorbance value.

The limit of linearity for each calibration curve was determined by plotting initial dA/dt versus concentration over a wide range of concentrations. For example, Figure 3.17 shows the calibration curve for ClO_4^- with concentrations up to 15 μM. Starting with this graph, a few points were removed to find the concentration at which the curve becomes

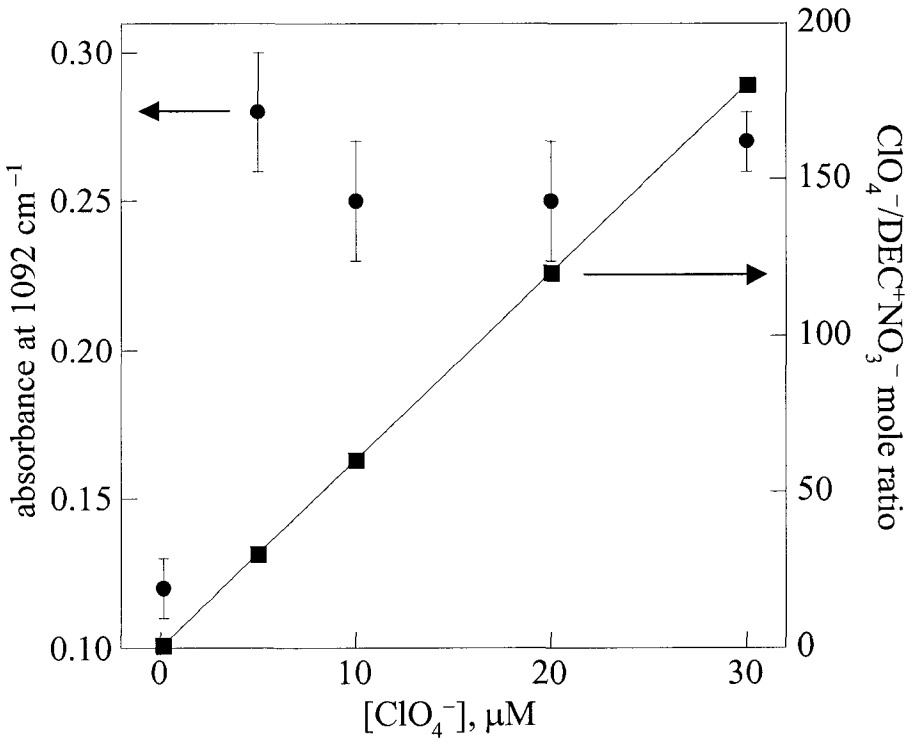

Figure 3.15. Graph of the maximum or final absorbance of the 1092 cm^{-1} ClO_4^- peak at various concentrations for the silicon probe coated with 20 μL of a 1 mM dichloromethane solution of $DEC^+NO_3^-$ is shown with circles and the left scale. The squares and the right scale represent the ratio of the number of moles of ClO_4^- in solution compared to the moles of $DEC^+NO_3^-$ on the ATR crystal. Error bars represent ±1σ.

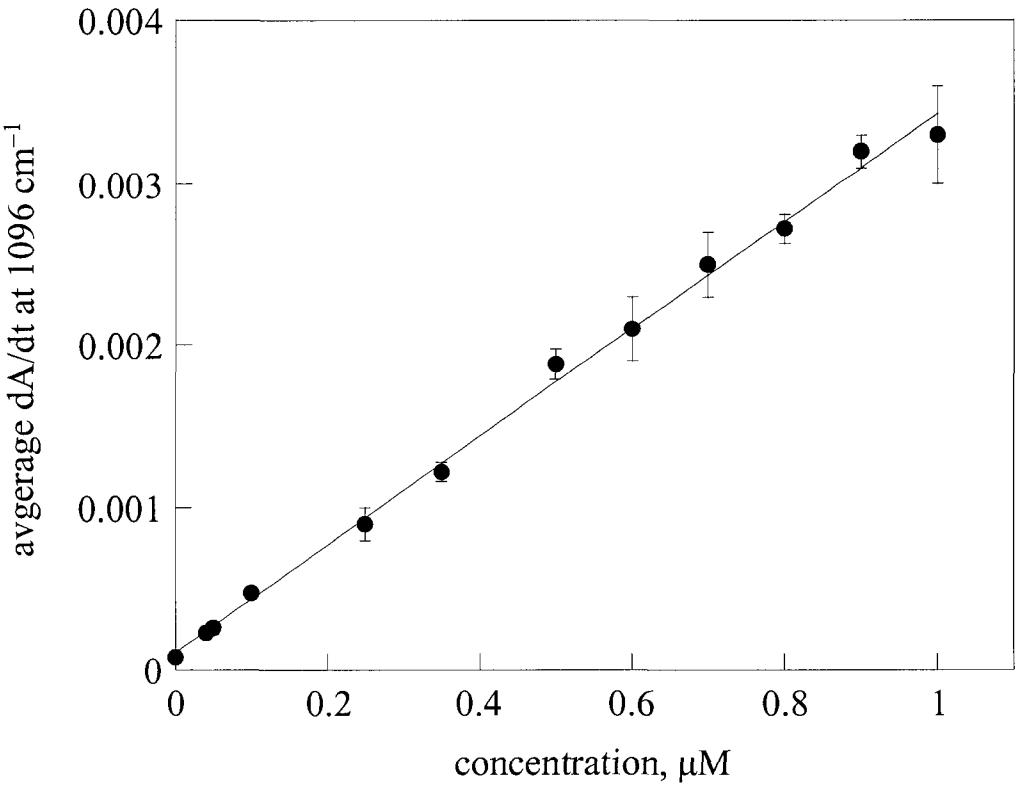

Figure 3.16. The initial d*A*/d*t* versus [ClO_4^-] calibration curve. Points are the average of at least three trials of each concentration in contact with the silicon probe coated with 20 μL of a 3 mM dichloromethane solution of $DEC^+NO_3^-$. Error bars, which are smaller than the points in some cases, represent ±1σ. The equation for the least-squares linear fit is $y = 3.32(6) \times 10^{-3}x + 1.1(3) \times 10^{-4}$ with a correlation coefficient of 0.997.

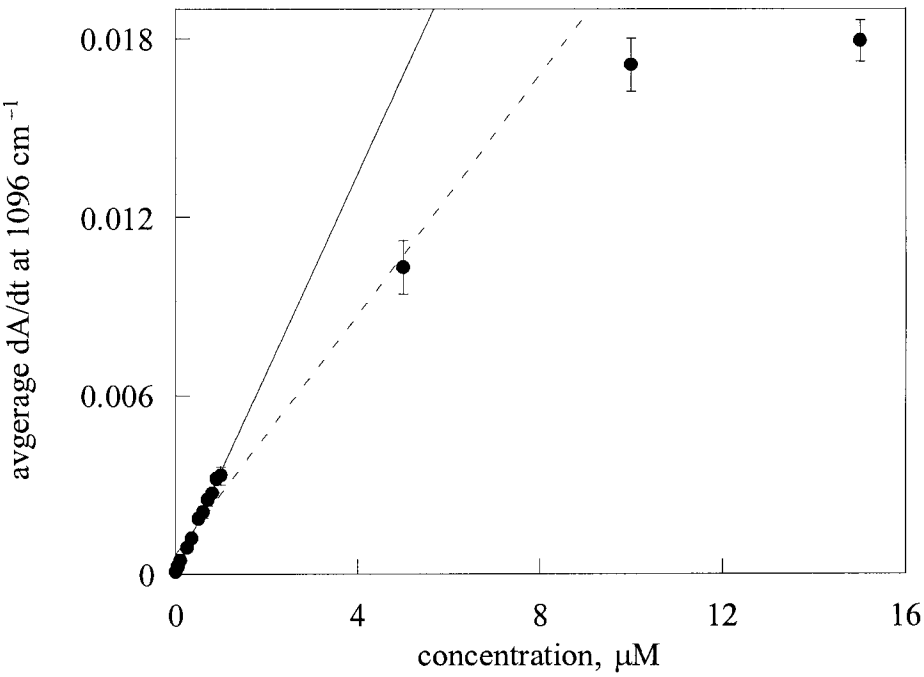

Figure 3.17. Initial d*A*/d*t* versus [ClO_4^-] calibration curves. Points are the average of at least three trials of each concentration in contact with the silicon probe coated with 20 μL of a 3 mM dichloromethane solution of $DEC^+NO_3^-$. Error bars, which are smaller than the points in some cases, represent ±1σ. A solid line is drawn representing the least-squares fit for the calibration curve up to 1 μM, shown in Figure 3.20. The dashed line is the least-squares fit for the data up to 5 μM with a correlation coefficient of 0.97.

linear. For the calibration curve up to 5 μM, the correlation coefficient is only 0.969 and it still does not appear to be linear. Thus, it was determined that the final calibration curve should be plotted only up to 1.0 μM as shown in Figure 3.16.

Linear initial dA/dt-versus-analyte-concentration calibration curves, which consisted of at least seven concentrations (points), were also constructed for $PFOS^-$ and $PMPA^-$, as shown in Figures 3.18 and 3.19, respectively. In both cases, the most intense IR band was chosen to determine the dA/dt values. The errors shown on the three calibration curves range from 3 to 26% relative standard deviation. These errors were typically larger at higher concentrations, contrary to what is commonly seen where large errors are generally associated with low concentrations near the detection limit. When using these ion-exchange coatings, high analyte concentrations saturate the coating quickly, making the determination of the initial dA/dt value less precise. One would think that this could be avoided by using data from only the first few minutes of ion exchange. However, if the analysis time is shortened, there will be fewer data points to define the initial linear portion of the A versus t curve, also increasing the error. Alternatively, if fewer scans per spectrum were collected, thereby collecting the same number of spectra in the shorter amount of time, the *SNR* will decrease, and this will also increase the error.

Now that several calibration curves have been created, the other IUPAC method of calculating LODs that was discussed in Chapter 1 (Equations 1.1 through 1.3) can be used. The LODs calculated from the calibration curves, reported as c_L in Table 3.8, are fairly close to the LODs determined using the *SNR*. This method of calculating LODs could not be used for all the anions listed in Table 3.1, because calibration curves were only created for ClO_4^-, $PFOS^-$, and $PMPA^-$.

During an ion-exchange process, one condition that is typically specified is that the number of moles of anion in solution must be large enough that during the course of the extraction, the concentration is not significantly changed. Therefore, the moles of anion in solution must be greater than the moles of extractant on the coated probe for the

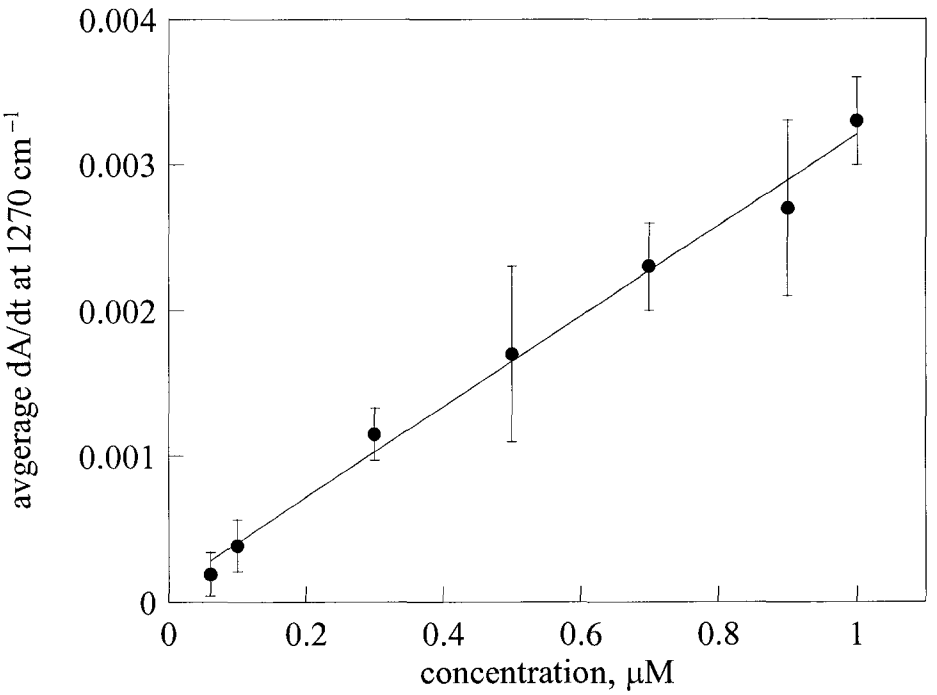

Figure 3.18. The initial d*A*/d*t* versus [$PFOS^-$] calibration curve. Points are the average of at least three trials of each concentration in contact with the silicon probe coated with 20 μL of a 1 mM dichloromethane solution of $DEC^+NO_3^-$. Error bars represent ±3σ. The equation for the least-squares linear fit is $y = 3.1(1) \times 10^{-3}x + 1.0(8) \times 10^{-4}$ with a correlation coefficient of 0.991.

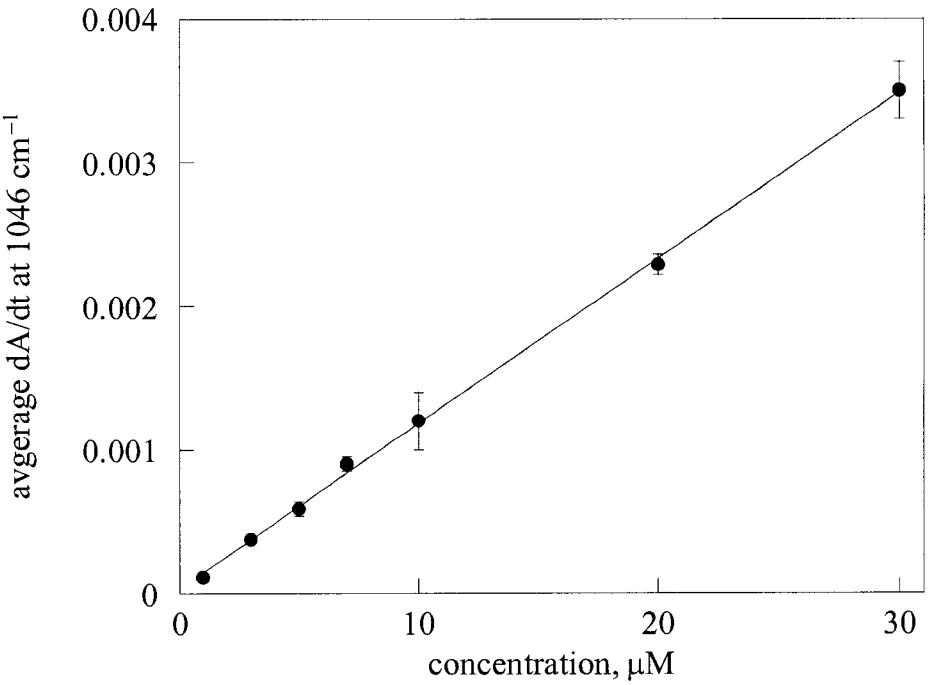

Figure 3.19. The initial d*A*/d*t* versus [$PMPA^-$] calibration curve. Points are the average of at least three trials of each concentration in contact with the diamond probe coated with 20 μL of a 5 mM dichloromethane solution of DEC^+Cl^-. Error bars, which are smaller than the points in some cases, represent ±1σ. The equation for the least-squares linear fit is $y = 1.15(2) \times 10^{-4}x + 3(2) \times 10^{-5}$ with a correlation coefficient of 0.999.

Table 3.8. Comparison of LODs calculated from two different IUPAC-recommended methods[126,127]

anion	s_b[a]	m[b]	$c_L = 3s_b/m$, μM[c]	LOD, μM[d]
ClO_4^-	3×10^{-5}	3.32×10^{-3}	0.027	0.04
$PFOS^-$	3×10^{-5}	3.1×10^{-3}	0.029	0.06
$PMPA^-$	3×10^{-5}	1.15×10^{-4}	0.79	0.7

[a] s_b is the standard deviation of the dA/dt values for the blank spectra. This was calculated by monitoring the wavenumber for the most intense analyte band (1096, 1270, and 1046 cm^{-1} for ClO_4^-, $PFOS^-$, and $PMPA^-$, respectively). [b] m is the slope of the dA/dt versus concentration calibration curve shown in Figures 3.16, 3.18, and 3.19. [c] c_L is the calculated LOD. [d] LOD found using the *SNR* as listed in Table 3.1.

determination of linear calibration curves. For example, the ratio of moles of aqueous $PFOS^-$ to moles of $DEC^+NO_3^-$ in the coating is 3–50 over the range of concentrations included in the $PFOS^-$ calibration curve (0.06–1.0 μM $PFOS^-$ in 100 mL). The ratio of moles of aqueous $PMPA^-$ to moles of DEC^+Cl^- in the coating is 10–300 over the range of concentrations included in the $PMPA^-$ calibration curve (1–30 μM $PMPA^-$ in 100 mL). For these examples, there will still be an excess of moles of the anion in solution even at equilibrium (saturated coating) for the lowest concentration on the calibration curve. However, the ratio of moles of aqueous ClO_4^- to moles of $DEC^+NO_3^-$ in the coating is only 0.7–17 over the range of concentrations included in the ClO_4^- calibration curve (0.04–1.0 μM ClO_4^- in 100 mL). Since the mole ratio at the lowest ClO_4^- concentration is only 0.7, if the ion exchange was permitted to proceed to completion, then all of the ClO_4^- would be depleted from the solution before the coating could become saturated.

This problem can be ignored since only the *initial* dA/dt value is needed to generate values for the calibration curve. It was determined that the absorbance change necessary to define a straight line from which a slope (dA/dt) can be reliably calculated occurs within the first 10 to 15 minutes of the ion-exchange reaction (given that a spectrum is collected every minute). For example, the absorbance versus time graph for 0.15 μM ClO_4^- in contact with the $DEC^+NO_3^-$-coated silicon probe is shown in Figure 3.20 where the mole ratio of ClO_4^- (in 100 mL solution) to NO_3^- (in the $DEC^+NO_3^-$ coating) is 0.75. After 15 minutes, the ν(ClO) peak absorbance is 0.0066 which is only ca. 5% of the maximum absorbance of 0.1233 that is reached when essentially all of the aqueous ClO_4^- has been depleted. According to the change in the absorbance of the ν(ClO) peak during the first 15 minutes of the ion-exchange reaction, the concentration of ClO_4^- in solution has only dropped from 0.1500 to 0.1425 μM (a 5% change). This small number of moles of ClO_4^- lost from aqueous solution (7.5×10^{-10}) was exchanged for NO_3^- in the DEC^+ coating which left 1.925×10^{-8} moles of NO_3^- remaining in the

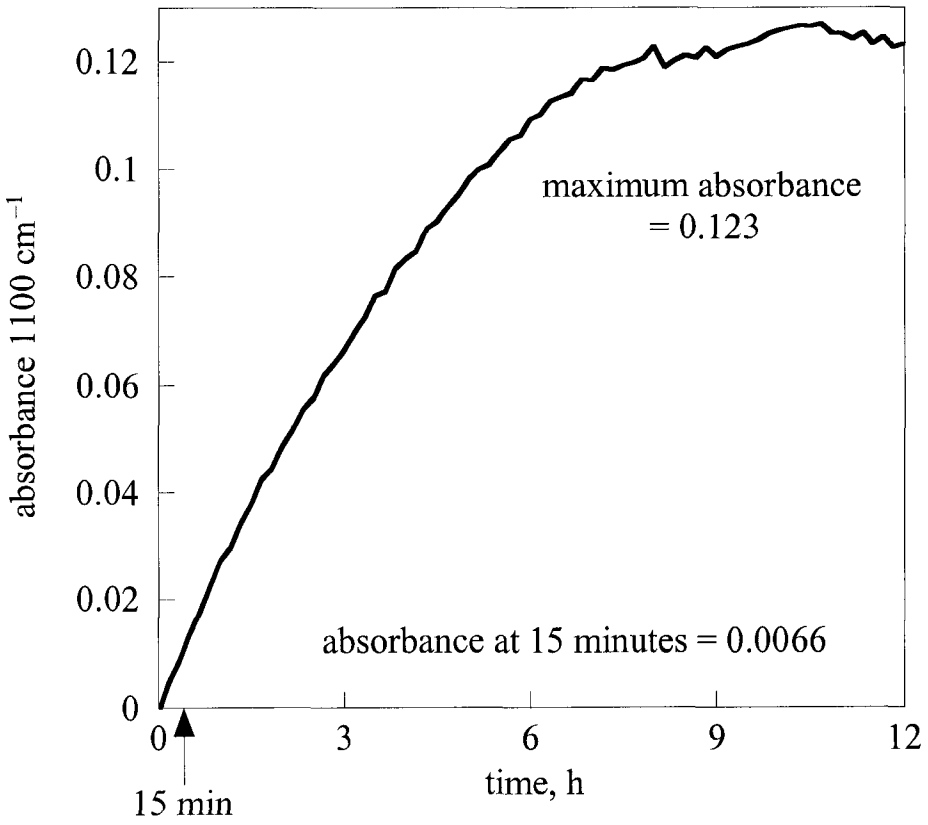

Figure 3.20. A plot of the absorbance increase versus time for the detection of 0.15 μM ClO_4^- using the silicon probe coated by the evaporation of 20 μL of a 1mM dichloromethane solution of $DEC^+NO_3^-$. The arrow indicates the location of 15 minutes when the absorbance is only ca. 5% of the maximum absorbance reached after more than 9 hours.

coating. Thus, the ClO_4^-/NO_3^- mole ratio only decreased from 0.75 to 0.74 (a 1.3% change). Therefore, during the period of time that the initial dA/dt is determined, there is an essentially constant concentration of ClO_4^- in solution.

Anion exchange kinetics. The kinetics of these ion-exchange extractions are similar to those modeled by Helfferich et al. for anion exchange kinetics in resins of high selectivity.[128] Although there are some obvious physical differences between ion-exchange beads and a layer of extractant on a smooth, flat crystal surface, the theory behind the rates should remain the same. In Helfferich's model there are three volumes that could potentially control the kinetics of the ion exchange, as shown in Figure 3.21: the bulk of solution; the stagnant liquid film layer; and the extractant coating. The layer of liquid close to the extractant is not affected by the stirring of the solution, much like the Nernst diffusion layer in stirred electrochemical experiments.[129] This stagnant layer is referred to as the liquid film and is a convection-free zone of defined thickness (ca. 10^{-3} to 10^{-2} cm) and has a sharp boundary with the bulk of the stirred solution.[130]

The ion-exchange reaction depicted in Equation 3.16 shows only the anions for simplicity and will be used to explain the kinetic model. This model is based on several

$$NO_3^-(coating) + ClO_4^-(bulk\ aq) \rightleftharpoons ClO_4^-(coating) + NO_3^-(bulk\ aq) \qquad (3.16)$$

assumptions including (i) no concentration gradient in the ion-exchange particle (extractant coating), (ii) quasi-stationary state of liquid-phase mass transfer, (iii) linear driving force, (iv) constant separation factor, α (defined in Equation 3.17), at a given

$$\alpha = \frac{[ClO_4^-]_{(coating)}[NO_3^-]_{(bulk\ aq)}}{[NO_3^-]_{(coating)}[ClO_4^-]_{(bulk\ aq)}} \qquad (3.17)$$

solution concentration, (v) constant individual diffusion coefficients of the exchanging ions, and (vi) constant volume of the ion exchange material (extractant coating).[128] Other

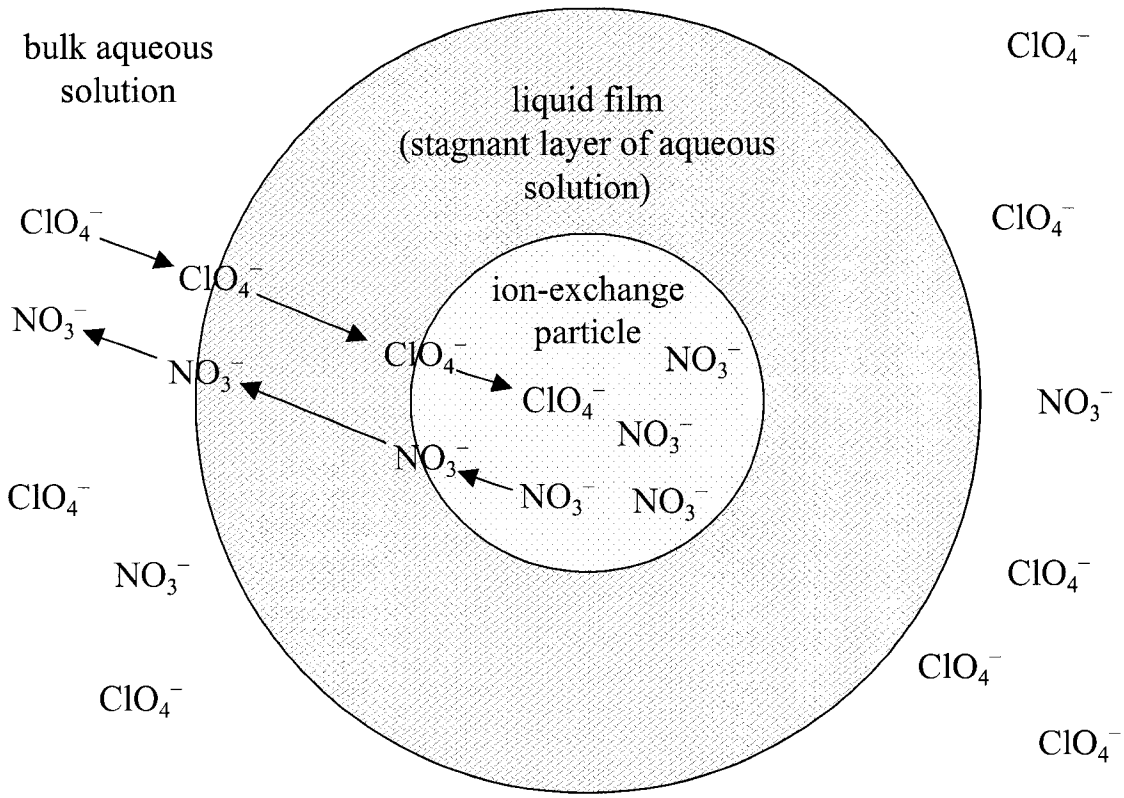

Figure 3.21. Schematic of an ion-exchange particle surrounded by a liquid film layer and then the bulk aqueous solution. This is similar to the model for anion exchange depicted by Helfferich et al.[130]

assumptions are that the ion exchanger initially contains only NO_3^- and that the aqueous solution contains a constant concentration of ClO_4^-, which is a similar condition to that discussed earlier for linear calibration curves. For $\alpha >> 1$ (corresponding to the uptake of a highly preferred anion), the anion exchange is governed by Equation 3.18, where F is

$$F \cong \frac{3D[X^-]_{(bulk\ aq)}\, t}{r\delta[X^-]_{(coating)}} \tag{3.18}$$

the fractional approach to equilibrium, D is the effective liquid-phase diffusivity ($cm^2\ s^{-1}$), t is time (s), r is the particle radius of the ion exchanger (cm), δ is the liquid film thickness (cm), and $[X^-]$ represents the total concentration of each anion in either the bulk of solution or the DEC^+ coating.[128]

Although the particle radius of the ion exchanger does not directly fit our application, this can most likely be related to the thickness of the $DEC^+NO_3^-$ coating on the ATR crystal, which is approximately constant. According to this model, there is a linear dependence of fractional conversion on time, which gives a initially constant rate of ion exchange. The theoretical graph of fractional conversion over time very closely resembles the graphs obtained for absorbance versus time for an anion in contact with an extractant coated probe.[128] In this case F is independent of α. However, a smaller α (i.e., a less selective extractant) should result in the absorbance versus time graph being linear for a shorter amount of time.

Several important points can be ascertained from Equation 3.18. Since there is a very high selectivity of the ion-exchanger, the concentration of ClO_4^- in the liquid film layer is negligible until ion exchange is almost complete. Thus, a constant driving force in the liquid film is maintained for any given concentration. Given that D is constant for any specified stirring rate, Equation 3.18 will give a constant rate of ion exchange for a given bulk concentration of ClO_4^- until F approaches 1 (equilibrium). Accordingly, the rate-controlling step is mass transfer of the anion from the bulk of solution to the liquid

film and F will be directly proportional to the concentration of ClO_4^- in the bulk solution. Because of these relationships, linear calibration curves were possible by plotting the initial dA/dt value (which is directly related to F when F is small) versus concentration.

To demonstrate the selectivity of the $DEC^+NO_3^-$ extractant, a solution of two anions, ClO_4^- and ClO_3^-, present at equal concentrations was put in contact with the $DEC^+NO_3^-$-coated silicon probe and spectra were collected every minute for 30 minutes. The resulting spectra are shown in Figure 3.22 where a peak is present only for ClO_4^-. The presence of ClO_4^- inhibited the uptake of ClO_3^- by the thin-film coating, not only at equilibrium but also at the beginning of the ion-exchange process. This agrees well with the theory that *at equilibrium*, only the most weakly hydrated anion will be extracted from a solution, which in this case is ClO_4^-. The hydration energies ($\Delta G°_{hyd}$) of ClO_4^- and ClO_3^- are –259 and –308 kcal mol^{-1},[54] respectively, which shows that ClO_4^- is the more weakly hydrated anion. Recall that $\Delta G°_{hyd}$ is –314 kcal mol^{-1} for NO_3^-.[54] However, the *initial* detection of only the most weakly hydrated anion (ClO_4^-) is not explained by the different hydration energies.

Since both ClO_4^- and ClO_3^- are less hydrated than NO_3^- (which is confirmed by the extraction of ClO_3^- by the $DEC^+NO_3^-$-coated probe and is shown in Figure 3.22), one would expect the simultaneous extraction of both anions from a solution containing equal concentrations of both anions. One possible explanation for the lack of ClO_3^- band in the extraction with an equal concentration of ClO_4^-, is that ClO_3^- has a significantly smaller molar absorptivity than ClO_4^-. However, the integrated absorbances of the ClO_4^- and ClO_3^- peaks from spectra taken using the uncoated probe were nearly equal. Therefore, it can be assumed that their molar absorptivities (at least in aqueous solution) are also similar. One other possibility is that the ν(ClO) band from $DEC^+ClO_3^-$ is significantly less intense than that for $DEC^+ClO_4^-$. This possibility was eliminated by examining the spectra in Figure 3.23 that were collected using solutions containing 20 μM of each anion in contact with the $DEC^+NO_3^-$-coated diamond probe after a 10-

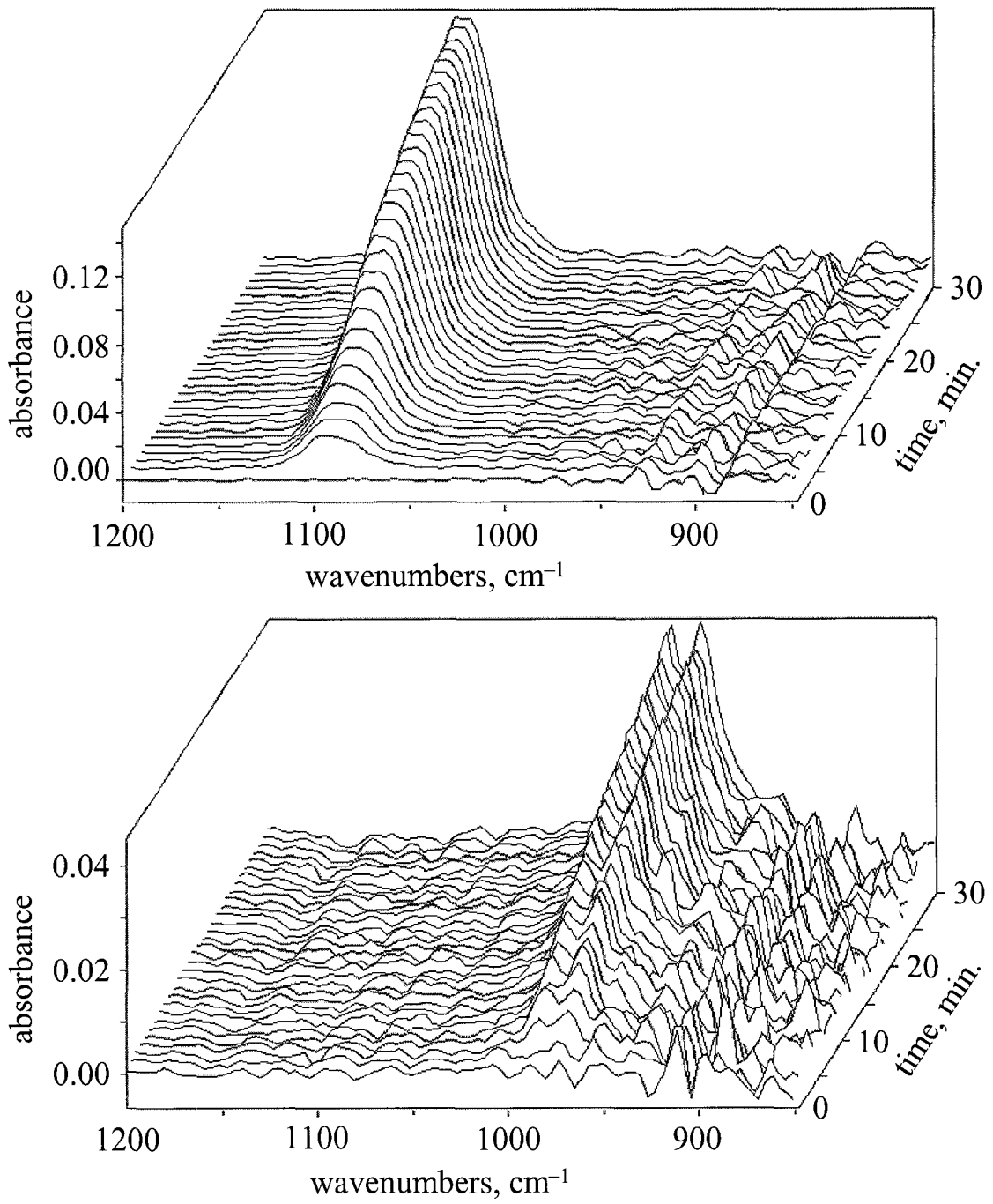

Figure 3.22. The top spectra are of the detection of 20 μM ClO_4^-, in the presence of 20 μM ClO_3^-, using the $DEC^+NO_3^-$-coated silicon probe. The bottom spectra are of the detection of 20 μM ClO_3^-, shown for comparison, using the $DEC^+NO_3^-$-coated silicon probe. Spectra (64 co-added scans) were recorded every minute for 30 minutes.

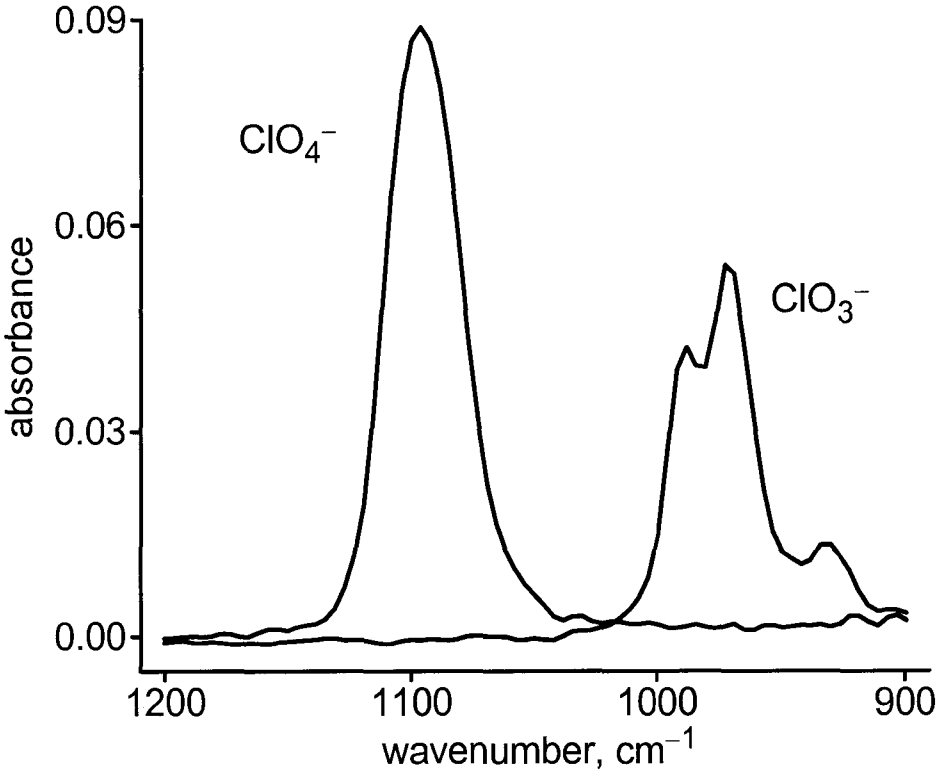

Figure 3.23. Comparison of the positions and relative intensities of IR bands for the structurally similar anions ClO_3^- and ClO_4^-. The displayed spectra were collected 10 minutes after the diamond ATR probe coated by evaporation of 20 μL of a 3 mM dichloromethane solution of $DEC^+NO_3^-$ was immersed in 20 μM aqueous $LiClO_4$ or $NaClO_3$. One major ν(ClO) band can be seen for $DEC^+ClO_4^-$ at 1096 cm^{-1} while the three ν(ClO) bands from $DEC^+ClO_3^-$ are located at 988, 973, and 931 cm^{-1}.

minute ion-exchange interval. The integrated absorbance of the ν(ClO) band of the $DEC^+ClO_4^-$-containing coating was found to be 55% larger than the integrated absorbance of the ν(ClO) bands of the $DEC^+ClO_3^-$-containing coating. It is important to note that at 10 minutes the absorbance versus time graph for both anions was still in the linear region. This would not be a valid comparison if one of the anions had saturated the DEC^+ coating before the collection of the 10-minute spectrum (i.e., if the absorbance versus time graph had leveled off). Therefore, since the intensities of the ν(ClO) bands for $DEC^+ClO_3^-$ are only ca. two times smaller than the intensity of the $DEC^+ClO_4^-$ band, one should observe both bands for the simultaneous extraction of the two anions at equal concentrations.

Preliminary experiments suggest that for competition experiments such as the one described here, the appearance of IR bands for both anions or only one anion may depend on their initial d*A*/d*t* values. For example, the d*A*/d*t* value for a 1 μM solution of ClO_3^- (0.00109(5)) is three times slower than the d*A*/d*t* value for a 1 μM solution of ClO_4^- (0.0033(3)) when using the $DEC^+NO_3^-$-coated silicon probe. The smaller initial d*A*/d*t* value for ClO_3^- is in agreement with the smaller absorbance of its ν(ClO) peak in Figure 3.23. It is plausible that ClO_3^- is not initially detected in the presence of an equal concentration of ClO_4^- because of its smaller initial d*A*/d*t* value. The investigation of the factors that affect the ATR-FTIR detection of analytes in the presence of a variety of interferants will be an important area of future research in our lab.

Another example of the differences between hydration energies and d*A*/d*t* values can be seen by the detection of 1 μM ClO_4^- using $DEC^+NO_3^-$- and DEC^+Cl^--coated probes. The silicon probe was coated by evaporation of 20 μL of 1 mM dichloromethane solutions of each extractant. According to their hydration energies ($\Delta G°_{hyd}$ is –259, –314, and –338 kcal mol^{-1} for ClO_4^-, NO_3^-, and Cl^-) the detection of ClO_4^- with DEC^+Cl^- is energetically more favorable than its detection with $DEC^+NO_3^-$. However, the initial d*A*/d*t* values do not seem to be related to hydration energy since the initial d*A*/d*t* for the

extraction with DEC^+Cl^-, 0.0017(1) min^{-1}, is similar to the value for the extraction with $DEC^+NO_3^-$, 0.0025(1) min^{-1}. The same experiments were repeated using 1 μM $CF_3SO_3^-$ and also resulted in similar d*A*/d*t* values for DEC^+Cl^- and $DEC^+NO_3^-$, 0.0025(3) min^{-1} and 0.0039(4) min^{-1}, respectively. The extraction of 1 μM ClO_4^- with the silicon probe coated by evaporation of a mixed solution of 10% DEC^+Cl^- and 90% $DEC^+NO_3^-$ also resulted in similar d*A*/d*t* values compared with those for 100% $DEC^+NO_3^-$. The d*A*/d*t* values for coatings made from 10% to 50% to 90% to 100% DEC^+Cl^- were also similar to that obtained from 100% $DEC^+NO_3^-$. Therefore, it seems that hydration energy only determines whether or not the ion exchange will occur and does not appear to influence the rate of ion exchange.

Identification of aqueous anions. One of the benefits of using IR as a detection method is that the analyte being detected can be positively identified by its unique IR bands in the fingerprint region of the spectrum. At least six major bands can be seen in Figures 3.10 and 3.11 for the extraction of $PMPA^-$ by a DEC^+Cl^- coating. Both the location and the relative intensities of these bands differ greatly from those of other anions. Examining anions that have similar structures can show the unique spectrum of each anion. Triflate ($CF_3SO_3^-$), $PFBS^-$ ($C_4F_9SO_3^-$), and $PFOS^-$ ($C_8F_{17}SO_3^-$) are structurally similar anions containing C–F and S–O bonds that are responsible for IR bands in the fingerprint region of the spectrum. As seen in Figure 3.24, lengthening the perfluorinated carbon chain from one to four to eight carbons results in significantly different IR spectra. For the sake of uniformity, all spectra displayed in Figure 3.24 were collected using 100 mL of a 1 μM anion solution in contact with the silicon probe coated with 20 μL of 1 mM $DEC^+NO_3^-$ after a 10-minute ion-exchange interval. The absorbance of the most intense peak in each spectrum is virtually the same because the initial d*A*/d*t* values for these three analytes were the same to within experimental error for a given concentration (this was true at 0.10, 1.0, and 10 μM). Since the extractant-coated

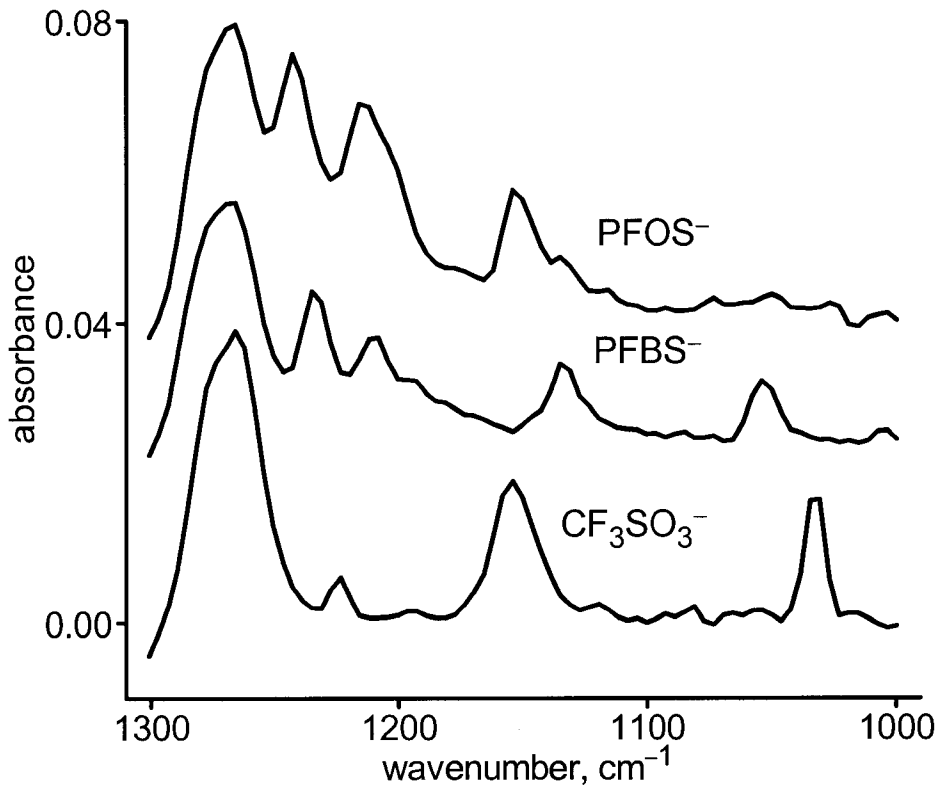

Figure 3.24. Comparison of the positions and relative intensities of IR bands for the structurally similar anions $PFOS^-$ (n-$C_8F_{17}SO_3^-$), $PFBS^-$ (n-$C_4F_9SO_3^-$), and $CF_3SO_3^-$. The displayed spectra were collected 10 minutes after the silicon ATR probe coated by evaporation of 20 μL of a 1 mM dichloromethane solution of $DEC^+NO_3^-$ was immersed in 1.0 μM aqueous K(PFOS), K(PFBS), or $LiCF_3SO_3$. Four major $PFOS^-$ bands for DEC^+PFOS^- can be seen at 1270, 1243, 1216 and 1154 cm^{-1}. The four $CF_3SO_3^-$ bands for $DEC^+CF_3SO_3^-$ are located at 1266, 1224, 1154, and 1031 cm^{-1} and the five $PFBS^-$ bands for DEC^+PFBS^- can be clearly seen at 1266, 1235, 1208, 1135, and 1054 cm^{-1}.

probe LOD values for these three analytes are all 0.06 ± 0.01 μM, it appears that the initial d*A*/d*t* values are also the same at concentrations lower than 0.10 μM.

Spectral differences can be seen even when two anions differ by only one atom, as seen with ClO_4^- and ClO_3^- in Figure 3.23. Not only does the location of the major peak shift from 1096 cm^{-1} for ClO_4^- to 973 cm^{-1} for ClO_3^-, but the peak shape changes from one single band to three distinct bands. Both spectra displayed in Figure 3.23 were collected using 100 mL of a 20 μM anion solution in contact with the $DEC^+NO_3^-$-coated diamond probe after a 10-minute analysis time.

Analysis of ClO_4^- in the presence of excess NO_3^-. Up to this point, most of the studies described in this dissertation were carried out with a single anionic analyte in DI water. The detection and quantification of ClO_4^- in hydroponic fertilizers containing high concentrations of nitrate salts was also studied.[15] As part of this study, the amount of excess NO_3^- that would affect both the initial d*A*/d*t* and the *SNR* of the perchlorate ν(ClO) band at 1096 cm^{-1} when using a $DEC^+NO_3^-$-coated silicon probe was determined. The results of several experiments with aqueous solutions of ClO_4^- containing various amounts of excess NO_3^- are listed in Table 3.9. All of these experiments were done using the silicon ATR crystal coated with 20 μL of a 1 mM dichloromethane solution of $DEC^+NO_3^-$. Depending on the ClO_4^- concentration, the d*A*/d*t* rate was lowered in the presence of 100 to 1,000-fold molar excess NO_3^-. The *SNR* did not appear to be affected by the addition of excess NO_3^- to the 0.15 μM ClO_4^-. At this concentration, however, the *SNR* is small and the relatively large error may mask any real change. At a higher concentration of ClO_4^-, 1 μM, the addition of only 100-fold excess NO_3^- resulted in significant lowering of the *SNR*.

Analysis of hydroponic fertilizers for perchlorate. Some aspects of this work have already been published.[15] Initial characterization of the fertilizer samples was accomplished by placing a sufficiently large aliquot of the stock solution (ca. 1 mL) on top of the uncoated silicon probe in the upright position so that the ATR crystal was

Table 3.9. Comparison of *SNR* and d*A*/d*t* rates for solutions of ClO_4^- with excess NO_3^- detected using the $DEC^+NO_3^-$-coated silicon probe[a]

$[ClO_4^-]$, μM	$[NO_3^-]$, μM	$\frac{[NO_3^-]}{[ClO_4^-]}$	*SNR*(σ)[b]	d*A*/d*t*(σ), min^{-1} [c]
0.15	0	na[d]	5.3(9)	0.0006(2)
0.15	15	100	7(1)	0.0006(1)
0.15	150	1000	6	0.0002
1	0	na	40(7)	0.0024(1)
1	10	10	41(7)	0.0024(1)
1	100	100	26	0.0015
1	250	250	18	0.0007
1	500	500	8	0.0003
1	1000	1000	6	0.0002

[a] The silicon ATR probe was coated by the evaporation of 20 μL of a 1 mM dichloromethane solution of $DEC^+NO_3^-$. [b] *SNR* calculated after 10 minutes in contact with the coated probe. σ = standard deviation. Only a single trial was done for values with no error listed [c] d*A*/d*t* values were determined at 1096 cm^{-1}. [d] na = not applicable.

completely covered by the sample and collecting a spectrum (64 co-added scans) that was ratioed to water. A peak at 1347cm^{-1} was observed due to the ν_{asym}(NO) band from aqueous NO_3^-, while no ν_{asym}(ClO) bands due to aqueous ClO_4^- at 1108 cm^{-1} were observed for any of the fertilizer stock solutions. The absence of the ν_{asym}(ClO) peak at 1108 cm^{-1} indicates that if there is ClO_4^- present in these fertilizers, it is at concentrations lower than 0.8 mM (i.e., the uncoated probe LOD listed in Table 3.1). The absorbance of the ν_{asym}(NO) peak at 1347 cm^{-1} was used in these experiments to determine the concentration of NO_3^- in each 10- or 3-g L^{-1} fertilizer stock solution. This was done by using the calibration curve of absorbance at 1347 cm^{-1} versus [NO_3^-] shown in Figure 3.14. The NO_3^- concentration determined for each of the fertilizer samples is listed in Table 3.10. A sample of Bulldog Soda was also analyzed. Bulldog Soda is sodium nitrate derived solely from mined Chilean caliche (a known natural source for perchlorate) and is sold as a single-component fertilizer product (N-P-K grade 16-0-0).

The concentration of nitrate in the fertilizer products listed in Table 3.10 is also presented as "% nitrate nitrogen" (weight percent of the fertilizer product that is nitrogen occurring as nitrate) so that the ATR-FTIR measurements can be compared to the concentration of NO_3^- listed by the manufacturer on the fertilizer product package. Note that our measurements, which reflect the NO_3^- levels in small laboratory samples, are not to be taken as a challenge to the manufacturers' reported levels, which are representative of much larger amounts of product. Instead, our results are presented in this manner to demonstrate their generally good agreement with the manufacturers' reported levels. The % nitrate nitrogen for the fertilizers was also analyzed by Raman spectroscopy by our EPA collaborators, Collette and Williams, and are listed in Table 3.10. There is a reasonably good correlation between the ATR-FTIR and the Raman results.

The seven hydroponic fertilizers were found to contain very different amounts of NO_3^-, with the weight percent nitrogen as nitrate varying from 4.1% to 16.7% (i.e., 18%

Table 3.10. Nitrate concentrations from ATR-FTIR and Raman spectroscopic analysis compared to the manufacturer reported levels

sample #	$[NO_3^-]$, mM in ATR-FTIR stock solution[b]	% nitrate nitrogen manufacturer[c]	% nitrate nitrogen ATR-FTIR[d]	% nitrate nitrogen Raman[d]
Bulldog Soda[a]	128 ± 6	16.0	18.1 ± 0.9	16.4 ± 0.3
1	103 ± 5	12.5	14.5 ± 0.7	12.6 ± 0.1
2	29 ± 1	5.0	4.1 ± 0.2	3.3 ± 0.1
3	112 ± 5	15.5	15.6 ± 0.7	14.1 ± 0.1
4	17 ± 1	8.9	8.1 ± 0.5	7.5 ± 0.1
5	120 ± 6	15.0	16.7 ± 0.9	14.5 ± 0.1
6	51 ± 3	7.0	7.2 ± 0.5	6.2 ± 0.1
7	31 ± 2	4.55	4.3 ± 0.2	3.7 ± 0.1

[a] Bulldog Soda is $NaNO_3$ derived solely from Chilean caliche. [b] $[NO_3^-]$ in the stock solution determined using the calibration curve in Figure 3.14. Stock solutions for the fertilizer samples were all 10 g L^{-1} except for #4 for which a 3 g L^{-1} stock solution was made. The errors listed are $\pm 1\sigma$. [c] The weight % nitrate nitrogen in the fertilizer as reported by the manufacturer on the product package (N-P-K grade). [d] The weight % nitrate nitrogen in the fertilizer as measured by ATR-FTIR or Raman spectroscopy. The errors listed are $\pm 1\sigma$.

to 74% NO_3^- by weight). Except for ClO_4^- and NO_3^-, the other components of the fertilizers were not determined in this study. However, the manufacturers' listed N-P-K grades indicate that the fertilizers also contained varying amounts of phosphate and potassium. Therefore, each fertilizer, when dissolved in water, resulted in a unique aqueous matrix.

The high content of dissolved solids and the high nitrate concentrations of the aqueous fertilizer solutions required the use of the method of standard additions to determine the ClO_4^- concentrations (and, ultimately, the weight percent of perchlorate in the fertilizers). The fertilizer solutions analyzed using the $DEC^+NO_3^-$-coated silicon probe were either 100 mg L^{-1} (for fertilizers #2 and #4) or 1,000 mg L^{-1} (for fertilizers #1, #3, #5, #6, and #7). Three of the samples exhibited a peak at 1096 cm^{-1}, indicating the presence of a measurable amount of ClO_4^-. FTIR spectra of the three fertilizer samples containing ClO_4^-, samples #1, #2, and #4, are shown in Figures 3.25, 3.26 and 3.27, respectively. To determine the ClO_4^- concentration, each of the fertilizer solutions shown to contain ClO_4^- were re-analyzed several times with varying amounts of an aqueous 1 mM ClO_4^- stock solution added to the sample. This procedure (three replicates each) was repeated for at least four different concentrations of added ClO_4^-.

In principle, each ClO_4^--spiked, standard-addition sample should give a dA/dt value that is linearly related to the total concentration of ClO_4^- in solution. A plot of dA/dt versus the concentration increment of added ClO_4^- was made for each of the three samples, and the absolute value of the x-axis intercept of a linear least-squares fit to the data was taken as the concentration of ClO_4^- in the unspiked fertilizer sample solution. The weight percent ClO_4^- in the solid fertilizer sample was then calculated using this value and the known dilution factor. These standard addition graphs for samples #1, #2, and #4 are shown in Figures 3.28, 3.29, and 3.30, respectively. Sample #1 contained 12 ± 3 μM ClO_4^- (10 g L^{-1} stock solution), sample #2 contained 39 ± 3 μM ClO_4^- (10 g L^{-1} stock solution), and sample #4 contained 10 ± 1 μM ClO_4^- (3 g L^{-1} stock solution). The

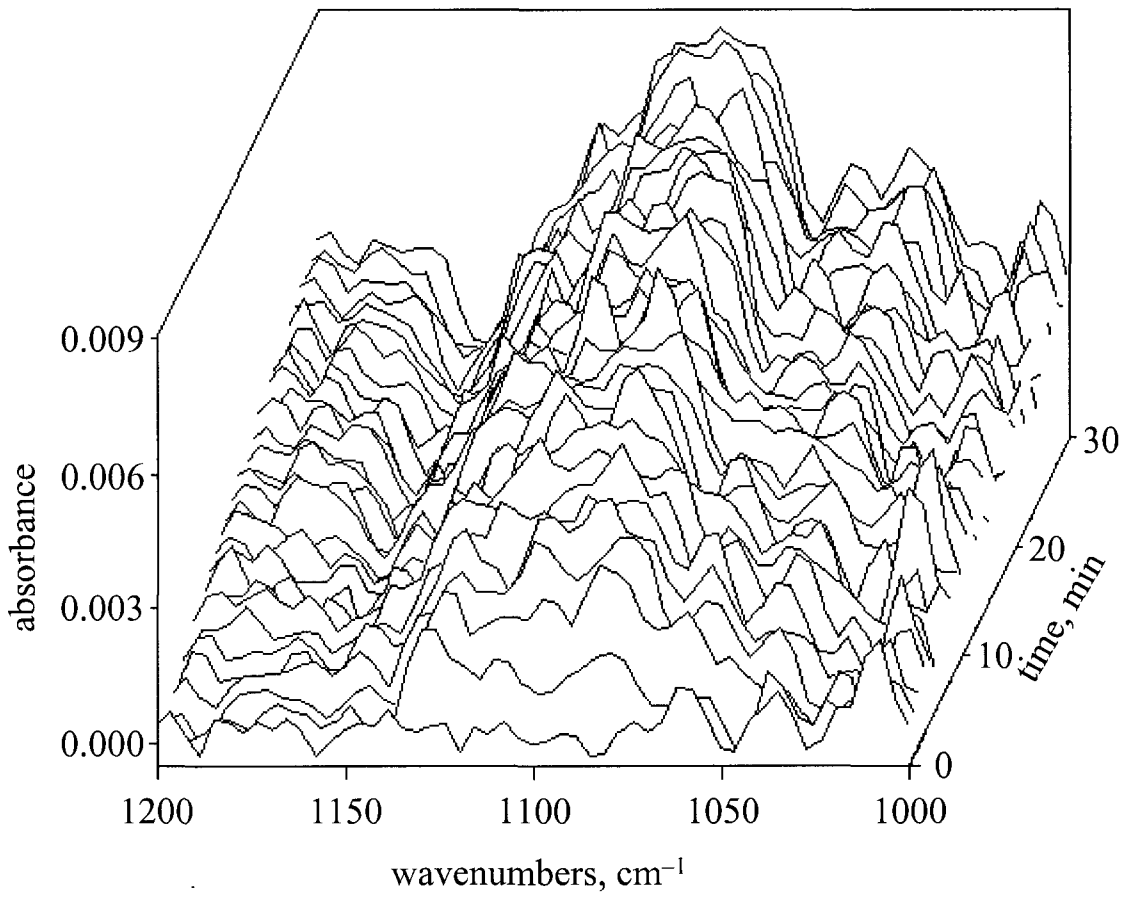

Figure 3.25. ATR-FTIR detection of ClO_4^- in 1,000 mg L^{-1} of fertilizer sample #1 (100 mL) using the silicon probe coated by evaporation of 20 μL of a 1 mM dichloromethane solution of $DEC^+NO_3^-$. A single band for $DEC^+ClO_4^-$ can be seen at 1096 cm^{-1}, which corresponds to 1.2 ± 0.3 μM aqueous ClO_4^- in this fertilizer solution.

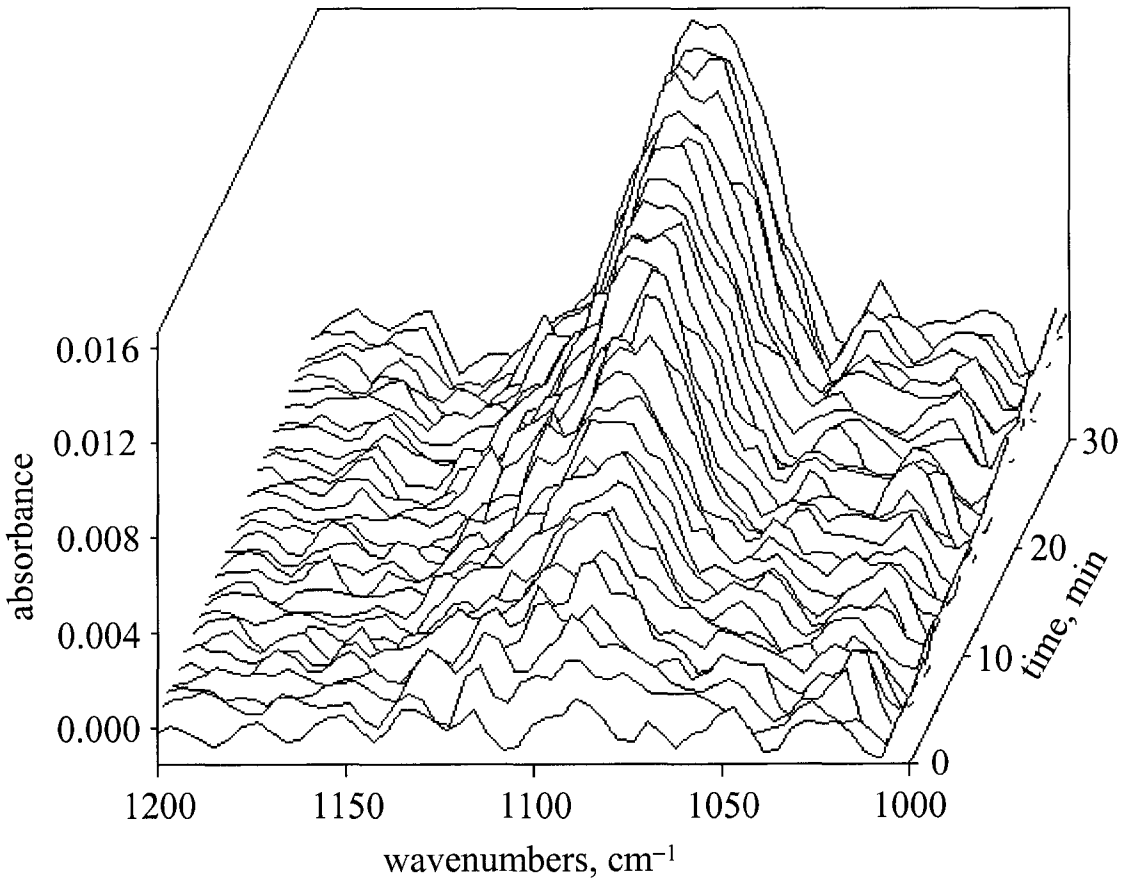

Figure 3.26. ATR-FTIR detection of ClO_4^- in 100 mg L^{-1} of fertilizer sample #2 (100 mL) using the silicon probe coated by evaporation of 20 μL of a 1 mM dichloromethane solution of $DEC^+NO_3^-$. A single band for $DEC^+ClO_4^-$ can be seen at 1096 cm^{-1}, which corresponds to 0.38 ± 0.03 μM aqueous ClO_4^- in this fertilizer solution.

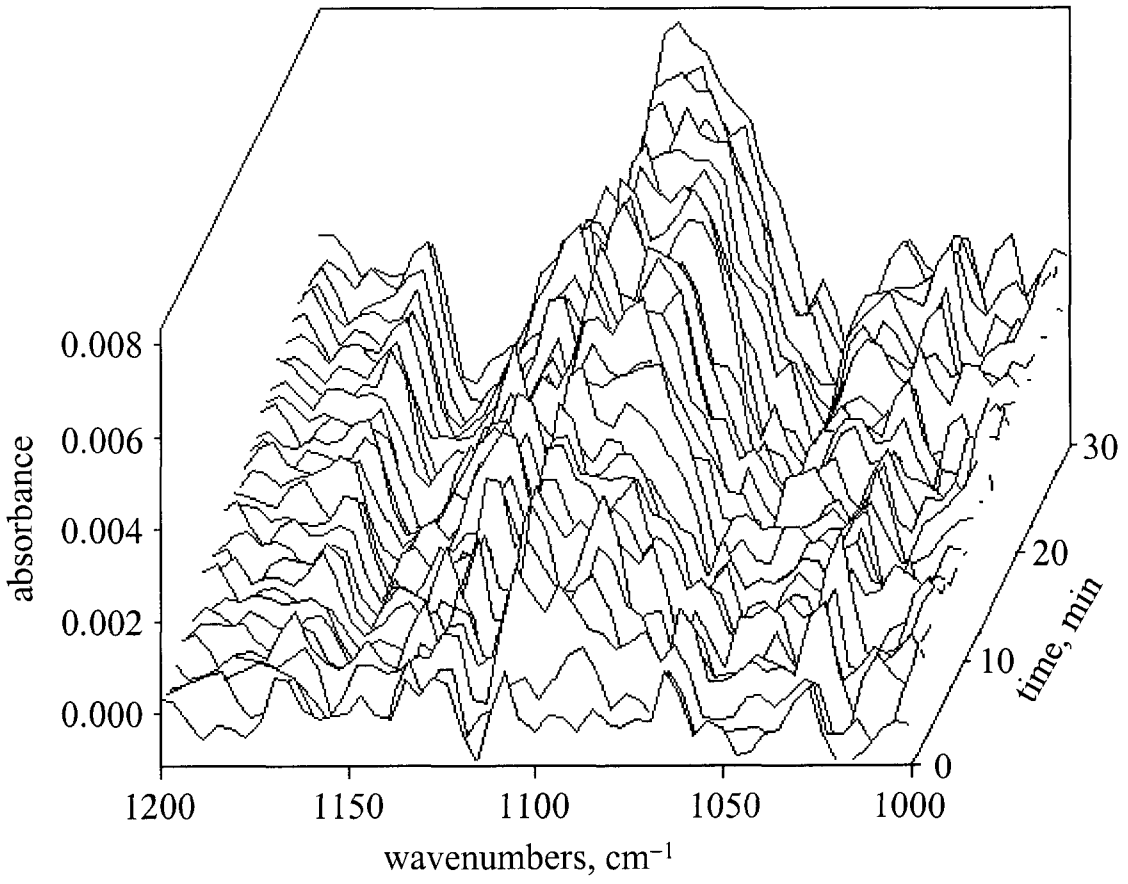

Figure 3.27. ATR-FTIR detection of ClO_4^- in 100 mg L^{-1} of fertilizer sample #4 (100 mL) using the silicon probe coated by evaporation of 20 μL of a 1 mM dichloromethane solution of $DEC^+NO_3^-$. A single band for $DEC^+ClO_4^-$ can be seen at 1096 cm^{-1}, which corresponds to 0.32 ± 0.04 μM aqueous ClO_4^- in this fertilizer solution.

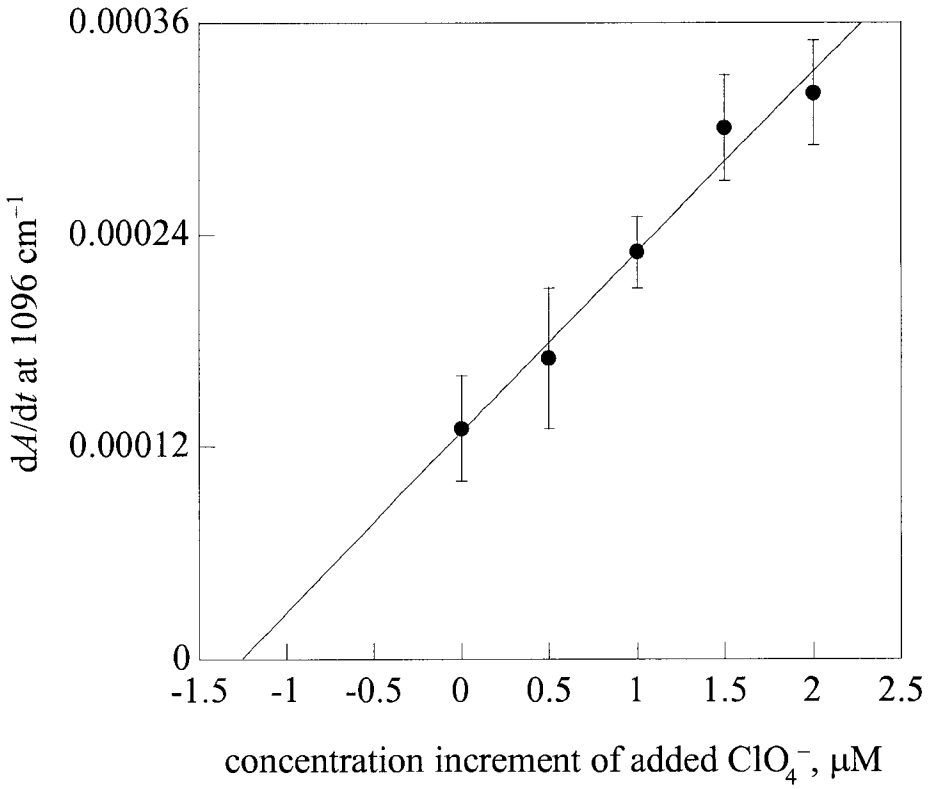

Figure 3.28. Standard addition graph for fertilizer sample #1. Using this graph, the absolute value of the *x*-axis intercept, 1.2 ± 0.3 μM, corresponds to the amount of ClO_4^- in the 1,000 mg L^{-1} fertilizer solution. After accounting for dilution, there was 12 ± 3 μM ClO_4^- in the 10 g L^{-1} stock solution of this fertilizer. The equation for the least squares linear fit is $y = 1.02(9) \times 10^{-4}x + 1.3(1) \times 10^{-4}$ with a correlation coefficient of 0.98. Error bars represent ±1σ.

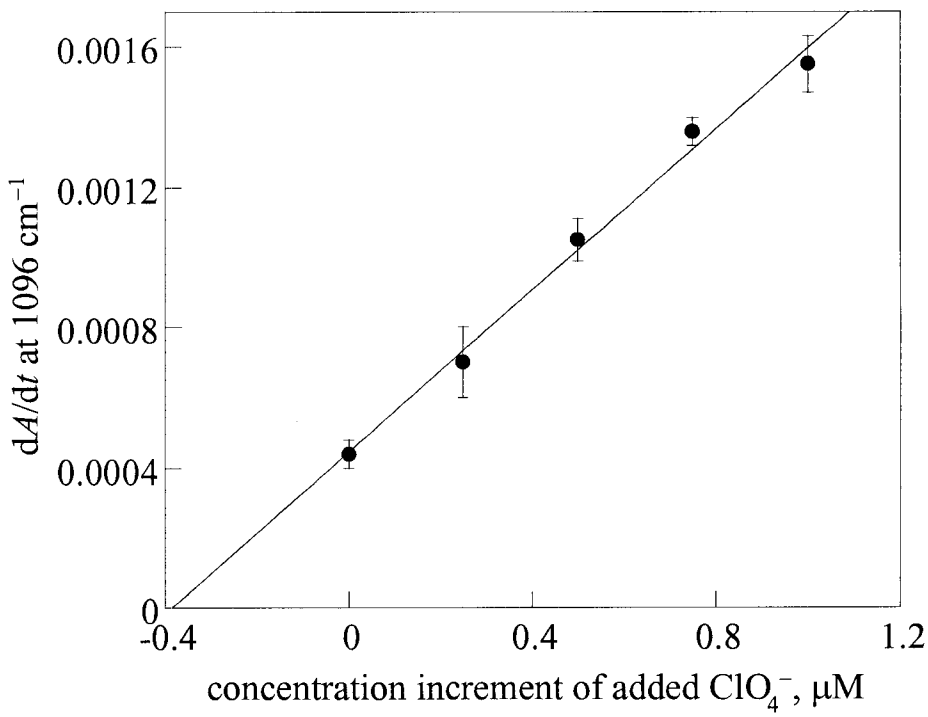

Figure 3.29. Standard addition graph for fertilizer sample #2. Using this graph, the absolute value of the *x*-axis intercept, 0.38 ± 0.03 μM, corresponds to the amount of ClO_4^- in the 100 mg L^{-1} fertilizer solution. After accounting for dilution, there was 39 ± 3 μM ClO_4^- in the 10 g L^{-1} stock solution of this fertilizer. The equation for the least squares linear fit is $y = 11.5(6) \times 10^{-3}x + 4.4(4) \times 10^{-4}$ with a correlation coefficient of 0.992. Error bars represent ±1σ.

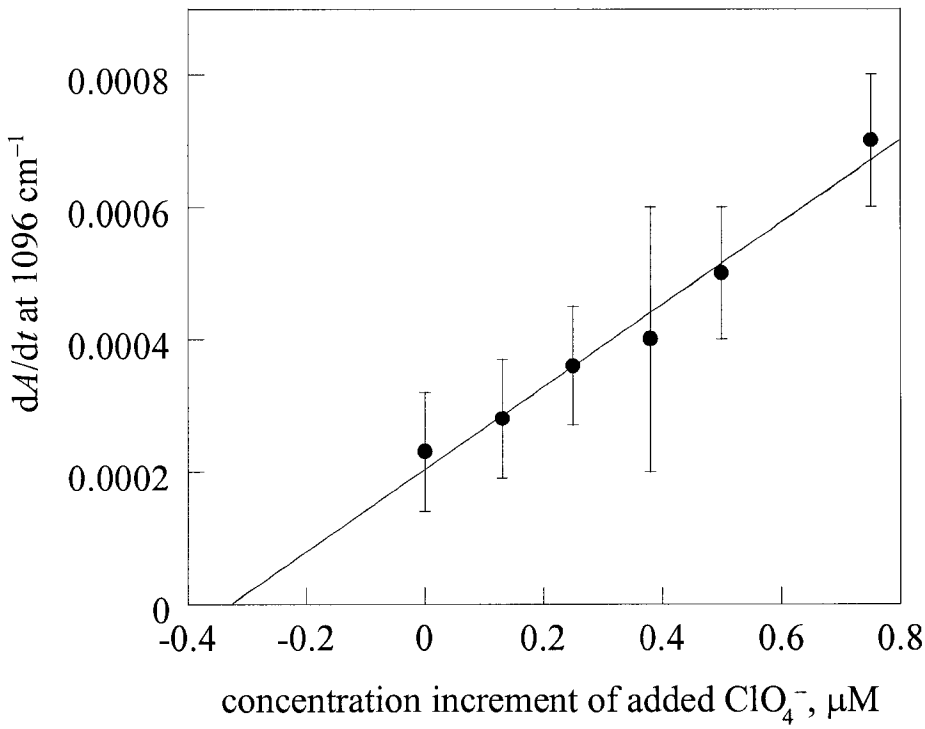

Figure 3.30. Standard addition graph for fertilizer sample #4. Using this graph, the absolute value of the *x*-axis intercept, 0.32 ± 0.04 μM, corresponds to the amount of ClO_4^- in the 100 mg L^{-1} fertilizer solution. After accounting for dilution, there was 10 ± 1 μM ClO_4^- in the 3 g L^{-1} stock solution of this fertilizer. The equation for the least squares linear fit is $y = 6.2(5) \times 10^{-4}x + 2.0(2) \times 10^{-4}$ with a correlation coefficient of 0.98. Error bars represent ±1σ.

reproducibility of dA/dt values for these standard addition graphs ranged from 3 to 50% relative standard deviation.

A sample of Bulldog Soda was also analyzed by the method of standard additions using the $DEC^{+}NO_3^{-}$-coated silicon probe. Since Bulldog Soda consists of sodium nitrate that was mined as Chili saltpeter, it was expected to contain some detectable amount of ClO_4^{-}. As shown in Figure 3.31, a large, well-defined ClO_4^{-} peak can be seen for the analysis of 10 mg L^{-1} Bulldog Soda. The standard addition quantification curve for Bulldog Soda is shown in Figure 3.32. The 10 g L^{-1} Bulldog Soda stock solution contained 0.23 ± 0.03 mM ClO_4^{-} which is ca. 10 times higher concentration ClO_4^{-} than in the three hydroponic fertilizer stock solutions shown to contain perchlorate.

In addition to analysis by ATR-FTIR done in our labs, the seven hydroponic fertilizers were also analyzed by Raman, complexation electrospray ionization mass spectrometry (cESIMS), and IC.[15] Perchlorate was not detected by any of the techniques in four of the seven hydroponic fertilizers. The concentrations of ClO_4^{-} for the fertilizers using the four different techniques are listed in Table 3.11. Note that the concentrations of NO_3^{-} and ClO_4^{-} reported in Tables 3.10 and 3.11, respectively, assume complete extraction of water-soluble analytes from the solid matrixes in all cases. This has not been independently established. All of the fertilizers were dissolved completely (i.e., no solids were visible in the stock solutions after thorough mixing) for the ATR-FTIR analyses. Complete extraction may not have been achieved for all of the solid fertilizer matrixes in the other three laboratories, particularly when high solid-to-water ratios were used and some undissolved solids remained (this was the case with some extracts for the Raman experiments[15]). However, reasonable quantitative agreement for perchlorate concentrations among all techniques is consistent with near-complete extraction of perchlorate, and possibly nitrate as well. In fact, ClO_4^{-} concentrations determined by ATR-FTIR are the same within $\pm 1\sigma$ for fertilizer #4, $\pm 2\sigma$ for Bulldog Soda, and $\pm 3\sigma$ for fertilizers #1 and #2, demonstrating the accuracy of the ATR-FTIR method.

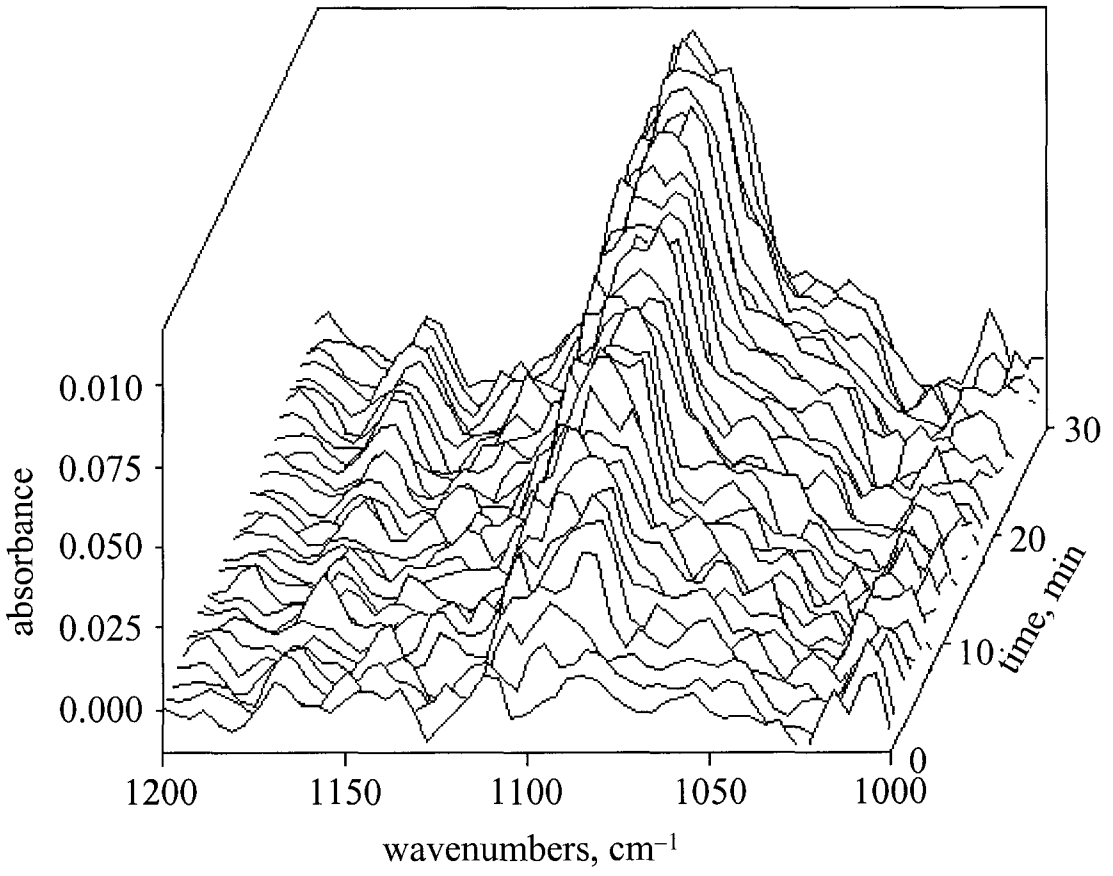

Figure 3.31. ATR-FTIR detection of ClO_4^- in 10 mg L^{-1} of Bulldog Soda (100 mL) using the silicon probe coated by evaporation of 20 μL of a 1 mM dichloromethane solution of $DEC^+NO_3^-$. A single band for $DEC^+ClO_4^-$ can be seen at 1096 cm^{-1}, which corresponds to 0.23 ± 0.03 μM aqueous ClO_4^- in this fertilizer solution.

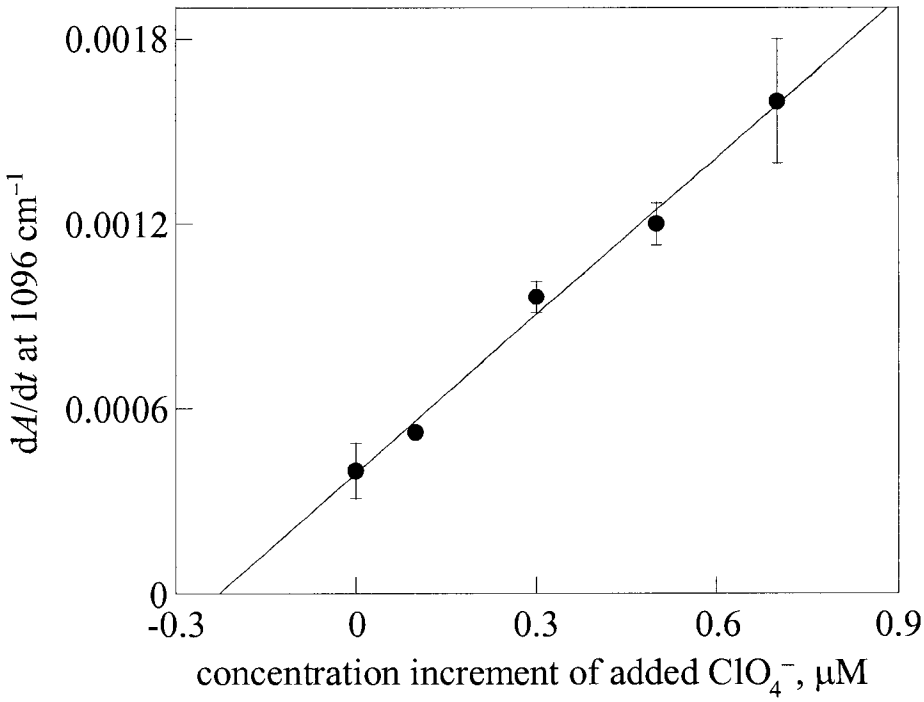

Figure 3.32. Standard addition graph for the fertilizer Bulldog Soda. Using this graph, the absolute value of the *x*-axis intercept, 0.23 ± 0.03 μM, corresponds to the amount of ClO_4^- in the 10 mg L^{-1} fertilizer solution. After accounting for dilution, there was 0.23 ± 0.03 mM ClO_4^- in the 10 g L^{-1} stock solution of this fertilizer. The equation for the least squares linear fit is $y = 1.71(8) \times 10^{-3}x + 3.9(3) \times 10^{-4}$ with a correlation coefficient of 0.993. Error bars, one of which is smaller than its point, represent ±1σ.

Table 3.11. Concentration of ClO_4^- in hydroponic fertilizers analyzed by ATR-FTIR spectroscopy, Raman spectroscopy, cESIMS, and IC[15]

sample #	ClO_4^- concentration, mg kg^{-1} [a]			
	ATR-FTIR[b]	Raman	cESIMS[c]	IC[d]
Bulldog Soda[e]	2200 ± 300	1759 ± 111	na[f]	na
1	120 ± 30	92 ± 5	230 ± 29	202 ± 2
2	380 ± 30	352 ± 87	483 ± 16	319 ± 16
3	nd[g]	nd	nd	nd
4	320 ± 40	268 ± 12	323 ± 15	285 ± 9
5	nd	nd	nd	nd
6	nd	nd	nd	nd
7	nd	nd	nd	nd

[a] ClO_4^- concentration in product as purchased. Value is mean ± sample standard deviation. To convert to weight percent perchlorate, divide by 10,000. [b] This work. [c] cESIMS = complexation electrospray ionization mass spectrometry. [d] IC = ion chromatography. [e] Bulldog Soda is $NaNO_3$ derived solely from Chilean caliche. [f] na = not analyzed. [g] nd = not detected. Detection limits differ for each technique and for each matrix, but nd can be approximated as $ClO_4^- < 30$ mg kg^{-1}.

In another study that used Raman spectroscopy to quantify ClO_4^- in nitrate fertilizers, Williams et al. calculated the perchlorate-to-nitrate concentration ratio (w/w).[12] They compared the ratios found from fertilizers that were commercially available in 1998 and 1999 to those from historical data from the soluble components in mined Chilean caliche. The historical minimum and maximum perchlorate-to-nitrate ratios, 3.7×10^{-4} and 9.0×10^{-2}, respectively, were based on eight samplings of large tonnages of ore mined by nitrate companies in northern Chile over a period of about 50 years.[131] If the perchlorate-to-nitrate ratio falls within or near this range, it is possible that the source of the ClO_4^- in that fertilizer could have originated from mined Chilean caliche.

The perchlorate-to-nitrate concentration ratios shown in Table 3.12 were determined for the three ClO_4^--containing hydroponic fertilizers and for Bulldog Soda using both ATR-FTIR (this work) and Raman spectroscopy.[15] Note that it is possible to determine perchlorate-to-nitrate concentration ratios with IC as well, but this would have been less convenient than the spectroscopic measurements because different IC columns and different IC methods are needed to measure NO_3^- and ClO_4^-. Since Bulldog Soda is known to be derived solely from mined Chilean caliche, its evaluation can serve as an independent assessment of the perchlorate-to-nitrate concentration ratio test. This test was informative, since the perchlorate-to-nitrate ratio for Bulldog Soda (2.8×10^{-3}) was between the aforementioned minimum and maximum ratios. The perchlorate-to-nitrate concentration ratios for the fertilizers, as well as the ratio for Bulldog Soda, are clustered near the lower end of the historical range for the mined ore (although the value for sample #1 falls just below the lower end of the range). Based on these observations, it is possible that the ClO_4^- found in these fertilizers could have originated from mined Chilean caliche. It is important to point out that improvements in the refinement process for Chilean caliche are resulting in a substantial reduction of the amount of ClO_4^- in fertilizer products containing components derived from Chile saltpeter.[13]

Table 3.12. Perchlorate-to-nitrate concentration ratios (w/w) from ATR-FTIR and Raman spectroscopic analysis[a]

sample #[b]	$[NO_3^-]/[ClO_4^-]$[c]	$10^3 \times ClO_4^-/NO_3^-$ w/w ratio ATR-FTIR[d]	$10^3 \times ClO_4^-/NO_3^-$ w/w ratio Raman[e]
Bulldog Soda	560 ± 80	2.8 ± 0.4	2.4 ± 0.2
1	9000 ± 2000	0.19 ± 0.05	0.17 ± 0.01
2	740 ± 60	1.9 ± 0.2	2.4 ± 0.6
4	1700 ± 200	0.8 ± 0.3	0.81 ± 0.05

[a] The historical minimum and maximum perchlorate-to-nitrate w/w ratios are 3.7×10^{-4} and 9.0×10^{-2}, respectively.[12] [b] Bulldog Soda is $NaNO_3$ derived solely from Chilean caliche. Samples #3 and #5–7 did not contain detectable amounts of perchlorate. Therefore they were not included in this table. [c] Molar ratios were calculated for the stock solution of each fertilizer (10 g L^{-1} for all fertilizers except #4, which was 3 g L^{-1}) from the NO_3^- concentration data in Table 3.11 and the ClO_4^- concentrations given in the text. [d] This work. [e] Colette et al.[15]

More importantly, Table 3.12 shows that low micromolar concentrations of aqueous ClO_4^- are able to be quantified using the method of standard additions with ATR-FTIR even in the presence of up to 9,000-times molar excess of aqueous NO_3^-. This large excess of NO_3^- is even greater than the 1,000-fold excess listed in Table 3.9 for the detection of 1 μM ClO_4^-. The ability to detect these small concentrations of ClO_4^- in complex fertilizer matrixes attests to the selectivity, and therefore the versatility, of the $DEC^+NO_3^-$-coated probe ATR-FTIR method.

Analysis of $CF_3SO_3^-$ in the presence of excess NO_3^-. Given the results for the analysis of ClO_4^- in the presence of large excesses of NO_3^-, it was desired to confirm this trend using a different target analyte, $CF_3SO_3^-$. The matrix anion was chosen to be NO_3^- since it is a ubiquitous contaminant in groundwater and surface water and its presence is easily monitored at a wavenumber (1351 cm^{-1}) that does not interfere with most extractable anions. Also, since the $DEC^+NO_3^-$-coated probe was being used, NO_3^- is already present in the equilibrium expression for the ion exchange and no new anions are being introduced to make the expression more complex. The presence of a 10-fold molar excess KNO_3 did not affect the initial dA/dt value for a 15 μM $CF_3SO_3^-$ solution (i.e., dA/dt = 0.061 min^{-1} for both 15 μM $CF_3SO_3^-$ in DI water and 15 μM $CF_3SO_3^-$ in the presence of 150 μM NO_3^-). A solution of 15 μM $CF_3SO_3^-$ in the presence of 0.1 M NO_3^- (ca. 7000 times molar excess NO_3^-) was also examined with the $DEC^+NO_3^-$-coated silicon probe. Even after six hours, no $CF_3SO_3^-$ peaks were observed to grow in. This indicates that the $CF_3SO_3^-/NO_3^-$ ion-exchange equilibrium lies far to the side containing $DEC^+NO_3^-$ when the $[CF_3SO_3^-]/[NO_3^-]$ ratio is ca. 7000. Note that the difference between perchlorate and triflate ion exchange with $DEC^+NO_3^-$ in the presence of a large excess of nitrate suggests that the absolute value of the hydration energy of ClO_4^- is larger than that of $CF_3SO_3^-$.

Analysis of $PMPA^-$ in the presence of a complex matrix. The effect of a complex water matrix on the detection of $PMPA^-$ was examined. The ingredients of a

synthetic tap water matrix (currently used as a standard by the U.S. military) are listed in Table 3.13. As a point of reference, many of the components in this synthetic tap water are at concentrations near the upper concentration limits for Fort Collins, Colorado drinking water.[132] The 10-minute LOD for $PMPA^-$ in synthetic tap water using the uncoated diamond probe was found to be 0.4 mM with a *SNR* of 4 ± 1. The 10-minute LOD for $PMPA^-$ in synthetic tap water using the DEC^+Cl^--coated diamond probe was found to be 0.2 mM with a *SNR* of 4.0 ± 0.7 (the data for this LOD was collected by Dr. Stephanie C. Bowman in the Strauss Research Group). The details of these LOD determinations can be found in Appendix D. Although the $PMPA^-$ LOD in synthetic tap water using the uncoated probe is similar to that in DI water (0.3 mM), the DEC^+Cl^--coated probe LOD for $PMPA^-$ of 200 μM in synthetic tap water is significantly higher than the LOD in DI water (0.7 μM). Additionally, there is only a two-fold increase in sensitivity for the coated versus uncoated synthetic tap water LODs compared to a 430-fold increase in sensitivity for the coated versus uncoated DI water LODs.

The high LOD for $PMPA^-$ in synthetic tap water using the DEC^+Cl^--coated probe is probably caused by the high concentration of NO_3^- (12 μM) in the matrix, which will compete with $PMPA^-$ during the ion exchange with DEC^+Cl^-. The presence of a large number of other anions at various concentrations will also negatively affect the extraction of $PMPA^-$ by DEC^+Cl^-. The effect of these interferences can be seen in the 10-fold increase in the noise used to calculate the *SNR*, $1.9(2) \times 10^{-4}$ with DI water versus $1.9(2) \times 10^{-3}$ with synthetic tap water over the same wavenumbers range. Conversely, the noise for the uncoated probe LODs remained the same within error for DI water and synthetic tap water ($1.0(3) \times 10^{-4}$ and $8(2) \times 10^{-5}$, respectively).

Counter-ion effects. A control study was done using the $DEC^+NO_3^-$-coated silicon probe to detect 1 μM ClO_4^- with four different counter-ions (Li^+, Na^+, K^+, and NH_4^+). It was found that the initial dA/dt values were the same to within $\pm 3\sigma$ and the 10-minute *SNR*s were the same to within $\pm 2\sigma$ for 1 μM solutions of ClO_4^- with the four

Table 3.13. Synthetic tap water recipe[a]

compound	concentration, mg L^{-1}	concentration, μM
$NaHCO_3$	100	1200
$MgSO_4$	6.7	56
$CaSO_4$	27.0	199
K_2HPO_4	0.7	4
KH_2PO_4	0.3	2
$(NH_4)_2SO_4$	0.01	0.08
NaCl	0.01	0.2
$FeSO_4$	0.001	0.007
$NaNO_3$	1.0	12
Humic Acid	1.0	na[b]
Fulvic Acid	1.0	na
pH	7.6–7.8[c]	na

[a] This recipe was provided by Janet Jensen from the Joint Services Agent Water Monitor program of the US military in March 2003. [b] na = not applicable. [c] The pH range listed is dimensionless.

different counter-ions. Note that most of the experiments described in this dissertation were done using the perchlorate salts of one of these cations. Since these four salts are undoubtedly completely dissociated at 1 μM, it is sensible that there is no counter-ion effect.

Reproducibility. Various aspects of these ATR-FTIR experiments were monitored for reproducibility. When using the uncoated probes, for example, the relative standard deviations of the average absorbance values for all of the anions ranged from 1 to 33% (see Appendix B for individual values) with a median of 10%. The relative standard deviations of the average absorbance values for all of the anions using the coated probes ranged from 2 to 38% (see Appendix C for individual values), with a median of 14.5%. Table 3.7 shows the reproducibility of the noise values for both the coated and uncoated probes over various wavenumber ranges, which have standard deviations of 11–33% for 11–32 trials (all but one set of these noise values are within a range of 11–18% error). The absolute absorbance of ν(CH) and ν(NO) bands from 46 $DEC^+NO_3^-$ coatings on the silicon probe were within ±6%, as shown in Appendix A. For nine $DEC^+NO_3^-$ coatings on the silicon probe, the initial dA/dt values for a solution of 5 μM ClO_4^- were reproducible to within ±11%. Finally, the error in the initial dA/dt values determined for the three calibration curves ranged from 3 to 26%. For the four fertilizer standard addition plots, the range was 1 to 50% . As can be seen by these statistics, the ATR-FTIR method is reasonably precise.

Analysis of extractant coating thickness. The coating thickness was optimized for perchlorate detection by coating the silicon probe with 20 μL of dichloromethane solutions of $DEC^+NO_3^-$ ranging in concentration from 0.1 to 10 mM. The more concentrated extractant solutions resulted in more intense ν(CH) and ν(NO) IR bands due to the thicker coatings on the ATR crystal. For each experiment, the coated probe was immersed in 5 μM aqueous $LiClO_4$ and spectra were recorded every minute for 15 minutes. As can be seen from the graph in Figure 3.33, coatings prepared from the 3 mM

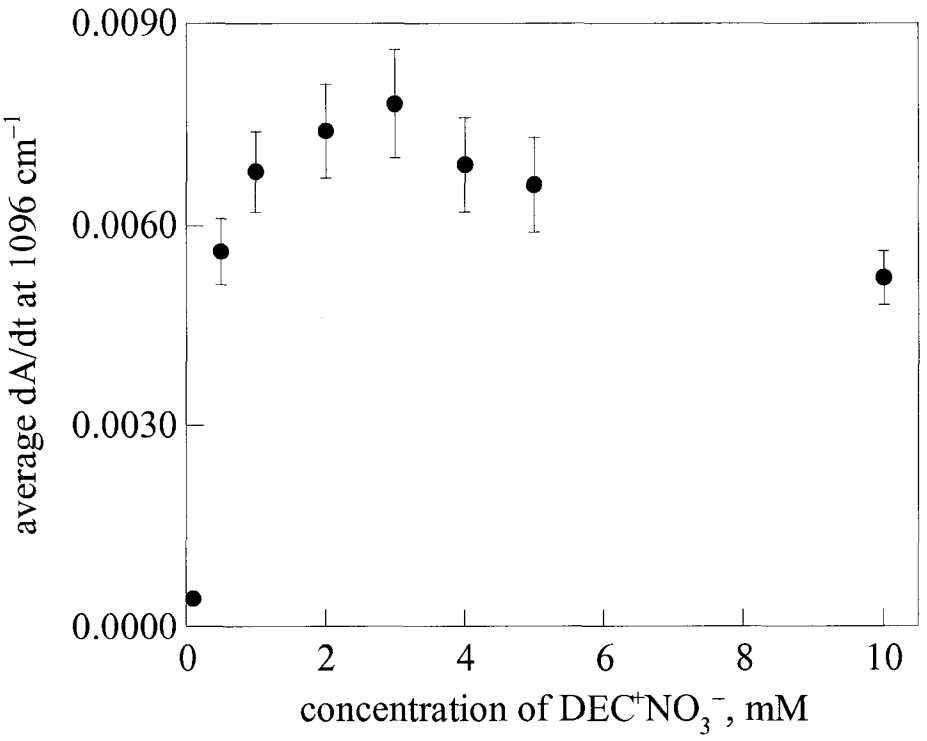

Figure 3.33. The initial d*A*/d*t* for the detection of 5 μM ClO_4^- using the silicon probe coated with various concentrations of $DEC^+NO_3^-$. Points are the average of at least three trials of each concentration of $DEC^+NO_3^-$ and the silicon probe was coated with 20 μL of each dichloromethane solution. Error bars represent ±1σ.

$DEC^+NO_3^-$ solution resulted in the largest initial dA/dt values while coatings made from both higher and lower concentrations of $DEC^+NO_3^-$ had smaller initial dA/dt values. After this set of experiments was completed, all subsequent experiments were done using a 3 mM $DEC^+NO_3^-$ solution to coat the surface of the ATR crystal. Some experiments that had been completed before this optimization was performed are also reported in this dissertation. The DEC^+Cl^--coating thickness for $PMPA^-$ detection was not optimized.

The measured and calculated thicknesses of these $DEC^+NO_3^-$ coating can be compared to the penetration depths (d_p) of the evanescent wave for the various ATR crystals. An approximate coating thickness of 0.2 μm was calculated using the equation for the volume of a cylinder and the known density of $DEC^+NO_3^-$ (1.1 g cm^{-3}), which was previously determined by X-ray crystallography.[61] An actual coating thickness of ca. 0.1 μm was estimated by ellipsometry (WVASE 32, J. A. Woolam Co Inc, Lincoln, NE) using a $DEC^+NO_3^-$-coated silicon wafer. Table 3.14 lists d_p values at four different IR wavenumbers calculated using Equation 3.14 for both the uncoated and $DEC^+NO_3^-$-coated silicon and diamond crystals. The wavenumber range, 4000 to 650 cm^{-1}, was chosen since it is the range of the IR spectra in this study. The other two points, 1555 and 1000 cm^{-1}, are the boundaries of the useful part of the fingerprint region that is most commonly examined when using either the silicon or diamond ATR probes. The index of refraction of a thin-film coating of $DEC^+NO_3^-$ was determined to be ca. 1.5 by ellipsometry. Both of the ATR probes used have a manufacturer-specified θ value of 45°.

As can be seen from Table 3.14, the evanescent wave penetrates 0.40 to 1.75 μm beyond the surface of the ATR crystal in the fingerprint region of the IR spectrum for $DEC^+NO_3^-$-coated ATR crystals. Therefore, the entire thickness of the coating, 0.1–0.2 μm, is sensed by the evanescent wave. In addition, the evanescent wave also penetrates into the aqueous solution in contact with the thin-film coating. However, since the analyte concentrations used for the coated probe experiments are much too dilute, by orders of magnitude, for the analyte to be detected in aqueous solution, only the analyte

Table 3.14. Calculated evanescent wave penetration depths (d_p)

interface	n_1	n_2	d_p (μm) at the indicated wavenumber[a]			
			4000 cm^{-1}	1555 cm^{-1}	1000 cm^{-1}	650 cm^{-1}
silicon/water	3.5	1.3	0.15	0.39	0.61	0.93
silicon/$DEC^+NO_3^-$	3.5	1.5	0.16	0.40	0.62	0.96
diamond/water	2.4	1.3	0.26	0.67	1.05	1.61
diamond/$DEC^+NO_3^-$	2.4	1.5	0.28	0.73	1.14	1.75

[a] Evanescent wave penetration depths (d_p) were calculated using Equation 3.14 where $\theta = 45°$.

that has undergone ion exchange with NO_3^- or Cl^- in the coating can be detected. In other words, the aqueous analyte is "invisible" in the DEC^+X^--coated probe experiments.

In a different set of experiments, it was determined that the maximum absorbance of the ClO_4^- peak and the time required to reach this maximum is linearly related to the concentration of the $DEC^+NO_3^-$ solution used to coat the silicon probe. A solution of 5 μM ClO_4^- was put in contact with the $DEC^+NO_3^-$-coated silicon probe (coated with four different concentrations of the $DEC^+NO_3^-$ coating solution) and the extraction was allowed to proceed to completion (equilibrium). As can be seen from Figure 3.34, the maximum absorbance of the ClO_4^- peak gradually increases as the concentration of the $DEC^+NO_3^-$ coating solution increases. As expected, the more $DEC^+NO_3^-$ available on the probe for ion exchange, the higher the absorbance due to ClO_4^- at equilibrium. This relationship is approximately linear until the coating becomes thick enough that the evanescent wave can not penetrate the entire coating. When using a 10 mM $DEC^+NO_3^-$ solution to coat the silicon probe, it was estimated that the coating is ca. 4.4 μm thick, thicker than the 1 μm penetration depth for the evanescent wave at 650 cm^{-1}. In this case, the entire thickness of the $DEC^+NO_3^-$ coating is not being sensed by the evanescent wave, therefore, the relationship between the maximum absorbance and the coating solution concentration is no longer linear. Note that it took more time to reach the maximum absorbance of the ClO_4^- peak for coatings made from the more concentrated $DEC^+NO_3^-$ solutions.

Temperature effects. Preliminary experiments demonstrated that initial dA/dt values for aqueous solutions of ClO_4^- in contact with a $DEC^+NO_3^-$-coated probe depend on the temperature of the aqueous solution. As would be expected, the initial dA/dt values increased with temperature (2, 23, and 35 °C) for the $DEC^+NO_3^-$-coated silicon probe in contact with a 5 μM solution of $CF_3SO_3^-$. At 45 °C, the initial dA/dt values decreased slightly to within the range for 2 or 23 °C. It is possible that this higher temperature may

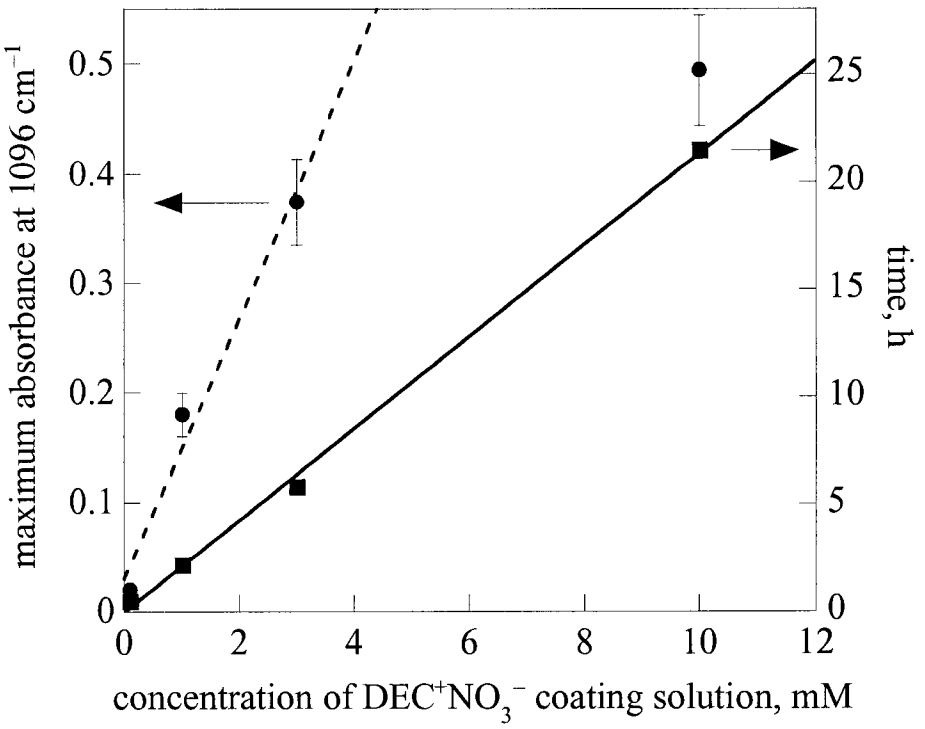

Figure 3.34. The maximum absorbance (circles, left axis) and time to reach the maximum absorbance (squares, right axis) for the detection of 5 μM ClO_4^- using the silicon probe coated with various concentrations of $DEC^+NO_3^-$. Points are the average of at least three trials of each concentration of $DEC^+NO_3^-$ and the silicon probe was coated with 20 μL of each dichloromethane solution. Error bars, some of which are smaller than the points, represent ±1σ.

cause the $DEC^+NO_3^-$ coating to become unstable and possibly undergo nucleophilic decomposition at a faster rate, which will be discussed in detail below.

Stability of DEC^+X^- coated probes in water. It has been determined by a previous member of the Strauss Research Group that tetraalkylated ferricenium salts, such as HEP^+X^-, undergo nucleophilic decomposition in the presence of anionic nucleophiles.[133] Gansle's study, as well as the extensive literature on ferricenium salt decomposition, support a 3:2 conversion of ferricenium to ferrocene upon decomposition with an anionic nucleophile as shown in Equation 3.19.[133-138] Because of this precedent, it was desired to determine if nucleophilic decomposition occurs when using $DEC^+NO_3^-$-coated silicon ATR crystals.

$$3DEC^+X^- \longrightarrow 2DEC^0 + Fe^{2+} + 3X^- + \text{organics} \qquad (3.19)$$

The $DEC^+NO_3^-$-coated silicon probe was contacted with DI water (i.e., an analyte was not added) and spectra were collected for 24 hours. The absorbance of the ν(CH) band at 2926 cm^{-1} and the ν(NO) band at 1355 cm^{-1} from the $DEC^+NO_3^-$ coating were monitored as shown in Figure 3.35. Both of these bands initially decreased and then leveled off at an approximately constant absorbance. The initial decrease in the ν(CH) band occurs during the first 10 minutes of analysis which is the time typically used to equilibrate the coating before an analyte is added to the solution. After 24 hours, the ν(CH) bands can still be clearly seen as shown in Figure 3.36. However, the decrease in the ν(NO) band occurs over a longer time range and apparently results from the complete loss of NO_3^- from the coating. After ca. four hours, no ν(NO) band is observed in the spectrum.

The loss of NO_3^- from the $DEC^+NO_3^-$ coating during contact with water could indicate that NO_3^- is acting as a nucleophile and facilitating the decomposition of $DEC^+NO_3^-$ to DEC^0. Even if all of the NO_3^- is removed from the coating into the

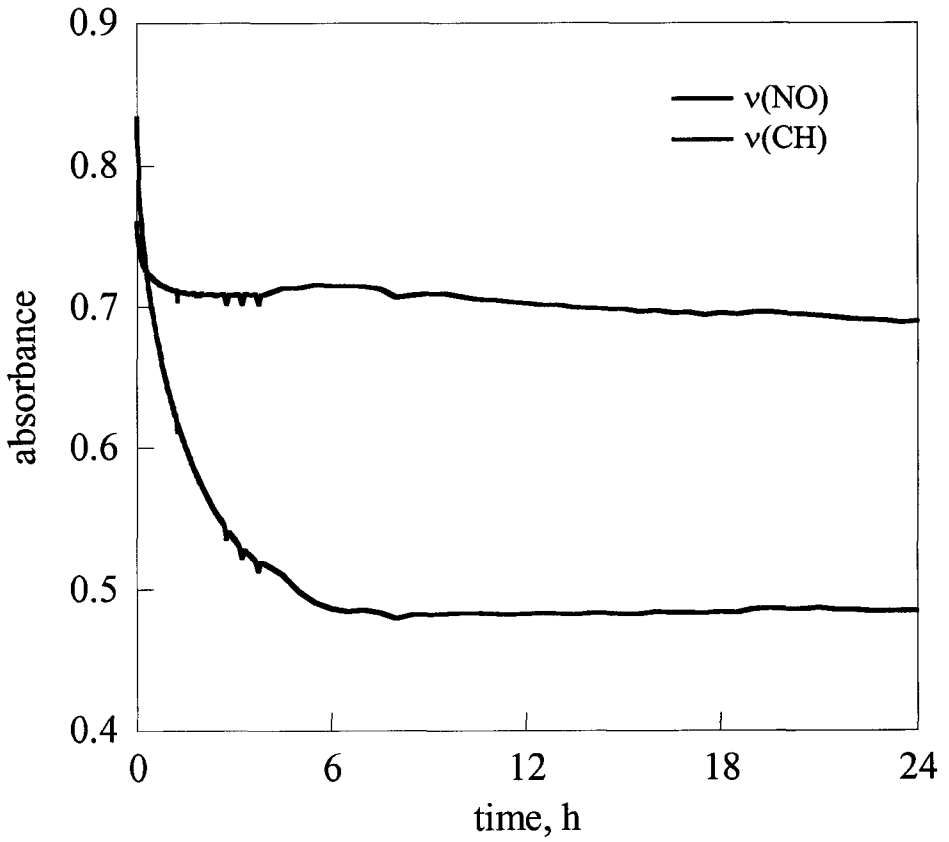

Figure 3.35. Absorbance of the ν(NO) band at 1355 cm^{-1} and the ν(CH) band at 2926 cm^{-1} for the analysis of the silicon probe coated with 20 μL of a 1 mM dichloromethane solution of $DEC^{+}NO_3^{-}$ in contact with only DI water for 24 hours.

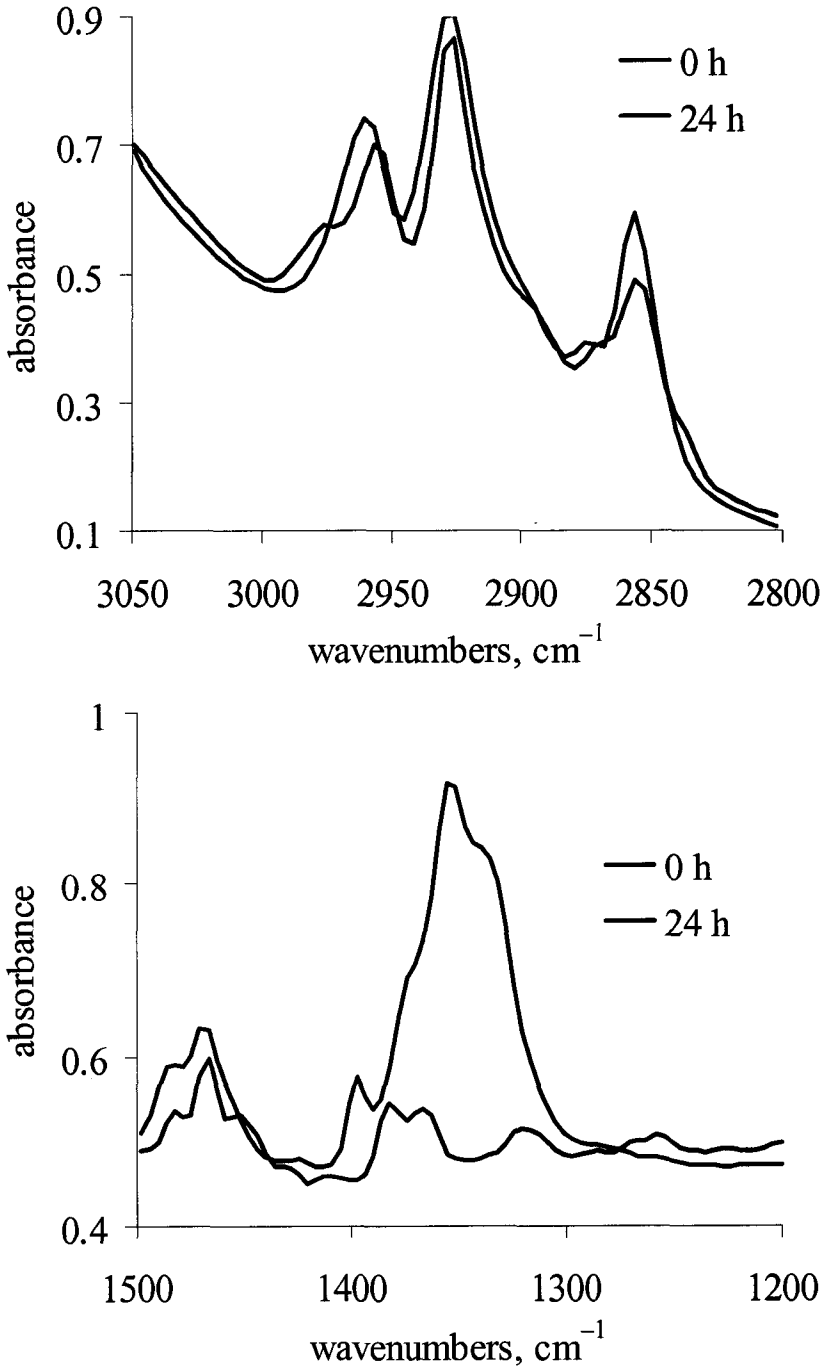

Figure 3.36. ATR-FTIR spectra collected immediately after the $DEC^{+}NO_3^{-}$-coated silicon probe was contacted with DI water and after 24 hours in contact with DI water. The top graph shows the region of the spectrum containing the ν(CH) bands while the bottom graph shows the region containing the ν(NO) band.

solution the concentration of aqueous NO_3^- (ca. 0.2 μM) would be too small to be detected. Note that the 10-minute LOD for NO_3^- using the uncoated probe is ca. 1 mM. A separate experiment was set up to mimic the conditions of the coated silicon probe at much larger volumes so that changes in the $DEC^+NO_3^-$ coating could be monitored by UV-vis. Using an amount proportional to that used on the silicon probe, a large circular silicon wafer (10 cm diameter) was coated with a 1 mM dichloromethane solution of $DEC^+NO_3^-$. The coated wafer was immersed in 1 L of DI water and stirred for seven days. After removal from the water, the wafer was air dried and the coating was dissolved in an appropriate volume of dichloromethane.

A standard 1 mM $DEC^+NO_3^-$ solution (before contact with water) and the ca. 1 mM solution made from the coating after contact with water for seven days were examined by UV-vis spectroscopy. This allowed the change in color that occurs when green $DEC^+NO_3^-$ (λ_{max} at 686 nm) is converted to orange DEC^0 (λ_{max} at 467 nm) to be monitored quantitatively. The UV-vis spectra in Figure 3.37 show the complete conversion of $DEC^+NO_3^-$ to DEC^0 over the seven day period, which indicates that $DEC^+NO_3^-$ is being either reduced or otherwise decomposed in a manner that includes partial reduction. Since there are no known reducing agents present in the system, it can be assumed that $DEC^+NO_3^-$ is undergoing auto-nucleophilic decomposition (i.e., the nitrate ion is the nucleophile). To investigate this further, the dichloromethane solution made from the coating after contact with water for seven days was oxidized with $Fe(NO_3)_3$ to see if the expected 66% (i.e., 2/3) of the original $DEC^+NO_3^-$ could be recovered. The absorbance of the 686 nm peak after oxidation was 69% of the absorbance of the $DEC^+NO_3^-$ solution before contact with the silicon wafer. Combined with the IR evidence, this suggests that when $DEC^+NO_3^-$ is on a silicon surface *in the presence of water* it undergoes nucleophilic decomposition, presumably with NO_3^- acting as the nucleophile.

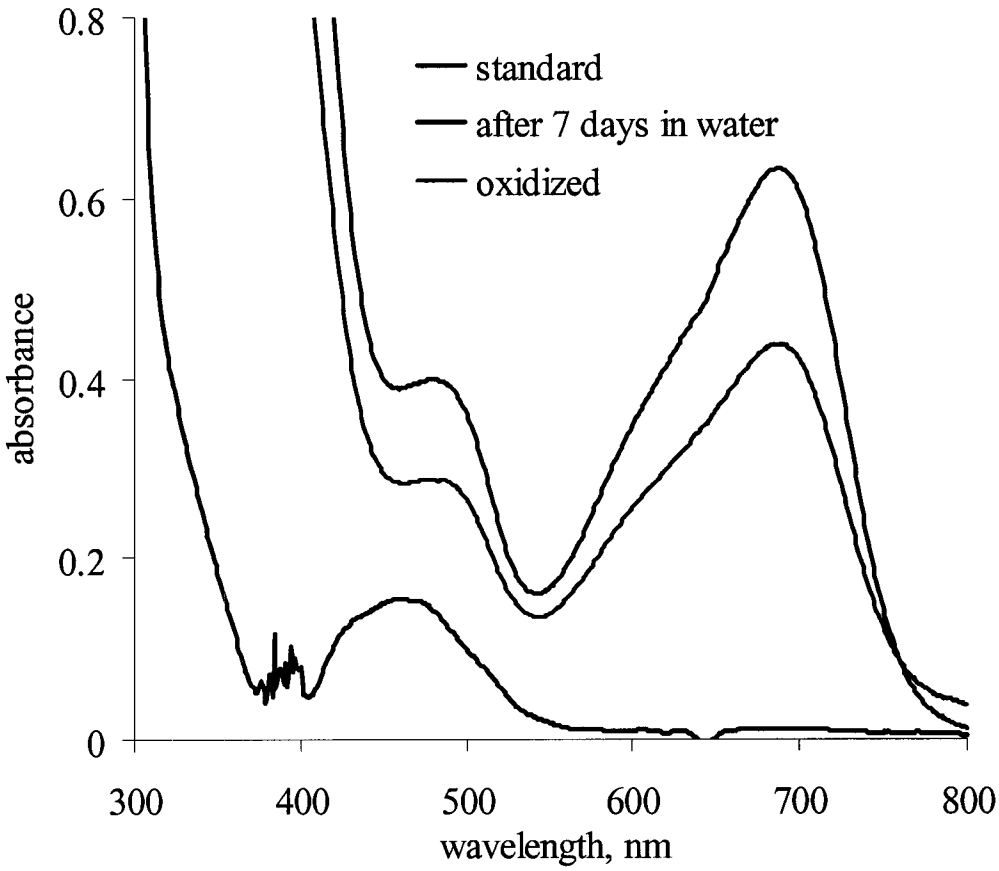

Figure 3.37. UV-vis spectra of three dichloromethane solutions. The black spectrum is of a 1 mM solution of $DEC^{+}NO_3^{-}$ before it was used to coat a large silicon wafer. The blue spectrum is of a ca. 1 mM solution made from the coating after contact with water for seven days. The red spectrum is the same solution as the blue spectrum after it was oxidized with $Fe(NO_3)_3$.

If $DEC^+NO_3^-$ on the coated silicon probe in contact with water is undergoing nucleophilic decomposition, then this decomposition should be slower or should not occur at all when the DEC^+X^- coating is made with an X^- anion that is a weaker nucleophile than nitrate. Two weaker nucleophiles, ClO_4^- and $CB_{11}H_{12}^-$, were ion paired with DEC^+ in dichloromethane by liquid-liquid ion-exchange reactions, and the solutions of $DEC^+ClO_4^-$ and $DEC^+CB_{11}H_{12}^-$ were used to coat the silicon ATR probe. The coatings were exposed to DI water for 24 hours while the DEC^+X^- coatings were monitored by IR. For both the $DEC^+ClO_4^-$- and $DEC^+CB_{11}H_{12}^-$-coated probes, the ν(CH) bands initially decreased within the first 10 minutes, and then leveled off. Large ν(CH) bands were observed after 24 hours, similar to what was observed in the case of $DEC^+NO_3^-$ coatings.

The time dependence of the absorbance of the ν(ClO) and ν(BH) bands from the $DEC^+ClO_4^-$ and $DEC^+CB_{11}H_{12}^-$ coatings, respectively, are compared to that of the ν(NO) band from the $DEC^+NO_3^-$ coating over a 24 hour period in Figure 3.38. After an initial rapid decrease of both the ClO_4^- and $CB_{11}H_{12}^-$ peaks, the ClO_4^- peak continued to decrease at a slow rate, while the $CB_{11}H_{12}^-$ peak stayed constant. The spectrum of the $DEC^+CB_{11}H_{12}^-$-coated silicon probe in Figure 3.39 shows the presence of both the ν(BH) and ν(CH) bands even after 24 hours. Similarly, although the ν(ClO) band had decreased slightly after 24 hours, it was still readily observable in the spectrum of the $DEC^+ClO_4^-$-coated silicon probe. The slow decrease of the ν(ClO) band over the 24 hour period could be due to the slower nucleophilic decomposition of $DEC^+ClO_4^-$, which one would expect to be slower than for $DEC^+NO_3^-$ but faster than for $DEC^+CB_{11}H_{12}^-$ based on the presumed relative strengths of the three nucleophiles, $NO_3^- > ClO_4^- > CB_{11}H_{12}^-$. All of these experiments support the hypothesis that $DEC^+NO_3^-$ undergoes nucleophilic decomposition when it is a coating on a silicon crystal in contact with DI water for long periods of time.

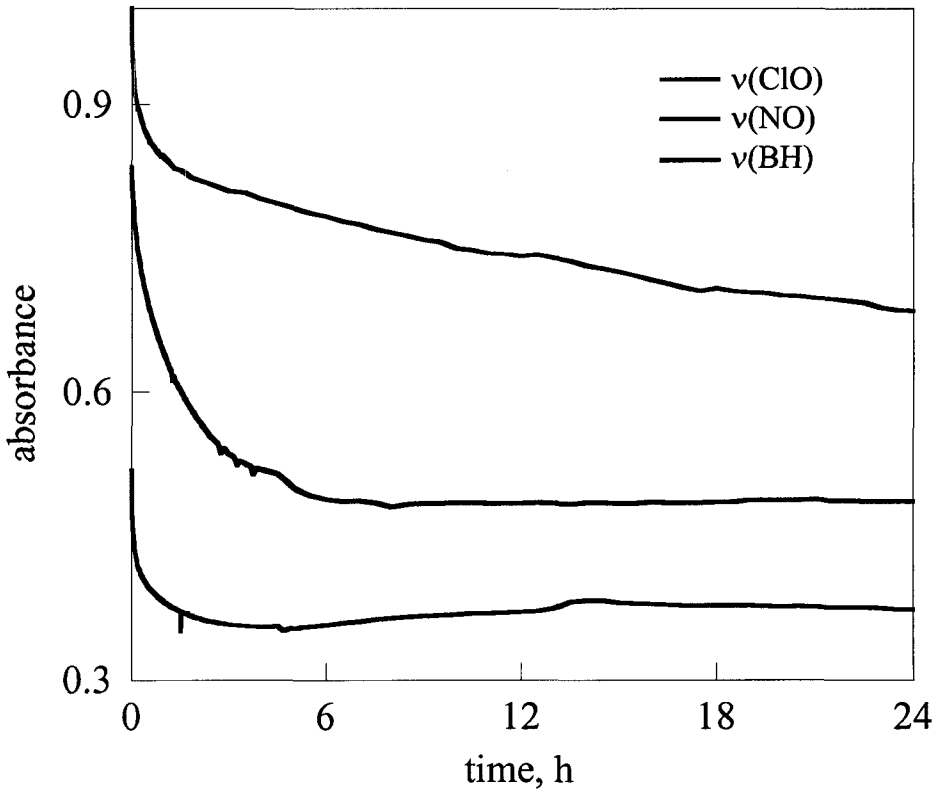

Figure 3.38. Absorbance of the ν(ClO) band at 1089 cm^{-1} from the $DEC^+ClO_4^-$-coated probe, the ν(NO) band at 1355 cm^{-1} from the $DEC^+NO_3^-$-coated probe, and the ν(BH) band at 2548 cm^{-1} from the $DEC^+CB_{11}H_{12}^-$-coated probe. In each case the silicon probe was coated by evaporation of 20 μL of a 1 mM dichloromethane solution of the DEC^+X^- extractant and contacted with DI water for 24 hours.

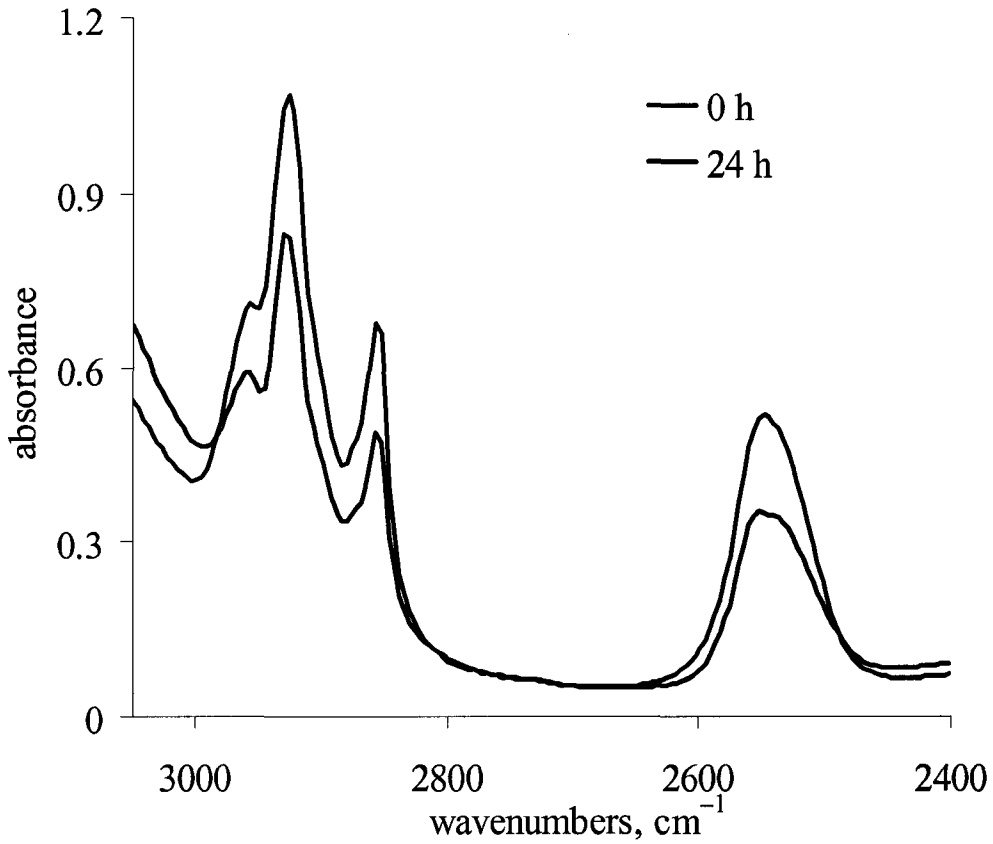

Figure 3.39. ATR-FTIR spectra collected immediately after the $DEC^{+}CB_{11}H_{12}^{-}$-coated silicon probe was contacted with water and after 24 hours in contact with water. Several ν(CH) bands are observed ca. 2900 cm^{-1} and one ν(BH) band is observed at 2548 cm^{-1}.

Redox-recycling of the extractant coating. One of the benefits of using a ferrocene-based ion-exchange compound as the ATR crystal coating is the possibility of recycling the coating through a redox cycle which would allow it to be used multiple times. The redox recycling of $HEP^+NO_3^-$ was detailed earlier in Figure 3.1. Work in the Strauss Research Group with redox-recyclable ferrocenes is related to the electrochemical or redox switching studies published by other groups.[139-145] These groups, as well as several members of the Strauss Research Group, have shown that the reversible binding of ions can be accomplished by electrochemically switching or redox switching an extractant molecule.[46,47,133]

A preliminary study was carried out with the $DEC^+CB_{11}H_{12}^-$-coated silicon probe to explore the possibility of recycling the coating. Due to the lack of long-term stability of $DEC^+NO_3^-$ coatings on the silicon probe, recycling was only possible using $DEC^+CB_{11}H_{12}^-$ coatings. After a 3 minute water equilibration, the $DEC^+CB_{11}H_{12}^-$-coated crystal was treated with an aqueous solution containing 0.1 M $Na_2S_2O_4$, a strong reducing agent ($E°(S_2O_4^{2-}/SO_3^{2-})$ = –0.94 V vs. NHE[146]). The IR spectra in Figure 3.40 showed that the ν(BH) band at 2548 cm^{-1} due to the $DEC^+CB_{11}H_{12}^-$ coating decreased over time until it almost reached the baseline while the intensities of the ν(CH) bands decreased only slightly. This corresponds to the reduction of the $DEC^+CB_{11}H_{12}^-$ coating to a neutral DEC^0 coating with the concomitant release of the $CB_{11}H_{12}^-$ anion to the aqueous solution, as shown in Equation 3.20.

$$2DEC^+CB_{11}H_{12}^-(s) + S_2O_4^{2-}(aq) + 2H_2O \longrightarrow 2DEC^0(s) + 2CB_{11}H_{12}^-(aq) + 2H_2SO_3(aq) \quad (3.20)$$

The reducing agent was removed after 17 minutes and the coating was gently rinsed with water. It was then treated with an aqueous solution containing 10 mM $Fe(NO_3)_3$ (an oxidizing agent) and 10 mM $CsCB_{11}H_{12}$ for the following 73 minutes. IR

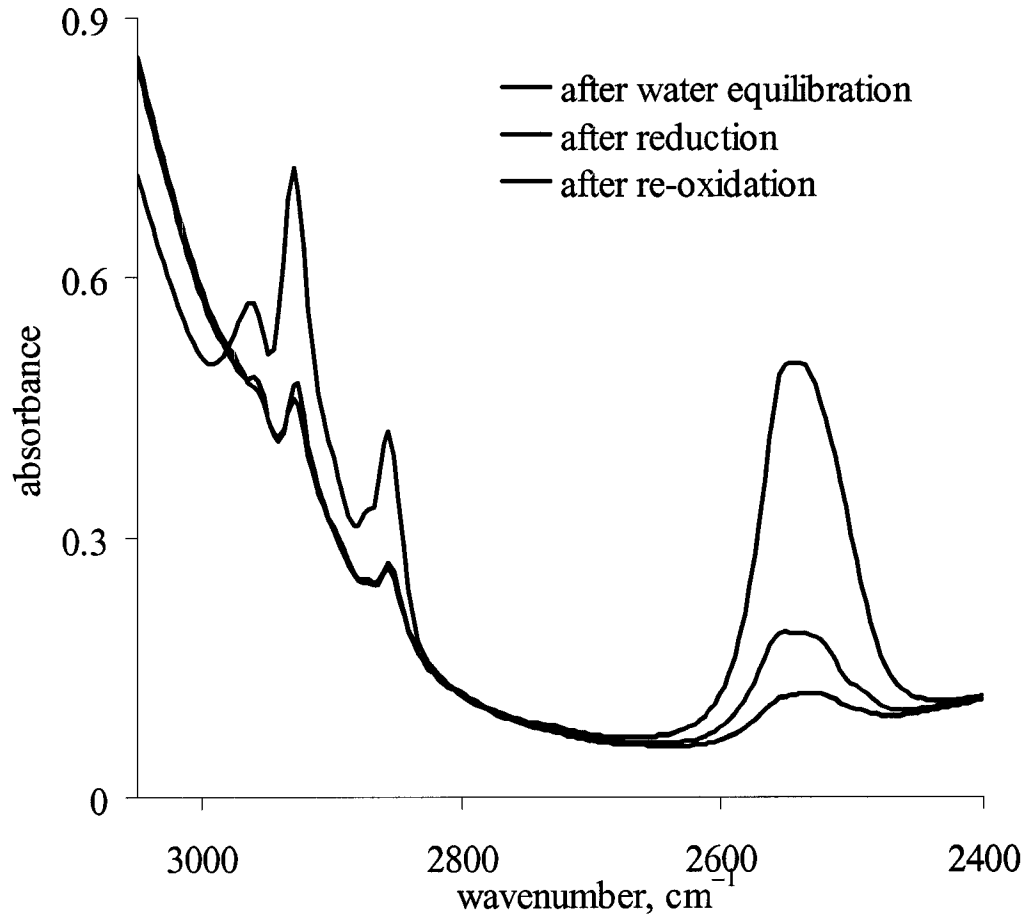

Figure 3.40. ATR-FTIR spectra of the reduction and oxidation of a $DEC^{+}CB_{11}H_{12}^{-}$-coating on the silicon probe. The first spectrum was collected after a 3 minute water equilibration, the second spectrum was collected after 17 minutes in contact with an aqueous solution containing 0.1 M $Na_2S_2O_4$ (reducing agent), and the third spectrum was collected after 73 minutes in contact with an aqueous solution containing 10 mM $Fe(NO_3)_3$ (oxidizing agent) and 10 mM $CsCB_{11}H_{12}$.

spectra showed that the ν(BH) band at 2548 cm^{-1} grew back in over time as the coating was reactivated (i.e., as the DEC^0 extractant was re-oxidized to $DEC^+CB_{11}H_{12}^-$), as also shown in Figure 3.40. The reactivation of the extractant and the detection of aqueous $CB_{11}H_{12}^-$ occur in one step in this example (Equation 3.21). Therefore, the

$$DEC^0(s) + Fe^{3+}(aq) + CB_{11}H_{12}^-(aq) \longrightarrow DEC^+CB_{11}H_{12}^-(s) + Fe^{2+}(aq) \quad (3.21)$$

$DEC^+CB_{11}H_{12}^-$ coating can be redox recycled, not only in principle but in practice. However, after only one redox cycle, the intensity of the ν(CH) bands decreased significantly. Therefore, a more permanent (i.e., more stable) DEC^+-like coating needs to be used before the coating can be efficiently redox recycled and reused.

Conclusions

This chapter has described the detection and identification of ≤ 0.7 μM perchlorate, chlorate, three perfluoroalkanesulfonates, and pinacolylmethylphosphonate in water *in 10 minutes* using ATR crystals coated with thin-films of the nitrate and chloride salts of the organometallic ion-exchange cation DEC^+. Although the method for depositing these coatings is very simple (i.e., evaporation of 20 μL of a dichloromethane solution on the ATR crystal surface), these thin-film coatings gave reproducible LODs to within ±33%. In general, the lowest LODs were obtained using the $DEC^+NO_3^-$-coated diamond probe prepared with a 3 mM dichloromethane solution of $DEC^+NO_3^-$. The use of the $DEC^+NO_3^-$-coated probes resulted in a large increase in sensitivity (170–23,000-fold) for weakly hydrated aqueous anions compared to the unmodified, commercially available probes.

Calibration curves for ClO_4^-, $PFOS^-$, and $PMPA^-$ were shown to be linear over at least one order of magnitude of concentration starting at or near the quantification limit with errors in the average dA/dt values ranging from 3 to 26%. To our knowledge, this is

the first time that analyte concentrations have been determined by the kinetics of ion exchange monitored by IR spectroscopy. Calibration curves based on initial dA/dt values versus analyte concentration offer a significant time advantage compared to using final absorbance values that require waiting until the extractant coating becomes saturated. The kinetics of these ion-exchange reactions has been compared to a model for anion exchange kinetics in resins of high selectivity proposed by Helfferich.[130] On a simple level the model compares well and seems to indicate that the rate limiting step at low analyte concentrations is diffusion of the analyte from the bulk of solution into the stagnant liquid film layer.

Several matrixes more complex than DI water were investigated. In most cases the addition of other anions to the aqueous matrix negatively affected the extraction of the target anion. However, using the method of standard additions, trace quantities of ClO_4^- were detected in hydroponic nitrate fertilizers (the $[NO_3^-]/[ClO_4^-]$ concentration ratios were as high as 9,000 in these fertilizers). A collaborative study with EPA scientists allowed us to validate our methodology: the concentrations of perchlorate in four fertilizers determined by ATR-FTIR were found to be the same at the $\pm 3\sigma$ level of confidence as those determined in other laboratories by Raman spectroscopy, cESIMS, and IC.[15]

The use of nonpermanent DEC^+X^- coatings was surprisingly reproducible. However, to further reduce the error and to achieve lower LODs, more work will need to be done in the future to aid in the stability of the ferricenium salts when they are used as extractant coatings. It is possible that more permanent coatings prepared using sol-gels or polymers could improve the stability of the coating. This may also enable better redox-recycling and reuse of the DEC^+X^- coatings, but it may also slow down the ion-exchange reaction.

References

1. Richardson, S. D. *Anal. Chem.* **2003**, *75*, 2831–2857.
2. Urbansky, E. T. *Environ. Sci. Pollut. Res. Int.* **2002**, *9*, 187–192.
3. Hogue, C. *Chem. Eng. News* **2003**, *81*, 37–46.
4. "Perchlorate environmental contamination: toxicological review and risk characterization. Second external review draft, NCEA-1-0503," U.S. EPA, Office of Research and Development, National Center for Environmental Assessment, U.S. Government Printing Office: Washington, DC, 2002.
5. Clark, J. J. J. In *Perchlorate in the Environment*; Urbansky, E. T., Ed.; Kluwer/Plenum: New York, 2000, pp 15–29.
6. Christen, K. *Environ. Sci. Technol.* **2000**, *34*, 374A–375A.
7. Urbansky, E. T. *Bioremediation J.* **1998**, *2*, 81–95.
8. Urbansky, E. T.; Schock, M. R. *J. Environ. Manage.* **1999**, *56*, 79–95.
9. http://www.epa.gov/safewater/perchlorate/perchlorate.html, September 2003.
10. Ericksen, G. E. *Am. Scientist* **1983**, *71*, 366–374.
11. Urbansky, E. T.; Brown, S. K.; Magnuson, M. L.; Kelty, C. A. *Environ. Pollut.* **2001**, *112*, 299–302.
12. Williams, T. L.; Martin, R. B.; Collette, T. W. *Appl. Spectrosc.* **2001**, *55*, 967–983.
13. Urbansky, E. T.; Collette, T. W.; Robarge, W. P.; Hall, W. L.; Skillen, J. M.; Kane, P. F. "Survey of fertilizers and related materials for perchlorate (ClO_4^-), EPA/600/R-01/tba," U.S. EPA, Office of Research and Development: Cincinnati, 2001.
14. De Borba, B. M.; Urbansky, E. T. *J. Environ. Monit.* **2002**, *4*, 149–155.
15. Collette, T. W.; Williams, T. L.; Urbansky, E. T.; Magnuson, M. L.; Hebert, G. N.; Strauss, S. H. *Analyst* **2003**, *128*, 88–97.

16. "Public health goal for perchlorate in drinking water, draft," Office of environmental health hazard assessment, California EPA, Dec. 2002.

17. *Fed. Regist.* **1998**, *63*, 10273–10287.

18. *Fed. Regist.* **1999**, *64*, 50555–50620.

19. Malmqvist, A.; Welander, T.; Gunnarsson, L. *Appl. Environ. Microbiol.* **1991**, *57*, 2229–2232.

20. Warrington, P. D. "Ambient Water Quality Guidelines for Chlorate," British Columbian Ministry of Water, Land and Air Protection, Canada: British Columbia, Feb. 2002.

21. "Alternative disinfectants and oxidants guidance manual, 815-R-99-014," U.S. EPA, Office of Water, April 1999.

22. "Trihalomethanes in drinking water: sampling, analysis, monitoring, and compliance, 570/9-83-002," U.S. EPA, Office of Drinking Water, August 1983.

23. Schultz, M. M.; Barofsky, D. F.; Field, J. A. *Environ. Eng. Sci.* **2003**, *20*, 487–501.

24. *Fed. Regist.* **2000**, *65*, 62319–62333.

25. *Fed. Regist.* **2002**, *67*, 11008–11030.

26. Brown, D.; Mayer, C. E. *The Washington Post*, May 17, 2000, p A1.

27. Key, B. D.; Howell, R. D.; Criddle, C. S. *Environ. Sci. Technol.* **1997**, *31*, 2445–2454.

28. Moody, C. A.; Field, J. A. *Environ. Sci. Technol.* **2000**, *34*, 3864–3870.

29. Purdy, R. Proceedings of the Society of Environmental Toxicology and Chemistry Conference, Nashville, TN, 2000, PMP124, p 160.

30. Renner, R. *Environ. Sci. Technol.* **2001**, *35*, 154A–160A.

31. Renner, R. *Sci. Am.* **2001**, *March 17*, 18.

32. Tullo, A. *Chem. Eng. News* **2000**, *May 22*, 9–10.

33. Tullo, A. *Chem. Eng. News* **2000**, *May 29*, 12–13.

34. Wood, A.; Clarin, W. *Chem. Week* **2000**, *May 24*, 9.

35. Nassar, A.-E. F.; Lucas, S. V.; Smith, P. B. W.; Hoffland, L. D. In *Surfactant-Based Separations: Science and Technology*; Scamehorn, J. F., Harwell, J. H., Eds.; American Chemical Society: Washington, DC, 2000; Vol. 740, pp 329–350.

36. "Guidelines for Chemical Warfare Agents in Drinking Water," Subcommittee on Guidelines for Military Field Drinking Water Quality, National Academy Press: Washington DC, 1995.

37. Epstein, J.; Bauer, V. E.; Saxe, M.; Demek, M. M. *J. Am. Chem. Soc.* **1956**, *78*, 4068–4071.

38. Kingery, A. F.; Allen, H. E. *Toxicol. Environ. Chem.* **1995**, *47*, 155–184.

39. Kawasaki, M.; Omori, T.; Hasegawa, K. *Radiochim. Acta* **1993**, *63*, 53.

40. Ashley, K. R.; Ball, J. R.; Pinkerton, A. B.; Abney, K. D.; Schroeder, N. C. *Solvent Extr. Ion Exch.* **1994**, *12*, 239.

41. Liang, L.; Gu, B.; Yin, X. *Sep. Sci. Technol.* **1996**, *6*, 111.

42. Bonnesen, P. V.; Alexandratos, S. D.; Brown, G. M. Proceedings of the American Institute of Chemical Engineers 1995 Annual Meeting, Miami, FL, Nov. 12–17, 1995, Vol. 2, pp 294–299.

43. Rogers, R. D.; Griffin, S. T.; Horwitz, E. P.; Diamind, H. *Solvent Extr. Ion Exch.* **1997**, *15*, 547.

44. Rogers, R. D.; Zhaung, J.; Griffin, S. T. *Sep. Sci. Technol.* **1997**, *32*, 699.

45. Rogers, R. D.; Bond, A. H.; Griffin, S. T.; Horwitz, E. P. *Solvent Extr. Ion Exch.* **1996**, *14*, 919.

46. Clapsaddle, B. J. Synthesis and Characterization of Tetraalkylated and Functionalized Polyalkylated Ferrocenes and Their Applications for the Selective Redox-Recyclable Extraction and Detection of Aqueous Anions. Ph.D. Dissertation, Colorado State University, Fort Collins, CO, 2002.

47. Odom, M. A. Development of Strategies for the Detection, Extraction, and Recovery of Aqueous Anions Using Highly Selective Redox-Recyclable Materials. Ph.D. Dissertation, Colorado State University, Fort Collins, CO, 2001.

48. Chambliss, C. K.; Martin, C. R.; Strauss, S. H.; Moyer, B. A. *Solvent Extr. Ion Exch.* **1999**, *17*, 553–584.

49. Chambliss, C. K.; Odom, M. A.; Martin, C. R.; Moyer, B. A.; Strauss, S. H. *Inorg. Chem. Commun.* **1998**, *1*, 435–438.

50. Chambliss, C. K.; Odom, M. A.; Morales, C. M. L.; Martin, C. R.; Strauss, S. H. *Anal. Chem.* **1998**, *70*, 757–765.

51. Clark, J. F.; Clark, D. L.; Whitener, G. D.; Schroeder, N. C.; Strauss, S. H. *Environ. Sci. Technol.* **1996**, *30*, 3124–3127.

52. Strauss, S. H. In *ACS Sym. Series 716*; Bond, A. H., Dietz, M. L., Rogers, R. D., Eds.; American Chemical Society: Washington DC, 1999; Vol. 716, pp 156–165.

53. Clark, J. F.; Chamberlin, R. M.; Abney, K. D.; Strauss, S. H. *Environ. Sci. Technol.* **1999**, *33*, 2489–2491.

54. Moyer, B. A.; Bonnesen, P. V. In *Supramolecular Chemistry of Anions*; Bianchi, A., Bowman-James, K., Garcia Espana, E., Eds.; VCH Publishers: New York, 1997, pp 1–44.

55. Griffiths, P. R.; de Haseth, J. *Fourier Transform Infrared Spectrometry*; John Wiley & Sons: New York, 1986.

56. Skoog, D. A.; Leary, J. J. *Principles of Instrumental Analysis*; 4th ed.; Saunders College Publishing: New York, 1992.

57. Harrick, N. J. *Internal Reflection Spectroscopy*; Interscience: New York, 1967.

58. Urban, M. W. *Attenuated Total Reflectance Spectroscopy of Polymers. Theory and Practice*; American Chemical Society: Washington DC, 1996.

59. Hebert, G. N.; Odom, M. A.; Bowman, S. C.; Strauss, S. H. *Anal. Chem.* **2004**, *76*, 781–787.

60. Strauss, S. H.; Odom, M. A.; Hebert, G. N.; Clapsaddle, B. J. *J. Am. Water Works Assoc.* **2002**, *94*, 109–115.

61. Clapsaddle, B. J.; Clark, J. F.; Clark, D. L.; Gansle, K. M.; Gash, A. E.; Chambliss, C. K.; Odom, M. A.; Miller, S. M.; Anderson, O. P.; Hughes, R. P.; Strauss, S. H. *Inorg. Chem.*, unpublished work.

62. Jelinet, T.; Plesek, J.; Hermanek, S.; Stibr, B. *Collect. Czech. Chem. Commun.* **1986**, *51*, 818–829.

63. Mercier, J.-P.; Morin, P.; Dreux, M.; Tambute, A. *Chromatographia* **1998**, *48*, 529–534.

64. Bossle, P. C.; Martin, J. J.; Sarver, E. W.; Sommer, H. Z. *J. Chromatogr.* **1983**, *267*, 209–212.

65. Saito, N.; Sasaki, K.; Nakatome, K.; Harada, K.; Yoshinaga, T.; Koizumi, A. *Arch. Environ. Contam. Toxicol.* **2003**, *45*, 149–158.

66. Favier, R.; Pascal, J. L. *Analyst* **1991**, *116*, 479–481.

67. Hautman, D. P.; Munch, D. J.; Eaton, A. D.; Haghani, A. W. "Method 314.0 Determination of perchlorate in drinking water using ion chromatography," U.S. EPA, Office of Research and Development, National Exposure Research Laboratory: Cincinnatti, OH, 1999.

68. Doyle, J. M.; Miller, M. L.; McCord, B. R.; McCollam, D. A.; Mushrush, G. W. *Anal. Chem.* **2000**, *72*, 2302–2307.

69. Jackson, P. E.; Gokhale, S.; Rohrer, J. S. In *Perchlorate in the Environment*; Urbansky, E. T., Ed.; Klewer/Plenum: New York, 2000, pp 37–44.

70. Jackson, P. E.; Gokhale, S.; Streib, T.; Rohrer, J. S.; Pohl, C. A. *J. Chromatogr., A* **2000**, *888*, 151–158.

71. Wagner, H. P.; Pepich, B. V.; Hautman, D. P.; Munch, D. J.; Salhi, E.; von Gunten, U. "Method 326.0 Determination of inorganic oxyhalide disinfection by-products in drinking water using ion chromatography incorporating the addition

of a suppressor acidified postcolumn reagent for trace bromate analysis," U.S. EPA, Office of Ground Water and Drinking Water: Cincinnati, OH, 2002.

72. Hebert, G. N.; Odom, M. A.; Craig, P. S.; Dick, D. L.; Strauss, S. H. *J. Environ. Monit.* **2002**, *4*, 90–95.

73. Jenkins, A. L.; Uy, O. M.; Murray, G. M. *Anal. Chem.* **1999**, *71*, 373–378.

74. Magnuson, M. L.; Urbansky, E. T.; Kelty, C. A. *Anal. Chem.* **2000**, *72*, 25–29.

75. Barnett, D. A.; Horlick, G. *J. Anal. At. Spectrom.* **1997**, *12*, 497–501.

76. Handy, R.; Barnett, D. A.; Purves, R. W.; Horlick, G.; Guevremont, R. *J. Anal. At. Spectrom.* **2000**, *15*, 907–911.

77. Hauser, P. C.; Renner, N. D.; Hong, A. P. C. *Anal. Chim. Acta* **1994**, *295*, 181–186.

78. Urbansky, E. T.; Magnuson, M. L.; Kelty, C. A.; Brown, S. K. *Sci. Total Environ.* **2000**, *256*, 227–232.

79. Ellington, J. J.; Evans, J. J. *J. Chromatogr., A* **2000**, *898*, 193–199.

80. Ellington, J. J.; Wolfe, N. L.; Garrison, A. W.; Evans, J. J.; Avants, J. K.; Teng, Q. *Environ. Sci. Technol.* **2001**, *35*, 3213–3218.

81. Hansen, K. J.; Johnson, H. O.; Eldridge, J. S.; Butenhoff, J. L.; Dick, L. A. *Environ. Sci. Technol.* **2002**, *36*, 1681–1685.

82. Moody, C. A.; Kwan, W. C.; Martin, J. W.; Muir, D. C. G.; Mabury, S. A. *Anal. Chem.* **2001**, *73*, 2200–2206.

83. Takino, M.; Daishima, S.; Nakahara, T. *Rapid Commun. Mass Spectrom.* **2003**, *17*, 383–390.

84. Lakso, H.-A.; Ng, W. F. *Anal. Chem.* **1997**, *69*, 1866–1872.

85. Nassar, A.-E. F.; Lucas, S. V.; Hoffland, L. D. *Anal. Chem.* **1999**, *71*, 1285–1292.

86. Nassar, A.-E. F.; Lucas, S. V.; Jones, W. R.; Hoffland, L. D. *Anal. Chem.* **1998**, *70*, 1085–1091.

87. Zi-Hui, M.; Qin, L. *Anal. Chim. Acta* **2001**, *435*, 121–127.

88. Asbury, G. R.; Wu, C.; Siems, W. F.; Hill Jr., H. H. *Anal. Chim. Acta* **2000**, *404*, 273–283.

89. Steiner, W. E.; Clowers, B. H.; Matz, L. M.; Siems, W. F.; Hill Jr., H. H. *Anal. Chem.* **2002**, *74*, 4343–4352.

90. Janotta, M.; Mizaikoff, B. *Proc. SPIE-Int. Soc. Opt. Eng.* **2002**, *4616*, 1–8.

91. Spichiger-Keller, U. E. *Sens. Actuators, B* **1997**, *38–39*, 68–77.

92. Kraft, M.; Karlowatz, M.; Mizaikoff, B.; Stuck, R.; Steden, M.; Ulex, M.; Amann, H. *Meas. Sci. Technol.* **2002**, *13*, 1294–1303.

93. Mizaikoff, B. *Meas. Sci. Technol.* **1999**, *10*, 1185–1194.

94. Mizaikoff, B.; Gobel, R.; Krska, R.; Taga, K.; Kellner, R.; Tacke, M.; Katzir, A. *Sens. Actuators, B* **1995**, *29*, 58–63.

95. Jakusch, M.; Mizaikoff, B.; Kellner, R.; Katzir, A. *Sens. Actuators, B* **1997**, *38*, 83–87.

96. Heinrich, P.; Wyzgol, R.; Schrader, B.; Hatzilazaru, A.; Lubbers, D. W. *Appl. Spectrosc.* **1990**, *44*, 1641–1646.

97. Gobel, R.; Seitz, R. W.; Tomellini, S. A.; Krska, R.; Kellner, R. *Vib. Spectrosc.* **1995**, *8*, 141–149.

98. Acha, V.; Meurens, M.; Naveau, H.; Agathos, S. N. *Med. Fac. Landbouww. Univ. Gent.* **1998**, *63*, 1795–1801.

99. Acha, V.; Meurens, M.; Naveau, H.; Agathos, S. N. *Water Sci. Technol.* **1999**, *40*, 41–47.

100. Acha, V.; Meurens, M.; Naveau, H.; Agathos, S. N. *Biotechnol. Bioeng.* **2000**, *68*, 473–487.

101. Chittur, K. K. *Biomaterials* **1998**, *19*, 357–369.

102. Hahn, P.; Tacke, M.; Jakusch, M.; Mizaikoff, B.; Spector, O.; Katzir, A. *Appl. Spectrosc.* **2001**, *55*, 39–43.

103. Meuse, C. W.; Tomellini, S. A. *Anal. Lett.* **1989**, *22*, 2065–2073.

104. Lu, Y.; Han, L.; Brinker, C. J.; Niemczyk, T. M.; Lopez, G. P. *Sens. Actuators, B* **1996**, *35–36*, 517–521.

105. Han, L.; Niemczyk, T. M.; Lu, Y.; Lopez, G. P. *Appl. Spectrosc.* **1998**, *52*, 119–122.

106. Regan, R.; Meaney, M.; Vos, J. G.; MacCraith, B. D.; Walsh, J. E. *Anal. Chim. Acta* **1996**, *334*, 85–92.

107. Rivera, D.; Harris, J. M. *Anal. Chem.* **2001**, *73*, 411–423.

108. Wolfbeis, O. S. *Anal. Chem.* **2002**, *74*, 2663–2678.

109. Hug, S. J. *J. Colloid Interface Sci.* **1997**, *188*, 415–422.

110. Weisz, A. D.; Rodenas, L. G.; Morando, P. J.; Regazzoni, A. E.; Blesa, M. A. *Catal. Today* **2002**, *76*, 103–112.

111. Duckworth, O. W.; Martin, S. T. *Geochim. Cosmochim. Acta* **2001**, *65*, 4289–4301.

112. Elzinga, E. J.; Peak, D.; Sparks, D. L. *Geochim. Cosmochim. Acta* **2001**, *65*, 2219–2230.

113. Borda, M. J.; Strongin, D. R.; Schoonen, M. A. *Spectrochim. Acta, Part A* **2003**, *59*, 1103–1106.

114. Peak, D.; Luther, G. W., III; Sparks, D. L. *Geochim. Cosmochim. Acta* **2003**, *67*, 2551–2560.

115. Voegelin, A.; Hug, S. J. *Environ. Sci. Technol.* **2003**, *37*, 972–978.

116. Jakusch, M.; Janotta, M.; Mizaikoff, B. *Anal. Chem.* **1999**, *71*, 4786–4791.

117. Degenhardt, J.; McQuillan, A. J. *Langmuir* **1999**, *15*, 4595–4602.

118. Dobson, K. D.; McQuillan, A. J. *Spectrochim. Acta, Part A* **1999**, *55*, 1395–1405.

119. Dobson, K. D.; McQuillan, A. J. *Langmuir* **1997**, *13*, 3392–3396.

120. Wijnja, H.; Schulthess, C. P. *Soil Sci. Soc. Am. J.* **2001**, *65*, 324–330.

121. Sheals, J.; Sjoberg, S.; Persson, P. *Environ. Sci. Technol.* **2002**, *36*, 3090–3095.

122. Kellner, R.; Zippel, E.; Pungor, E.; Toth, K.; Lindner, E. In *Comtemporary Electroanalytical Chemistry*; Ivaska, A., Lewenstam, A., Sara, R., Eds.; Plenum Press: New York, 1990, pp 223–230.

123. Eggleston, C. M.; Hug, S.; Stumm, W.; Sulzberger, B.; Afonso, M. D. S. *Geochim. Cosmochim. Acta* **1998**, *62*, 585–593.

124. Gillette, P. C.; Lando, J. B.; Koenig, J. L. In *Fourier Transform Infrared Spectroscopy Applications to Chemical Systems*; Ferraro, J. R., Basile, L. J., Eds.; Acedemic Press: New York, 1985; Vol. 4, pp 1–47.

125. Wilhite, R. N.; Ellis, R. F. *Appl. Spectrosc.* **1963**, *17*, 168.

126. *Spectrochim. Acta B* **1978**, *33B*, 241–245.

127. *Spectrochim. Acta B* **1978**, *33B*, 248–265.

128. Helfferich, F. G.; Liberti, L.; Petrusselli, D.; Passino, R. *Israel J. Chem.* **1985**, *26*, 3–7.

129. Bard, A. J.; Faulkner, L. R. *Electrochemical Methods Fundamentals and Applications*; John Wiley & Sons: New York, 1980.

130. Helfferich, F. G. *Ion Exchange*; McGraw-Hill: New York, 1962.

131. Ericksen, G. E. "Geology and Origin of the Chilean Nitrate Deposits," US Department of the Interior: Washington DC, 1981.

132. "City of Fort Collins Drinking Water Quality Summary," Fort Collins Utilities: Fort Collins, CO, 2002.

133. Gansle, K. M. R. Investigation and Development of Liquid-Liquid Extraction Systems For the Removal of Pertechnetate From Aqueous Nuclear Waste Stream Simulants. Ph.D. Dissertation, Colorado State University, Fort Collins, CO, 1998.

134. Pendin, A. A.; Zakhar'evskii; Leont'evskaya, P. K. *Kinetics and Catalysis* **1966**, *7*, 922–925.

135. Pendin, A. A.; Leont'evskaya, P. K. *Kinetics and Catalysis* **1976**, *17*, 297–302.

136. Pendin, A. A.; Leont'evskaya, P. K. *Kinetics and Catalysis* **1976**, *17*, 303–306.

137. Pendin, A. A.; Leont'evskaya, P. K.; Bundina, T. K. *Kinetics and Catalysis* **1977**, *18*, 1087–1090.

138. Prins, R.; Korswagen, A. R.; Kortbeek, A. G. T. G. *J. Organomet. Chem.* **1972**, *39*, 335–344.

139. Deinhammer, R. S.; Ting, E.-Y.; Porter, M. D. *Anal. Chem.* **1995**, *67*, 237–246.

140. De Santis, G.; Fabbrizzi, L.; Licchelli, M.; Monichino, A.; Pallavicini, P. *J. Chem. Soc., Dalton Trans.* **1992**, 2219–2224.

141. Kingston, J. E.; Ashford, L.; Beer, P. D.; Drew, M. G. B. *J. Chem. Soc., Dalton Trans.* **1999**, 251–258.

142. Ghatak-Roy, A. R.; Martin, C. R. *Anal. Chem.* **1986**, *58*, 1574–1575.

143. Lilga, M. A.; Orth, R. J.; Sukamto, J. P. H.; Haight, S. M.; Schwartz, D. T. *Sep. Purif. Technol.* **1997**, *11*, 147–158.

144. Medina, J. C.; Gay, I.; Chen, Z.; Echegoyen, L.; Gokel, G. W. *J. Am. Chem. Soc.* **1991**, *113*, 365–366.

145. Shinkai, S. In *Comprehensive Supra-molecular Chemistry*; Gokel, G. W., Ed.; Elsevier: Oxford, U.K., 1996.

146. Bard, A. J.; Parsons, R.; Jordan, J., Eds. *Standard Potentials in Aqueous Solution*; Marcel Dekker: New York, 1985, p 799.

Chapter 4

ATR-FTIR Detection and Quantification of Low Concentrations of Aqueous Cyanide

Introduction

Historically, cyanide was introduced into the environment by seepage from mine tailing ponds near gold mining operations.[1,2] More recently, it has been found in water that has been discharged from sheet-metal and fertilizer factories.[3] The gas, HCN, evolves from aqueous solutions with pH values below 9.2. At low concentrations gaseous HCN can cause nerve damage or thyroid problems and at high concentrations can cause death within minutes.[4] As a result of these health risks, the EPA has set a drinking water maximum contaminant level (MCL) for cyanide of 7.7 μM.[5]

A standard method has been approved by the EPA to measure total cyanide present in solution, including that in weak or intermediate-strength metal cyano complexes. (e.g., Zn^{2+}, Cu^{+}, Cd^{2+}, Hg^{2+}, Ni^{2+}, and Ag^{+}).[6] The method consists of ligand exchange (with two proprietary reagents[7]) to release any CN^{-} that is weakly complexed by metals followed by flow injection analysis and amperometric detection with an Ag electrode, Ag/AgCl reference electrode, and Pt/stainless steel counter electrode. This method has a limit of detection (LOD) of 0.02 μM CN^{-} with a ca. two minute analysis time, not including time for the ligand exchange and other sample preparation steps.[6] The linear range for CN^{-} is 0.05–130 μM. It is important to note that the presence of sulfide in solution is an interferant that will cause a false positive electrode response. More importantly, this method will not determine cyanide from the thermodynamically or

kinetically stable complexes of cobalt, gold, palladium, platinum, ruthenium, and iron. The release of cyanide from complexes with these metals requires the harsher conditions of digestion in the presence of intense UV radiation prior to detection.[7]

The two most commonly used methods of cyanide detection (as found in the reference *Standard Methods for the Examination of Water and Wastewater*)[8] are the total cyanide by distillation method (LOD = 1 μM)[8] and the cyanide amenable to chlorination method (LOD = 1 μM)[9] both of which have significant short-comings.[10] That is, the distillation method can take many hours depending on how many times the distillation process needs to be repeated and the chlorination method has many known interferences, mainly other anions, and has challenges with the prescribed colorimetric determination.

Several reviews are available that describe the numerous other methods for cyanide analysis.[2,11-14] Recently, Zheng et al. reviewed seven common analytical methods used to evaluate cyanide species in municipal and industrial waters.[10,14] These methods include analysis for free cyanide by microdiffusion,[15] metal cyano complexes by ion chromatography,[16] total cyanide by low power UV digestion,[17] total cyanide by UV digestion and thin film distillation,[18] weak acid dissociable cyanide by colorimetric, electrode, or titrimetric detection,[19] total and weak acid dissociable cyanide by flow injection analysis,[20] and the EPA standard method discussed above,[6] all of which have LODs less then 50 nM. Several other methods have been reported in the literature, all of which were capable of achieving cyanide LODs equal to or lower than the EPA standard method LOD of 19 nM.[6] These methods include an electrochemical minisensor that incorporates cyanide into a self-assembled bilayer lipid membrane (LOD = 4.9 nM),[21] atomic absorption spectroscopy (LOD = 2 nM),[22] spectrophotometric detection (LODs = 19–23 nM),[11,23] UV photodissociation and detection with an ion-selective electrode (LOD = 0.4 nM),[24] and flow injection analysis with gas-diffusion membrane and fluorescence detection (LOD = 0.015 nM).[25] Other recently reported methods with higher cyanide LODs include ion chromatography (LOD = 50 μM),[26] quartz crystal microbalance-based

methods (LODs = 0.2–11 μM),[27,28] ion-interaction chromatography with UV photodissociation and fluorescence detection (LOD = 0.4 μM),[29] surface enhanced Raman spectroscopy (LODs = 0.04–0.4 μM),[30-33] phosphorescence (LOD = 0.12μM),[34] and flow injection analysis with UV digestion and amperometric detection (LOD = 0.08 μM).[35]

In this chapter an ATR-FTIR method using a Ni-based organometallic ligand-exchange complex will be presented that has been designed for the detection of free (uncomplexed) CN^-. Preliminary results using this method including an LOD have been previously reported by the Strauss Research Group.[36] Additionally, a similar ATR-FTIR method using a variety of organometallic ligand-exchange complexes (e.g., *cis*-$PdCl_2$(diphenylphosphino)(ferrocene), $RhCl(CO)(PPh_3)_2$, and *cis*-$PtCl_2(PPh_3)_2$; PPh_3 = triphenylphosphine) was studied by Elisha Kosak, a former member of the Strauss Research Group.[37]

Detection of CN^- using the DEC^+X^--coated probes, as described in Chapter 3, was not possible since CN^- is more strongly hydrated than either NO_3^- or Cl^- and because of the possibility of CN^- causing nucleophilic decomposition of the ferrocenium complex. Instead, the compound 1,3-bis(diphenylphosphino)propanedichloronickel(II) ($NiCl_2$(dppp)), shown below, was used to complex aqueous cyanide. Note that this

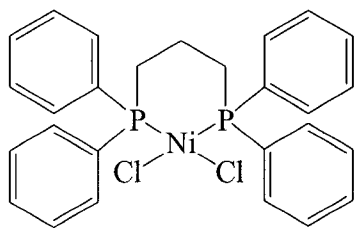

extractant is not redox recyclable. It is proposed that extraction of CN^- with $NiCl_2$(dppp) may form the new water-insoluble complex NiCl(CN)(dppp) by Cl^-/CN^- ligand exchange. Its formation may be due to the essentially irreversible, ligand-exchange reaction shown in Equation 4.1. The use of this nickel complex as a thin-film coating on

$$NiCl_2(dppp)\,(s) + CN^-\,(aq) \rightleftharpoons NiCl(CN)(dppp)\,(s) + Cl^-\,(aq) \quad (4.1)$$

silicon ATR crystals for the detection of low concentrations of cyanide will be discussed in this chapter. In addition to calculating 10-minute LODs for CN^-, a linear calibration curve was generated over two orders of magnitude of concentration. Some preliminary studies will also be described in this chapter that investigate the effects of a more complex matrix on the LOD and the rate of extraction.

Experimental Section

Reagents. Chemicals that were obtained commercially were used without further purification unless otherwise noted. Potassium cyanide (99.9%), sodium hydroxide (98.7%), sodium chloride (99.5%), and dichloromethane (ACS grade) were obtained from Fisher Scientific. The metal complex 1,3-bis(diphenylphosphino)propane-dichloronickel(II) ($NiCl_2$(dppp), 97%) was purchased from Aldrich.

Instrumentation. The pH was measured using an Orion meter (Boston, MA) with a Corning® pH electrode (Corning, NY). IR spectra were recorded using an ATR-FTIR spectrometer (ReactIR™-1000, Applied Systems Inc., Millersville, MD) described in detail in the Experimental Section of Chapter 3. Only the silicon (SiComp®) ATR probe (Applied Systems Inc, Millersville, MD) probe was used, with a spectral window of 4000 to 650 cm^{-1}. A nominal spectral resolution of 8 cm^{-1}, an electronic gain of 1. Happ-Ganzel apodization with no post-run spectral smoothing were used.

Procedure. All aqueous stock solutions were prepared in Class A volumetric glassware using distilled deionized (DI) water (Barnstead NANOpure, Dubuque, IA) that had an initial resistivity of 18 MΩ cm. All experiments were performed at 24 ± 1 °C (room temperature). The pH of all aqueous solutions containing CN^- was adjusted to pH 10.0 ± 0.2 using sodium hydroxide, since gaseous HCN may evolve from solutions with a pH less than 9.2.

The general steps for ATR-FTIR analysis of an aqueous analyte using both the coated and uncoated ATR probes were detailed in Chapter 3. The following is a brief description of the procedure used for cyanide detection. All experiments were done using the silicon ATR crystal since the region where the ν(CN) band occurs (ca. 2100 cm^{-1}) had little to no transmittance using the diamond ATR crystal. For experiments using the uncoated probe, the silicon probe was placed in the inverted position, and immersed in a beaker of 100 mL of water adjusted to pH 10 that was stirred with a magnetic stir bar and stir plate at ca. 200 rpm. A background spectrum was collected by scanning continually for 10 minutes (1,660 co-added scans). An aliquot (0.01–10 mL) of a concentrated CN^- stock solution (also at pH 10) was then added to the pH 10 water with stirring after the same volume had been removed. A 10-minute spectrum (1,660 co-added scans) of the resulting solution was then collected.

For experiments using the coated silicon probe, the exposed surface of the ATR crystal was treated with 20 ± 3 μL of a fresh (a new solution was made daily) 5 mM dichloromethane solution of $NiCl_2$(dppp). The coated ATR probe was used for a single analysis, after which the thin-film coating was removed by washing with acetone or dichloromethane. The coated ATR probe was then immersed in 100 mL of pH 10 water, which was stirred at ca. 200 rpm using a 3 cm magnetic stir bar. The coating was allowed to equilibrate with water for 10 minutes, at which time a background spectrum (64 co-added scans) was collected. Immediately following the collection of the background spectrum a spectrum (64 co-added scans) was collected every minute for an appropriate amount of time (usually 10–60 minutes). Between the collection of the 1st and 2nd spectra (0 and 1 minute), an appropriate amount (usually 0.01–10 mL) of a CN^- stock solution was added to the pH 10 water, with stirring, to achieve the desired final CN^- concentration. Note that prior to the addition of an aliquot of the stock solution, that same volume was removed from the 100 mL of water to maintain a total volume of 100 mL. The solution was stirred continuously during the entire experiment. ATR-FTIR results

from a typical CN^- extraction experiment for the detection of 5 μM CN^- (pH 10) in contact with the $NiCl_2$(dppp)-coated silicon probe are shown in Figure 4.1. A ν(CN) band at 2104 cm^{-1} was clearly visible within minutes.

Results and Discussion

10-Minute limits of detection (LODs). As discussed in Chapter 3, the sensitivity of the commercially-available ATR-FTIR spectrometer used in this study can be dramatically improved simply by applying a thin-film coating of an ion-exchange material to the surface of the ATR crystal. A dramatic improvement in the LOD for aqueous CN^- was observed between the uncoated silicon probe and the $NiCl_2$(dppp)-coated silicon probe. Recall that the LOD is defined as the concentration of analyte which yields a signal-to-noise ratio (*SNR*) $\geq 3 \pm 1$ for a 10-minute analysis. All *SNR*s reported are averages of three or more trials at that concentration.

The 10-minute LOD for CN^- using the $NiCl_2$(dppp)-coated silicon probe was 0.09 μM, as listed in Table 4.1. Since the 10-minute LOD for aqueous CN^- with the unmodified silicon probe was found to be 2 mM, the nickel-complex coating lowered the 10-minute detection limit for aqueous CN^- by a factor of 22,000. Details of the calculation of these LODs can be found in Appendix E. A spectrum of 0.09 μM CN^- after 10 minutes in contact with the $NiCl_2$(dppp)-coated probe is shown in Figure 4.2. Even at this low concentration, the ν(CN) band is discernable compared to the blank spectrum.

The coated-probe LOD of 0.09 μM CN^- is significantly lower than the EPA drinking-water MCL of 7.7 μM.[5] The 10-minute coated-probe LOD is five times higher than the 0.019 μM CN^- LOD for the EPA standard method.[6] However, this ATR-FTIR method is less time-consuming and has a lower LOD than the standard methods for total cyanide by distillation or cyanide amenable to chlorination (LODs = 1 μM).[8,9]

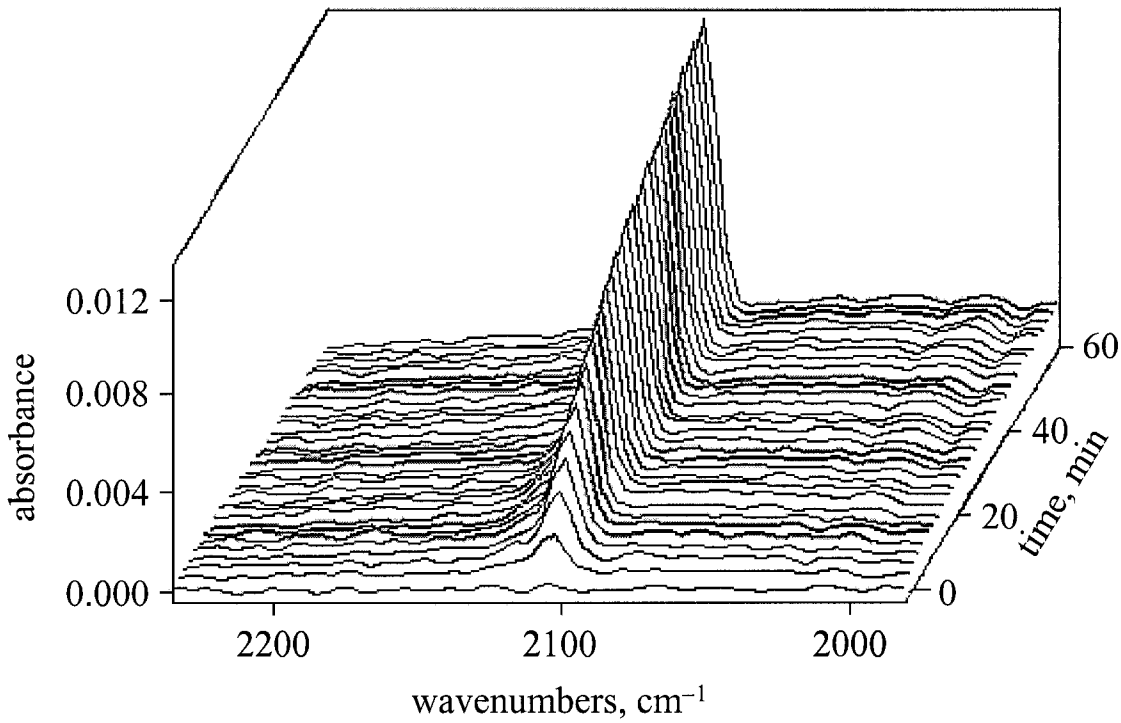

Figure 4.1. ATR-FTIR spectra collected every minute for 60 minutes of the $NiCl_2$(dppp)-coated silicon probe immersed in a 5 μM CN^- aqueous solution adjusted to pH 10 with NaOH. The ν(CN) band at 2104 cm^{-1} is attributed to the solid complex NiCl(CN)(dppp) on the surface of the silicon probe.

Table 4.1. Ten-minute limits of detection (LODs) for aqueous CN^- determined by ATR-FTIR[a]

matrix	uncoated probe[b]			extractant coated probe[c]			LOD ratio[d]
	ν, cm^{-1}	LOD, mM	*SNR*(σ)	ν, cm^{-1}	LOD, μM	*SNR*(σ)	
pH 10 water	2081	2	4(1)	2104	0.09	4(1)	22,000
synthetic tap water[e]	2081	3[f]	4(1)	2104	0.2	4.2(9)	15,000

[a] Abbreviations: ν, IR spectral band monitored; *SNR*, signal-to-noise ratio. [b] Uncoated-probe LODs were determined from sample and background spectra (1,660 co-added scans each) collected over 10-minute intervals. [c] Extractant-coated-probe LODs were determined from sample spectra collected after a 10-minute extraction period and ratioed to background spectra (64 co-added scans each). The silicon crystal was coated by evaporation of 20 μL of a 5 mM dichloromethane solution of $NiCl_2$(dppp). [d] Ratio of the uncoated probe LOD to the coated probe LOD. [e] The components of synthetic tap water are listed in Table 3.13 [f] This LOD was determined by Dr. Stephanie C. Bowman in the Strauss Research Group.

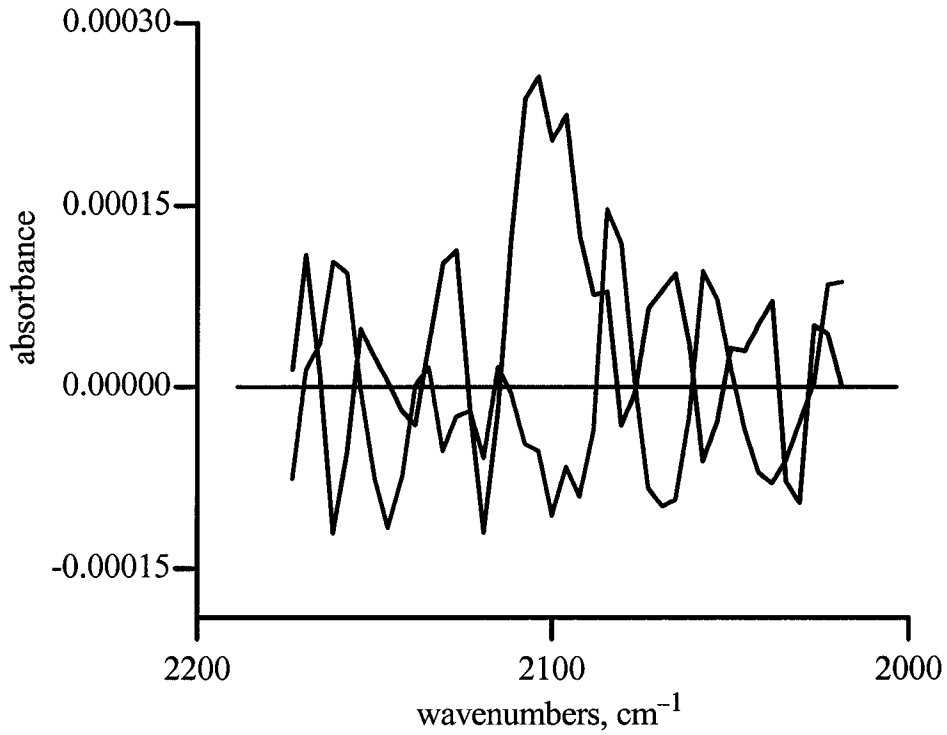

Figure 4.2. Spectrum of 0.09 μM CN^- in pH 10 water after 10 minutes in contact with the $NiCl_2$(dppp)-coated silicon probe is shown in black. A blank spectrum (pH 10 water in contact with the $NiCl_2$(dppp)-coated probe) is shown in blue, and the baseline ($y = 0$) in red. The *SNR* of the ν(CN) band is 4 ± 1 at 2104 cm^{-1}.

Calibration curves. Quantification was done using calibration curves that were prepared according to the method described in Chapter 3. In general, the initial rate of increase in the absorbance of the ν(CN) band over time, hereinafter referred to as d*A*/d*t*, was found to be directly proportional to [CN^-] up to a limiting concentration. For example, a plot of d*A*/d*t* versus [CN^-] (Figure 4.3) was linear only from 0.1 to 10.0 μM. At higher concentrations, it is possible that the ligand exchange is going beyond the formation of NiCl(CN)(dppp) on the surface of the silicon crystal to the formation of other Ni complexes (e.g., possibly $Ni(CN)_2$(dppp) or $Ni(CN)_4^{2-}$). The formation these complexes, or others, could contribute to the higher relative error (ca. 30%) for the 50 and 100 μM points on the non-linear portion of the calibration curve in Figure 4.3.

Reproducibility. Several experiments were performed to test the reproducibility of the $NiCl_2$(dppp)-coated probe method. First, the entire calibration curve was reproduced one year later using different $NiCl_2$(dppp) solutions, CN^- stock solutions, and instrument operators (Karen S. Wendling, an undergraduate summer student, generated one of the calibration curves). As can be seen from Figure 4.4, both of the calibration curves have good correlation coefficients and very similar slopes.

In addition to the calibration curves, the d*A*/d*t* values for 1 μM CN^- in contact with the $NiCl_2$(dppp)-coated silicon probe were also compared for three sets of experiments as shown in Table 4.2. Three trials were done for each set of experiments done over a three year time period by two different operators. New $NiCl_2$(dppp) and CN^- stock solutions were used for each set of experiments. Even though a large number of variables were changed, the d*A*/d*t* values for 1 μM CN^- were the same within the listed errors. This same level of reproducibility has been shown for d*A*/d*t* values for 5 μM CN^- for two sets of experiments (three trials each) done on the same day. In this case, different $NiCl_2$(dppp) and CN^- stock solutions were used. Nevertheless, as shown in Table 4.2, the average d*A*/d*t* values were the same within the listed errors.

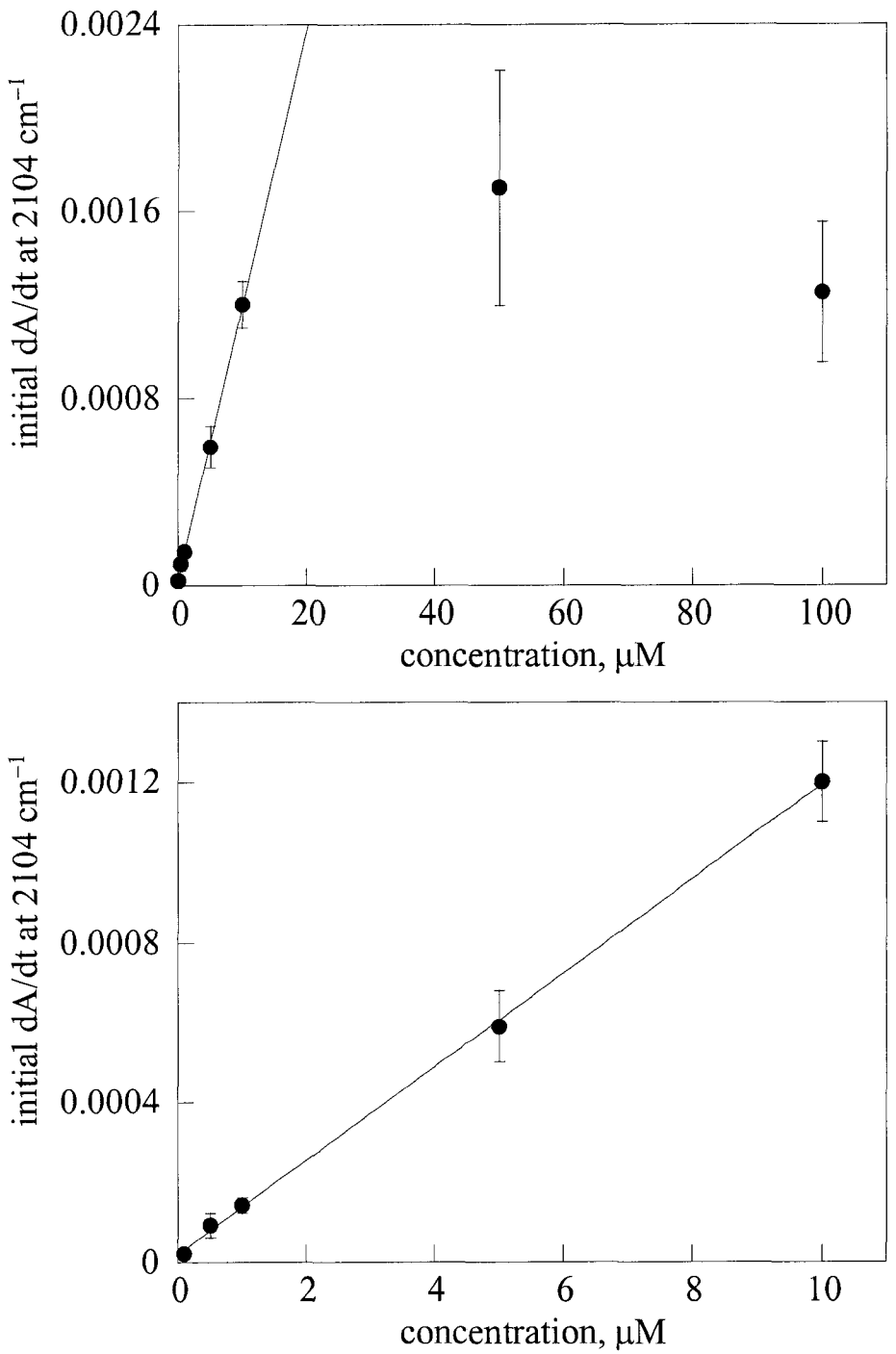

Figure 4.3. Calibration curves for aqueous CN^- in contact with the silicon probe coated with 20 μL of a 5 mM dichloromethane solution of $NiCl_2$(dppp). The lines drawn in both graphs are the linear fit to the points up to 10 μM with the equation $y = 1.18(6) \times 10^{-4}x + 1.8(8) \times 10^{-5}$ and a correlation coefficient of 0.999. The error bars represent ±1σ.

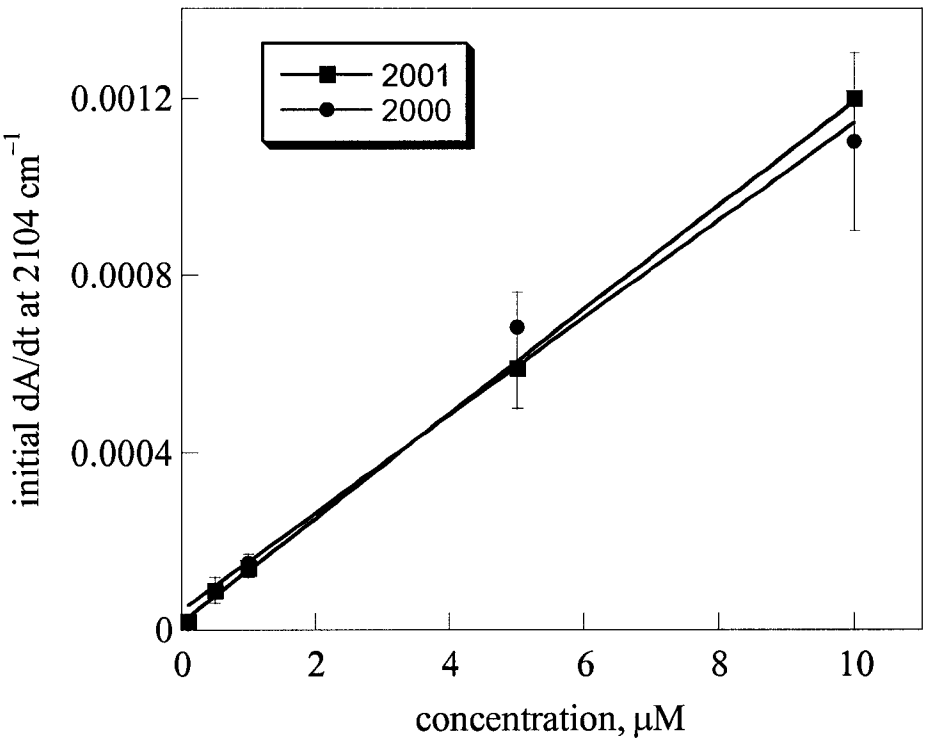

Figure 4.4. Comparison of CN^- calibration curves produced in two different years (September 2000 and July 2001) by two instrument operators (Karen S. Wendling generated the 2001 calibration curve), using different $NiCl_2$(dppp) and CN^- stock solutions. The 2000 linear fit has the equation $y = 1.11(9) \times 10^{-4}x + 4(3) \times 10^{-5}$ and a correlation coefficient of 0.985. The 2001 linear fit has the equation $y = 1.18(6) \times 10^{-4}x + 1.8(8) \times 10^{-5}$ and a correlation coefficient of 0.999. Error bars represent $\pm 1\sigma$.

Table 4.2. Reproducibility of dA/dt values over a three year time period

$[CN^-]$, μM	date	operator[a]	$dA/dt(\sigma)$, min^{-1} [b]
1	September 2000	GNH	$1.7(2) \times 10^{-4}$
1	June 2001	KSW	$1.5(2) \times 10^{-4}$
1	June 2003	GNH	$1.4(2) \times 10^{-4}$
5	June 2003	GNH	$5.4(9) \times 10^{-4}$
5	June 2003	GNH	$5.6(6) \times 10^{-4}$

[a] GNH = Gretchen N. Hebert, KSW = Karen S. Wendling. [b] dA/dt values were calculated using the ν(CN) band at 2104 cm^{-1} for the $NiCl_2$(dppp)-coated silicon probe; σ = estimated standard deviation.

Another measure of the reproducibility of the these experiments is the relatively low error in the average noise values from blank spectra using both the uncoated and $NiCl_2$(dppp)-coated silicon probe. The relative standard deviation associated with the average noise values listed in Table 4.3 ranged from 12 to 30%. An error of only 29% was obtained from a large number of trials (54) of blank spectra using the $NiCl_2$(dppp)-coated probe.

One of the main problems encountered with the use of the $NiCl_2$(dppp)-coated probe method is that the metal complex is not stable over time when it is stored in dichloromethane. This was initially noted by a change in the color of the solution from clear salmon (freshly prepared) to colorless with a white precipitate (after ca. one week). When an old extractant solution was used to coat the silicon probe and it was immersed in a CN^- solution, no ν(CN) band was observed. To counter this problem, a new $NiCl_2$(dppp) stock solution was prepared each day. It is possible that the change in the Ni complex solution within one day may cause some of the error associated with the coated-probe experiments. Some experiments have been done by another member of the Strauss Research Group to find different metal complexes that are more stable in dichloromethane solutions and that can be used for the extraction of aqueous CN^-.[37] Preliminary results indicated that the complex $RhCl(CO)(PPh_3)_2$, where PPh_3 is triphenylphosphine, can detect 0.75 μM CN^- when it was used as a coating on the silicon probe and that it may be stable in the presence of air as a chloroform solution.[37]

Detection of aqueous CN^- in complex matrixes. Several different chloride-containing matrixes were tested to check for interferences with the detection of CN^- by the $NiCl_2$(dppp)-coated probe. First, the $NiCl_2$(dppp)-coated silicon probe was immersed in a solution containing 10 μM CN^- in synthetic tap water. The components of synthetic tap water, which contains 0.17 μM Cl^- as well as other ions, are listed in Table 3.13. After 10 minutes, the ν(CN) band was significantly above the noise with a *SNR* of 49 ± 7, which is the same within error as for a 10 μM CN^- solution in pH 10 water (*SNR* 71 ±

Table 4.3. Comparison of noise values over various wavenumber regions using the silicon ATR crystal

uncoated[a] or coated[b] probe	noise window, cm^{-1}	number of trials	average noise(σ)[c]
uncoated	2157–2054	11	$2.3(7) \times 10^{-5}$
uncoated[d]	2157–2054	9	$1.9(4) \times 10^{-5}$
coated	2135–2057	54	$7(2) \times 10^{-5}$
coated[d]	2135–2057	11	$8(1) \times 10^{-5}$

[a] Each uncoated probe noise value was determined from a blank spectrum (1,660 co-added scans) of pH 10 water collected over a 10-minute interval. [b] Each extractant-coated probe noise value was determined from a blank spectrum (64 co-added scans) of pH 10 water in contact with the $NiCl_2$(dppp)-coated silicon probe. [c] The noise is calculated as the root-mean-square noise using a blank spectrum; σ = standard deviation. [d] These trials were done using synthetic tap water, which has components listed in Table 3.13.

25). This indicates that the components of synthetic tap water do not interfere with the detection of CN^- using the $NiCl_2$(dppp) extractant. However, the LODs for CN^- in synthetic tap water (3 mM and 0.2 μM for the uncoated and $NiCl_2$(dppp)-coated probes, respectively) are slightly higher than the 10-minute LODs for CN^- in pH 10 water (2 mM and 0.09 μM for the uncoated and $NiCl_2$(dppp)-coated probes, respectively), as shown in Table 4.1. Details of the calculation of these LODs can be found in Appendix E. These higher LODs may indicate a small effect of the more complex synthetic tap water matrix compared to the pH 10 water. Even though synthetic tap water affects the ratio of extraction of CN^- by the $NiCl_2$(dppp)-coated probe and hence the 10-minute LOD, there is still a 15,000-fold lowering of the LOD compared to the uncoated probe in the synthetic tap water matrix.

A second chloride-containing matrix was tested when the $NiCl_2$(dppp)-coated probe was immersed in a solution containing 10 μM CN^- and 1.0 M Cl^-. Even though the Cl^- co-contaminant is present in 100,000-fold excess compared to CN^-, the *SNR* after 10 minutes was very large (93 ± 27) and was the same within error as for a solution of 10 μM CN^- with no added Cl^-. Finally, 10 μM CN^- was put in a solution of simulated seawater that contains a high concentration of many salts (see Table 4.4) and the *SNR* was measured after 10 minutes in contact with the $NiCl_2$(dppp)-coated probe. Although the ν(CN) band was visible after 10 minutes with a *SNR* of 13 ± 4, the presence of 53,500-fold excess Cl^- in addition to the other co-contaminants (i.e., sulfate, carbonate, and bromide) significantly slowed down the extraction of CN^- by the $NiCl_2$(dppp) coating. Spectra of this extraction over a 60 minute time period can be seen in Figure 4.5. The presence of a detectable ν(CN) band after 10 minutes in 10 μM CN^- suggests that CN^- may be detectable in real seawater and other aqueous brines using the $NiCl_2$(dppp)-coated silicon probe, although the method of standard additions might have to be used for quantification.

Table 4.4. Components of a seawater simulant[a]

salts[b]	concentration, mM
NaCl	458
KCl	5
$CaCl_2$	10
$MgCl_2$	26
$MgSO_4$	26
$KHCO_3$	2.3
KBr	0.75
H_3BO_3	0.32

[a] The recipe was taken from a book by J. E. Fergusson.[38] [b] The total concentration of aqueous Cl^- is 535 mM. Concentrations of seawater components vary somewhat by location, and additional components are commonly found in seawater but are generally less than 20 ppm.

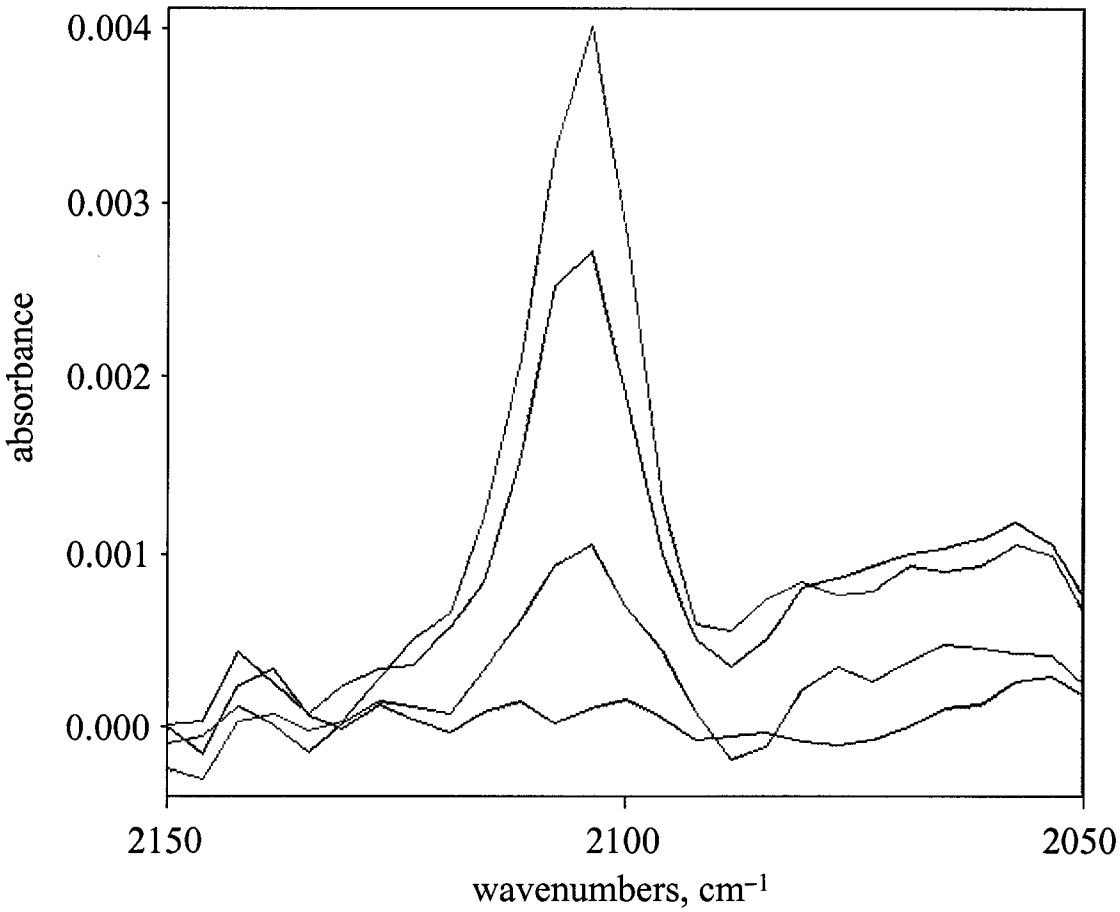

Figure 4.5. ATR-FTIR spectra of 10 μM CN^- in a simulated seawater matrix collected after 0, 10, 30, and 60 minutes (black, blue, green, and red spectra, respectively) in contact with the $NiCl_2$(dppp)-coated silicon probe.

Conclusions

This chapter has described the detection of low concentrations of aqueous CN^- in 10 minutes using silicon ATR crystals coated with a thin-film of the extractant $NiCl_2$(dppp). The use of the $NiCl_2$(dppp)-coated silicon probe decreased the 10-minute LOD 22,000-fold compared to that of the commercially available, unmodified silicon probe. A linear calibration curve was produced over the concentration range 0.1 to 10.0 μM CN^- using the $NiCl_2$(dppp)-coated silicon probe, which allows for the quantification of low concentrations of aqueous CN^-. Calibration curves and individual concentrations have been shown to be reproducible over two different years when the experiments were conducted by different operators using different $NiCl_2$(dppp) and CN^- stock solutions. In general, LODs determined from this method were reproducible with error less than 30%.

Three different chloride-containing matrixes were examined to determine if any interference with the detection of CN^- by the $NiCl_2$(dppp)-coated silicon probe would occur. Although the CN^- LOD was slightly higher for synthetic tap water compared to pH 10 water, the *SNR*s after 10 minutes were the same within error for solutions of 10 μM CN^- in the two matrixes. Likewise, there was also no significant effect on the *SNR* of the ν(CN) peak for a solution of 10 μM CN^- with a 100,000-fold excess of Cl^-. Additionally, the 10-minute LOD of 0.2 μM CN^- using the $NiCl_2$(dppp)-coated probe in synthetic tap water is significantly below the MCL of 7.7 μM CN^- set by the EPA.[5] This indicates that even in tap water that contains many impurities, the ATR-FTIR method using a $NiCl_2$(dppp)-coated probe can detect CN^- significantly below the EPA-regulated limits. However, the presence of a complex combination of salts commonly found in seawater significantly lowered the *SNR* of the ν(CN) peak compared to pH 10 water. Quantification of CN^- in seawater would probably require the use of the method of standard additions. Even so, the ATR-FTIR method using the $NiCl_2$(dppp)-coated silicon probe is appropriate for detection of CN^- in a wide variety of aqueous matrixes.

References

1. Boening, D. W.; Chew, C. M. *Water, Air, Soil, Pollut.* **1999**, *109*, 67–79.
2. Otu, E. O.; Byerley, J. J.; Robinson, C. W. *Int. J. Environ. Anal. Chem.* **1996**, *63*, 81–90.
3. http://www.epa.gov/safewater/contaminants/dw_contamfs/cyanide.html, September 2003.
4. Hardman, J. G.; Limbird, L. E.; Molinoff, P. B.; Ruddon, R. W.; Gilman, A. G., Eds. *Goodman and Gilman's Pharmacological Basics of Therapeutics*; 9th ed.; McGraw-Hill: New York, 1996, p 1688.
5. http://www.epa.gov/safewater/mcl.html, September 2003.
6. "Method OIA-1677 Available cyanide by flow injection, ligand exchange, and amperometry, 821-R-99-013," U.S. EPA, Office of Water, August 1999.
7. http://www.oico.com/cyan.htm, December 2003.
8. APHA-AWWA-WPCF, Ed. *Standard Methods for the Examination of Water and Wastewater*; 20th ed.; American Public Health Association: Washington DC, 1998, pp 4-37–4-41.
9. APHA-AWWA-WPCF, Ed. *Standard Methods for the Examination of Water and Wastewater*; 20th ed.; American Public Health Association: Washington DC, 1998, pp 4-41–4-44.
10. Zheng, A.; Dzombak, D. A.; Luthy, R. G.; Sawyer, B.; Lazouskas, W.; Tata, P.; Delaney, M.; Zilitinkevitch, L.; Sebroski, J. R.; Swartling, R. S.; Drop, S. M.; Flaherty, J. M. *Environ. Sci. Technol.* **2003**, *37*, 107–115.
11. Sun, B.; Noller, B. N. *Water Res.* **1998**, *32*, 3698–3704.
12. Karube, I.; Yano, K.; Sasaki, S.; Nomura, Y.; Ikebukuro, K. *Annals NY Acad. Sci.* **1998**, *864*, 23–36.
13. Singh, H. B.; Wasi, N.; Mehra, M. C. *Int. J. Environ. Anal. Chem.* **1986**, *26*, 115–136.

14. Zheng, A.; Dzombak, D. A.; Luthy, R. G.; Delaney, M. F.; Drop, S. M.; Flaherty, J. M.; Sawyer, B.; Sebroski, J. R.; Swartling, R. S.; Tata, P.; Zilitinkevitch, L. Proceedings of the 73rd Annual Conference on Water Quality and Wastewater Treatment, Anaheim, CA, 2000, session 66.

15. "ASTM Designation: D 4282-95; Standard Test Method for Determination of Free Cyanide in Water and Wastewater by Microdiffusion" In *Annual Book of ASTM Standards*; ASTM: Philadelphia, PA, 1998; Vol. 14.02, pp 468–472.

16. "Determination of Metal Cyanides," Application Note No. 55; Dionex Corporation: Sunnyvale, CA, 1988.

17. "Method 335.3 Methods for Chemical Analysis of Water and Wastes, 4-79-020," U.S. EPA, Office of Research and Development: Cincinnati, OH, 1983.

18. "ASTM Designation: D 4374-93, Standard Test Method for Cyanides in Water-Automated Methods for Total Cyanide, Dissociable Cyanide, and Thiocyanate" In *Annual Book of ASTM Standards*; ASTM: Philadelphia, PA, 1998; Vol. 14.02.

19. APHA-AWWA-WPCF, Ed. *Standard Methods for the Examination of Water and Wastewater*; 20th ed.; American Public Health Association: Washington DC, 1998, pp 4-44–4-45.

20. APHA-AWWA-WPCF, Ed. *Standard Methods for the Examination of Water and Wastewater*; 20th ed.; American Public Health Association: Washington DC, 1998, pp 4-52–4-53.

21. Siontorou, C. G.; Nikolelis, D. P. *Anal. Chim. Acta* **1997**, *355*, 227–234.

22. Rosentreter, J. J.; Skogerboe, R. K. *Anal. Chem.* **1991**, *63*, 682–688.

23. Meeusen, J. C. L.; Temminghoff, E. J. M.; Keizer, M. G.; Novozamsky, I. *Analyst* **1989**, *114*, 959–963.

24. Vallejo-Pecharroman, B.; de Castro, L. *Analyst* **2002**, *127*, 267–270.

25. Nomura, Y.; Nagakubo, K.; Ji, H.-S.; Watanabe, A.; Akimoto, T.; McNiven, S.; Hayashi, K.; Arikawa, Y.; Karube, I. *Environ. Sci. Technol.* **2000**, *34*, 2618–2622.

26. Caliamanis, A.; McCormick, M. J.; Carpenter, P. D. *J. Chromatogr., A* **2000**, *884*, 75–80.

27. Gering, K. L.; Rosentreter, J. J. In *Cyanide: Social, Industrial and Economic Aspects*; Young, C., Ed.; The Mineral, Metals and Materials Society: Warrendale, PA, 2001, pp 141–150.

28. Mirmohseni, A.; Alipour, A. *Sens. Actuators, B* **2002**, *84*, 245–251.

29. Miralles, E.; Compano, R.; Granados, M.; Prat, M. D. *Anal. Chim. Acta* **2000**, *403*, 197–204.

30. Spencer, K. M.; Sylvia, J. M.; Clauson, S. L.; Janni, J. A. *Proc. SPIE-Int. Soc. Opt. Eng.* **2002**, *4577*, 158–165.

31. Tessier, P. M.; Christensen, S. D.; Ong, K. K.; Clemente, E. M.; Lenhoff, A. M.; Kaler, E. W.; Velev, O. D. *Appl. Spectrosc.* **2002**, *56*, 1524–1530.

32. Shelton, R. D.; Haas III, J. W.; Wachter, E. A. *Appl. Spectrosc.* **1994**, *48*, 1007–1010.

33. Premasiri, W. R.; Clarke, R. H.; Londhe, S.; Womble, W. E. *J. Raman Spectrosc.* **2001**, *32*, 919–922.

34. Fernandez-Arguelles, M. T.; Costa-Fernandez, J. M.; Pereiro, R.; Sanz-Medel, A. *Anal. Chim. Acta* **2003**, *491*, 27–35.

35. Weinberg, H. S.; Cook, S. J. *Anal. Chem.* **2002**, *74*, 6055–6063.

36. Strauss, S. H.; Odom, M. A.; Hebert, G. N.; Clapsaddle, B. J. *J. Am. Water Works Assoc.* **2002**, *94*, 109–115.

37. Kosak, E. D. Determination of Pseudohalide Anions at ppb Levels and a Chemical Warfare Agent Hydrolysis Product at sub-ppm Levels in Aqueous Samples by Attenuated Total Reflectance Fourier Transform Infrared Spectroscopy. M.S. Thesis, Colorado State University, Fort Collins, CO, 2003.

38. Fergusson, J. E. *Inorganic Chemistry and the Earth, Chemical Resources, Their Extraction, Use and Environmental Impact*; Pergamon Press: New York, 1982.

Appendix A

Table A.1. Reproducibility of the ATR-FTIR absorbance values of the $DEC^{+}NO_3^{-}$-coated silicon probe[a]

	ν(CH), 2926 cm^{-1}	ν(NO), 1332 cm^{-1}	ratio ν(CH)/ν(NO)
	1.07552	1.0255	1.049
	1.14979	1.10149	1.044
	1.0948	1.03961	1.053
	1.14328	1.10144	1.038
	1.04346	0.973823	1.072
	1.05895	1.02104	1.037
	1.0958	1.05249	1.041
	1.09303	1.03467	1.056
	1.13891	1.0995	1.036
	1.11588	1.06903	1.044
	1.10047	1.05341	1.045
	1.09961	1.03958	1.058
	1.10233	1.04308	1.057
	1.12473	1.06946	1.052
	1.08815	1.01821	1.069
	1.04588	0.99044	1.056
	1.13347	1.08252	1.047
	1.13782	1.0958	1.038
	1.06323	0.991293	1.073
	1.11972	1.07413	1.042
	1.12652	1.07328	1.050
	1.10616	1.04949	1.054
	1.13713	1.08028	1.053
	1.13806	1.08202	1.052
	1.12118	1.09805	1.021
	1.07691	1.04596	1.030
	1.15893	1.11425	1.040
	1.13043	1.07322	1.053
	1.17572	1.14723	1.025
	1.16416	1.11521	1.044
	1.05459	0.91956	1.147
	1.09551	0.969367	1.130
	1.18743	1.03604	1.146

	ν(CH), 2926 cm^{-1}	ν(NO), 1332 cm^{-1}	ratio ν(CH)/ν(NO)
	1.07599	0.907701	1.185
	1.08523	0.914866	1.186
	1.07856	0.93066	1.159
	1.16029	1.11945	1.036
	1.16526	1.11445	1.046
	1.15317	1.0841	1.064
	1.01684	1.03705	0.981
	1.04445	1.01487	1.029
	1.0602	1.03194	1.027
	1.02866	0.991616	1.037
	1.01641	1.01634	1.000
	1.02395	1.00046	1.023
	1.04622	1.02553	1.020
average[b]	1.10	1.04	1.06
standard deviation	0.05	0.06	0.04
RSD[c]	5%	6%	4%

[a] Each trial listed was from a separate film made by evaporating 20 μL of a 3 mM dichloromethane solution of $DEC^{+}NO_3^{-}$ on the silicon probe. [b] Average of 46 trials. [c] RSD = relative standard deviation.

Appendix B

Calculation of 10-minute ATR-FTIR LODs using the uncoated probes

The 10-minute LOD for ClO_4^- using the uncoated diamond probe is 0.7 mM with a *SNR* of 4 ± 1, as shown in Table B.1, and the 10-minute LOD for ClO_4^- using the uncoated silicon probe is 0.8 mM with a *SNR* of 4.0 ± 0.6, as shown in Table 3.2. The 30-minute LOD for ClO_4^- using the uncoated silicon probe is 0.40 mM with a *SNR* of 5 ± 1, as shown in Table B.2. The 10-minute ClO_3^- LOD using the uncoated silicon probe is 2 mM with a *SNR* of 3.0 ± 0.7, as shown in Table B.3 and the 10-minute ClO_3^- LOD using the uncoated diamond probe is 1 mM with a *SNR* of 4 ± 1, as shown in Table B.4. The 10-minute $PFOS^-$ LOD using the uncoated silicon probe is 0.01 mM with a *SNR* of 4 ± 1, as shown in Table B.5. The 10-minute $PFBS^-$ LOD using the uncoated silicon probe is 0.25 mM with a *SNR* of 3.5 ± 0.7, as shown in Table B.6. The 10-minute $CF_3SO_3^-$ LOD using the uncoated silicon probe is 0.3 mM with a *SNR* of 3.7 ± 0.7, as shown in Table B.7. The 10-minute $PMPA^-$ LOD using the uncoated diamond probe 0.3 mM with a *SNR* of 4 ± 1, as shown in Table B.8. In all of these tables, the bold values are the LODs as listed in Table 3.1.

Table B.1. Determination of the 10-minute ClO_4^- LOD using the uncoated diamond ATR probe[a]

concentration, mM	ν(ClO) signal[b]	average signal (σ)[c]	average *SNR* ± error[d]
10	0.007595	0.0076(2)	84 ± 28
10	0.007488		
10	0.007862		
2	0.0015	0.0014(1)	14 ± 6
2	0.00156		
2	0.00124		
1.5	0.00121	0.0010(2)	10 ± 4
1.5	0.00105		
1.5	0.000644		
1	0.0006999	0.0006(2)	6 ± 3
1	0.000388		
1	0.000733		
1	0.000431		
0.8	0.00031	0.00035(7)	4.4 ± 1.4
0.8	0.000287		
0.8	0.000450		
0.8	0.000497		
0.7	**0.000358**	**0.00032(2)**	**4 ± 1**
0.7	**0.000313**		
0.7	**0.000302**		

[a] Distilled/deionized water. Each 10-minute spectrum was the result of 1660 co-added scans. [b] Absorbance at 1108 cm^{-1}. [c] σ = standard deviation. [d] Signal-to-noise ratio (*SNR*) where average noise = $9(3) \times 10^{-5}$ and the error was propagated from the signal and noise standard deviations.

Table B.2. Calculation of the 30-minute ClO_4^- LOD using the uncoated silicon ATR probe[a]

concentration, mM	ν(ClO) signal[b]	average signal (σ)[c]	average *SNR* ± error[d]
0.8	0.00125		12.5[e]
0.5	0.000759	0.0007(1)	7 ± 2
0.5	0.000566		
0.4	**0.000442**	**0.0005(1)**	**5 ± 1**
0.4	**0.000735**		
0.4	**0.00057**		
0.4	**0.000416**		
0.3	0.00011	0.0002(1)	2 ± 1
0.3	0.000387		
0.3	0.0000305		

[a] Distilled/deionized water. Each 30-minute spectrum was the result of 5000 co-added scans. [b] Absorbance at 1108 cm^{-1}. [c] σ = standard deviation. [d] Signal-to-noise ratio (*SNR*) where average noise = $1.0(2) \times 10^{-4}$ and the error was propagated from the signal and noise standard deviations. [e] No error is listed for those concentrations for which only one experiment was performed.

Table B.3. Determination of the 10-minute ClO_3^- LOD using the uncoated silicon ATR probe[a]

concentration, mM	ν(ClO) signal[b]	average signal (σ)[c]	average *SNR* ± error[d]
100	0.0407	0.0413(5)	83 ± 15
100	0.041997		
100	0.04122		
10	0.00496		10[e]
2	**0.001561**	**0.0015(2)**	**3.0 ± 0.7**
2	**0.00118**		
2	**0.00161**		
1	0.00074		1.5

[a] Distilled/deionized water. Each 10-minute spectrum was the result of 1660 co-added scans. [b] Absorbance at 988 cm^{-1}; [c] σ = standard deviation. [d] Signal-to-noise ratio (*SNR*) where average noise = 5.0(9) × 10^{-4} and the error was propagated from the signal and noise standard deviations. [e] No error is listed for those concentrations for which only one experiment was performed.

Table B.4. Determination of the 10-minute ClO_3^- LOD using the uncoated diamond ATR probe[a]

concentration, mM	ν(ClO) signal[b]	average signal (σ)[c]	average *SNR* ± error[d]
10	0.00654	0.0064(1)	49 ± 8
10	0.00619		
10	0.00642		
2	0.00123	0.00117(7)	9 ± 1
2	0.00110		
1.5	0.000638	0.00068(7)	5.2 ± 0.9
1.5	0.000627		
1.5	0.000774		
1.2	0.00078	0.0008(1)	6 ± 1
1.2	0.00091		
1.2	0.000662		
1.1	0.000574	0.00057(1)	4.4 ± 0.7
1.1	0.000585		
1.1	0.000561		
1	**0.000362**	**0.0005(1)**	**4 ± 1**
1	**0.0005**		
1	**0.000658**		

[a] Distilled/deionized water. Each 10-minute spectrum was the result of 1660 co-added scans; [b] Absorbance at 973 cm^{-1}. [c] σ = standard deviation; [d] Signal-to-noise ratio (*SNR*) where the average noise = $1.3(2) \times 10^{-4}$ and the error was propagated from the signal and noise standard deviations.

Table B.5. Determination of the 10-minute $PFOS^-$ LOD using the uncoated silicon ATR probe[a]

concentration, mM	signal[b]	average signal (σ)[c]	average *SNR* ± error[d]
1	0.01535	0.012(2)	63 ± 17
1	0.01106		
1	0.010385		
0.1	0.00203		11[e]
0.05	0.00135		7
0.02	0.00115		6
0.01	**0.000503**	**0.0008(2)**	**4 ± 1**
0.01	**0.00101**		
0.01	**0.000745**		

[a] Distilled/deionized water. Each 10-minute spectrum was the result of 1660 co-added scans. [b] Absorbance at 1243 cm^{-1}. [c] σ = standard deviation. [d] Signal-to-noise ratio (*SNR*) where average noise = $1.9(4)\times10^{-4}$ and the error was propagated from the signal and noise standard deviations. [e] No error is listed for those concentrations for which only one experiment was performed.

Table B.6. Determination of the 10-minute $PFBS^-$ LOD using the uncoated silicon ATR probe[a]

concentration, mM	signal[b]	average signal (σ)[c]	average *SNR* ± error[d]
5	0.019705	0.01968(5)	68 ± 12
5	0.019723		
5	0.01961		
0.5	0.00188	0.0017(2)	6 ± 1
0.5	0.00152		
0.25	**0.00087**	**0.0010(1)**	**3.5 ± 0.7**
0.25	**0.001101**		
0.25	**0.001032**		

[a] Distilled/deionized water. Each 10-minute spectrum was the result of 1660 co-added scans. [b] Absorbance at 1254 cm^{-1}. [c] σ = standard deviation. [d] Signal-to-noise ratio (*SNR*) where the average noise = $2.9(5) \times 10^{-4}$ and the error was propagated from the signal and noise standard deviations.

Table B.7. Determination of the 10-minute $CF_3SO_3^-$ LOD using the uncoated silicon ATR probe[a]

concentration, mM	signal[b]	average signal (σ)[c]	average *SNR* ± error[d]
10	0.01467		113[e]
5	0.007649	0.0075(1)	58 ± 13
5	0.007392		
1	0.00127	0.00136(9)	10 ± 2
1	0.00145		
0.5	0.000722		5.6
0.3	**0.000542**	**0.00048(6)**	**3.7 ± 0.7**
0.3	**0.000406**		
0.3	**0.000485**		

[a] Distilled/deionized water. Each 10-minute spectrum was the result of 1660 co-added scans. [b] Absorbance at 1258 cm^{-1}. [c] σ = standard deviation. [d] Signal-to-noise ratio (*SNR*) where average noise = $1.3(2) \times 10^{-4}$ and the error was propagated from the signal and noise standard deviations. [e] No error is listed for those concentrations for which only one experiment was performed.

Table B.8. Determination of the $PMPA^-$ 10-minute LOD using the uncoated diamond ATR probe[a]

concentration, mM	signal[b]	average signal (σ)[c]	average *SNR* ± error[d]
0.5	0.0009263		9.3[e]
0.5	0.000477	0.00054(5)	5 ± 1
0.4	0.000548		
0.4	0.000608		
0.3	**0.000382**	**0.0004(1)**	**4 ± 1**
0.3	**0.000249**		
0.3	**0.000440**		
0.3	**0.000236**		
0.3	**0.000505**		
0.3	**0.000350**		

[a] Distilled/deionized water. Each 10-minute spectrum was the result of 1660 co-added scans. [b] Absorbance at 1042 cm^{-1}. [c] σ = standard deviation. [d] Signal-to-noise ratio (*SNR*) where the average noise = $1.0(3) \times 10^{-4}$ and the error was propagated from the signal and noise standard deviations. [e] No error is listed for concentrations for which only one experiment was performed.

Table B.9. The signal-to-noise ratios (*SNR*s) for the major $PMPA^-$ peaks from the 10-minute detection of 0.3 mM $PMPA^-$ using the uncoated diamond ATR probe

ν, cm^{-1}	average *SNR* ± error
1162	3 ± 1
1065	2 ± 1
1046[a]	4 ± 1
1015	1.5 ± 0.5

[a] The 1046 cm^{-1} peak was the peak used for determining the 10-minute LOD listed in Tables 3.1 and B.8.

Appendix C

Calculation of 10-minute ATR-FTIR LODs using the extractant-coated probes

The 10-minute LOD for ClO_4^- using the $DEC^+NO_3^-$-coated silicon probe is 0.04 μM with a *SNR* of 3.5 ± 0.8, as shown in Table C.1, and the 10-minute LOD for ClO_4^- using the $DEC^+NO_3^-$-coated diamond probe is 0.03 μM with a *SNR* of 2.8 ± 0.6, as shown in Table C.2. The 30-minute LOD for ClO_4^- using the $DEC^+NO_3^-$-coated silicon probe is 0.02 μM with a *SNR* of 3.7 ± 0.9, as shown in Table C.3. The 10-minute ClO_3^- LOD using the $DEC^+NO_3^-$-coated diamond probe is 0.2 μM with a *SNR* of 3.2 ± 0.9, as shown in Table C.4, and the 10-minute ClO_3^- LOD using the $DEC^+NO_3^-$-coated silicon probe is 0.7 μM with a *SNR* of 3.4 ± 0.6, as shown in Table C.6. The 10-minute $PFOS^-$ LOD using the $DEC^+NO_3^-$-coated silicon probe is 0.06 μM with a *SNR* of 3 ± 1, as shown in Table C.8. The 10-minute $PFBS^-$ LOD using the $DEC^+NO_3^-$-coated silicon probe is 0.07 μM with a *SNR* of 3.5 ± 0.8, as shown in Table C.10. The 10-minute $CF_3SO_3^-$ LOD using the $DEC^+NO_3^-$-coated silicon probe is 0.05 μM with a *SNR* of 2.9 ± 0.5, as shown in Table C.12. In all of these tables, the bold values are the LODs as listed in Table 3.1.

Table C.1. Determination of 10-minute ClO_4^- LOD using the $DEC^+NO_3^-$-coated silicon ATR probe[a]

concentration, μM	ν(ClO) signal[b]	average signal (σ)[c]	average *SNR* ± error[d]
5	0.14018	0.13(1)	220 ± 40
5	0.10723		
5	0.13716		
1	0.04833	0.045(5)	75 ± 15
1	0.05136		
1	0.04753		
1	0.03943		
1	0.03894		
1	0.04422		
0.1	0.004475	0.0041(7)	7 ± 2
0.1	0.003065		
0.1	0.00466		
0.05	0.00163	0.0027(8)	5 ± 2
0.05	0.003282		
0.05	0.0032		
0.04	**0.001715**	**0.0021(3)**	**3.5 ± 0.8**
0.04	**0.00212**		
0.04	**0.002556**		

[a] Distilled/deionized water. Each trial was done using the silicon probe coated with 20 μL of a 3 mM dichloromethane solution of $DEC^+NO_3^-$. [b] Absorbance at 1096 cm^{-1}. [c] σ = standard deviation. [d] Signal-to-noise ratio (*SNR*) where the average noise = $1.9(3) \times 10^{-4}$ and the error was propagated from the signal and noise standard deviations.

Table C.2. Determination of 10-minute ClO_4^- LOD using $DEC^+NO_3^-$-coated diamond ATR probe[a]

concentration, μM	ν(ClO) signal[b]	average signal (σ)[c]	average *SNR* ± error[d]
0.1	0.00173		9.1[e]
0.05	0.000969		5.1
0.03	**0.000666**	**0.00054(9)**	**2.8 ± 0.6**
0.03	**0.000446**		
0.03	**0.000511**		

[a] Distilled/deionized water. Each trial was done using the diamond probe coated with 20 μL of a 3 mM dichloromethane solution of $DEC^+NO_3^-$. [b] Absorbance at 1096 cm^{-1}. [c] σ = standard deviation. [d] Signal-to-noise ratio (*SNR*) where the average noise = 1.9(3) × 10^{-4} and the error was propagated from the signal and noise standard deviations. [e] No error is listed for those concentrations for which only one experiment was performed.

Table C.3. Determination of 30-minute ClO_4^- LOD using the $DEC^+NO_3^-$-coated silicon ATR probe[a]

concentration, μM	ν(ClO) signal[b]	average signal (σ)[c]	average *SNR* ± error[d]
0.04	0.002964	0.0034(5)	6 ± 1
0.04	0.003909		
0.02	**0.002295**	**0.0022(4)**	**3.7 ± 0.9**
0.02	**0.002212**		
0.02	**0.002196**		
0.02	**0.00273**		
0.02	**0.00127**		
0.02	**0.00231**		

[a] Distilled/deionized water. Each trial was done using the silicon probe coated with 20 μL of a 3 mM dichloromethane solution of $DEC^+NO_3^-$. [b] Absorbance at 1096 cm^{-1}. [c] σ = standard deviation. [d] Signal-to-noise ratio (*SNR*) where the average noise = 1.9(3) × 10^{-4} and the error was propagated from the signal and noise standard deviations.

Table C.4. Determination of 10-minute ClO_3^- LOD using $DEC^+NO_3^-$-coated diamond ATR probe[a]

concentration, μM	ν(ClO) signal[b]	average signal (σ)[c]	average *SNR* ± error[d]
20	0.05364		89[e]
0.5	0.00422	0.0044(1)	8 ± 1
0.5	0.00451		
0.5	0.00441		
0.3	0.00354	0.0031(4)	5 ± 1
0.3	0.00292		
0.3	0.00273		
0.2	**0.00211**	**0.0019(4)**	**3.2 ± 0.9**
0.2	**0.00224**		
0.2	**0.00134**		
0.1	0.000837		1.4

[a] Distilled/deionized water. Each trial was done using the diamond probe coated with 20 μL of a 3 mM dichloromethane solution of $DEC^+NO_3^-$. [b] Absorbance at 973 cm^{-1}. [c] σ = standard deviation. [d] Signal-to-noise ratio (*SNR*) where the average noise = 6(1) × 10^{-4} and the error was propagated from the signal and noise standard deviations. [e] No error is listed for those concentrations for which only one experiment was performed.

Table C.5. The signal-to-noise ratios (*SNR*s) for the major ν(ClO) bands from the 10-minute detection of 0.2 μM ClO_3^- using the $DEC^+NO_3^-$-coated diamond ATR probe

ν, cm^{-1}	average *SNR* ± error
988	3.2 ± 0.7
973[a]	3.2 ± 0.9

[a] The 973 cm^{-1} peak was the peak used for determining the 10-minute LOD listed in Tables 3.1 and C.4.

Table C.6. Determination of the 10-minute ClO_3^- LOD using $DEC^+NO_3^-$-coated silicon ATR probe[a]

concentration, μM	ν(ClO) signal[b]	average signal (σ)[c]	average *SNR* ± error[d]
20	0.05066		28[e]
1	0.0109	0.0108(4)	5.4 ± 0.9
1	0.0112		
1	0.0103		
0.8	0.00831	0.008(1)	4.2 ± 0.8
0.8	0.00604		
0.8	0.00843		
0.7	**0.00608**	**0.0062(4)**	**3.4 ± 0.6**
0.7	**0.00575**		
0.7	**0.00674**		

[a] Distilled/deionized water. Each trial was done using the silicon probe coated with 20 μL of a 3 mM dichloromethane solution of $DEC^+NO_3^-$. [b] Absorbance at 988 cm^{-1}. [c] σ = standard deviation. [d] Signal-to-noise ratio (*SNR*) where the average noise = $1.8(3) \times 10^{-3}$ and the error was propagated from the signal and noise standard deviations. [e] No error is listed for those concentrations for which only one experiment was performed.

Table C.7. The signal-to-noise ratios (*SNR*s) for the major ν(ClO) bands from the 10-minute detection of 0.7 μM ClO_3^- using the $DEC^+NO_3^-$-coated silicon ATR probe

ν, cm^{-1}	average *SNR* ± error
988	3.4 ± 0.6
973[a]	3.6 ± 0.8

[a] The 988 cm^{-1} peak was the peak used for determining the 10-minute LOD listed in Tables 3.1 and C.6.

Table C.8. Determination of 10-minute $PFOS^-$ LOD using the $DEC^+NO_3^-$-coated silicon ATR probe[a]

concentration, μM	signal[b]	average signal (σ)[c]	average *SNR* ± error[d]
0.1	0.00444	0.0037(5)	10 ± 2
0.1	0.00358		
0.1	0.0033		
0.1	0.00334		
0.07	0.00304	0.0024(6)	6 ± 2
0.07	0.00245		
0.07	0.00157		
0.06	**0.00105**	**0.0013(5)**	**3 ± 1**
0.06	**0.00196**		
0.06	**0.000772**		
0.05	0.00059	0.0009(3)	2.4 ± 0.4
0.05	0.00132		
0.05	0.00084		

[a] Distilled/deionized water. Each trial was done using the silicon probe coated with 20 μL of a 1 mM dichloromethane solution of $DEC^+NO_3^-$. [b] Absorbance at 1270 cm^{-1}. [c] σ = standard deviation. [d] Signal-to-noise ratio (*SNR*) where the average noise = $3.9(6) \times 10^{-4}$ and the error was propagated from the signal and noise standard deviations.

Table C.9. The signal-to-noise ratios (*SNR*s) for the major $PFOS^-$ peaks from the 10-minute detection of 0.06 μM $PFOS^-$ using the $DEC^+NO_3^-$-coated silicon ATR probe

ν, cm^{-1}	average *SNR* ± error
1270[a]	3 ± 1
1243	2 ± 1
1212	1.0 ± 0.8
1154	1.5 ± 0.8

[a] The 1270 cm^{-1} peak was the peak used for determining the 10-minute LOD listed in Tables 3.1 and C.8.

Table C.10. Determination of 10-minute $PFBS^-$ LOD using the $DEC^+NO_3^-$-coated silicon ATR probe[a]

concentration, μM	signal[b]	average signal (σ)[c]	average *SNR* ± error[d]
10	0.40169	0.42(2)	910 ± 130
10	0.41883		
10	0.44954		
1	0.03178		69[e]
0.1	0.00205	0.0025(6)	5 ± 1
0.1	0.00202		
0.1	0.00263		
0.07	**0.00158**	**0.0016(3)**	**3.5 ± 0.8**
0.07	**0.0013**		
0.07	**0.00192**		

[a] Distilled/deionized water. Each trial was done using the silicon probe coated with 20 μL of a 1 mM dichloromethane solution of $DEC^+NO_3^-$. [b] Absorbance at 1270 cm^{-1}. [c] σ = standard deviation. [d] Signal-to-noise ratio (*SNR*) where the average noise = $4.6(6) \times 10^{-4}$ and the error was propagated from the signal and noise standard deviations. [e] No error is listed for those concentrations for which only one experiment was performed.

Table C.11. The signal-to-noise ratios (*SNR*s) for the major $PFBS^-$ peaks from the 10-minute detection of 0.07 μM $PFBS^-$ using the $DEC^+NO_3^-$-coated silicon ATR probe

ν, cm^{-1}	average *SNR* ± error
1270[a]	3.5 ± 0.8
1193	2.4 ± 0.1
1131	5 ± 1
1050	1.7 ± 0.1

[a] The 1270 cm^{-1} peak was the peak used for determining the 10-minute LOD listed in Tables 3.1 and C.10.

Table C.12. Determination of 10-minute $CF_3SO_3^-$ LOD using $DEC^+NO_3^-$-coated silicon ATR probe[a]

concentration, μM	signal[b]	average signal (σ)[c]	average *SNR* ± error[d]
0.1	0.00282	0.0037(9)	8 ± 2
0.1	0.00315		
0.1	0.00517		
0.1	0.00353		
0.07	0.00198	0.0024(3)	5.0 ± 0.8
0.07	0.00265		
0.07	0.00249		
0.05	**0.0016**	**0.0014(2)**	**2.9 ± 0.5**
0.05	**0.00137**		
0.05	**0.00118**		
0.05	**0.00157**		

[a] Distilled/deionized water. Each trial was done using the silicon probe coated with 20 μL of a 1 mM dichloromethane solution of $DEC^+NO_3^-$. [b] Absorbance at 1266 cm^{-1}. [c] σ = standard deviation. [d] Signal-to-noise ratio (*SNR*) where the average noise = $4.9(5) \times 10^{-4}$ and the error was propagated from the signal and noise standard deviations.

Table C.13. The signal-to-noise ratios (*SNR*s) for the major $CF_3SO_3^-$ peaks from the 10-minute detection of 0.05 μM $CF_3SO_3^-$ using the $DEC^+NO_3^-$-coated silicon ATR probe

ν, cm^{-1}	average *SNR* ± error
1266[a]	2.9 ± 0.5
1154	2.0 ± 0.6
1034	3 ± 1

[a] The 1266 cm^{-1} peak was the peak used for determining the 10-minute LOD listed in Tables 3.1 and C.12.

Appendix D

Calculation of 10-minute $PMPA^-$ LODs in synthetic tap water by ATR-FTIR

A synthetic tap water recipe was given to us by Janet Jensen (Joint Services Agent Water Monitor), and seven batches were prepared using the recipe shown in Table 3.13. Several of these batches were used to determine the 10-minute $PMPA^-$ LODs using the coated and uncoated diamond probe. The 10-minute LOD for $PMPA^-$ in synthetic tap water using the DEC^+Cl^--coated diamond probe is 0.2 mM with a *SNR* of 4.0 ± 0.7, as shown in Table D.1. The 10-minute LOD for $PMPA^-$ in synthetic tap water using the uncoated diamond probe is 0.4 mM with a *SNR* of 4 ± 1, as shown in Table D.2. In all of these tables, the bold values are the LODs.

Table D.1. Determination of the 10-minute $PMPA^-$ LOD in synthetic tap water using the DEC^+Cl^--coated diamond ATR probe[a]

concentration, mM	signal[b]	average signal (σ)[c]	average *SNR* ± error[d]
0.5	0.01051		5.8[e]
0.2	**0.007385**	**0.007(1)**	**4.0(7)**
0.2	**0.006003**		
0.2	**0.006905**		
0.2	**0.00914**		
0.1	0.007071	0.005(1)	2.8(6)[f]

[a] This data was collected by Dr. Stephanie S. Bowman. Each trial was done using the diamond probe coated with 20 μL of a 5 mM dichloromethane solution of DEC^+Cl^-. [b] Absorbance at 1112 cm^{-1}. [c] σ = standard deviation. [d] Signal-to-noise ratio (*SNR*) where the average noise = 1.8(2) × 10^{-3} and the error was propagated from the signal and noise standard deviations. [e] No error is listed for those concentrations for which only one trial was performed. [f] Due to the low absorbance for one of the trials at 0.1 mM, which gives *SNR* < 2, this concentration was determined not to be the LOD.

Table D.2. Determination of the 10-minute $PMPA^-$ LOD in synthetic tap water using the uncoated diamond ATR probe[a]

concentration, mM	signal[b]	average signal (σ)[c]	average *SNR* ± error[d]
1	0.00218		27[e]
0.5	0.000306	0.0004(1)	5 ± 2
0.5	0.000381		
0.5	0.000544		
0.4	**0.00026**	**0.00031(7)**	**4 ± 1**
0.4	**0.000408**		
0.4	**0.000264**		

[a] Each 10-minute spectrum was the result of 1660 co-added scans. [b] Absorbance at 1046 cm^{-1}. [c] σ = standard deviation. [d] Signal-to-noise ratio (*SNR*) where the average noise = $8(2) \times 10^{-5}$ and the error was propagated from the signal and noise standard deviations. [e] No error is listed for those concentrations for which only one experiment was performed.

Table D.3. The signal-to-noise ratios (*SNR*s) for the major $PMPA^-$ peaks from the 10-minute detection of 0.4 mM $PMPA^-$ using the uncoated diamond ATR probe

ν, cm^{-1}	average *SNR* ± error
1162	7 ± 3
1065	3 ± 1
1046[a]	4 ± 1
1015	3 ± 2

[a] The 1046 cm^{-1} peak was the peak used for determining the 10-minute LOD listed in Tables 3.1 and D.2.

Appendix E

Calculation of 10-minute ATR-FTIR LODs for cyanide

The 10-minute LOD for CN^- using the uncoated silicon probe is 2 mM with a *SNR* of 4 ± 1 is shown in Table E.1. The 10-minute LOD for CN^- using the $NiCl_2$(dppp)-coated silicon probe is 0.09 μM with a *SNR* of 4 ± 1 is shown in Table E.2. The 10-minute LOD for CN^- in synthetic tap water using the uncoated silicon probe is 3 mM with a *SNR* of 4 ± 1 is shown in Table E.3. The 10-minute LOD for CN^- in synthetic tap water using the $NiCl_2$(dppp)-coated silicon probe is 0.2 μM with a *SNR* of 4.2 ± 0.9 is shown in Table E.4. In all of these tables, the bold values are the LODs as listed in Table 4.1.

Table E.1. Calculation of the 10-minute LOD for CN^- using the uncoated silicon ATR probe[a]

concentration, mM	ν(CN) signal[b]	average signal (σ)[c]	average *SNR* ± error[d]
10	0.000357		15.5
4	0.0001901		8.3
3	0.000188	0.00018(2)	8 ± 3
3	0.000154		
3	0.000196		
2	**0.000095**	**0.00010(1)**	**4 ± 1**
2	**0.000117**		
2	**0.000083**		

[a] Each 10-minute spectrum was the result of 1,660 co-added scans. [b] Absorbance at 2081 cm^{-1}. [c] σ = standard deviation. [d] Signal-to-noise ratio (*SNR*) where the average noise = $2.3(7) \times 10^{-5}$ and the error was propagated from the signal and noise standard deviations.

Table E.2 Calculation of the 10-minute LOD for CN^- using the $NiCl_2$(dppp)-coated silicon ATR probe[a]

concentration, μM	ν(CN) signal[b]	average signal (σ)[c]	average *SNR* ± error[d]
10	0.02385	0.023(4)	330 ± 110
10	0.01895		
10	0.01799		
10	0.02471		
10	0.02856		
10	0.020057		
0.5	0.001204	0.0015(2)	21 ± 7
0.5	0.00161		
0.5	0.00166		
0.3	0.000847	0.00095(8)	14 ± 4
0.3	0.00105		
0.3	0.000966		
0.2	0.000621	0.00069(7)	10 ± 3
0.2	0.000681		
0.2	0.00078		
0.1	0.000314	0.00031(4)	4.4 ± 1.4
0.1	0.000259		
0.1	0.000345		
0.09	**0.000256**	**0.00027(7)**	**4 ± 1**
0.09	**0.000393**		
0.09	**0.000251**		
0.09	**0.000199**		
0.08	0.00018	0.00017(1)	2.4 ± 0.7
0.08	0.000177		
0.08	0.000153		

[a] Each trial was done using the silicon probe coated with 20 μL of a 5 mM dichloromethane solution of $NiCl_2$(dppp). [b] Absorbance at 2104 cm^{-1}. [c] σ = standard deviation; [d] Signal-to-noise ratio (*SNR*) where the average noise = 7(2) × 10^{-5} and the error was propagated from the signal and noise standard deviations.

Table E.3. Calculation of the 10-minute LOD for CN^- in synthetic tap water using the uncoated silicon ATR probe[a]

concentration, mM	ν(CN) signal[b]	average signal (σ)[c]	average *SNR* ± error[d]
10	0.0004454		23[e]
5	0.0002054		11
3	**0.0000711**	**0.00008(1)**	**4 ± 1**
3	**0.000101**		
3	**0.0000785**		
2	0.00004326		2.3

[a] This data was collected by Dr. Stephanie C. Bowman. Each 10-minute spectrum was the result of 1,660 co-added scans. The recipe for synthetic tap water is listed in Table 3.13. [b] Absorbance at 2081 cm^{-1}. [c] σ = standard deviation. [d] Signal-to-noise ratio (*SNR*) where the average noise = $1.9(4) \times 10^{-5}$ and the error was propagated from the signal and noise standard deviations. [e] No error is listed for those concentrations for which only one experiment was performed.

Table E.4. Calculation of the 10-minute LOD for CN^- in synthetic tap water using the $NiCl_2$(dppp)-coated silicon ATR probe[a]

concentration, μM	ν(CN) signal[b]	average signal (σ)[c]	average *SNR* ± error[d]
1	0.001361		17[e]
0.5	0.001189		15
0.3	0.000618		7.8
0.2	**0.00033**	**0.00034(6)**	**4.2 ± 0.9**
0.2	**0.000273**		
0.2	**0.000414**		

[a] Each trial was done using the silicon probe coated with 20 μL of a 5 mM dichloromethane solution of $NiCl_2$(dppp). The recipe for synthetic tap water is listed in Table 3.13. [b] Absorbance at 2104 cm^{-1}. [c] σ = standard deviation. [d] Signal-to-noise ratio (*SNR*) where the average noise = 8(1) × 10^{-5} and the error was propagated from the signal and noise standard deviations. [e] No error is listed for those concentrations for which only one experiment was performed.

Appendix F

Reprints of published papers

Table of Contents

Method for the determination of sub-ppm concentrations of perfluoroalkylsulfonate anions in water

Gretchen N. Hebert, Matthew A. Odom, Preston S. Craig, Donald L. Dick and Steven H. Strauss*

Department of Chemistry, Colorado State University, Fort Collins, CO 80523, USA. E-mail: strauss@chem.colostate.edu; Tel: (970)491-5104

Received 18th September 2001, Accepted 8th January 2002
First published as an Advance Article on the web 14th January 2002

The determination of sub-ppm concentrations of aqueous perfluoroalkylsulfonate (PFS†) anions, including perfluorooctylsulfonate (PFOS), has been accomplished with a relatively simple mass spectrometric procedure that does not require extraction of the analytes into an organic solvent or a chromatographic separation prior to injection into the negative-ion electrospray ionization mass spectrometer. Sample pretreatment was minimized and consisted of dilution of the aqueous samples of groundwater, surface water, tap water, and distilled water with acetonitrile, addition of dodecylsulfate (DDS) as an internal standard, and, in some cases, addition of known amounts of perfluorobutylsulfonate (PFBS) or PFOS for standard-addition experiments. The linear-response range for PFOS is 25.0 μg L^{-1} to 2.5 mg L^{-1}. The lower limit of this range is three orders of magnitude lower than an equally straightforward chromatographic method. The relative errors for standard aqueous solutions containing only 25.0 μg L^{-1} and 2.5 mg L^{-1} PFOS are ±14% and ±7%, respectively, with 133 μg L^{-1} DDS as the internal standard. The detection limit and quantification limit for PFOS in these standards are 5.0 μg L^{-1} and 25.0 μg L^{-1}, respectively. Six different PFS anions, containing three to eight carbon atoms, were identified and quantified in an aqueous film-forming foam (AFFF) formulation using the method of standard additions. Two alkylsulfate anions and two perfluoroalkylcarboxylate anions were also identified in the AFFF formulation.

Introduction

The 3M Company recently announced that it is discontinuing production and distribution of perfluorooctylsulfonate-based products because of the suspected toxicity of $C_8F_{17}SO_3^-$ (PFOS) and the persistence of some PFOS-based chemicals in workers, in animals, and in the environment.[1–13] The single-dose LD_{50} of tetraethylammonium perfluorooctylsulfonate for Wistar rats has long been known to be 190 mg kg^{-1}.[3] In a recent 3M study, however, more than one-third of the rat pups whose mothers were fed only 1.6 mg kg^{-1} per day during pregnancy died within four days of birth.[4] Although the mechanism(s) of toxicity is not known, the persistence of PFOS in the environment is probably related to the inert nature of C–F bonds in perfluoroalkyl chains.[14–16] For example, PFOS was not metabolized by *Pseudomonas* sp. strain D2.[17] Laboratory rats were only able to excrete 26% of the ^{14}C-labeled PFOS that was administered.[18]

The PFOS anion, its 4-, 5-, 6-, and 7-carbon homologs, and their derivatives are important components in two widely used commercial formulations, Scotchgard protection and repellant products and LIGHT WATER brand aqueous film-forming (fire-fighting) foams (AFFF's).[4,5,12,13] Both have been in use for many years. AFFF's are especially effective at extinguishing liquid-fuel fires and have been used extensively at military and civilian fire-fighting training facilities as well as at military airfields and municipal airports.[12,19–23] In a recent seminal study, Moody and Field detected and quantified several perfluoroalkylcarboxylate anions at concentrations between 125 μg L^{-1} and 7.1 mg L^{-1} in groundwater contaminated with untreated AFFF wastewater at Naval Air Station Fallon, NV, and at Tyndall Air Force Base, Panama City, FL.[24] Their study confirmed two earlier reports that tentatively identified "fluorinated surfactants" in groundwater at the Tyndall site.[25,26] More recently, perfluoroalkylcarboxylate anions have been quantified from the groundwater around a fire training area at the former Wurtsmith Air Force Base in Oscoda, MI.[13] Although perfluoroalkylcarboxylate anions are not listed as components of AFFF's in patents or in MSDS sheets,[27,28] their presence in at least one AFFF formulation will be reported in this paper.

Before this work, there were only two published methods for the identification of perfluoroalkylsulfonate (PFS) anions in water, and neither of them is suitable for the quantitative determination of sub-ppm amounts of individual PFS anions. In the first study, PFS anions were identified, but not quantitatively determined, using fast-atom-bombardment and collision-activated-dissociation mass spectrometry.[29] In the second study, two commercially available suites of PFS anions at concentrations between 5 and 50 mg L^{-1} in aqueous acid were quantitatively determined collectively by extraction by a polymeric reverse-phase resin followed by elution onto a multiphase HPLC column and detection by suppressed conductivity.[30] However, each PFS anion was not individually quantified by this method.

While this manuscript was in preparation, Hansen *et al.* reported a mass-spectral method for determining concentrations of PFOS and other fluorochemical anions in blood serum and whole liver tissue.[31] Due to the complex nature of these matrixes, their method requires (i) extraction of PFOS (and the other fluorochemical anions) into an organic solvent using an ion-pairing reagent, (ii) evaporation of the solvent and reconstitution in another solvent, (iii) HPLC separation of the anions on a Betasil C_{18} column, and (iv) negative-ion electrospray *tandem* mass spectrometry (the latter was

†Abbreviations: PFS, perfluoroalkylsulfonate; PFOS, perfluorooctylsulfonate; DDS, dodecylsulfate; PFBS, perfluorobutylsulfonate; PFHxS, perfluorohexylsulfonate; AFFF, aqueous film-forming foam; (−)ES-MS, negative-ion electrospray mass spectrometry

DOI: 10.1039/b108463c

necessary because of possible biological interferrents).[31] This important new method, however complex, has now been used to determine the accumulation of PFOS in marine mammals and the global distribution of PFOS in wildlife.[8–10]

A second mass-spectral method for the determination of perfluorinated surfactants in surface water was also reported while this manuscript was in preparation.[32] Moody *et al.* describe two techniques, liquid chromatography-tandem mass spectrometry and ^{19}F NMR spectroscopy, that required the use of solid-phase extraction to preconcentrate the analytes. Using these techniques, PFS anions were quantified in the low μg L^{-1} concentration range (the linear response range using liquid chromatography-tandem mass spectrometry is 0.85–208 μg L^{-1}). While useful when analyzing surface water, both of these methods require significant sample preparation and relatively long analysis times.

In this paper, we report a simpler mass-spectral method for the quantitative determination of individual PFS anions, ranging from four to eight carbon atoms, in groundwater and other homogeneous aqueous samples. The method is simpler and less time consuming because these matrixes are significantly less complex than blood serum, whole tissue, and surface water. The linear-response range for PFOS is 25.0 μg L^{-1} to 2.5 mg L^{-1}. The lower limit is three orders of magnitude lower than the lower limit for the HPLC method discussed above.[30] Although the linear-response range we report is for a higher concentration range than that reported by Moody *et al.*,[32] our direct-injection mass spectral method is less complex since it does not require preconcentration steps. The direct-injection method has already been used to determine that $C_6F_{13}SO_3^-$ (PFHxS) and PFOS anions are still present in groundwater contaminated with untreated AFFF wastewater at the former Wurtsmith Air Force base, Oscoda, MI, six years after the cessation of fire-training activities.[13] The detection limit (signal-to-noise ratio greater than three) and quantification limit (signal-to-noise ratio greater than five) for PFOS are 5.0 μg L^{-1} and 25.0 μg L^{-1}, respectively.

Experimental section

Standards and reagents

Sodium dodecylsulfate (Na(DDS), Sigma, >99%) was dried under vacuum at 25 °C for 24 h and was stored in a helium-filled glovebox. Two perfluoroalkylcarboxylic acids, $C_{11}F_{23}CO_2H$ and $C_5F_{11}CO_2H$ (Aldrich), were used as received. Acetonitrile (Fisher, HPLC grade) was used as received. Distilled water was purified and deionized to 18 MΩ with a Barnstead NanoPure purification system. Potassium perfluorooctylsulfonate, K(PFOS), was synthesized from perfluorooctylsulfonyl fluoride (3M) by adding it to KOH in water. The white crystalline compound K(PFOS) is the major product from this reaction, while perfluoroalkylsulfonates with other chain lengths (C7, C6) are also present in small amounts. Five recrystallizations from hot water were carried out to take advantage of the lower solubility of K(PFOS) in cold water compared to PFS salts with shorter chain lengths. The purity of K(PFOS) was determined to be >99% by negative-ion electrospray ionization mass spectrometry ((−)ES-MS) and by ^{19}F NMR spectroscopy. A yield of 65% was achieved based on perfluorooctylsulfonyl fluoride. Purified K(PFOS) was dried under vacuum and stored in a helium-filled glovebox. The synthesis of potassium perfluorobutylsulfonate, K(PFBS), from perfluorobutylsulfonyl fluoride (3M) and KOH was the same in every respect except that the higher solubility of this salt in water resulted in a much lower yield of purified material (30% based on perfluorobutylsulfonyl fluoride).

The AFFF formulation FC-203CF LIGHT WATER Brand Aqueous Film Forming Foam® (3M) was used as received. The MSDS sheet for this formulation lists the components as water (70%), 2-(2-butoxyethoxy)ethanol (20%), two alkylsulfate salts (5%), amphoteric fluoroalkylamide derivative (3%), five perfluoroalkylsulfonate salts (1%), triethanolamine (1%), and methyl-1H-benzotriazole (0.1%).[27]

A groundwater sample was collected from the former Wurtsmith Air Force base near Oscoda, MI by Cheryl Moody Bartel and Jennifer Field.[13] The sample collection protocols as well as the analysis of field blanks were addressed in a study to be published elsewhere.[13] The groundwater was withdrawn in June 1999 from a well (labeled FT3) in an area used for fire-fighting training from 1952 to 1993. These fire-training exercises included the use of AFFF formulations that probably contained PFS anions including PFOS.[13]

Water samples from the Ohio River and Cincinnati tap water were donated by E. T. Urbansky of the US Environmental Protection Agency in high-density polyethylene bottles. Horsetooth Reservoir water (Fort Collins, CO) was collected in December 2001 in high-density polyethylene bottles.

Sample preparation

Due to the sensitivity of (−)ES-MS peak intensities to minor changes in experimental conditions, a strict experimental procedure was followed when preparing and analyzing all samples. A 1 : 1 (v : v) acetonitrile : water matrix was used to efficiently nebulize the anions present in solution. Matrixes containing only water as the solvent were significantly less efficient. All samples were prepared using gas-tight syringes accurate to ±1% or less of their total volume (10, 50 and 500 μL). The syringes were rinsed with 1 : 1 (v : v) acetonitrile : water at least five times after each use and conditioned by rinsing three times with each new sample before an aliquot of the sample was withdrawn for analysis.

Standard-addition samples were prepared as follows. A groundwater sample was centrifuged for 15 min at 5,000 rpm to separate any fine particulates that cannot be injected into the (−)ES-MS instrument. The samples were not filtered since this might result in some loss of PFOS by adsorption onto the filter. A series of 200-μL aliquots of the centrifuged groundwater supernatant were treated with appropriate volumes of a 5.0 mg L^{-1} solution of PFOS in 1 : 1 (v : v) acetonitrile : water. The series of samples were then diluted with 200 μL of acetonitrile and 25 μL of a 2.7 mg L^{-1} DDS solution in 1 : 1 (v : v) acetonitrile : water. The diluted sample was then diluted further with a sufficient amount of 1 : 1 (v : v) acetonitrile : water so that the final volume was 500 μL. This sample preparation process resulted in a 2.5 fold dilution of the original groundwater sample.

The samples used to generate the calibration curve for the direct-injection method were prepared as above except that deionized water was used instead of the groundwater supernatant. Much larger volumes (*e.g.*, 10 mL) of these samples were prepared, but the dilution factors were the same. In this paper, the direct-injection method is defined as a method that requires only dilution and addition of DDS, the internal standard, prior to analysis. This greatly reduces both the sample preparation time and the number of samples to be analyzed.

All samples were prepared using glass laboratory equipment. Since it was not known whether PFS anions might adhere differently to different surfaces and thus interfere with our analyses, we investigated whether 10 mL samples containing known concentrations of K(PFOS) and K(PFBS) gave different results after being rolled for 20 min and left still for 24 h in 1 L Pyrex and high-density polypropylene bottles. It was found that samples not rolled in the large bottles gave the same mass spectral responses as the samples rolled in either glass or plastic.

The quantitative accuracy of the instruments was checked at the beginning, middle and end of each data set collected using a

single standard equimolar solution containing 250 μg L^{-1} PFOS and 133 μg L^{-1} DDS in a 1 : 1 (v : v) acetonitrile : water solution. Three to five replicates of each sample were analyzed and the Q test was used to eliminate spurious data. All experimental values in this paper are reported with ±1 standard deviation. Blanks were run after the replicates of each sample to insure that there was no carry-over between samples.

Instrumentation

Both a Fisons VG Quattro single quadrupole mass spectrometer and a Finnigan LCQ Duo mass spectrometer were used to collect the (−)ES-MS data. Instrumental parameters are compared in Table 1. Samples were introduced into the LCQ Duo by continuous infusion from a syringe and into the Quattro by flow injection from a 10 μL sample loop. Results were similar for both instruments with the exception that the Fisons instrument had slightly lower detection and quantification limits (3 μg L^{-1} and 5 μg L^{-1}, respectively) although it also had higher relative errors. Standard-addition experiments were conducted using only the Finnigan LCQ Duo instrument. All other experiments were done using both instruments.

Several experiments were specifically performed to compare the two spectrometers. A set of two standards containing low and high PFOS concentrations was prepared with four replicates each. The first standard contained 250 μg L^{-1} PFOS and 133 μg L^{-1} DDS and had a ratio of (−)ES-MS intensities, $I(499)/I(265)$, of 3.9 ± 0.9 (Fisons) and 4.8 ± 0.4 (Finnigan). The second standard contained 2.5 mg L^{-1} PFOS and 133 μg L^{-1} DDS and had values of $I(499)/I(265)$ of 26 ± 4 (Fisons) and 33 ± 3 (Finnigan). In both cases, the ratios of intensities were the same within the error of each spectrometer. In addition, log-log calibration plots were made using each spectrometer. The slopes of the plots were 1.02 ± 0.04 (Fisons) and 0.93 ± 0.02 (Finnigan).

Fluorine-19 NMR spectra of K(PFOS) and K(PFBS) dissolved in acetonitrile-d_3 were recorded using a Varian Inova-300 spectrometer at 25 °C. The ^{19}F frequency was 282 MHz and the chemical shift was referenced to an external $CFCl_3$ standard (δ 0.0). Peaks for PFOS were located at δ −80.3 (triplet (t), 3F), −114.2 (multiplet (m), 4F), −120.2 (m, 2F), −121.1 (m, 4F), −121.9 (m, 2F), −125.3 (t, 2F).

The pH was measured using an Orion meter with a Ross® pH electrode. The conductivity was measured with a Yellow Springs conductivity probe and meter.

Results and discussion

Internal standard choice

Dodecylsulfate (DDS) was used as an internal standard for all (−)ES-MS samples to allow for the quantification of PFS anions. In general, it is important that an ES-MS internal standard has properties similar to the analyte, so that both species will tend to form ions under the same conditions. Several researchers have used an isotopically labeled form (*e.g.*, a perdeuterated or polydeuterated isotopomer) of their analyte as their internal standard, but that is not convenient for perfluorinated compounds.[33–35] By keeping the internal standard similar in structure and mass, it will have a similar sensitivity coefficient to the analyte. The sensitivity coefficient is a constant that is related to the efficiency of an analyte to form individual molecular ions in the electrospray source.[34,35] The ratio of anion peak intensities is equal to the ratio of sensitivity coefficients when the concentrations of the anions are equal.[34,35] In this work, samples were analyzed containing equal concentrations of PFOS and DDS to compare their sensitivity coefficients. The anions PFOS and DDS have different sensitivity coefficients, which were manifested by two different (−)ES-MS peak intensities for the same concentration of the two ions. However, the ratio of these intensities, $I(499)/I(265)$, was relatively constant (to within experimental error) at 1.4–2.2 over the concentration ranges 5.0 μg L^{-1} to 25.0 mg L^{-1} PFOS and 2.7 μg L^{-1} to 13.3 mg L^{-1} DDS for equimolar concentrations of the two surfactant anions, which makes DDS an appropriate internal standard for PFOS. The validity of DDS as an internal standard should be evaluated for each new matrix. In addition, the sensitivity coefficients for the two perfluorinated anions PFOS and PFBS were found to be the same to within experimental error over the concentration range 5.0 μg L^{-1} to 499 μg L^{-1} PFOS and 3.0 μg L^{-1} to 299 μg L^{-1} PFBS (these limiting concentrations correspond to equal numbers of moles of the two anions). Based on these observations, we assume that the sensitivity coefficients of $C_5F_{11}SO_3^-$, $C_6F_{13}SO_3^-$, and $C_7F_{15}SO_3^-$ are also equal to that of PFOS and PFBS over equimolar concentration ranges.

Table 1 Comparison of instrumental parameters for the Finnigan LCQ Duo and the Fisons VG Quattro mass spectrometers

Finnigan LCQ Duo		Fisons VG Quattro	
Spray voltage[a]	−3.5 kV	Capillary voltage	−2.9 kV
Capillary voltage	−39 V	Cone voltage	−30 V
Capillary temperature	200 °C	Source temperature	75 °C
Infusion rate	5 μL min^{-1}	Flow injection rate	4 μL min^{-1}

[a]Different names have been given to the same components by the two companies.

Method of standard additions

Two methods of determining unknown concentrations of PFOS (and therefore unknown concentrations of $C_4F_9SO_3^-$, $C_5F_{11}SO_3^-$, $C_6F_{13}SO_3^-$, and $C_7F_{15}SO_3^-$) were investigated. A groundwater sample from the former Wurtsmith Air Force base near Oscoda, MI, that was part of a larger study[13] will serve to exemplify the first method.

The groundwater sample, labeled FT3, consisted of a clear, colorless supernatant and a small amount of solid particles. The pH and specific conductivity of the supernatant were 6.2 and 736 μS cm^{-1}, respectively. Four replicate aliquots of each of four different standard-addition samples were prepared. Along with four replicate aliquots of FT3 that did not contain added PFOS, the spiked aliquots were examined by (−)ES-MS after each was made to be 133 μg L^{-1} DDS in 1 : 1 (v : v) acetonitrile : water.

A plot of $I(499)/I(265)$ *vs.* the concentration of added PFOS is shown in Fig. 1 (each data point is the average over the four replicates). The mass spectrometer detector was found to be linear over the concentration range from 25 μg L^{-1} to 2.5 mg L^{-1} PFOS. The absolute value of the *x*-axis intercept of a linear least-squares fit to the data, 120 ± 20 μg L^{-1}, represents the experimentally determined concentration of PFOS in the diluted groundwater sample. The concentration of PFOS in undiluted FT3 groundwater is 2.5 times that value, 300 ± 50 μg L^{-1} (17% relative error). The dilution process is described in the *Experimental Section*.

No peaks were detected in the (−)ES-MS spectra of these samples for other PFS anions with three, four, five, or seven carbon atoms. However, there was a detectable peak corresponding to $C_6F_{13}SO_3^-$ (PFHxS, *m/z* 399). A separate standard-addition experiment was not possible since neither PFHxS nor its sulfonyl fluoride precursor are commercially available. Based on the assumption that the sensitivity coefficient of PFOS and PFHxS are equal (see above), the concentration of PFHxS present was determined by comparing the intensity ratio $I(499)/I(265)$ of the sample with no added PFOS with the intensity ratio $I(399)/I(265)$. The result of this data analysis is that the concentration of PFHxS in undiluted

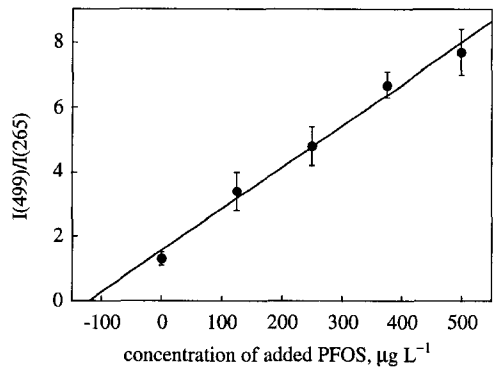

Fig. 1 A plot of the mass-spectral intensity ratio $I(499)/I(265)$ *vs.* concentration of the perfluorooctylsulfonate anion (PFOS, $C_8F_{17}SO_3^-$) added to groundwater sample FT3 (collected at Wurtsmith Air Force Base, Oscoda, MI) that was diluted 2.5 times with 1 : 1 (v : v) acetonitrile : water and spiked with 133 μg L^{-1} dodecylsulfate. Each data point is the average over the four replicates and the error bars shown are for ±1 standard deviation. The absolute value of the *x*-axis intercept, 120 ± 20 μg L^{-1}, represents the experimentally determined concentration of PFOS in the diluted groundwater sample. Therefore, the concentration of PFOS in undiluted FT3 groundwater is 2.5 times that value, 300 ± 50 μg L^{-1}.

FT3 groundwater is 210 ± 50 μg L^{-1}. Therefore, the PFOS to PFHxS molar ratio is 1.2 ± 0.3.

Note that the method of standard additions takes into account variations in the composition of different groundwater samples (*i.e.*, the method employs matrix matching).[36] Furthermore, as noted above, the new method reported herein allows a much simpler sample preparation to be used than required by the method developed by Hansen *et al.* for blood sera and tissue samples[31] or that described for the method recently reported by Moody *et al.*[32]

Direct-injection method

In some situations, the standard-addition method may be more time consuming than desired for a quick estimate of unknown concentrations of PFS anions. To explore the possibility of a direct measurement (*i.e.*, after addition of DDS but with no added PFOS), the following experiments were performed. A series of twenty aqueous samples (four replicates of five different concentrations) that were spiked with 133 μg L^{-1} DDS and that varied in concentration of 25.0 μg L^{-1} to 2.5 mg

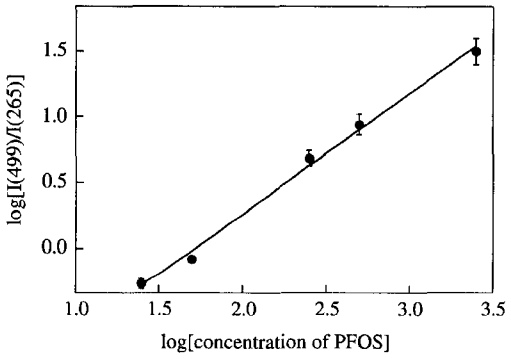

Fig. 2 A log-log plot of the mass-spectral intensity ratio $I(499)/I(265)$ *vs.* concentration of perfluorooctylsulfonate for a series of five standards with five different concentrations (four replicates at each concentration). Each standard was spiked with 133 μg L^{-1} dodecylsulfate (the solvent was 1 : 1 (v : v) acetonitrile : water). The correlation coefficient for this calibration graph is 0.995 and the slope is 0.93 ± 0.02. For some points the error bars (±1 standard deviation) are smaller than the point.

L^{-1} PFOS were prepared. A log-log plot of $I(499)/I(265)$ *vs.* the PFOS concentration with a linear least-squares slope of 0.93 ± 0.02 and a correlation coefficient of 0.995 is shown in Fig. 2. Each point on this calibration graph has a relative standard error ranging from 6 to 14%. This plot demonstrates that unknown concentrations of PFOS in water can be reliably determined over this concentration range using a linear fit to the data.

The FT3 groundwater sample was analyzed using the direct-injection method by preparing samples (four replicates each) diluted by a factor 2.5 that contained 133 μg L^{-1} DDS as the only added standard. Using the calibration graph, the concentration of PFOS in the FT3 groundwater sample was determined to be 240 ± 40 μg L^{-1} (*cf.* 300 ± 50 μg L^{-1} PFOS by the standard-addition method). The concentration of PFHxS in the FT3 groundwater sample was calculated by the same method described in the *Method of standard additions* section for PFHxS. The concentration of PFHxS was determined to be 160 ± 40 μg L^{-1} (*cf.* 210 ± 50 μg L^{-1} PFHxS by the standard-addition method).

Several experiments were performed to explore the effects of the water matrix on the intensity ratio $I(499)/I(265)$. First, three natural water matrixes (Horsetooth Reservoir (Fort Collins, CO), Cincinnati tap water, and Ohio River water) were tested using a modified standard-addition method. Spectra for all three matrixes with no added PFOS or DDS exhibited no peak for either PFOS or DDS. Samples (four replicates each) were made from each matrix to contain 133 μg L^{-1} DDS and two different concentrations of PFOS (50 μg L^{-1} and 250 μg L^{-1}). The (−)ES-MS intensity ratios $I(499)/I(399)$ for these standard additions are listed in Table 2. Both Cincinnati tap water and water from the Ohio River had significantly different values of $I(499)/I(399)$ compared to the standards. The intensity ratios of Horsetooth Reservoir water were very close to the expected intensity ratio for the 50 μg L^{-1} PFOS sample and it had the same intensity ratio for the 250 μg L^{-1} PFOS sample, indicating that this matrix had the least effect on the ionization efficiency of the standards within the spectrometer. Therefore, the direct-injection method can to be used with the Horsetooth Reservoir water samples. However, the variation of the intensity ratios of Cincinnati tap water and Ohio River water shows that the method of standard additions must be used for quantification. Each new matrix would have to be tested as described here to determine the proper method of quantification.

Next, the ionic strength was varied to check for changes in the intensity ratio $I(499)/I(265)$ compared with low ionic strength standards. The (−)ES-MS spectra of a series of four aqueous samples (three replicates each) that were 50 μg L^{-1} PFOS and 133 μg L^{-1} DDS and varied in specific conductivity from 1.4 μS cm^{-1} to 742 μS cm^{-1} by addition of Na_2SO_4 were recorded (the 1.4 μS cm^{-1}-samples had no added Na_2SO_4). The values of $I(499)/I(265)$ varied randomly from 0.18 to 0.36, indicating that a change in specific conductivity over the range 1.4–742 μS cm^{-1} resulting from a change in ionic strength will result in concentrations of PFOS determined by the direct-injection method that are reliable to within a factor of two.

Table 2 Comparison of the (−)ES-MS intensity ratio $I(499)/I(265)$ of standards with the $I(499)/I(265)$ ratio of natural water samples spiked with 133 μg L^{-1} DDS and two different concentrations of PFOS[a]

	50 μg L^{-1} PFOS	250 μg L^{-1} PFOS
Standards	1.0 ± 0.1	4.7 ± 0.7
Horsetooth Reservoir water	1.3 ± 0.1	5.4 ± 0.2
Cincinnati tap water	1.9 ± 0.3	9 ± 2
Ohio River water	1.9 ± 0.2	7 ± 1

[a]The data are reported with ±1 standard deviation.

Finally, the (−)ES-MS spectra of a series of three aqueous samples (three replicates each) that were 50 μg L^{-1} PFOS and 133 μg L^{-1} DDS and varied in pH from 6–8 were recorded. The pH was adjusted with solid Na_2HPO_4/KH_2PO_4 buffer (pHydrion buffer; Micro Essential Lab, Inc.) The values of $I(499)/I(265)$ varied randomly from 0.36 to 0.60, indicating that concentrations of PFOS determined by the direct-injection method are reliable to within a factor of 2 over this pH range.

We did not investigate the use of tandem mass spectrometry since the goal of the study was to develop a simple, fast method for quantification of PFS anions. The use of MS-MS fragmentation experiments could be used when evaluating samples from sources where PFS anions could be confused with other anions present in solution.

Analysis of an AFFF concentrate

One formulation of AFFF, FC-203CF LIGHT WATER Brand Aqueous Film Forming Foam® (3M), was analyzed by (−)ES-MS for the quantitative determination of PFS anions. Four samples were prepared by diluting the AFFF concentrate with a solution of 1 : 1 (v : v) acetonitrile : water to a 40,000-fold final dilution. The samples also contained 133 μg L^{-1} DDS as an internal standard. The (−)ES-MS spectrum of the dilute AFFF is shown in Fig. 3. The characteristic peaks of six PFS anions can be seen at *m/z* 249 ($C_3F_7SO_3^-$), 299 ($C_4F_9SO_3^-$), 349 ($C_5F_{11}SO_3^-$), 399 ($C_6F_{13}SO_3^-$), 449 ($C_7F_{15}SO_3^-$), and 499 ($C_8F_{17}SO_3^-$). Note that only five PFS anions are listed in the MSDS sheet for this formulation of AFFF.[27] Two alkylsulfate salts are listed in the MSDS sheet and their peaks can be seen at *m/z* 209 ($C_8H_{17}OSO_3^-$) and 237 ($C_{10}H_{21}OSO_3^-$).[27] In a parallel experiment for which DDS was not added, no (−)ES-MS peak was observed at *m/z* 265. Therefore, since DDS or another species with *m/z* 265 is not present in this formulation of AFFF, DDS is an appropriate internal standard. Peaks are also present for $C_7F_{15}CO_2^-$ (*m/z* 413) and $C_5F_{11}CO_2^-$ (*m/z* 313) as well as for their $C_7F_{15}^-$ and $C_5F_{11}^-$ fragments at *m/z* 369 and 269, respectively. Although (−)ES-MS is a soft ionization technique that does not normally cause fragmentation, control experiments with pure samples of $C_{11}F_{23}CO_2H$ and $C_5F_{11}CO_2H$ proved that decarboxylation fragments do form under the instrumental conditions used in this study. Therefore, perfluoroalkylcarboxylate anions are present in at least one formulation of AFFF even though they are not listed in either the patent or the MSDS sheet.[27,28]

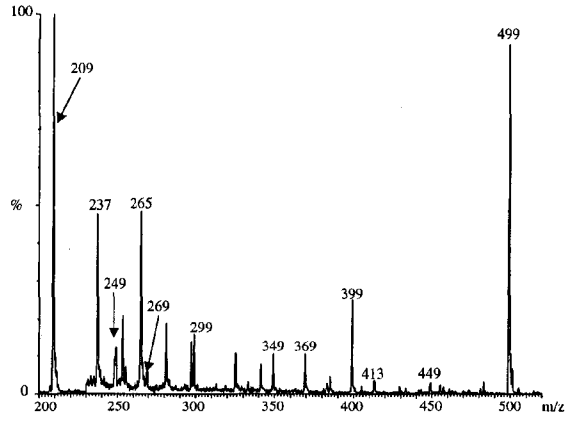

Fig. 3 Negative-ion electrospray ionization mass spectrum of FC203-LIGHT WATER aqueous film-forming foam. The commercial concentrate was diluted 40,000 times with 1 : 1 (v : v) acetonitrile : water and spiked with 133 μg L^{-1} dodecylsulfate (*m/z* 265). The vertical scale from *m/z* 230–520 has been expanded eight times. The peaks at *m/z* 249, 299, 349, 399, 449, 499 are assigned to the perfluoropropyl-, perfluorobutyl-, perfluoropentyl-, perfluorohexyl-, perfluoroheptyl-, and perfluorooctylsulfonate anions, respectively. The peaks at *m/z* 209 and 237 are assigned to $C_8H_{17}OSO_3^-$ and $C_{10}H_{21}OSO_3^-$, respectively. The peaks at *m/z* 413, 369, 313, and 269 are assigned to $C_7F_{15}CO_2^-$, $C_7F_{15}^-$, $C_5F_{11}CO_2^-$, and $C_5F_{11}^-$, respectively.

Concentrations of the PFS anions present in this formulation of AFFF were determined using a modified version of the method of standard additions. Four samples were prepared by adding 250 μg L^{-1} PFOS, 150 μg L^{-1} PFBS, and 133 μg L^{-1} DDS to the 40,000-fold diluted AFFF. Four samples were also prepared by adding only 133 μg L^{-1} DDS to the dilute AFFF. The concentrations of PFOS and PFBS in the AFFF concentrate were determined by comparing intensity ratios of the unspiked AFFF samples to the samples containing the known concentrations of the three standards and AFFF, to be 9 ± 1 mg L^{-1} PFOS and 0.6 ± 0.1 mg L^{-1} PFBS. The concentrations of the other four PFS anions were determined by comparing the intensity ratios of the unspiked samples and concentrations of both PFOS and PFBS to the intensity ratios of the PFS anion of unknown concentrations. This method gives concentration ranges of 0.4–1.5 mg L^{-1} for $C_3F_7SO_3^-$, 0.3–1.3 mg L^{-1} for $C_5F_{11}SO_3^-$, 0.6–2.7 mg L^{-1} for $C_6F_{13}SO_3^-$, and 0.1–0.4 mg L^{-1} for $C_7F_{15}SO_3^-$.

Conclusions

We have herein presented a method for the quantification of perfluoroalkylsulfonate (PFS) anions in aqueous solution. The method allows for the identification and quantification of individual PFS anions instead of the total (collective) concentration of PFS anions present in solution.[30] Other published methods for quantifying these anions require at least one extraction or separation step, making the methods more time consuming and more complex.[31,32] Our method has a limit of detection of 5.0 μg L^{-1} and a linear calibration range of 25.0 μg L^{-1} to 2.5 mg L^{-1} for $C_8F_{17}SO_3^-$ (PFOS). Both of these values are within the same order of magnitude as those reported by Hansen *et al.*[31] Moody *et al.* have reported a linear calibration range of 0.85–208 μg L^{-1} for PFOS using liquid chromatography–tandem mass spectrometry,[32] slightly lower than that reported here. They also reported a ^{19}F NMR method that has a much higher linear calibration range and a higher detection limit.[32] Importantly, the two methods reported by Moody *et al.* gave quantitative results for PFOS in surface water that were significantly different from each other, presumably because of the presence of other surfactants that yield ^{19}F NMR spectra similar to that of PFS anions. We recommend that the method of standard additions presented in this paper be used to quantify PFOS in aqueous solutions. The direct-injection method can be used when the matrix involved is less complex or when a less precise determination of PFOS concentration is acceptable.

Acknowledgement

This work was supported by a grant from the National Science Foundation (CST-9726143) and, in part, by Electrox, Inc. We thank B. J. Clapsaddle and Dr. J. A. Field for expert advice, Dr. F. E. Behr of 3M Company for samples of $C_8F_{17}SO_2F$ and $C_4F_9SO_2F$ and Dr. E. T. Urbansky of the US Environmental Protection Agency for the samples of Cincinnati tap water and Ohio River water.

References

1 A.-K. Sohlenius, A. M. Eriksson, C. Hogstrom, M. Kimland and J. W. DePierre, *Pharmacol. Toxicol.*, 1993, **72**, 90.
2 R. G. Schnellmann, *Toxic. in Vitro*, 1990, **4**, 71.
3 J. N. Meussdoerffer and H. Niderprüm, *Chem. Z.*, 1980, **104**, 45.
4 A. Tullo, *Chem. Eng. News*, 2000, **78**(May 29), 12.
5 A. Tullo, *Chem. Eng. News*, 2000, **78**(May 22), 9.
6 D. B. Chan and E. S. K. Chian, *Environ. Prog.*, 1986, **5**, 104.

7 *Fed. Regist.*, 2000, **65**, (202), p. 62319.
8 J. P. Giesy and K. Kannan, *Environ. Sci. Technol.*, 2001, **35**, 1339.
9 K. Kannan, J. Koistinen, K. Beckmen, T. Evans, J. F. Gorzelany, K. J. Hansen, P. D. Jones, E. Helle, M. Nyman and J. P. Giesy, *Environ. Sci. Technol.*, 2001, **35**, 1593.
10 K. Kannan, J. C. Franson, W. W. Bowerman, K. J. Hansen, P. D. Jones and J. P. Giesy, *Environ. Sci. Technol.*, 2001, **35**, 3065.
11 G. W. Olsen, J. M. Burris, J. H. Mandel and L. R. Zobel, *J. Occup. Environ. Med.*, 1999, **41**, 799.
12 C. A. Moody and J. A. Field, *Environ. Sci. Technol.*, 2000, **34**, 3864.
13 C. A. Moody, G. N. Hebert, S. H. Strauss and J. A. Field, *Environ. Sci. Technol.*, submitted for publication.
14 B. Smart, in *Chemistry of Organic Fluorine Compounds II (ACS Monograph 187)*, ed. M. Hudlicky and A. E. Pavlath, American Chemical Society, Washington, DC, 1995, p. 979.
15 V. Gloeckner, K. Lunkwitz and D. Prescher, *Tenside, Surfactants, Deterg.*, 1989, **26**, 376.
16 E. Kissa, *Fluorinated Surfactants: Synthesis, Properties, Applications*, Marcel Dekker: New York, 1994.
17 B. D. Key, R. D. Howell and C. S. Criddle, *Environ. Sci. Technol.*, 1998, **32**, 2283.
18 J. D. Johnson, S. J. Gibson and R. E. Ober, *Fundam. Appl. Toxicol.*, 1984, **4**, 972.
19 R. L. Darwin, R. E. Ottman, E. C. Norman, J. E. Gott and C. P. Hanauska, *NFPA Journal*, 1995, **May/June**, 67.
20 Y. Hashimoto, *DIC Tech. Rev.*, 1995, **1**, 9.
21 S. Szonyi and A. Cambon, *Fire Saf. J.*, 1990, **16**, 353.
22 F. Szonyi, S. Szonyi and A. Cambon, *Comun. Jorn. Com. Esp. Deterg.*, 1991, **22**, 297.
23 A. A. Briggs, *Fire Technol.*, 1979, **15**, 20.
24 C. A. Moody and J. A. Field, *Environ. Sci. Technol.*, 1999, **33**, 2800.
25 M. Henley, H. Mayfield, and T. Shelley, presented at the American Chemical Society Pittsburgh Conference, Atlanta, GA, 1997.
26 A. D. Levine, E. L. Libelo, G. Bugna, T. Shelley, H. Mayfield and T. B. Stauffer, *Sci. Total Environ.*, 1997, **208**, 179.
27 MSDS sheet for 3M's FC-203CF LIGHT WATER Brand Aqueous Film Forming Foam.
28 R. Alm and R. M. Stern, *US Pat.*, 5085786, 1992.
29 P. A. Lyon, K. B. Tomer and M. L. Gross, *Anal. Chem.*, 1985, **57**, 2984.
30 M. Laikhtman and J. S. Rohrer, *J. Chromatogr., A*, 1998, **822**, 321.
31 K. J. Hansen, L. A. Clemen, M. E. Ellefson and H. O. Johnson, *Environ. Sci. Technol.*, 2001, **35**, 766.
32 C. A. Moody, W. C. Kwan, J. W. Martin, D. C. G. Muir and S. A. Mabury, *Anal. Chem.*, 2001, **73**, 2200.
33 R. B. Cole, *Electrospray Ionization Mass Spectrometry: Fundamentals, Instrumentation, and Applications*, John Wiley and Sons, New York, 1997.
34 K. S. Webb, P. B. Baker, N. P. Cassells, J. M. Francis, D. E. Johnston, S. L. Lancaster, P. S. Minty, G. D. Reed and S. A. White, *J. Forensic Sci.*, 1996, **41**, 938.
35 P. Kebarle and L. Tang, *Anal. Chem.*, 1993, **65**, 972A.
36 D. C. Harris, *Quantitative Chemical Analysis*, W. H. Freeman and Company, New York, 4th edn., 1995, pp. 139–142.

Occurrence and persistence of perfluorooctanesulfonate and other perfluorinated surfactants in groundwater at a fire-training area at Wurtsmith Air Force Base, Michigan, USA†

Cheryl A. Moody,[a]‡ Gretchen N. Hebert,[b] Steven H. Strauss*[b] and Jennifer A. Field*[c]

[a]*Department of Chemistry, Oregon State University, Corvallis, Oregon 97331, USA.*
[b]*Department of Chemistry, Colorado State University, Fort Collins, Colorado 80523, USA. E-mail: strauss@lamar.colostate.edu; Tel: (970)491-5104*
[c]*Department of Environmental and Molecular Toxicology, Oregon State University, Corvallis, Oregon 97331, USA. E-mail: jennifer.field@orst.edu; Tel: (541)737-2265*

Received 24th December 2002, Accepted 26th February 2003
First published as an Advance Article on the web 10th March 2003

Various formulations of fire-extinguishing materials, including aqueous film-forming foams (AFFFs), were used as part of fire-training exercises conducted at Wurtsmith Air Force Base (WAFB) in northeastern Michigan from the 1950s until the base was decommissioned in 1993. As a result of past fire-training exercises, AFFF-laden wastewater containing fuels, solvents, and other materials directly entered groundwater without prior treatment. Perfluorinated surfactants are key components in some AFFF formulations. In this study, groundwater was analyzed for perfluoroalkanesulfonates and perfluorocarboxylates. Perfluoroalkanesulfonates were directly detected using negative-ion electrospray ionization mass spectrometry. Derivatized perfluorocarboxylates were detected using electron impact gas chromatography-mass spectrometry. Groundwater from wells around fire-training area FTA-02 at WAFB contained four perfluorinated surfactants ranging in concentration from 3 to 120 μg L^{-1}: perfluorooctanesulfonate (PFOS); perfluorohexanesulfonate; perfluorooctanoate; and perfluorohexanoate. This is the first report demonstrating that PFOS, recently shown to be toxic to organisms ranging from zooplankton to primates, is still present in groundwater in measurable quantities five or more years after its last known use.

Introduction

Some perfluorinated surfactant anions, including perfluorooctanesulfonate, $C_8F_{17}SO_3^-$ (PFOS), have recently become pollutants of concern.[1–11] Salts of PFOS are known to cause significant toxic effects, including mortality, in cynomolgus monkeys (oral doses of 0.75 mg kg^{-1} day^{-1}),[12] rabbits (oral doses of 3.75 mg kg^{-1} day^{-1}),[13] rats (oral doses of 1.6 mg kg^{-1} day^{-1}),[9] and zooplankton (exposure to 10 mg L^{-1}).[14] Other biological effects of PFOS exposure have also been reported.[1,15–23] The growing evidence that PFOS is toxic to higher organisms is noteworthy because it has been found in the tissues of many animals around the globe, including white rabbits in New Zealand, eagles near the Baltic Sea, various birds in Italy, Korea, Japan, and the southeastern US, polar bears in Alaska, river otters in Washington and Oregon, seals in the arctic regions of Canada and Norway, penguins in Antarctica, fish in the Pacific Ocean, Mediterranean Sea, and Lake Michigan, and oysters in the Gulf of Mexico and Chesapeake Bay.[24–30] It is clear from this list that PFOS is distributed globally in the environment. Furthermore, PFOS concentrations up to 13 mg L^{-1} have been found in serum of fluorochemical plant employees in Alabama and Belgium.[31] Additionally, 65 human serum samples obtained from four different US biological supply companies had PFOS concentrations ranging from 7 to 82 μg L^{-1}.[32]

Salts of PFOS, or compounds that may degrade to PFOS, were used for years in many consumer and industrial formulations, including fabric treatments, anti-static agents, paper coatings approved for food contact, shampoos, corrosion inhibitors, insecticides, and fire-fighting foams known as AFFFs (aqueous film-forming foams).[1,2] AFFFs, some of which contain perfluoroalkanesulfonates[33] including PFOS,[34] have proven to be effective at extinguishing liquid-fuel fires and are widely and routinely used by civilian and US military fire-fighters.[35–37] Historically, effluents from AFFF fire-fighting activities were neither impounded nor pre-treated prior to discharge to wastewater treatment systems or to the environment. Such releases may be responsible for the presence of PFOS in specific, localized environments. As far as the global distribution of PFOS is concerned, volatile perfluorooctanesulfonyl-containing compounds that may degrade to PFOS under environmental or biological conditions[38] were recently detected in ambient air in rural southern Ontario and in Toronto, ON.[39]

The PFOS anion, like many other perfluorinated chemical species, is very stable.[40] It is resistant to thermal degradation and chemical attack in aqueous solution. For example, PFOS has been shown not to be metabolized by some pseudomonads,[41] and its resistance to degradation in wastewater treatment systems causes excessive foaming that inhibits nitrification.[42] Perfluorinated surfactants were detected in surface water downstream from an accidental spill site five months after the release.[43,44] In addition, PFOS concentrations as high as 140 ng L^{-1} were detected in the Tennessee River 45 miles (72 km) downstream of a fluorochemical manufacturing facility in Decatur, AL (this value is significantly higher than the *ca.* 30 ng L^{-1} concentrations found upstream of the facility).[45] However, nothing has been published to date on the occurrence and persistence of perfluoroalkanesulfonates in the sub-surface environment. In this study, we report that PFOS and the related perfluorinated surfactants $C_6F_{13}SO_3^-$ (PFHxS), $C_5F_{11}COO^-$ (PFHxA), and

†Electronic supplementary information (ESI) available: Map of location of Wurtsmith Air Force Base, Oscoda, MI and surrounding states. See http://www.rsc.org/suppdata/em/b2/b212497a/

‡Current address: Lawrence Livermore National Laboratory, P.O. Box 808, Mail Stop L-232, Livermore, California 94551, USA

DOI: 10.1039/b212497a

$C_7F_{15}COO^-$ (PFOA) are present at concentrations up to 120 μg L^{-1} in Michigan groundwater (1) up to 500 m from a site where AFFFs were routinely used for fire-fighting training activities and (2) at least five years after the cessation of fire-fighting activities.

Experimental section

Field site description and characterization

Wurtsmith Air Force Base (WAFB), which was decommissioned in 1993, is located in northeastern Michigan (see Fig. 1). Beginning in 1952, Fire-Training Area Two (FTA-02) at WAFB was used to train US military personnel in fire-fighting procedures. Training exercises consisted of flooding a concrete pad with flammable liquids, igniting the fluids, and extinguishing the fire with fire-fighting agents including AFFF.[46,47] Although, the pad was the central location of recent fire-training activity, AFFF and other fire-extinguishing materials may have been used to extinguish fires in other areas at FTA-02.[48]

The soil and groundwater at WAFB in the area around FTA-02 has been studied in detail.[46–53] Benzene, toluene, ethylbenzene, and xylenes were found in the groundwater at concentrations ranging from 10 to 2,000 μg L^{-1}.[46,48] In this study, groundwaters from 68 wells at FTA-02 were tested for non-volatile total organic carbon (TOC) using a TOC analyzer (Model Dohrman DC-190, Rosemount Analytical, Santa Clara, CA). The TOC values ranged from 1 mg L^{-1} (detection limit) to 225 mg L^{-1} and confirmed previous findings that the groundwater in this area is contaminated with a variety of fuel-related contaminants.[46–48] In addition to non-aqueous phase liquids,[49] a discontinuous 0.1 m thick layer of a black, tar-like substance occurs 0.3 to 0.9 m below the surface up to 50 m downgradient from the fire-training pad.[47] Groundwater from wells proposed to contain anionic surfactants from the use of AFFFs were tested for total anion concentrations using a standard method for methylene blue active substances.[54] Anion concentrations (calculated as PFOA, *m/z* 413) ranged from 400 to 10,200 μg L^{-1}.

A contaminant plume at FTA-02 was previously defined in several studies by examining groundwater from the numerous wells around the fire-training area for volatile organic compounds and specific conductance. The general plume boundary was approximated by specific conductance values greater than 250 μS cm^{-1}.[46–48] For this study, specific conductances (Purge Saver Model FC 2000, QED Environmental Systems, Inc., Ann Arbor, MI) of groundwater collected from 68 wells ranged from 110 to 3,170 μS cm^{-1}, with the highest values measured near the fire-training pad area. The pH of the groundwater samples varied from 5.5 to 8.6.

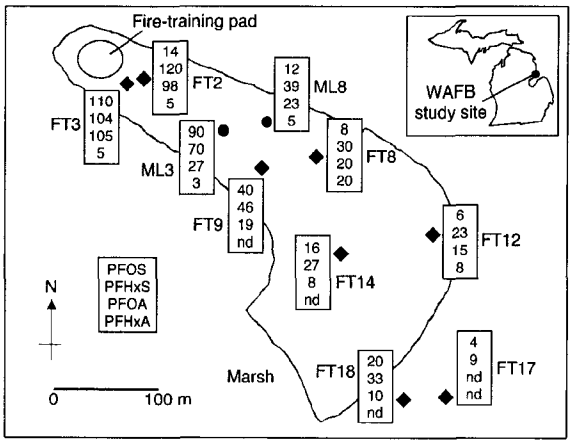

Fig. 1 Map showing the FTA-02 groundwater plume at retired Wurtsmith Air Force Base (WAFB), Oscoda, MI, USA. The inset shows the location of WAFB on a map of Michigan. (A larger area map showing surrounding states, south-central Canada, and the Great Lakes is available as Electronic Supplementary Information (ESI)†.) Groundwater samples from the indicated wells (diamonds and circles) were analyzed for perfluorooctanesulfonate (PFOS), perfluorohexanesulfonate (PFHxS), perfluorooctanoate (PFOA), and perfluorohexanoate (PFHxA). The boxes next to each well list the concentrations of the four analytes, in the order shown in the legend, in μg L^{-1} (nd = not detected).

Sample collection

Groundwater samples were collected from two types of monitoring wells at FTA-02 (Fig. 1). The position of the wells relative to the plume boundary are illustrated in Fig. 1 using the previously reported well designations.[46–48,50–52] Monitoring wells with the identifier FT (fire-training) denote iron-cased 10 cm inner diameter wells with 1 to 2 m stainless steel screened intervals located 3 to 6 m below the water table.[52] Wells with ML notations describe multilevel wells constructed from 2.5 cm inner diameter PVC casing with 0.3 m screened intervals that are vertically spaced from 0.5 to 2 m.[50] More detailed descriptions of these wells have been reported.[46–48,50–52] Groundwater samples from ML3 and ML8 were collected in November 1998 and samples from the other wells were collected in June 1999. All samples were collected in high-density polypropylene bottles due to a report that perfluorinated carboxylates adsorb to glass.[55] It has since been shown that neither PFOS nor PFHxS adsorb to glass or to high-density polypropylene.[34] Samples were shipped on ice without preservation and stored at 4 °C prior to analysis.

Standards and reagents

Potassium perfluorooctanesulfonate, K(PFOS), was synthesized from perfluorooctanesulfonyl fluoride (3M Company, St. Paul, MN) by adding potassium hydroxide in water and was recrystallized from water five times to a final purity of >99%.[34] It was dried under vacuum at 25 °C before use. Sodium dodecyl sulfate (DDS, Sigma, St. Louis, MO, 99%) was dried under vacuum at 25 °C for 24 h and stored in a helium-filled glovebox. Perfluorooctanoic acid (98%), 2-chlorolepidine (99%; used as an internal standard), and iodomethane (used for perfluorocarboxylate methylations) were used as received from Aldrich (Milwaukee, WI).

Perfluoroalkanesulfonate and perfluorocarboxylate analyses

Quantitative perfluoroalkanesulfonate concentrations in the groundwater samples were determined using direct-injection negative-ion electrospray ionization mass spectrometry ((−)ES-MS) by the method of Hebert *et al.*[34] The sample preparation method included centrifugation to separate any fine particulates and dilution of each groundwater sample with acetonitrile to obtain solutions that were 1 : 1 (v : v) acetonitrile : water. These solutions were spiked with 133 μg L^{-1} DDS as an internal standard. Five replicate samples of each groundwater sample were analyzed. The concentrations of PFHxS in the samples were also determined using the DDS internal standard. This assumes that the (−)ES-MS sensitivity coefficients of PFOS and PFHxS are the same, a reasonable assumption since it is known that the sensitivity coefficients of PFOS and perfluorobutanesulfonate are the same.[34] Intensity ratios of PFOS (*m/z* = 499) and DDS (*m/z* = 265), *I*(499)/*I*(265), were averaged and converted to PFOS concentrations using a calibration curve of *I*(499)/*I*(265) ratio *vs.* PFOS concentration previously prepared using the purified K(PFOS) standard.[34] The calibration curve was linear over a range of PFOS concentrations from 5 to 2,500 μg L^{-1} (R^2 = 0.99). The detection limit (defined as a signal-to-noise ratio greater than 3)

and quantification limit (defined as a signal-to-noise ratio greater than 10) for PFOS were 3 and 5 μg L^{-1}, respectively.

Perfluorocarboxylate concentrations were measured by the method of Moody and Field.[56] Strong anion exchange Empore disks were used to extract perfluorocarboxylates (6 to 8 carbons) from groundwater. The perfluorocarboxylates were simultaneously eluted from the disks and derivatized to their methyl esters by treatment with iodomethane for direct analysis by electron impact gas chromatography-mass spectrometry (GC-MS). A single analysis was conducted for each groundwater sample. The detection limit (defined as a signal-to-noise ratio greater than 3) and quantification limit (defined as a signal-to-noise ratio greater than 10) for perfluorocarboxylates were 3 and 13 μg L^{-1}, respectively, using 2-chlorolepidine as the internal standard. The concentrations of PFHxA and perfluoroheptanoate (PFHpA) in the samples were also determined using the 2-chlorolepidine internal standard, assuming a response factor equal to an equimolar amount of PFOA. Additionally, electron capture negative chemical ionization GC-MS was employed to confirm the identity of PFOA, PFHpA, and PFHxA in groundwater samples.

Results

Because one class of perfluorinated surfactants, perfluorocarboxylates, was detected in a limited number of groundwater samples from two other US military fire-training areas[56] as well as in commercial AFFF mixtures (unpublished data), the groundwater from FTA-02 was analyzed for these specific perfluorinated compounds as well as other perfluorinated surfactants found in commercial AFFFs. The concentrations of PFOS in WAFB groundwater from the wells shown in Fig. 1 ranged from 4 μg L^{-1} to 110 μg L^{-1} and the concentrations of PFHxS ranged from 9 μg L^{-1} to 120 μg L^{-1}. Groundwater from all of the wells in Fig. 1 contained measurable concentrations of both PFOS and PFHxS. Relative errors in PFOS and PFHxS concentrations are listed in Table 1 and ranged from *ca.* 3% for the higher concentrations to *ca.* 50% near the detection limit. In addition to PFOS and PFHxS, some AFFF formulations contain relatively small amounts of at least three other perfluoroalkanesulfonate anions, perfluorobutanesulfonate, perfluoropentanesulfonate, and perfluoroheptanesulfonate.[34] However, these perfluoroalkanesulfonate homologues were not observed in any of the groundwater samples that were analyzed for this study.

The groundwater samples from FTA-02 had total perfluorocarboxylate concentrations ranging from the detection limit of 3 μg L^{-1} to 110 μg L^{-1}, as shown in Table 1. Groundwater from half of the wells in Fig. 1 contained measurable concentrations of both PFOA and PFHxA. The PFHpA anion was observed in a few of the groundwater samples at the detection limit (3 μg L^{-1}). Groundwater from a background well located at WAFB, but not at FTA-02, contained no detectable perfluorinated carboxylates (*i.e.*, <3 μg L^{-1}), indicating that the occurrence of perfluorocarboxylates in groundwater downgradient from the fire-training pad at FTA-02 are likely the result of AFFF applications and discharge during fire-training exercises. Of the three perfluorocarboxylate surfactants detected, PFOA was the dominant homologue, accounting for greater than 90% of the total mass of perfluorocarboxylates present. The observation of a suite of perfluorocarboxylates, as well as a suite of perfluoroalkanesulfonates, was expected since the raw materials used by the chemical industry to synthesize many perfluorinated organic compounds are mixtures.[40]

Discussion

The highest concentrations of perfluoroalkanesulfonates and perfluorocarboxylates were observed in groundwater collected near the fire-training pad. Groundwater collected from wells located downgradient from the pad had lower concentrations. The data in Table 1 show that the total concentration of perfluoroalkanesulfonates was generally greater than the total concentration of perfluorocarboxylates. The ratios of total mass of perfluoroalkanesulfonates to total mass of perfluorocarboxylates varied from 0.95 to 5.4.

The presence of perfluoroalkanesulfonates in groundwater up to 500 m downgradient of the fire-training pad may indicate that this class of anionic surfactants migrates in the sub-surface environment. One important consideration for anionic perfluorinated surfactant transport is the organic content of soil. For example, Sullivan and Mabury determined that soil partition coefficients were linearly related to organic carbon content and sorption increased with increasing perfluorinated chain length.[57] More research will be required to fully investigate the factors that govern the transport behavior of perfluorinated surfactants.

The total concentrations of perfluorocarboxylates at WAFB FTA-02 were generally lower than previously observed in groundwater at Tyndall Air Force Base, FL and Naval Air Station Fallon, NV (124 to 298 μg L^{-1} and 540 to 7,090 μg L^{-1}, respectively).[56] Groundwater samples were collected at these bases from wells around fire-training areas seven to ten years after cessation of fire-fighting activity. The frequency with which fire-training tests were conducted at the individual sites undoubtedly varied between sites and is only poorly documented. However, the presence of similar perfluorinated surfactants in the WAFB groundwater samples indicates the likely use of AFFFs of similar composition. Groundwater samples from Tyndall Air Force Base and Naval Air Station Fallon were not analyzed for perfluoroalkanesulfonates[56]

Table 1 Concentrations of perfluoroalkanesulfonates and perfluorocarboxylates measured in the groundwater at FTA-02 at Wurtsmith Air Force Base

Well	Approximate distance from pad/m	PFOS/μg L^{-1}[a]	PFHxS/μg L^{-1}[a]	PFOA/ μg L^{-1}[b,c]	PFHxA/ μg L^{-1}[b,c]
FT2	17	14 ± 2	120 ± 20	98	5
FT3	18	110 ± 10	104 ± 3	105	5
ML3	114	90 ± 8	70 ± 10	27	3
ML8	121	12 ± 2	39 ± 4	23	5
FT8	183	8 ± 2	30 ± 10	20	20
FT9	183	40 ± 10	46 ± 8	19	nd
FT12	305	6.0 ± 0.8	23 ± 2	15	8
FT14	305	16 ± 2	27 ± 4	8	nd
FT18	518	20 ± 10	33 ± 4	10	nd
FT17	540	4.0 ± 0.2	9 ± 1	nd	nd

[a]The errors shown are ±1 standard deviation and were calculated from five replicate analyses. [b]The values listed are for a single analysis in each case. Based on past experience with this type of analysis,[56] the relative errors for these values probably range from 4% to 14%. [c]nd = not detected.

because a routine and reliable analytical method was unavailable at the time of analysis.

Recently, several reports of perfluorinated surfactants in surface waters have been published. Surface water collected from the Tennessee River near a fluorochemical manufacturing site contained concentrations of PFOS (17 to 144 ng L^{-1}) and PFOA (<25 to 598 ng L^{-1}) significantly lower than groundwater at WAFB FTA-02.[45] The observation of lower concentrations of perfluorinated surfactants in surface water is consistent with concentrations of PFOA (8 to 33 ng L^{-1}) found upstream of an accidental spill of fire-fighting foam into Etobicoke Creek, Toronto, ON.[44] The higher concentrations of PFOS (up to ~1000 μg L^{-1}) and PFOA (up to ~10 μg L^{-1}) found in the surface water downstream from the Ontario spill site are closer to the concentrations of perfluorinated surfactants found in the groundwater at WAFB FTA-02.

Conclusions

Despite a minimum of five years since active fire-fighting activity occurred at WAFB FTA-02, significant concentrations of perfluoroalkanesulfonates and perfluorocarboxylates were found in the groundwater. It is believed that the observed perfluorinated surfactants were components of some of the fire-fighting materials used at this site until 1993. The groundwater velocity is known to be 0.1 to 0.3 m day^{-1} at this site.[46,48,52] Assuming that the source of perfluorinated surfactants was the fire-training pad, we estimate that the perfluorinated surfactants found in groundwater *ca.* 500 m from the fire-training pad have been in the groundwater environment for a minimum of five years and potentially for as long as 15 years. The observation of perfluoroalkanesulfonates and perfluorocarboxylates in WAFB groundwater indicates that the compounds are resistant to degradation under the prevailing groundwater conditions at this site.

Acknowledgements

We thank M. J. Barcelona and S. K. Haack for facilitating sampling collection and technical assistance, and D. L. Dick, P. S. Craig, M. A. Odom, and B. J. Clapsaddle for experimental advice and assistance. We acknowledge Supelco, Inc. for the donation of vacuum manifolds and a GC column. This work was supported by the US NSF (grants CST-9726143 and CST-0085892 to Colorado State University) and by the US NIEHS (EHSC grant ES00210 to Oregon State University to support the Mass Spectrometry Core Facility).

References

1 US Environmental Protection Agency, *Fed. Regist.*, 2000, **65**, 62319.
2 US Environmental Protection Agency, *Fed. Regist.*, 2002, **67**, 11008.
3 D. Brown and C. E. Mayer, in The Washington Post, Washington DC, May 17, 2000, p. A1.
4 B. D. Key, R. D. Howell and C. S. Criddle, *Environ. Sci. Technol.*, 1997, **31**, 2445.
5 C. A. Moody and J. A. Field, *Environ. Sci. Technol.*, 2000, **34**, 3864.
6 R. Purdy, presented at the Society of Environmental Toxicology and Chemistry Conference, Nashville, TN, 2000, p. 160, abstract number PMP124.
7 R. Renner, *Environ. Sci. Technol.*, 2001, **35**, 154A.
8 R. Renner, *Sci. Am.*, March 17, 2001, p. 18.
9 A. Tullo, *Chem. Eng. News*, May 29, 2000, p. 12.
10 A. Tullo, *Chem. Eng. News*, May 22, 2000, p. 9.
11 A. Wood and W. Clarin, *Chem. Week*, May 24, 2000, p. 9.
12 A. M. Seacat, P. J. Thomford, K. J. Hansen, G. W. Olsen, M. T. Case and J. L. Butenhoff, *Toxicol. Sci.*, 2002, **68**, 249.
13 M. T. Case, R. G. York and M. S. Christian, *Int. J. Toxicol.*, 2001, **20**, 101.
14 H. Sanderson, T. M. Boudreau, S. A. Mabury, W.-J. Cheong and K. R. Solomon, *Environ. Toxicol. Chem.*, 2002, **21**, 1490.
15 J. Berthiaume and K. B. Wallace, *Toxicol. Lett.*, 2002, **129**, 23.
16 M. Derbel, M. Hosokawa and T. Satoh, *Biol. Pharm. Bull.*, 1996, **19**, 765.
17 T. Ikeda, K. Fukuda, I. Mori, M. Enomoto, T. Komai and T. Suga, in *Peroxisomes in Biology and Medicine*, ed. H. D. Fahimi and H. Sies, Springer-Verlag, Berlin, 1987, pp. 304–308.
18 A.-K. Sohlenius, A. M. Eriksson, C. Hogstrom, M. Kimland and J. W. DePierre, *Pharmacol. Toxicol.*, 1993, **72**, 90.
19 A. A. Starkov and K. B. Wallace, *Toxicol. Sci.*, 2002, **66**, 244.
20 D. J. Leubker, K. J. Hansen, N. M. Bass, J. L. Butenhoff and A. M. Seacat, *Toxicology*, 2002, **176**, 175.
21 B. Haughom and O. Spydevold, *Biochim. Biophys. Acta*, 1992, **1128**, 65.
22 T. M. Boudreau, R. Janutka, K. R. Solomon, P. K. Sibley, D. C. G. Muir and S. A. Mabury, presented at the Society of Environmental Toxicology and Chemistry Conference, Nashville, TN, 2000, p. 77, abstract number 348.
23 T. M. Boudreau, R. Janutka, K. R. Solomon, P. K. Sibley, D. C. G. Muir and S. A. Mabury, presented at the Society of Environmental Toxicology and Chemistry Conference, Madrid, Spain, 2001, p. 129, abstract number M/MF144.
24 J. P. Giesy and K. Kannan, *Environ. Sci. Technol.*, 2001, **35**, 1339.
25 K. Kannan, J. Koistinen, K. Beckmen, T. Evans, J. F. Gorzelany, K. J. Hansen, P. D. Jones, E. Helle, M. Nyman and J. P. Giesy, *Environ. Sci. Technol.*, 2001, **35**, 1593.
26 K. Kannan, J. C. Franson, W. W. Bowerman, K. J. Hansen, P. D. Jones and J. P. Giesy, *Environ. Sci. Technol.*, 2001, **35**, 3065.
27 K. Kannan, K. J. Hansen, T. L. Wade and J. P. Giesy, *Arch. Environ. Contam. Toxicol.*, 2002, **42**, 313.
28 K. Kannan, S. Corsolini, J. Falandysz, G. Oehme, S. Focardi and J. P. Giesy, *Environ. Sci. Technol.*, 2002, **36**, 3210.
29 K. Kannan, J. Newsted, R. S. Halbrook and J. P. Giesy, *Environ. Sci. Technol.*, 2002, **36**, 2566.
30 K. Kannan, J.-W. Choi, N. Iseki, K. Senthilkumar, D. H. Kim, S. Masunaga and J. P. Giesy, *Chemosphere*, 2002, **49**, 225.
31 G. W. Olsen, J. M. Burris, J. H. Mandel and L. R. Zobel, *J. Occup. Environ. Med.*, 1999, **41**, 799.
32 K. J. Hansen, L. A. Clemen, M. E. Ellefson and H. O. Johnson, *Environ. Sci. Technol.*, 2001, **35**, 766.
33 *Material Safety Data Sheet for FC-203CF Light Water AFFF 3%*, 3M Company, Saint Paul, MN, 1999.
34 G. N. Hebert, M. A. Odom, P. S. Craig, D. L. Dick and S. H. Strauss, *J. Environ. Monit.*, 2002, **4**, 90.
35 R. D. Howell and E. E. Tucker, *Am. Environ. Lab.*, 1996, **12**, 10.
36 R. L. Darwin, R. E. Ottman, E. C. Norman, J. E. Gott and C. P. Hanauska, *Natl. Fire Protect. Assoc.*, 1995, 67.
37 D. B. Chan and E. S. K. Chian, *Environ. Prog.*, 1986, **5**, 104.
38 US Environmental Protection Agency, *Fluorochemical Use, Distribution and Release Overview*, 3M Company, 1999, pp. AR-226-0550.
39 J. W. Martin, D. C. G. Muir, C. A. Moody, D. A. Ellis, W. C. Kwan, K. R. Solomon and S. A. Mabury, *Anal. Chem.*, 2002, **74**, 584.
40 E. Kissa, *Fluorinated Surfactants: Synthesis, Properties and Applications*, Marcel Dekker, New York, 1994.
41 B. D. Key, R. D. Howell and C. S. Criddle, *Environ. Sci. Technol.*, 1998, **32**, 2283.
42 M. Erten-Unal, G. C. Schafran, S. Paranjape, E. Garcia-Cardona, H. Yan, F. Williams, D. Cotnoir, K. Clark and D. Kirk, *Proceedings of the 52nd Purdue Industrial Waste Conference*, 1998, **52**, 47.
43 C. A. Moody, W. C. Kwan, J. W. Martin, D. C. G. Muir and S. A. Mabury, *Anal. Chem.*, 2001, **73**, 2200.
44 C. A. Moody, J. W. Martin, W. C. Kwan, D. C. G. Muir and S. A. Mabury, *Environ. Sci. Technol.*, 2002, **36**, 545.
45 K. J. Hansen, H. O. Johnson, J. S. Eldridge, J. L. Butenhoff and L. A. Dick, *Environ. Sci. Technol.*, 2002, **36**, 1681.
46 *Phase II—Confirmation/Quantification Stage 1: Wurtsmith Air Force Base, MI: Investigations of Groundwater and Soil Contamination at Selected Sites*, United States Geological Survey, Lansing, MI, 1991.
47 *Phase II—Confirmation/Quantification Stage 2: Wurtsmith Air Force Base, MI, Investigation of Soil and Groundwater Contamination at Selected Sites, vol. I*, United States Geological Survey, Lansing, MI, 1995.
48 M. J. Barcelona, *Symposium on Natural Attenuation of Chlorinated Organics in Groundwater, September 1996*, p. 98.
49 J. L. Bermejo, W. A. Sauck and E. A. Atekwana, *Ground Water Monit. Rem.*, 1997, 131.

50 F. H. Chapelle, S. K. Haack, P. Adriaens, M. A. Henry and P. M. Bradley, *Environ. Sci. Technol.*, 1996, **30**, 3565.
51 M. A. Dojka, P. Hugenholtz, S. K. Haack and N. R. Pace, *Appl. Environ. Microbiol.*, 1998, **64**, 3869.
52 J. L. Gillespie, *Installation Restoration Program Phase II—Confirmation/Quantification Stage 2*, United States Geological Survey, Lansing, MI, 1990.
53 J. T. McGuire, D. T. Long, M. J. Klug, S. K. Haack and D. W. Hyndman, *Environ. Sci. Technol.*, 2002, **36**, 2693.
54 APHA-AWWA-WPCF, *Standard Methods for the Examination of Water and Wastewater*, American Public Health Association, Washington DC, 24th edn., 1998, ch. 5, pp. 47–49.
55 J. Belisle and D. F. Hagen, *Anal. Biochem.*, 1980, **101**, 369.
56 C. A. Moody and J. A. Field, *Environ. Sci. Technol.*, 1999, **33**, 2800.
57 R. C. Sullivan and S. A. Mabury, presented at the Society of Environmental Toxicology and Chemistry Conference, Baltimore, MD, 2001, p. 193, abstract number PM278.

BY STEVEN H. STRAUSS,
MATTHEW A. ODOM, GRETCHEN N. HEBERT, AND BRADY J. CLAPSADDLE

Attenuated total reflectance–Fourier transform infrared (ATR–FTIR) sensors have been developed that can detect polyatomic anions in aqueous solution in the micrograms-per-litre range. The ability to detect and potentially quantify aqueous anions is important for several applications including groundwater, surface water, and wastewater testing. The surface of a commercially available ATR crystal was modified with highly selective films of organometallic extractants, resulting in sensitivity enhancements of three to five orders of magnitude relative to the unmodified crystal. No pretreatment of the aqueous solution was required for the detection and identification of three analytes. Detection limits for cyanide, perchlorate, and perfluorooctylsulfonate using the modified crystal were 5, 3, and 25 µg/L, respectively, for 60-min analyses. The significance of this work is the prospect that a common and easily portable spectroscopic technique can be used to detect and identify aqueous anions at microgram-per-litre concentrations—in favorable cases even in the presence of competing anions.

ATR–FTIR detection of ≤ 25 µg/L AQUEOUS CYANIDE, PERCHLORATE, AND PFOS

An ongoing need exists to detect and quantify anionic pollutants such as cyanide (CN^-) (Boening & Chew, 1999; Otu et al, 1996), perchlorate (ClO_4^-) (Christen, 2000; Okamoto et al, 1999; Susarla et al, 1999; Urbansky, 1998), and perfluorooctylsulfonate ($C_8F_{17}SO_3^-$; PFOS) (Moody & Field, 2000; Renner, 2000; Tullo, 2000a; Tullo, 2000b; Olsen et al, 1999; Moody et al, unpubl.) at low concentrations in aqueous media. The current US Environmental Protection Agency drinking water standard and drinking water reference dose for cyanide and perchlorate are 200 µg/L (USEPA, 2000; Pontius, 2000) and 4–18 µg/L (Urbansky, 1998), respectively. The surfactant PFOS, which was formerly used in fabric treatments* and aqueous film-forming foams used to fight liquid fuel fires (Moody & Field, 2000; Renner, 2000; Tullo, 2000a; Tullo, 2000b; Moody et al, unpubl.), is a major wastewater problem in that its presence can cause excessive foaming and shutdowns of publicly owned treatment facilities (Moody & Field, 2000; Darwin et al, 1995).

Quantitative methods based on Fourier transform infrared (FTIR) spectroscopy are generally considered to be insufficiently sensitive for the analysis of trace contaminants in water (i.e., < 1 mg/L) (Urban, 1996; Griffiths & de Haseth, 1986). Nevertheless, there are examples of attenuated total reflectance (ATR) crystals coated with submicron-thick layers of polymeric or sol-gel materials that enhance

*Scotchgard®-brand, 3M, St. Paul, Minn.

TABLE 1 1-h detection limits for the unmodified and modified attenuated total reflectance–Fourier transform infrared probe*

Anion†	Wavenumber Monitored‡ cm^{-1}	Detection Limit		Organometallic Extractant§
		Unmodified Probe—μg/L	Modified Probe—μg/L	
CN^-	2,104	130,000	5	$NiCl_2$(dppp)
ClO_4^-	1,092	288,000	3	$DEC^+NO_3^-$
$n\text{-}C_8F_{17}SO_3^-$	1,270	100,000	25	$DEC^+NO_3^-$

*The detection limit is defined as the concentration at which a band with a signal/noise ratio ≥ 3 was observed after 60 min.
†CN^-—cyanide, ClO_4^-—perchlorate, $C_8F_{17}SO_3^-$—perfluorooctylsulfonate
‡The wavenumber monitored for the modified probe experiments; the wavenumber monitored for the unmodified probe experiments differed by a few wavenumbers in all three cases.
§dppp—1,3-bis(diphenylphosphino)propane; DEC^+—1,1′,3,3′-tetrakis(2-methyl-2-nonyl)ferrocenium cation

FIGURE 1 Time-dependent ATR–FTIR spectra of $NiCl_2$(dppp)-coated probe immersed in 130 μg/L aqueous CN^-

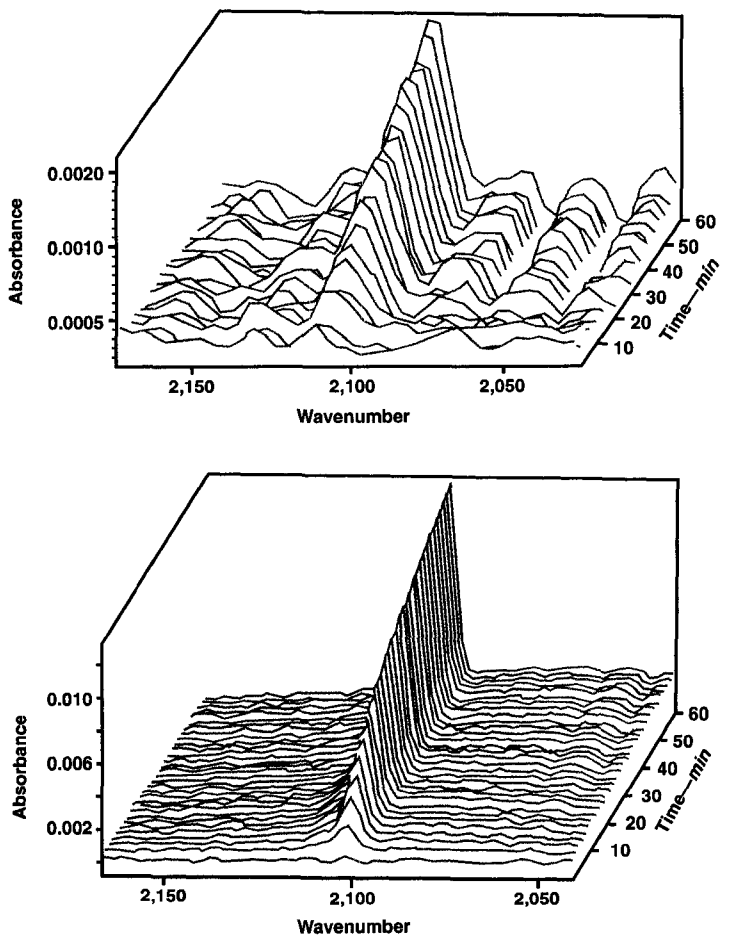

Spectra are of two thin films of the water-insoluble compound $NiCl_2$(dppp) on the probe immersed in pH 10 aqueous KCN ([CN^-] = 5.0 μg/L in the top spectrum; [CN^-] = 0.13 μg/L in the bottom spectrum). The band that grows in over time at 2,104 cm^{-1} is assigned to the water-insoluble compound NiCl(CN)(dppp), which is formed throughout the film by the CN^-/Cl^- ion-exchange reaction that occurs in the film.
ATR–FTIR—attenuated total reflectance–Fourier transform infrared, $NiCl_2$(dppp)—1,3-bis(diphenylphosphino)-propanedichloronickel(II)

the sensitivity of FTIR spectrometers by concentrating an analyte in the region probed by the evanescent wave (i.e., in the coating). Most analytes that have been detected in this manner are neutral organic molecules such as atrazine (3 mg/L), 1,1-bis(4-chlorophenyl)-2,2,2-trichloroethane (50 mg/L), trichloroethylene (100 mg/L), and benzonitrile (350 μg/L) (the lowest aqueous concentrations studied to date are shown in parentheses) (Han et al, 1998; Regan et al, 1996; Göbel et al, 1995). Only a few coatings that can concentrate ions have been reported, and none are known to detect aqueous ions at concentrations below 1,000 μg/L (Barja et al, 1999; Degenhardt & McQuillan, 1999; Dobson & McQuillan, 1999; Dobson & McQuillan, 1997; Hug, 1997; Persson et al, 1996; Yang & Saavedra, 1995; Ahn & Franses, 1994). In this initial report, the authors demonstrate that CN^-, ClO_4^-, and $C_8F_{17}SO_3^-$ can be detected in water at concentrations equal to 25 μg/L using a commercially available silicon ATR–FTIR immersion probe that has been coated with thin films of suitable organometallic ion-exchange compounds (Chambliss et al, 1999a; Chambliss et al, 1999b; Clark et al, 1999; Strauss, 1999; Chambliss et al, 1998; Clark et al, 1996; Clapsaddle et al, unpubl.).

MATERIALS AND METHODS

Reagents and chemicals. The following chemicals were obtained from vendors and were used without further purification: potassium cyanide,* sodium hydroxide,* sodium chloride,* dichloromethane,* 1,3-bis(diphenylphosphino)-propanedichloronickel(II)† [$NiCl_2$(dppp)]; lithium perchlorate,‡ and buffer salt§ (pH 10.00 ± 0.02) containing sodium carbonate and sodium bicarbonate. The potassium salt of PFOS was synthesized according to a literature procedure (Hebert et al, in press). The polyalkylated ferrocenium salt 1,1′,3,3′-tetrakis(2-methyl-2-nonyl)ferrocenium nitrate ($DEC^+NO_3^-$) was synthesized according to a literature method (Clark et al, 1996; Clapsaddle et al, unpubl.). All aqueous stock solutions were prepared in class A volumetric glassware using

distilled deionized water** that had an initial resistivity of 18 MΩ cm. All experiments were performed at 24 ± 1°C.

FTIR spectrometer and ATR immersion probe. The spectrometer used in all experiments was an ATR–FTIR†† equipped with a silicon ATR‡‡ probe. The spectrometer was equipped with a liquid-nitrogen-cooled mercury cadmium telluride detector. The spectral window was 4,000–650 cm^{-1}. The spectrometer was interfaced to a dedicated personal computer. Data collection and manipulation were carried out using software.§§ The probe used consisted of a 30-bounce silicon ATR crystal mated to a zinc selenide optical focusing element and housed in a 1.5-in.-long × 1-in.-diameter cylindrical stainless-steel conduit. The exposed surface of the silicon ATR crystal (a circular area 10 mm in diameter) was treated with a 0.542-g/L dichloromethane solution of $NiCl_2$(dppp) (80 µL) or 0.804 g/L DEC+NO_3^- (20 µL). Evaporation of dichloromethane left thin-film coatings of the water-insoluble organometallic ion-exchange compounds on the surface of the ATR crystal. Film thickness was determined by ellipsometry*** to be approximately 0.1 µm.

ATR–FTIR analysis of samples. In a typical analysis, the coated ATR probe was immersed into a known volume of water that was stirred at 200 rpm. The coating was allowed to equilibrate with water for 10 min, at which time a background spectrum was collected. An appropriate amount of an analyte stock solution was then added with stirring and FTIR spectra of the resulting dilute, analyte solution were collected every minute for 60 min. Happ-Ganzel apodization with no spectral smoothing was used, the nominal spectral resolution was 8 cm^{-1}, 64 scans were co-added for each spectrum, and the instrument gain was 1.

The detection limits listed in Table 1 (signal/noise ratio ≥ 3) using the unmodified and modified probe were determined in different ways. For the unmodified probe, an aqueous solution of the analyte was brought into contact with the probe and a spectrum ratioed to water was recorded by signal averaging continuously for 60 min (24,576 scans). The modified probe was immersed in aqueous solutions of specific analyte concentrations, which resulted in bands that were three times the signal-to-noise ratio at either 4 or 60 min. Each spectrum recorded was the result of co-adding 64 scans (30 s scan time). The lower the concentrations of analytes detected, the longer the modified probe was allowed to be in contact with the solution.

RESULTS AND DISCUSSION

The authors' goal was to show that ATR–FTIR spectroscopy can be used to detect polyatomic anions in water at concentrations three to five orders of magnitude lower than current ATR–FTIR detection limits. They accomplished this by modifying a commercially available 30-bounce silicon ATR–FTIR immersion probe with thin-film coatings of two different ion-exchange compounds as described earlier. No further modification of the ATR–FTIR probe and no sample pretreatment were necessary for the experiments reported in this article.

FIGURE 2 Schematic drawing of ion-exchange process

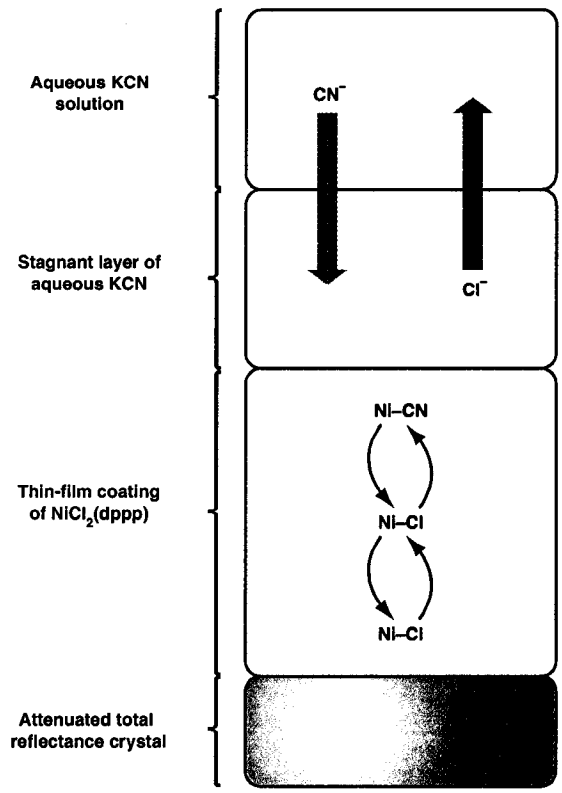

This drawing shows the CN^-/Cl^- ion-exchange reaction that occurs when a thin film of $NiCl_2$(dppp) (abbreviated Ni–Cl) is treated with an aqueous solution of KCN. The relative thickness of the layers is not to scale.

Each thin-film coating was used for only one analysis, after which it was removed from the ATR crystal by washing with dichloromethane. In other words, the ATR crystal was recoated with a thin film of the organometallic ion-exchange compound for each sample. Even though this simple evaporation procedure does not allow film thickness and uniformity to be precisely controlled, the authors found that different films of a given extractant afforded excellent reproducibility for multiple samples of a given aqueous analyte. For example, five replicates of 500 µg/L ClO_4^- with five new films gave a range of dA(1,092 cm^{-1})/dt from 0.0063 to 0.0081 s^{-1} (a relative

*Fisher, Fairlawn, N.J.
†Aldrich, Milwaukee, Wis.
‡G.F.S., Columbus, Ohio
§Micro Essential Lab, Brooklyn, N.Y.
**Type D4700 Nanopure™ Analytical Deionization System, Barnstead/Thermolyne Corp., Dubuque, Iowa
††ReactIR™, Applied Systems Inc., Millerville, Md.
‡‡SiComp®, Applied Systems Inc., Millerville, Md.
§§ASI Reactor™ software, version 2, Applied Systems Inc., Millerville, Md.
***WVASE32™, J.A. Wollman Co. Inc., Lincoln, Neb.

FIGURE 3 Infrared spectra after 5 and 10 min with coated probe immersed in 15 µg/L aqueous ClO_4^-

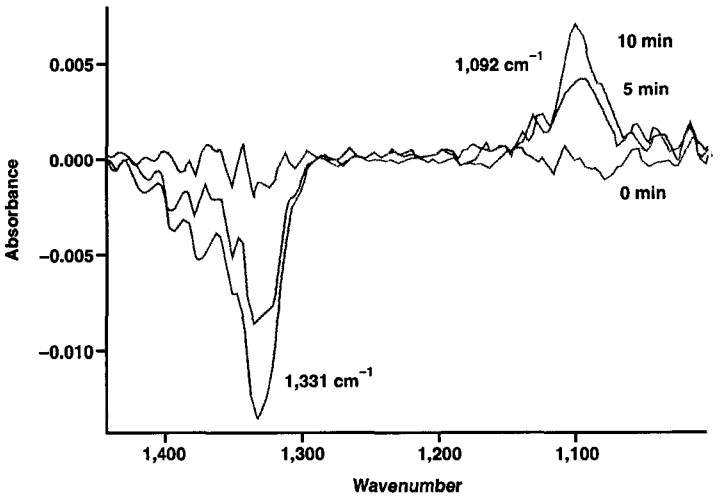

Spectra are of a thin film of water-insoluble $DEC^+NO_3^-$ on the probe immersed in a pH 5–6 aqueous solution of $LiClO_4$ (DEC^+ = 1,1',3,3'-tetrakis(2-methyl-2-nonylferrocenium) cation; $[ClO_4^-]$ = 15 µg/L). The positive band at 1,092 cm^{-1} and the negative band at 1,331 cm^{-1} that grow in over time are assigned to the water-insoluble compounds $DEC^+ClO_4^-$ and $DEC^+NO_3^-$, respectively. The appearance of $DEC^+ClO_4^-$ and the disappearance of $DEC^+NO_3^-$ throughout the film are the result of the ClO_4^-/NO_3^- ion-exchange reaction.
ClO_4^-—perchlorate

FIGURE 4 Plot of absorbance at 1,270 cm^{-1} versus time over 350 min for 25 µg/L PFOS

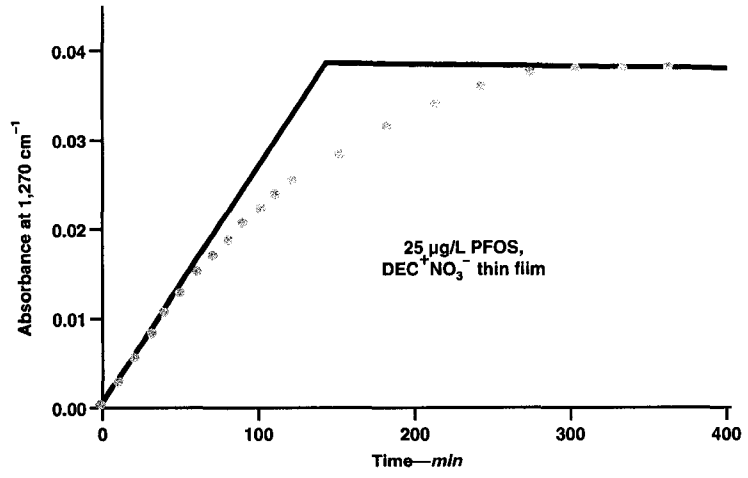

Plot is of a thin film of water-insoluble $DEC^+NO_3^-$ on the probe immersed in a pH 5–6 aqueous solution of K(PFOS) ([PFOS] = 25 µg/L); PFOS—perfluorooctylsulfonate

estimated standard deviation of 10% about the mean). By using water-insoluble but organic-soluble coatings in this manner, the authors were able to study several different ion-exchange compounds and aqueous analytes in a relatively brief period of time using only one ATR–FTIR probe. The rapid removal and reapplication of coatings would not have been possible if more robust, covalently linked coatings had been used instead. A subsequent article will describe experiments with a wider variety of extractants and aqueous analytes (Hebert et al, unpubl.).

$NiCl_2$(dppp)—a nonrecyclable extractant. When the probe coated with a thin film of this compound was immersed in a pH 10 aqueous solution of 5 µg/L CN^-, a new band at 2,104 cm^{-1} was clearly above the detection limit (i.e., signal/noise ≥ 3 at 2,104 cm^{-1}) in 60 min. Because the 1-h detection limit for aqueous CN^- with the unmodified probe was 130,000 µg/L, the nickel complex coating has lowered the detection limit for aqueous CN^- by a factor of 50,000. These and other results are listed in Table 1. When the concentration of aqueous CN^- was 130 µg/L, the time necessary to observe the band at 2,104 cm^{-1} was only 4 min. Figure 1 shows FTIR spectra recorded over time of the $NiCl_2$(dppp)-coated probe immersed in aqueous solutions containing 5 µg/L and 130 µg/L CN^-. Preliminary experiments indicate that the band at 2,104 cm^{-1} is due to the formation of the new water-insoluble complex NiCl(CN)(dppp). Its formation is undoubtedly due to the following, essentially irreversible, ion-exchange reaction:

$$NiCl_2(dppp)(s) + CN^-(aq) \rightarrow NiCl(CN)(dppp)(s) + Cl^-(aq)$$

A depiction of the ion-exchange process is shown in Figure 2. Three kinetic processes could potentially govern the rate of growth of the band at 2,104 cm^{-1}: (1) the diffusion of CN^- from the bulk solution into the stagnant aqueous layer and concomitant diffusion of Cl^- from the stagnant layer into the bulk solution (depicted with straight arrows), (2) the CN^-/Cl^- interchange at the surface of the film, and (3) CN^-/Cl^- ion exchange between adjacent nickel(II) centers (depicted with curved arrows). Because the appearance of the band at 2,104 cm^{-1} occurred at different times for different concentrations of CN^-, kinetic process 1 may be rate limiting under these conditions. In ongoing work, the authors will determine whether a reliable calibration curve of $dA(2{,}104\ cm^{-1})/dt$ versus CN^- concentration can be obtained.

When the $NiCl_2$(dppp)-coated probe was immersed in an aqueous solution containing 130 µg/L CN^- and 35.5 g/L Cl^-, the band at 2,104 cm^{-1} was also observed in about 4 min. Therefore, a 200,000-fold excess of the co-contami-

nant Cl^- does not interfere with the detection of CN^-. This shows the very high selectivity of $NiCl_2$(dppp) for CN^- and suggests that cyanide might be detectable at low concentrations in seawater and other aqueous brines using $NiCl_2$(dppp)-coated ATR–FTIR probes.

$DEC^+NO_3^-$—a redox-recyclable extractant. When the probe coated with a thin film of this compound was immersed in a solution of 3 µg/L ClO_4^- in distilled deionized water (pH 5–6), a new band at 1,092 cm^{-1} was observed in 60 min. This band is the T_2-symmetry ν (ClO) band of the tetrahedral perchlorate ion, now concentrated in the thin-film coating via the following, essentially irreversible ion-exchange reaction:

$$DEC^+NO_3^-(s) + ClO_4^-(aq) \rightarrow DEC^+ClO_4^-(s) + NO_3^-(aq)$$

The related compound $HEP^+NO_3^-$ [HEP^+ = 1,1′,3,3′- tetrakis(2-methyl-2-hexyl)ferrocenium cation] has been used to selectively extract and recover the related tetrahedral monoanions $^{99}TcO_4^-$ and ReO_4^- from aqueous solutions containing up to 100,000 times as much nitrate ion (Chambliss et al, 1999a; Chambliss et al 1999b; Strauss, 1999; Chambliss et al, 1998; Clark et al, 1996). The ion-exchange process can readily be seen in Figure 3, which displays IR spectra recorded after 5 and 10 min when the coated probe was immersed in 15 µg/L aqueous ClO_4^-. The negative band at 1,331 cm^{-1} (the E_u-symmetry ν [NO] band of the nitrate ion) represents the loss of an equivalent amount of NO_3^- from the thin-film coating (based on ClO_4^-) as the ion-exchange reaction proceeds and ClO_4^- is incorporated into the film, which gives rise to the positive band at 1,092 cm^{-1}. As was the case with CN^- detection using the $NiCl_2$(dppp) coating, the magnitude of dA(1,092 cm^{-1})/dt, and not final absorbance, is concentration-dependent. This suggests that it might be possible to prepare a calibration curve for the quantitative determination of aqueous perchlorate by FTIR spectroscopy at microgram-per-litre concentrations with little or no sample pretreatment. One experiment was performed to probe the effect of competing anions on dA(1,092 cm^{-1})/dt. When the aqueous solution contained 930 µg/L NO_3^- as well as 15 µg/L ClO_4^-, spectra similar to those shown in Figure 3 were reproduced in the same time intervals. Concentrations of added NO_3^- greater than or equal to 9,300 µg/L did affect the rise time of the band at 1,092 cm^{-1}. The functional form of dA/dt curves and the effect of competing anions on those curves are currently being studied and will be the subject of a forthcoming article (Hebert et al, unpubl.).

Because the 1-h detection limit for aqueous ClO_4^- (ν (ClO) = 1,104 cm^{-1}) with the unmodified probe was 288,000 µg/L, the $DEC^+NO_3^-$ coating has lowered the detection limit for aqueous perchlorate by a factor of

FIGURE 5 Time-dependent ATR–FTIR spectra of coated probe immersed in aqueous solution containing 250 µg/L PFOS

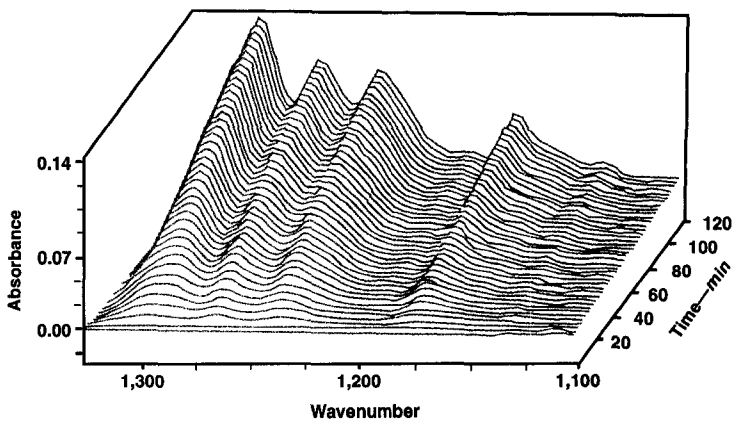

Spectra are of a thin film of water-insoluble $DEC^+NO_3^-$ on the probe immersed in a pH 5–6 aqueous solution of K(PFOS) (DEC^+ = 1,1′,3,3′-tetrakis(2-methyl-2-nonylferrocenium) cation; PFOS = $C_8F_{17}SO_3^-$; [PFOS] = 0.250 µg/L). The bands that grow in over time are assigned to the water-insoluble compound DEC(PFOS), which is formed throughout the film by the PFOS/NO_3^- ion-exchange reaction. ATR–FTIR—attenuated total reflectance–Fourier transform infrared; PFOS—perfluorooctylsulfonate

FIGURE 6 Complete redox-recyclable extraction and recovery cycle

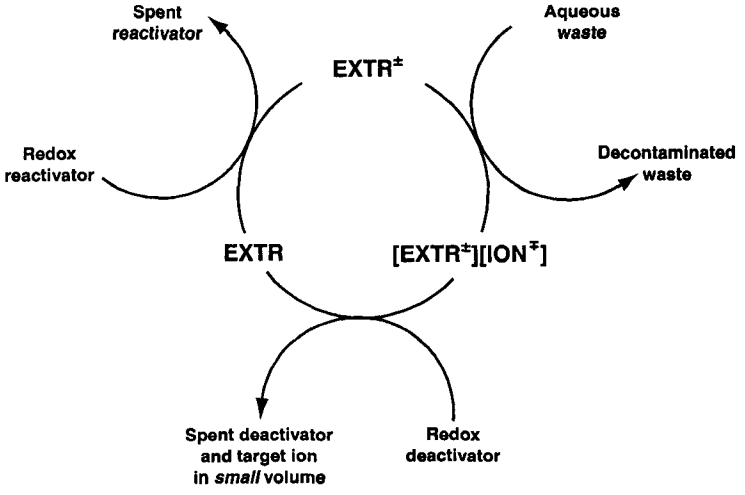

The deactivated extractant (EXTR) and activated extractant ($EXTR^+$ or $EXTR^-$) are confined to a nonaqueous phase throughout the cycle.

nearly 100,000 (Table 1). When the concentration of aqueous ClO_4^- was 500 µg/L, the time necessary to observe the band at 1,092 cm^{-1} was only 2 min.

When the probe coated with a thin film of $DEC^+NO_3^-$ was immersed in a solution of 25 µg/L PFOS in distilled deionized water (pH 5–6), several new bands in the fingerprint region were observed, undoubtedly because of an ion-exchange process similar to the one described earlier for ClO_4^-. The most intense band, at 1,270 cm^{-1}, had a signal/noise ratio ≥ 3 after 60 min. Figure 4 shows a plot of the absorbance at 1,270 cm^{-1} versus time over 350 min. Even though the maximum absorbance of the PFOS bands are not achieved in 60 min, this time is sufficient for the detection of PFOS. Because the 1-h detection limit for aqueous PFOS (ν = 1,243 cm^{-1}) with the unmodified probe was 100,000 µg/L, the $DEC^+NO_3^-$ coating has lowered the detection limit for aqueous PFOS by a factor of 4,000 (Table 1). When the concentration of aqueous PFOS was 250 µg/L, the time necessary to observe the band at 1,270 cm^{-1} was only 4 min. Figure 5 shows FTIR spectra recorded over time of the $DEC^+NO_3^-$-coated probe immersed in an aqueous solution containing 250 µg/L PFOS.

The compounds $DEC^+NO_3^-$ and $HEP^+NO_3^-$ are examples of redox-recyclable extractants, which are being developed in the authors' laboratory for the efficient removal and recovery from water of weakly hydrated aqueous ions, even in the presence of 10^5 times as much nitrate ion in the aqueous phase (Chambliss et al, 1999a; Chambliss et al, 1999b; Clark et al, 1999, Strauss, 1999; Chambliss et al, 1998; Clark et al, 1996; Clapsaddle et al, unpubl.). The basis of redox-recyclable extraction and recovery (R^2ER) is that the neutral extractant, in this case a hydrophobic ferrocene [$Fe(Cp')_2$], is the deactivated low-affinity form of the extractant. It is dissolved in an organic diluent or immobilized on a support. When treated with an aqueous reactivating solution, the high-affinity extractant $Fe(Cp')_2^+NO_3^-$ is formed within minutes. After ion-exchange equilibrium with an appropriate aqueous phase containing the target anion is complete (usually within minutes in bench-scale liquid–liquid experiments or whenever column breakthrough occurs), the R^2ER phase is treated with an aqueous deactivating solution. This causes reduction of $Fe(Cp')_2^+$ to $Fe(Cp')_2$ and release of the Y^- anion within minutes. Examples of reactivating solutions that have been used are aqueous $Fe(NO_3)_3$, $Ce(NH_4)_2(NO_3)_6$, and $NaClO/HNO_3$. Examples of deactivating solutions used are aqueous $Na_2S_2O_4$ and $K_4Fe(CN)_6$. A complete R^2ER cycle is shown in Figure 6. The authors believe that it will be possible to recycle ATR–FTIR thin-film coatings of R^2ER compounds using similar redox chemistry, once coatings that are more permanently bonded to the surface of an ATR crystal have been developed. The authors' work with R^2ER processes

REFERENCES

Ahn, D.J. & Franses, E.I., 1994. Ion Adsorption and Ion Exchange in Ultrathin Films of Fatty Acids. *AIChE Jour.*, 40:1046.

Barja, B.C. et al, 1999. Complexation of Methylphosphonic Acid With the Surface of Geothite Particles in Aqueous Solution. *Langmuir*, 15:2316.

Boening, D.W. & Chew, C.M., 1999. A Critical Review: General Toxicity and Environmental Fate of Three Aqueous Cyanide Ions and Associated Ligands. *Water, Air, Soil Pollut.*, 109:67.

Chambliss, C.K. et al, 1999a. Comparison of the Lipophilic Redox-recyclable Extractant [Fe(^{5}-$C_5H_3(t\text{-}C_7H_{15})_2)_2$][$NO_3$] With [N($n$-$C_7H_{15})_4$][$NO_3$] for Liquid–Liquid Anion-exchange of Aqueous $^{99}TcO_4^-$. *Solvent Extr. Ion Exch.*, 17:553.

Chambliss, C. K.et al, 1999b. Rapid and Selective Redox-recyclable Anion-exchange Materials Containing Polyalkylated Ferricenium Anion-exchange Sites. *Inorg. Chem. Communications*, 1:435.

Chambliss, C.K. et al, 1998. A New Strategy for Separating and Recovering Aqueous Ions: Redox-recyclable Ion-exchange Materials Containing a Physisorbed, Redox-active, Organometallic Complex. *Anal. Chem.*, 70:757.

Christen, K., 2000. Surprising Human Health–Perchlorate Link. *Envir. Sci. & Technol.*, 34:374A.

Clapsaddle, B.J. et al, unpubl. Synthesis and Characterization of Tetra-tert-alkyl Ferrocenes and Ferrocenium Salts, Including the Layered Structures of 1, 1′,3,3′-tetra(2-methyl-2-nonyl)ferrocene and 1,1′,3,3′-tetra(2-methyl-2-nonyl)ferrocenium Nitrate.

Clark, J.F. et al, 1999. Design and Use of a Redox-recyclable Organometallic Extractant for the Cationic Radionuclides $^{137}Cs^+$ and $^{90}Sr^{2+}$. *Envir. Sci. & Technol.*, 33:2489.

Clark, J.F. et al, 1996. Isolation of Soluble ^{99}Tc as a Compact Solid Using a Recyclable, Redox-active, Metal-complex Extractant. *Envir. Sci. & Technol.*, 30:3124.

Darwin, R.L. et al, 1995. Foam and the Environment: A Delicate Balance. *NFPA Jour.*, May/June:67.

Degenhardt, J. & McQuillan, A.J., 1999. In Situ ATR–FTIR Spectroscopic Study of Adsorption of Perchlorate, Sulfate, and Thiosulfate Ions Onto Chromium(III) Oxide Hydroxide Thin Films. *Langmuir*, 15:4595.

Deinhammer, R.S. et al, 1995. Dynamic Modification of Separations Using Electrochemically Modulated Liquid Chromatography. *Anal. Chem.*, 67:237.

De Santis, G. et al, 1992. Ferrocene Derivatives as Electron Carriers for Selective Oxidation and Reduction Reactions Through a Liquid Membrane. *Jour. Chem. Soc., Dalton Trans.*, 2219.

Dobson, K.D. & McQuillan, A.J., 1999. In Situ Infrared Spectroscopic Analysis of the Adsorption of Aliphatic Carboxylic Acids to TiO_2, ZrO_2, Al_2O_3, and Ta_2O_5 From Aqueous Solutions. *Spectrochim. Acta*, 55A:1395.

Dobson, K.D. & McQuillan, A. J., 1997. An Infrared Spectroscopic Study of Carbonate Adsorption to Zirconium Dioxide Sol-Gel Films From Aqueous Solutions. *Langmuir*, 13:3392.

Ghatak-Roy, A.R. & Martin, C.R., 1986. Electromodulated Ion Exchange Chromatography. *Anal. Chem.*, 58:1574.

Göbel, R. et al, 1995. Infrared Attenuated Total Reflection Spectroscopic Investigations of the Diffusion Behavior of Chlorinated Hydrocarbons Into Polymer Membranes. *Vibrational Spectroscopy*, 8:141.

Griffiths, P.R. & de Haseth, J., 1986. *Fourier Transform Infrared Spectrometry.* John Wiley & Sons, New York.

Han, L. et al, 1998. Use of CLS to Understand PLS IR Calibration for Trace Detection of Organic Molecules in Water. *Applied Spectroscopy*, 52:119.

is related to electrochemical or redox switching studies published by other groups (Kingston et al, 1999; Lilga et al, 1997; Shinkai, 1996; Deinhammer et al, 1995; De Santis et al, 1992; Medina et al, 1991; Ghatak-Roy & Martin, 1986), but with added emphasis on increasing the selectivity and decreasing the volume of the recovered target ion. These groups, as well as the authors, have shown that the reversible binding of ions can be accomplished by electrochemically switching or redox switching an extractant molecule.

The authors are pursuing the further development of the technology described in this article. The next obvious steps to be taken are to reduce detection times and to generate calibration (dose–response) curves. Future work will also include developing the ability to extract and therefore detect polyatomic cations of environmental concern in water at microgram-per-litre levels.

ACKNOWLEDGMENT

This research was supported in part by a research and development contract with Electrox Inc. and grants from the US National Science Foundation (CTS-9726143 and CTS-0085892), and is based on work supported in part by the US Army Research Laboratory and the US Army Research Office under grant number DAAD19-00-1-0417. The authors thank J.J. Rack for valuable suggestions.

ABOUT THE AUTHORS:

Steven H. Strauss is professor of analytical and inorganic chemistry, Dept. of Chemistry, Colorado State University, Fort Collins, CO 80523; e-mail <strauss@chem.colostate.edu>. He has a BA degree in chemistry from Franklin & Marshall College in Lancaster, Pa., and an MS degree and PhD, both also in chemistry, from Northwestern University in Evanston, Ill. He was also a postdoctoral research fellow in chemistry at Stanford University in California and Harvard University in Cambridge, Mass. He is a member of AWWA and the American Chemical Society. His previous work has been published in Environmental Science and Technology, Journal of the American Chemical Society, Analytical Chemistry, *and* Applied Spectroscopy. *Matthew A. Odom, Gretchen N. Hebert, and Brady J. Clapsaddle are all graduate research assistants in the Dept. of Chemistry at Colorado State University.*

If you have a comment about this article, please contact us at <journal@awwa.org>.

Hebert, G.N. et al, unpubl. ATR–FTIR Quantification of Aqueous Polyatomic Anions at µg/L Levels.

Hebert, G.N. et al, in press. Efficient Method for the Determination of Sub-ppm Concentrations of Perfluoroalkylsulfonate Anions in Water. *Jour. Envir. Monit.*

Hug, S.J., 1997. In Situ Fourier Transform Infrared Measurements of Sulfate Adsorption on Hematite in Aqueous Solutions. *Jour. Coll. Interface Sci.*, 188:415.

Kingston, J.E. et al, 1999. Anion Recognition and Sensing By Neutral and Charged Transition Metal Coordinated Ferrocene Phosphine Amide Receptors. *Jour. Chem. Soc., Dalton Trans.*, 251.

Lilga, M.A. et al, 1997. Metal Ion Separations Using Electrochemically Switched Ion Exchange. *Sep. Purif. Tech.*, 11:147.

Medina, J.C. et al, 1991. Redox-switched Molecular Aggregates: The First Example of Vesicle Formation From Hydrophobic Ferrocene Derivatives. *Jour. Amer. Chem. Soc.*, 113:365.

Moody, C.A. & Field, J.A., 2000. Perfluorinated Surfactants and the Environmental Implications of Their Use in Fire-fighting Foams. *Envir. Sci. & Technol.*, 34:18:3864.

Moody, C.A. et al, unpubl. Occurrence and Distribution of Perfluorinated Surfactants in Groundwater at the Wurtsmith Air Force Base Fire-training Area Two and KC-135 Crash Site. *Envir. Sci. & Technol.*

Okamoto, H.S. et al, 1999. Using Ion Chromatography to Detect Perchlorate. *Jour. AWWA*, 91:10:73.

Olsen, G.W. et al, 1999. Serum Perfluorooctane Sulfonate and Hepatic and Lipid Clinical Chemistry Tests in Fluorochemical Production Employees. *Jour. Occup. Envir. Med.*, 41:9:799.

Otu, E.O. et al, 1996. Ion Chromatography of Cyanide and Metal Cyanide Complexes: A Review. *Int. Jour. Envir. Anal. Chem.*, 63:81.

Persson, P. et al, 1996. Structure and Bonding of Orthophosphate Ions at the Iron Oxide–Aqueous Interface. *Jour. Coll. Interface Sci.*, 177:263.

Pontius, F.W., 2000. Regulations in 2000 and Beyond. *Jour. AWWA.*, 92:3:40.

Regan, F. et al, 1996. Determination of Pesticides in Water Using ATR–FTIR Spectroscopy on PVC/Chloroparaffin Coatings. *Anal. Chim. Acta*, 334:85.

Renner, R., 2000. Scotchgard Ban Highlights Unknowns. *Envir. Sci. & Technol.*, 34:371A.

Shinkai, S., 1996. Switchable Guest-binding Receptor Molecules. *Comprehensive Supra-molecular Chemistry* (G.W. Gokel, editor). Elsevier, Oxford, U.K.

Strauss, S.H., 1999. Redox-recyclable Extraction and Recovery of Heavy Metal Ions and Radionuclides From Aqueous Media. *Metal Ion Separation and Preconcentration: Progress and Opportunities* (A.H. Bond, M.L. Dietz, and R.D. Rogers, editors). ACS Sym. Series 716. Amer. Chem. Society, Washington.

Susarla, S. et al, 1999. Perchlorate Identification in Fertilizers. *Envir. Sci. & Technol.*, 33:3469.

Tullo, A., 2000a. 3M Discontinues Scotchgard Line. *Chem. Engrg. News*, May 22:9.

Tullo, A., 2000b. 3M Study Raised EPA's Concerns. *Chem. Engrg. News*, May 29:12.

Urban, M.W., 1996. *Attenuated Total Reflectance Spectroscopy of Polymers. Theory and Practice.* Amer. Chem. Society, Washington.

Urbansky, E.T., 1998. Perchlorate Chemistry: Implications for Analysis and Remediation. *Bioremediation Jour.*, 2:81.

USEPA, 2000. Current Drinking Water Standards <www.epa.gov/safewater/mcl.html> (Sept. 2000).

Yang, Lin & Saavedra, S.S., 1995. Chemical Sensing Using Sol-gel Derived Planar Waveguides and Indicator Phases. *Anal. Chem.*, 67:1307.

THE ANALYST
FULL PAPER
www.rsc.org/analyst

Analysis of hydroponic fertilizer matrixes for perchlorate: comparison of analytical techniques†

Timothy W. Collette,*[a] Ted L. Williams,[a] Edward T. Urbansky,*[b] Matthew L. Magnuson,[b] Gretchen N. Hebert[c] and Steven H. Strauss*[c]

[a] *United States Environmental Protection Agency, Office of Research and Development, National Exposure Research Laboratory, 960 College Station Road, Athens, GA 30605, USA. E-mail: collette.tim@epa.gov*

[b] *United States Environmental Protection Agency, Office of Research and Development, National Risk Management Research Laboratory, 26 West Martin Luther King Drive, Cincinnati, OH 45268, USA. E-mail: urbansky.edward@epa.gov*

[c] *Department of Chemistry, Colorado State University, Fort Collins, CO 80523, USA. E-mail: strauss@lamar.colostate.edu*

Received 1st August 2002, Accepted 22nd November 2002
First published as an Advance Article on the web 13th December 2002

Seven retail hydroponic nitrate fertilizer products, two liquid and five solid, were comparatively analyzed for the perchlorate anion (ClO_4^-) by ion chromatography (IC) with suppressed conductivity detection, complexation electrospray ionization mass spectrometry (cESI-MS), normal Raman spectroscopy, and infrared spectroscopy using an attenuated total reflectance crystal (ATR-FTIR) coated with a thin film of an organometallic ion-exchange compound. Three of the five solid products were found by all techniques to contain perchlorate at the level of approximately 100–350 mg kg^{-1}. The remaining products did not contain perchlorate above the detection level of any of the techniques. Comparative analysis using several analytical techniques that depend on different properties of perchlorate allow for a high degree of certainty in both the qualitative and quantitative determinations. This proved particularly useful for these samples, due to the complexity of the matrix. Analyses of this type, including multiple spectroscopic confirmations, may also be useful for other complicated matrixes (*e.g.*, biological samples) or in forensic/regulatory frameworks where data are likely to be challenged. While the source of perchlorate in these hydroponic products is not known, the perchlorate-to-nitrate concentration ratio (w/w) in the aqueous extracts is generally consistent with the historical weight percent of water soluble components in caliche, a nitrate-bearing ore found predominantly in Chile. This ore, which is the only well-established natural source of perchlorate, is mined and used, albeit minimally, as a nitrogen source in some fertilizer products.

Introduction

Perchlorate (ClO_4^-) has been identified, beginning in the late 1990's, as a contaminant in some natural waterways that are used extensively for recreation, drinking, and crop irrigation. Concern over perchlorate arises from its ability to interfere with the function of the thyroid,[1] which can affect metabolism and development. Based on the US Environmental Protection Agency's (EPA) latest risk assessment draft,[2] a concentration near 1 ppb is presumed to be safe for drinking water.[3] The EPA added perchlorate to the Contaminant Candidate List for drinking water in 1998,[4] and to the Unregulated Contaminant Monitoring Regulation list in 1999.[5] This has led to the development and application of a variety of techniques and methods for determining perchlorate in environmental samples, especially finished drinking water and the ground and surface waters that are used as drinking water sources. These include ion chromatography (IC),[6–8] complexation electrospray ionization mass spectrometry (cESI-MS),[9–12] and high field asymmetric waveform mass spectrometry (FAIMS).[13,14] With suitable sample clean-up, some of these techniques have also been applied to the analysis of aqueous extracts of plants that could absorb and accumulate perchlorate, *e.g.*, salt cedar,[15] fruits and vegetables,[16] and tobacco.[17]

Perchlorate contamination, which occurs mostly in the Western USA, can be attributed primarily to the defense and aerospace industry or to military operations,[11,18] where salts of perchlorate are used as oxidants in solid fuels for rockets and munitions. However, to properly assess the significance of perchlorate contamination, and to minimize its future impact, inquiries should be made into the possibility of additional sources of loading to the environment and to the food supply.

The only consistent and well-established natural occurrence of perchlorate is in nitrate-bearing ores, called caliche, that are located predominantly in Chile.[19–22] These ores are mined, and $NaNO_3$ (Chile saltpeter) is refined and sold as a finished fertilizer product (N–P–K grade 16–0–0, *i.e.*, 16% N, 0% P_2O_5, 0% K_2O by mass). Also, Chile saltpeter may be used infrequently in the manufacture of other fertilizer products, including some soluble plant foods that are sold to consumers at nurseries, home improvement centers, and other retail stores. Furthermore, KNO_3 made from Chile saltpeter by cation exchange is sold as a finished fertilizer product (N–P–K grade 14–0–45) and may similarly be incorporated into some soluble plant foods.

† This paper has been reviewed in accordance with the US Environmental Protection Agency's peer and administrative review policies and approved for publication. Mention of trade names or commercial products does not constitute endorsement or recommendation for use by the US EPA. This paper is the work of US government employees engaged in their official duties and is therefore exempt from US copyright protection pursuant to 17 USC 105.

DOI: 10.1039/b207523g

It is well-known that salts of perchlorate are carried-over with $NaNO_3$ in the process of refining Chile saltpeter. Therefore, products derived from Chilean caliche contain perchlorate as a minor component. For example, the finished 16-0-0 fertilizer product acquired in the last few years has been found to consistently contain perchlorate just below the level of 2000 mg kg^{-1}.[17,20,23] The only current vendor for this material has recently modified the caliche refinement process in order to reduce the level of perchlorate to less than 100 mg kg^{-1}.[24]

Fertilizer products derived from Chilean ores were widely used many decades ago. However, their usage has diminished to less than 0.2% of current USA fertilizer consumption,[25] due primarily to the low cost of synthetically produced nitrogen sources. Thus, it was surprising when reports of perchlorate occurrence in certain lawn-and-garden fertilizer products with no known link to Chile saltpeter, which were purchased from November 1998 to January 1999, began to appear (see Williams *et al.*[23] and references therein). While the initial work[26] on this topic relied mainly on IC for many of the materials tested, both it and later confirmatory works[23,27] included analysis of some samples by capillary electrophoresis, Raman spectroscopy, and NMR spectroscopy. Applying methods to confirm IC results with complicated matrixes, such as fertilizers, is important to prevent false positives (there are many unknown ions that might co-elute) as well as false negatives (there are many factors that raise detection limits). The utilities of Raman spectroscopy[23] and cESI-MS[28] in this regard have been demonstrated recently. In addition to describing confirmatory analytical techniques, these two recent studies[23,28] report on the absence or presence of perchlorate in approximately 70 fertilizer materials with no known link to Chile saltpeter that were acquired after May 1999. From among these approximately 70 materials, which span a wide range of type, perchlorate was detected in only two; both of these were fertilizer products formulated specifically for use in hydroponics.[23] (These two hydroponic fertilizers are a subset of the seven products analyzed in this work.)

EPA recently released a report [25] on the most comprehensive survey to date of the presence or absence of perchlorate in fertilizers and related materials. Samples were acquired in May 2000 and included products from all major national suppliers of large-scale agriculturally relevant materials. The survey also included some finished lawn-and-garden fertilizers, but did not include fertilizers targeted specifically for hydroponic use. Perchlorate was not found in any of the approximately 50 tested materials except for the few known to originate from Chile saltpeter.

It is important to note that all surveys of fertilizers for perchlorate represent only a temporal snapshot defined by the time at which samples were acquired. Nonetheless, there is clear consensus among researchers that currently used fertilizers are negligible contributors to perchlorate in the environment, based on the weight of evidence to date[23,25,28,29] and on consideration of the low usage of products derived from Chilean caliche. The source of perchlorate in some lawn-and-garden fertilizers acquired from November 1998 to January 1999,[23] and in the hydroponic fertilizer products described in this report (which were acquired during the Spring of 2000), remains unknown.

Apart from consideration of the magnitude of environmental loading, the finding of perchlorate in hydroponic fertilizers raises some particular concerns. To understand these concerns, note that hydroponics is defined as the production of crops without soil. This includes both water-based and media-based (*e.g.*, Rockwool) systems. Further note that hydroponic crop production is usually conducted in a greenhouse environment that supplies all water and nutrients, which are often re-circulated.[30]

If plants grown conventionally in soil are treated with perchlorate-containing fertilizers, the amount of perchlorate available to the plant will likely be attenuated over time *via* several mechanisms, including runoff and dilution due to rainfall, adsorption to soil, and biodegradation by soil microbes. On the other hand, hydroponic cultures seem more likely to experience accumulation of perchlorate within the media while maintaining bioavailability to growing plants since these natural attenuation mechanisms are absent. Furthermore, all perchlorate-reducing microbes identified to date favor nitrate over perchlorate as a terminal oxidant (electron acceptor) for metabolism.[31–35] In contrast to fertilizers for soil-based farming, nitrate is the primary source of nitrogen in hydroponic fertilizers, largely due to the high water solubility of its salts. Consequently, it is unlikely that significant consumption of perchlorate by water-borne microbes will be observed in hydroponic cultures where there normally would be excess nitrate ion present as a nutrient. This assertion is supported by recent investigations on the removal of perchlorate from water by willow trees grown in sand and hydroponic bioreactors,[36] using nutrient solutions containing nitrate at levels consistent with those used in hydroponic crop production.[37]

However, it should not be inferred that mere exposure of a plant to perchlorate in an aqueous hydroponic medium (*via* root or foliage) means that perchlorate absorption or accumulation definitely occurs. For example, absorption can be affected by a variety of factors, including the presence and concentrations of other ions in the medium, the types of transport proteins involved in the process, and species-, variety-, or cultivar-specific properties of the plant. None of these variables have yet been studied sufficiently in terms of their effects on perchlorate uptake. In addition, many plants can accumulate xylem-transportable ions in their stems or foliage, but not in their fruits, seeds, or nuts. Indeed, transformation of perchlorate (*i.e.*, reduction) has been shown to occur within the tissue of some plants following absorption.[38] Consequently, the focus of agronomic and botanical studies would have to be on uptake in the edible portions of food plants before implications for human or animal health can be inferred.

Although hydroponically grown crops constitute a small percentage of the total global market, the worldwide commercial hydroponics industry continues to grow steadily—about four-fold in known area harvested from 1990 to 2001.[30] Many developed western countries have some commercial hydroponic operations, and the industry is quite large and well-established in, for example, The Netherlands, United Kingdom, Spain, Canada, and Japan.[30,37,39,40] Indeed, a significant percentage of the global supply of a few fresh-market commercial fruits and vegetables (*e.g.*, tomatoes, cucumbers, capsicums, and lettuce) are now grown hydroponically. This increase in commercial hydroponic farming is driven by practical advantages that are perceived both by some producers (*e.g.*, higher and more consistent yield) and by some consumers (*e.g.*, better taste and appearance). Also, hydroponics is viewed by some as environmentally friendly since water is often recycled and pesticide use is often limited. Furthermore, hydroponic farming is attractive to countries where arable land and water are scarce (*e.g.*, Israel).[41] Apart from large-scale commercial businesses, hydroponics is also increasingly attractive for other horticultural activities such as hobby gardening and urban agriculture. The increase in hydroponic activity in all sectors is expected to continue into the foreseeable future.[30]

Therefore, in response to this situation, we have analyzed a small set of widely available hydroponic fertilizers, and herein report our results. Our goal was not to present an exhaustive survey of all such products or to comment on general occurrence. Instead, we sought to illuminate this potential exposure route, and to illustrate, for the first time, the benefits of jointly employing certain spectroscopic techniques that depend on different properties of perchlorate in order to confirm chromatographic identifications in complex matrixes.

Experimental

Sample procurement and preparation

Hydroponic fertilizers were purchased at a retail store in Athens, GA, during March and May of 2000 (see Table 1). To obtain a reasonably representative sample, the complete contents of a solid fertilizer (samples #1–5 of Table 1) container, ranging in weight from about 225–675 g, was riffled into two halves with one of these halves being riffled again; riffling of a subsequent half was repeated until less than 75 g of material was obtained in a half. The final riffled material was then placed in a large bottle where it was further mixed *via* rolling and shaking of the bottle. Next, the material was divided into three parts. One part was retained in Athens, GA, for analysis by Raman spectroscopy, one part sent to Cincinnati, OH, for analysis by IC and cESI-MS, and one part sent to Fort Collins, CO, for analysis by ATR-FTIR spectroscopy. Extracts of these solid fertilizers were then prepared under somewhat different conditions at each laboratory as described below, reflecting different instrument requirements. In particular, the solid-to-water ratio for the extracts varied considerably depending on the demands of the various techniques. The liquid fertilizer (samples #6 and #7 of Table 1) containers were shaken for at least 2 min and the contents were likewise divided among the three laboratories for analysis. All samples were stored in sealed amber glass bottles for overnight shipping from Athens, GA, to the other laboratories.

Note that the concentrations of perchlorate and nitrate reported in Tables 1 and 2, respectively, assume complete extraction of water-soluble analytes from the solid matrixes in all cases. This has not been independently established. Indeed, 100% extraction may not be achieved for all solid fertilizer matrixes, particularly when high solid-to-water ratios are used and some undissolved solids remain, as is the case with some extracts for Raman determination of perchlorate. However, reasonable quantitative agreement among all techniques (see Tables 1 and 2) is consistent with near-complete extraction. Nonetheless, concentrations reported here for solid products should be interpreted as approximate since matrix-specific extraction efficiencies are not accurately known.

Ion chromatography (IC)

A solution of each solid fertilizer product was prepared by dissolving the solid into deionized (DI) water at a ratio of 1.00 ± 0.05 g dL^{-1} (~ 1% w/w). The aqueous solutions were injected (100 μL loop) into a Dionex (Sunnyvale, CA) DX 300 ion chromatograph equipped with IonPac AG16 (guard) and AS16 (analytical separation) columns. The eluent was 0.100 M NaOH(aq) solution at a flow rate of 1.0 mL min^{-1}. Detection was by suppressed conductometry with a CDM2 conductivity detector; the current in the ASRS Ultra suppressor was set to 300 mA. The instrument was calibrated from 0.050 to 100 μg mL^{-1} perchlorate using multiple $NaClO_4$(aq) standards prepared from a stock solution of the reagent grade salt (GFS Chemical, Columbus, OH) using water deionized in-house by reverse osmosis. Water used for the eluent and the suppressor, which was operated in the external water mode, was obtained from a Waters (Milford, MA) Milli-Q polishing unit. Sodium hydroxide (50% w/w) used to make the eluent was obtained from Fisher Scientific (Pittsburgh, PA).

Under these conditions, the concentration of the bulk fertilizer constituent anions (*i.e.*, nitrate, sulfate, phosphate, and chloride) exceeded the perchlorate concentration by at least several hundredfold. Although these other anions are essentially not retained by the AS16 column, their combined concentration

Table 1 Hydroponic fertilizers analyzed by IC, cESI-MS, ATR-FTIR spectroscopy and Raman spectroscopy

			ClO_4^- concentration/mg kg^{-1} [c]			
Sample #[a]	N–P–K grade	Purchase date[b]	IC	cESI-MS	ATR-FTIR	Raman
1	20–6–16	3–2–00	202 ± 2	230 ± 29	120 ± 40	92 ± 5
2	5–18–22	3–2–00	319 ± 16	483 ± 16	340 ± 30	352 ± 87
3	15.5–0–0	3–2–00	ND	ND	ND	ND
4	9–5–18	5–22–00	285 ± 9	323 ± 15	300 ± 100	268 ± 12
5	15–0–0	5–22–00	ND	ND	ND	ND
6	7–0–5	5–22–00	ND	ND	ND	ND
7	5–2–6	5–22–00	ND	ND	ND	ND

[a] Samples 1–5 were solid fertilizers. Samples 6 and 7 were liquid fertilizers. [b] All fertilizers were purchased at a retail store in Athens, GA, USA. [c] Perchlorate concentration in product as purchased. Value is mean ± sample standard deviation. ND denotes that perchlorate was not detected. As discussed in the text, detection levels differ for each technique and for each matrix, but ND for all techniques can be interpreted as perchlorate < 30 mg kg^{-1}. Note: These results do not necessarily represent a continuing level of perchlorate in these or other fertilizer products. (See text for elaboration.)

Table 2 Nitrate concentrations and perchlorate-to-nitrate concentration ratios (w/w) from Raman and ATR-FTIR spectroscopic analysis

Sample[a]	% Nitrate nitro gen as listed[b]	% Nitrate nitro gen Raman[c]	% Nitrate nitro gen ATR-FTIR[c]	ClO_4^-/NO_3^- w/w ratio Raman[d]	ClO_4^-/NO_3^- w/w ratio ATR-FTIR[d]
Bulldog Soda	16.0	16.4 ± 0.3	18.1 ± 0.9	$(2.4 \pm 0.2) \times 10^{-3}$	$(2.8 \pm 0.4) \times 10^{-3}$
#1	12.5	12.6 ± 0.1	14.5 ± 0.7	$(1.7 \pm 0.1) \times 10^{-4}$	$(1.9 \pm 0.5) \times 10^{-4}$
#2	5.0	3.3 ± 0.1	4.1 ± 0.2	$(2.4 \pm 0.6) \times 10^{-3}$	$(1.9 \pm 0.2) \times 10^{-3}$
#3	15.5	14.1 ± 0.1	15.6 ± 0.7	N/A	N/A
#4	8.9	7.5 ± 0.1	8.1 ± 0.5	$(8.1 \pm 0.5) \times 10^{-4}$	$(8.0 \pm 3.0) \times 10^{-4}$
#5	15.0	14.5 ± 0.1	16.7 ± 0.9	N/A	N/A
#6	7.0	6.2 ± 0.1	7.2 ± 0.5	N/A	N/A
#7	4.55	3.7 ± 0.1	4.3 ± 0.2	N/A	N/A

[a] #1–#7 refer to samples listed in Table 1. Bulldog Soda is sodium nitrate derived solely from mined Chilean caliche. The Raman and ATR-FTIR measured values for perchlorate in Bulldog Soda are 1759 ± 111 and 2200 ± 300 mg kg^{-1}, respectively. [b] The weight % nitrate nitrogen in the fertilizer as reported by the manufacturer on the product package. [c] The weight % nitrate nitrogen in the fertilizer as measured by Raman spectroscopy or by ATR-FTIR spectroscopy. [d] The perchlorate-to-nitrate concentration ratio (w/w), as determined by Raman spectroscopy or by ATR-FTIR spectroscopy. If this ratio is in or near the range of 3.7×10^{-4} to 9.0×10^{-2}, the level of perchlorate relative to nitrate is consistent with products derived from mined Chile saltpeter at the time these products were purchased. See text for details. N/A denotes not applicable since perchlorate was not detected.

is so great that they produce a large, tailing peak. The peak of perchlorate, which has a retention time of ~8.4 min, sits on this tail, as shown in Fig. 1a. Fortifications of 2 μg mL^{-1} were used to verify the identity of the perchlorate peak as illustrated in Fig. 1b; this concentration was chosen so as to roughly double the peak area (*i.e.*, about twice the analyte concentration found in unspiked samples).

Complexation electrospray ionization mass spectrometry (cESI-MS) combined with IC eluate fraction collection

Perchlorate-containing fractions of the IC eluate were collected and analyzed by cESI-MS. (The very complex matrix of these samples interferes with effective cESI-MS analysis when the technique of standard addition[9,10,28] is used without prior anion isolation.) In this fashion, each injected aliquot is analyzed both by conductivity and, subsequently, by mass spectrometry. An increase in selectivity is afforded with the combined use of retention time (from IC) and mass-to-charge ratio (from cESI-MS). Unfortunately, analyte concentration is reduced because of dilution during fraction collection. However, the dilution factor was not prohibitive due to the high sensitivity of the cESI-MS technique.

IC fractions eluting between 8.0 and 10.0 min (2.0 mL total per fraction) were collected for multiple injections and subsequently combined using a Gilson (Middleton, WI) model FC 203B fraction collector. (The perchlorate peak elutes over the course of ~1.5 min with 0.10 M NaOH eluent.) With more pristine samples, the analyte-free post-suppressor eluate from the IC can be collected and used successfully as a blank for cESI-MS analyses of IC fractions. However, for most fertilizer solutions the post-suppressor eluate does not constitute a useful blank with these IC fractions because the perchlorate peak elutes on the large tail of the bulk nutrient anions peak. These anions reduce the efficiency of the electrospray process, adversely affecting the background mass spectrometer signal.

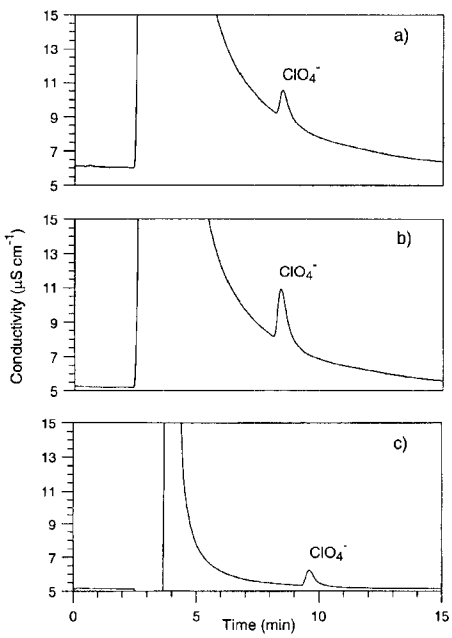

Fig. 1 (a) Ion chromatogram of a 1.0 g dL^{-1} solution of fertilizer sample #1 listed in Table 1. Conditions: 0.10 M NaOH(aq) as eluent; flow rate: 1.0 mL min^{-1}; AG16/AS16 columns; 100 μL loop; suppressed conductivity detection. (b) Same after fortification with 2.0 μg mL^{-1} perchlorate. (c) Ion chromatogram of the 8.0–10.0 min eluate fraction of the sample whose chromatogram is (a). The fraction was reinjected onto the IC using a 1.0 mL sample loop; otherwise, conditions are the same.

Therefore, to further reduce the level of these anions, the combined IC eluate fractions were reinjected on the IC using a 1.00 mL loop, and multiple fractions were collected/combined a second time.

The large injection volume used in the second set of collections resulted in some broadening of the perchlorate peak and also increased its retention time to ~9.6 min, as verified by injecting a standard solution. Accordingly, the eluate was taken during the period 9.0–11.0 min. As illustrated in Fig. 1c, the baseline conductivity (L) of the chromatogram for the second set of collections (L = 5.3 μS cm^{-1}) was significantly less than that for the first set (L > 8.0 μS cm^{-1}, see Fig. 1a). For these fertilizer samples, the combined fractions gathered from the second set of collections proved adequate, and were subsequently used in the cESI-MS analyses described below.

To prepare the IC eluate for cESI-MS analysis, a 1.0 mL aliquot of the collected eluate was transferred to a 4.0 mL glass vial using a pipettor. The following were then added to the eluate: 30 μL 0.20 M $C_{10}H_{21}NMe_3Br$(aq) (Fluka, Buchs, Switzerland) and 500 μL CH_2Cl_2 (Fisher Optima). The vial was capped with a PTFE-lined septum and shaken for 90 s. After phase separation (2–5 min), the dichloromethane layer was drawn off with a gas-tight syringe; a volume of ~350 μL was recovered. This dichloromethane extract was injected into the electrospray interface with a Rheodyne (Rohnert Park, CA) model 7725 injector with a 200 μL loop. The carrier liquid, Optima grade methanol, was pumped at 0.3 mL min^{-1} by a Waters 600 pump (Milford, MA). The mass spectrometer was a Finnigan MAT TSQ-700 (San Jose, CA) equipped with a standard Finnigan electrospray interface. Mass spectra were acquired in the negative ion mode by scanning Q3 over appropriate mass ranges with a scan time of 0.5 s. The ESI spray voltage was 4.0 kV, the interface capillary temperature was 200 °C, and the sheath gas pressure was 70 psi (480 kPa).

Attenuated total reflectance-Fourier transform infrared (ATR-FTIR) spectroscopy

Dichloromethane (Fisher, Fairlawn, NJ) and lithium perchlorate ($LiClO_4$, GFS Chemical, Columbus, OH) were obtained and used without further purification. The polyalkylated ferrocenium salt 1,1′,3,3′-tetrakis(2-methyl-2-nonyl)ferrocenium nitrate ($DEC^+NO_3^-$) was synthesized according to a literature method.[42,43] This compound is one of a number of selective, ferrocene-based, water-insoluble, organometallic ion-exchange compounds.[42–46] All aqueous stock solutions were prepared in Class A volumetric glassware using distilled DI water (Barnstead NANOpure, Dubuque, IA) that had an initial resistivity of 18 MΩ cm. All experiments were performed at 24 ± 1 °C. The seven fertilizer samples were dissolved in water to make 10 g L^{-1} stock solutions of all samples except for #4 for which a 3 g L^{-1} stock solution was made.

The spectrometer used in all experiments was an ASI (Applied Systems Inc, Millersville, MD) ReactIR™-1000 equipped with an ASI SiComp® ATR-FTIR immersion probe. The spectrometer was equipped with a liquid-nitrogen-cooled MCT detector. The spectral window was 4000–650 cm^{-1} with a nominal spectral resolution of 8 cm^{-1}. Happ-Ganzel apodization was used with no post-run spectral smoothing. Data collection and manipulation was carried out using ASI ReactIR™ software (version 2.1). The probe consisted of a 30-bounce silicon ATR crystal mated to a ZnSe optical focusing element and housed in a 1.5 in. long × 1 in. diameter cylindrical stainless-steel conduit. The exposed surface of the ATR crystal was a circular area 1 cm in diameter. For some experiments, the immersion probe was inverted so that a small amount of aqueous solution could wet the entire surface of the crystal. In other experiments, the probe was immersed in a beaker containing 100 mL of aqueous sample.

Initial characterization of the fertilizer samples was accomplished by placing a sufficiently large aliquot of the stock solution on top of the inverted SiComp® probe so that the ATR crystal was completely covered by the sample (this was generally 1 mL) and collecting a spectrum (64 co-added scans; 35 s total collection time) that was ratioed to DI water. The absorbance (A) of the ν_3 peak of nitrate at 1347 cm^{-1}, which is due to the asymmetric NO_3 stretching vibration,[47] was used in these experiments to determine the concentration of nitrate in each 10 or 3 g L^{-1} fertilizer stock solution. This was done by using a calibration curve of A(1347 cm^{-1}) *vs.* nitrate concentration, which was found to be linear over the concentration range 0.62 g L^{-1} to 25 g L^{-1} (a similar linear calibration curve has been reported in the literature).[48] The ν_3 peak of perchlorate in water at 1104 cm^{-1}, which is due to the asymmetric ClO_4 stretching vibration,[47] was not observed in any of the stock solutions, indicating that the concentration of perchlorate in the samples was less than 230 ppm (see below).

The LOD of perchlorate in DI water using the SiComp® probe was found to be 230 ppm, which is more than four orders of magnitude higher than early estimates of a safe level for drinking water (4–18 ppb).[18] In this case, the LOD is defined as the concentration of perchlorate that results in an absorbance at 1104 cm^{-1} after 15 min (3750 co-added scans) that is three times the signal to noise ratio (S/N) at ~1100 cm^{-1}. To lower the perchlorate LOD of the ATR-FTIR spectrometer, the silicon ATR crystal was coated with a thin film of $DEC^+NO_3^-$. Some aspects of this procedure have been published elsewhere.[49] The thin film was prepared by treating the crystal with 20 μl of a 0.81 g L^{-1} (1 mM) dichloromethane solution of $DEC^+NO_3^-$. Evaporation of dichloromethane left a thin-film coating of $DEC^+NO_3^-$ on the surface of the ATR crystal. The film thickness was determined to be ~0.1 μm by ellipsometry (WVASE 32TM, J.A. Wollman Co., Inc., Lincoln, NE). The coated ATR probe was immersed into 100 mL of a stirred (200 rpm) aqueous sample and a spectrum (64 co-added scans) was recorded every minute for 15 min. At this time, the film, which now contained $DEC^+ClO_4^-$ in some cases as well as $DEC^+NO_3^-$, was removed using dichloromethane and replaced with a fresh coating of $DEC^+NO_3^-$ for the next analysis. The relevant ion-exchange equilibrium is:[44–46]

$$DEC^+NO_3^-(film) + ClO_4^-(aq) \rightleftharpoons DEC^+ClO_4^-(film) + NO_3^-(aq)$$

In a typical analysis, the coated SiComp® probe was immersed in 100 mL of DI water for 10 min and a new single-beam background was collected. An appropriate volume of one of the fertilizer stock solutions was then added to make a solution for ATR-FTIR analysis that was either 100 mg L^{-1} (for fertilizers #2 and #4) or 1000 mg L^{-1} (for fertilizers #1, #3, #5, #6, and #7) in fertilizer concentration. The aforementioned 15 minute-by-minute spectra were then recorded. The set of spectra for fertilizer #2 (which is typical for samples that contained detectable perchlorate) is shown in Fig. 2. Each sample solution was analyzed in triplicate (*i.e.*, using a fresh coating of DEC^+NO3^- for each of the three analyses).

Several of the fertilizer solutions gave a positive indication for the presence of perchlorate by the growth of the ν_3 peak of perchlorate in the film at 1096 cm^{-1} as ion-exchange equilibration took place. We have established that the initial rate of growth of an absorbance peak associated with a particular anion is linearly related to the concentration of that anion in solution when exposed to an ATR probe coated with the appropriate ion-exchange film. For these fertilizer solutions, quantification of perchlorate was determined by the method of standard additions, using the initial rate of peak growth as the dependent variable.

First, a plot of the absorbance of the 1096 cm^{-1} peak *vs.* time was made, and the slope of the initial, apparently linear, portion (dA(1096 cm^{-1})/dt) was determined. This plot for sample #2 is shown in Fig. 3a. Note that, while the plot is apparently linear from 0 to about 15 min (the region over which the slope was determined), the overall approach to ion-exchange equilibrium is apparently exponential.

Next, each of the fertilizer solutions shown to contain perchlorate was analyzed several more times using this procedure, but with a known amount of a 0.11 g L^{-1} lithium perchlorate stock solution added to the sample. This procedure was repeated for at least four different concentrations of added perchlorate (three replicates each). Each perchlorate-spiked, standard-addition sample gave a dA(1096 cm^{-1})/dt value that

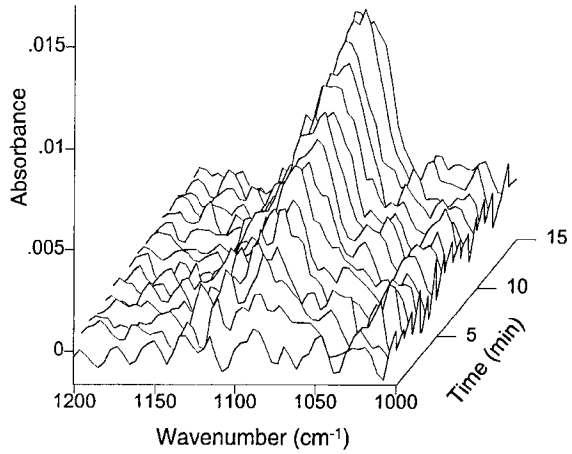

Fig. 2 ATR-FTIR spectra of an aqueous solution of 100 mg L^{-1} of fertilizer sample #2 listed in Table 1 collected every minute for 15 min using the SiComp® probe coated with a thin film of the ion-exchange compound $DEC^+NO_3^-$.

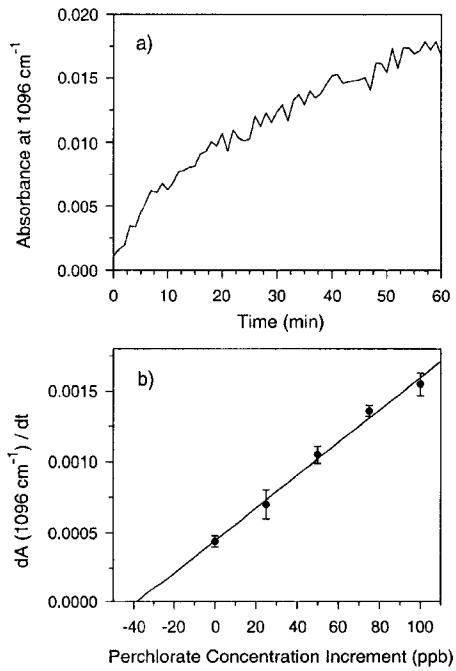

Fig. 3 (a) Plot of absorbance at 1096 cm^{-1} *vs.* time for the ATR-FTIR spectra displayed in Fig. 2, along with those collected for the same sample from 16 to 60 min. The slope of the approximately linear initial portion of this graph, dA(1096 cm^{-1})/dt, was used as one of the data points in the standard addition graph below it. (b) ATR-FTIR standard addition graph for fertilizer sample #2 listed in Table 1. Using this graph, the absolute value of the x-axis intercept corresponds to the amount of perchlorate in the 100 mg L^{-1} fertilizer solution. After accounting for dilution, there is 340 ± 30 mg kg^{-1} perchlorate in this fertilizer.

was linearly related to the overall concentration of perchlorate in solution.

Finally, a plot of $dA(1096\ cm^{-1})/dt$ *vs.* the perchlorate concentration increment was made, and the absolute value of the *x*-axis intercept of a linear least-squares fit to the data was taken as the concentration of perchlorate in the unspiked fertilizer sample solution. The perchlorate concentration in the solid fertilizer sample was then calculated using this value and the known dilution factor. The plot of $dA(1096cm^{-1})/dt$ *vs.* the perchlorate concentration increment for sample #2 is shown in Fig. 3b.

Raman spectroscopy

Extracts for perchlorate determination by Raman analysis were prepared using a protocol similar to that described by Williams *et al.*[23] Briefly, for the solid fertilizers (*i.e.*, samples #1-#5 of Table 1), about 5 g of the riffled material was extracted with 20–25 mL of DI water with an 18 MΩ cm resistivity. The mixture/solution was vortexed for 1 min and subsequently filtered through a Millipore Millex-HV 0.45 μm poly(vinylidene fluoride) (PVDF) filter. Note that perchlorate was not detected by Raman spectroscopy in sample #1 using these conditions. Later, after perchlorate was observed with the three other techniques, an additional extract of solid fertilizer sample #1 was prepared in a similar fashion, but using a higher solid-to-water ratio (*i.e.*, 5 g in 5 mL). A 2 mL portion of this more concentrated extract of fertilizer sample #1 was treated (after filtration) with 1 g of activated alumina adsorbent (DD6 by Alcoa), in order to decrease the very high level of some of the fertilizer nutrients. The treatment with DD6 generally followed the procedure of Ellington and Evans,[16] who have shown that DD6 significantly decreases (by competitive sorption) the concentration of ionic fertilizer nutrients in aqueous samples with no detectable loss of perchlorate when the nutrients are present at higher levels, as is the case here. Perchlorate was observed with Raman analysis in this more concentrated extract and was confirmed (both qualitatively and quantitatively) using a spike-and-recover procedure.

The liquid fertilizers (samples #6 and #7 of Table 1) were analyzed for perchlorate directly after passing 5 mL aliquots through Millex-HV filters. The aliquots were taken from the original containers that where hand-shaken for at least 2 min.

Separate extracts for nitrate determination by Raman analysis were prepared in a similar fashion, but using a much lower fertilizer-to-water w/w ratio. In this case, for both solid and liquid fertilizers, about 0.14 g of fertilizer was dissolved in 25 mL of dionized water.

The Raman spectra were acquired with a Kaiser Optical Systems HoloProbe, using 785 nm laser excitation from a 300 mW SDL-8530 external-cavity-stabilized diode laser. This type of Raman instrument has been described fully elsewhere.[23,50] Briefly, light from the laser was coupled to a remote probe head *via* a fiber optic cable. This laser light was then brought to focus with a series of lenses at approximately 7.5 cm beyond the end of the probe head assembly. A standard quartz cuvette, containing the aqueous fertilizer solution, was placed in the path of the beam such that the focus of the beam fell in the center of the solution. The power of the laser light at the solution was generally about 100 mW.

Raman scattered light from the solution was collected by the probe head along the same path as the excitation laser beam (*i.e.*, 180° backscattering geometry), and was coupled to a separate fiber optic cable for delivery to the spectrograph. Inside the spectrograph, the Raman scattered light was focused through a 50 μm slit and directed through a volume holographic grating and focused onto the charge-coupled device (CCD) detector. This spectrograph permits acquisition of the entire Raman spectrum, with a useable Stokes Raman shift of about 3280 to 95 cm^{-1} in a single exposure, with about 5 cm^{-1} spectral resolution. The CCD detector uses a high quantum efficiency Princeton CCD-1024EHRB back-illuminated, deep depletion, near-infrared-optimized chip, which is thermoelectrically cooled to −65 °C. A Kaiser Optical Systems, Inc., HoloLab calibration accessory was used in determining system response for frequency and intensity calibration.[51]

For perchlorate determinations, Raman spectra were typically collected with an exposure time of 20 s with five accumulations co-added. Spectra were collected in this fashion for each of the seven fertilizer sample solutions, for numerous perchlorate standards in water, and for pure water. These settings resulted in a total analysis time of ~7 min per spectrum. In a few cases, a higher exposure or more accumulations were employed to improve S/N for solutions containing lower perchlorate levels, thereby increasing the total analysis time to about 40 min. No solution exhibited significant fluorescence under any conditions.

For nitrate determinations, Raman spectra of extracts, standards, and water were collected in a similar manner. However, in this case, all spectra were collected with an exposure time of 15 s with three accumulations co-added. This resulted in a total analysis time of ~3 min per spectrum.

All sample and standard solutions were analyzed in triplicate. The perchlorate concentrations in the hydroponic fertilizer solutions were determined for all spectra based on the fitted area of the symmetric ClO_4 stretching peak (ν_1),[47] which occurs near Raman shift of 934 cm^{-1}. (A linear calibration curve was constructed using perchlorate standards prepared in DI water. Details of the method of quantification can be found elsewhere.)[23] Then, the perchlorate concentrations for the solid fertilizer samples were determined based on the solid-to-water ratio of the extracts, assuming 100% extraction efficiency. Finally, the mean perchlorate concentration of each solid sample was determined, along with the sample standard deviation (*s*); these values are reported in Table 1.

The nitrate concentrations in the fertilizer extracts, and in the original solid and liquid products, were determined in the same manner using the fitted area of the symmetric NO_3 stretching peak (ν_1),[47] which occurs near Raman shift of 1047 cm^{-1}. In Table 2, we present these results as '% nitrogen as nitrate,' which is the weight percent of the fertilizer product that is nitrogen occurring as nitrate.

The following reagents were used as calibration standards: ammonium perchlorate (NH_4ClO_4) 99+%, Aldrich; sodium perchlorate ($NaClO_4$) 99+%, Acros; sodium nitrate ($NaNO_3$) 99+%, Fisher. Each was used as received without further purification.

Results and discussion

Unequivocal identification of perchlorate, particularly in complex aqueous samples, is a challenging analytical problem. For obvious reasons, many convenient and widely accepted techniques for definitive analysis of environmental contaminants (*e.g.*, GC-MS) cannot be applied directly to inorganic ions occurring in aqueous media. The most common technique for perchlorate analysis is IC with suppressed conductivity detection.[7,52] IC is widely available, exhibits a low LOD for perchlorate in relatively pure water (~1 ppb), and can be equipped with autosamplers for unattended operation. However, identification is based solely on retention time matching since all ions are amenable to conductivity detection. Also, analysis by IC is greatly hindered when samples contain high total dissolved solids (TDS), as is the case with these hydroponic fertilizer solutions; TDS roughly equates to ionic strength. Both qualitative and quantitative analysis of perchlorate in fertilizers is compromised because the small

perchlorate peak elutes on the tail of a very large peak due to the major fertilizer components. Samples generally must be diluted to bring the TDS down to a manageable level. This raises the w/w LOD (relative to that for perchlorate in pure water), typically by orders of magnitude. While detection limits will vary from fertilizer to fertilizer, previous results[17,27,28] and the work here indicate a typical w/w LOD of about 30 mg kg^{-1}. Quite often, a series of runs is necessary in order to find the level of dilution that yields acceptable results. This significantly increases the total analysis time. Also, high TDS samples rapidly degrade the IC column and foul the suppressor and detector.

For qualitative chemical identifications to be considered definitive, a detection method more specific than retention-time matching is usually required. Historically, information-rich spectroscopic methods (*e.g.*, MS, IR, and NMR) have been used to satisfy this need. Certain types of these methods have been coupled to chromatographic instruments and have become valuable and routine tools for analysis of multi-component samples (*e.g.*, GC-MS, GC-IR, and LC-MS).

Unfortunately, none of these off-the-shelf coupled tools are directly amenable to analysis of perchlorate in fertilizer extracts. In some cases, the limitation is imposed by the separation technique. Fortunately, although fertilizer extracts are complex (*i.e.*, containing very high levels of TDS), the total number of unique components is limited, and chromatographic separation is not required if the detection method has adequate selectivity. All of the spectroscopy-based approaches described here rely on this principle. However, the selectivity afforded by each technique differs, one from the other, in the physical property of perchlorate upon which the measurement depends. The qualitative and semi-quantitative agreement observed among these techniques provides a highly confident determination of perchlorate in the hydroponic fertilizers tested (see Table 1). It is useful to briefly discuss a few salient points of the application of each spectroscopic technique to hydroponic fertilizer analysis to illustrate how these techniques together contribute to these results.

cESI-MS analysis

The use of cESI-MS provides confident identification of low molecular weight ions by MS without prior analyte separation.[10,53–55] The cESI-MS method is the most sensitive for detection of perchlorate in relatively pure water (LOD ~0.3 ppb) among those described here. Perchlorate determination by cESI-MS involves the use of a quaternary ammonium ion that forms an ion pair with perchlorate that can be selectively extracted into dichloromethane, and has been described in detail elsewhere.[10,53] The procedure allows the extraction of perchlorate from water, which is a problematic matrix for MS detection. This approach provides excellent selectivity, and is definitive for perchlorate identification. Unfortunately, cESI-MS is adversely affected by high TDS, roughly to the same degree as IC, based on difficulties in quantification. Other anions present in the aqueous sample (in this case, fertilizer nutrients) also form complexes with the quaternary ammonium base molecules and are extracted along with the perchlorate complex. High TDS affects the MS background signal and reduces the efficiency with which the electrospray apparatus produces perchlorate-complex ions. As with IC, the net effect is to raise the w/w LOD (relative to that in pure water), due to the need to dilute the sample. The selectivity, however, is not significantly affected by high TDS because of the unique mass spectrum of the perchlorate complex.

As described in the Experimental section, samples that were subjected to cESI-MS analysis were obtained from two successive IC fractionation runs. The organic extracts of the final fractions (after addition of the complexing agent) were injected into the ESI-MS instrument and the mass spectra of the perchlorate complexes were obtained. The most sensitive and selective method of analysis involves single ion monitoring using *m/z* 380, which corresponds to the most abundant perchlorate complex anion: $C_{10}H_{21}N(CH_3)_3Br(ClO_4)^-$. An example of three successive 50 μL injections of the organic extract for fertilizer sample #1 is shown in Fig. 4.

The experiments reported here are not useful for estimating LOD's of cESI-MS for perchlorate directly in fertilizer extracts because isolated IC fractions, which were much lower in TDS, were used. Some of us have previously used cESI-MS for analysis of perchlorate in fertilizers without IC fractionation and have observed LOD's of about 100 mg kg^{-1} or less.[28] In the present work, the LOD's are reduced by incorporating IC fractionation; however, the improvement is limited by the concomitant dilution. The LOD of cESI-MS with IC fractionation as described herein is expected for most samples to be at least as low as that of IC (*i.e.*, ~ 30 mg kg^{-1}).

ATR-FTIR analysis

Attenuated total reflectance FTIR spectroscopy is directly applicable to determination of polyatomic ions such as perchlorate in water.[48] However, using a commercially available 30-bounce silicon ATR probe, the perchlorate LOD of 230 ppm in DI water is rather high. The method described herein (and in more detail elsewhere)[49] involves the use of a thin-film coating consisting of a water-insoluble organometallic ion-exchange compound that is selective for perchlorate on the ATR crystal. When the modified probe was immersed in a perchlorate-containing aqueous solution, nitrate ions in the thin film were replaced by perchlorate ions, and an infrared spectral peak corresponding to perchlorate (the asymmetric ClO_4 stretching vibration, ν_3, which is of T_2-symmetry and occurs at 1096 cm^{-1})[47] appeared and grew in intensity over time. The initial rate of growth of the absorbance of this peak, $dA(1096\ cm^{-1})/dt$, is linearly correlated with the concentration of perchlorate in solution. Use of the extractant-coated probe leads to a lowering of the LOD from 230 ppm to 15 ppb in DI water.[49]

Although a new thin-film coating is required for each analysis, a relatively high degree of reproducibility can be achieved. For example, when three replicate films were treated with a given standard aqueous solution of lithium perchlorate, the $dA(1096\ cm^{-1})/dt$ values typically varied by ±10% about the mean over the concentration range 15 ppb to 1 ppm. The high TDS content and high nitrate concentrations of the aqueous fertilizer solutions required the use of the method of standard additions, and the reproducibility of $dA(1096\ cm^{-1})/dt$ values for a given sample varied from ±50% relative error for small

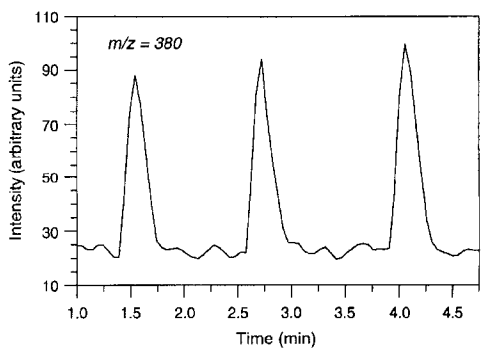

Fig. 4 cESI-MS single ion monitoring (negative ion mode) spectrum for three successive 50 μL injections of a CH_2Cl_2 extract of the IC eluate fraction collected at 9.0–11.0 min, whose IC chromatogram is shown in Fig. 1(c), after complexation. The most abundant complex anion, $C_{10}H_{21}N(CH_3)_3(Br)(ClO_4)^-$, peak is observed at *m/z* 380.

amounts of added perchlorate to ±14% relative error for large amounts of added perchlorate. In addition, the high TDS and high nitrate content of the fertilizer solutions had an adverse effect, in most cases, on the perchlorate LOD. For example, a control experiment showed the perchlorate LOD is 0.6 ppm in a 1.55 g L^{-1} aqueous solution of nitrate (added as sodium nitrate), whereas the perchlorate LOD is 0.015 ppm in DI water for a 15 min contact.

The ATR-FTIR results for perchlorate and nitrate are shown in Tables 1 and 2, respectively. Note in Table 2 that the seven hydroponic fertilizers were found to contain very different amounts of nitrate, with the weight percent nitrogen as nitrate varying from about 4.1% to 16.7% (*i.e.*, weight percent nitrate 18% to 74%). Except for perchlorate and nitrate, the components of the fertilizers were not determined in this study. However, the manufacturers' listed N-P-K grades, which are shown in Table 1, indicate that the fertilizers also contained various amounts of phosphate and potassium. Therefore, each fertilizer, when dissolved in water, resulted in a unique aqueous matrix.

Perchlorate was not detected by any technique in four of the seven hydroponic fertilizers. Extracts of these four samples were used to estimate the LOD for perchlorate in fertilizer solutions using the extractant-coated SiComp® probe. Specifically, we determined the amount of added perchlorate that was required to obtain an absorbance peak at 1096 cm^{-1} with height equal to three times the peak-to-peak noise level at ~1100 cm^{-1} for 64 co-added scans taken after an equilibration time of 15 min. The concentration of perchlorate in the extract at that point (assuming it contained zero perchlorate prior to addition) was taken as the estimate of LOD for that extract. As expected, the LOD was somewhat different for each fertilizer solution because each one represents a different matrix of dissolved solids. Specifically, LOD estimates ranged from 200 to 700 ppb, with the lower LOD estimates generally being observed for fertilizers with lower levels of nitrate.

Raman analysis

Perchlorate is measured in the bulk aqueous fertilizer solutions using normal Raman spectroscopy without complexation or sorption onto a surface. This is convenient, but not sensitive. Approximately 20 ppm is the LOD for perchlorate in DI water for Raman analysis (using the conditions described above) when no post-run data manipulation is performed. This is based on S/N = 3, using the height of the 934 cm^{-1} peak of perchlorate relative to peak-to-peak noise in the baseline in the same region of the spectrum. Subtraction of a spectrum of DI water (*i.e.*, an ideal blank) decreases the Raman LOD to about 10 ppm, which is still more than two orders of magnitude above that of the other techniques described here for DI water.

Although not very sensitive, Raman is a useful tool in this application because it can easily tolerate very high levels of TDS with only limited impact on the perchlorate LOD. Raman essentially has no upper limit of detection; therefore, samples that are very concentrated in both analyte and in other matrix components can be analyzed if there is adequate resolution of matrix-component and analyte peaks. (It has been shown recently that the Raman spectral features of common fertilizer components do not directly interfere with the 934 cm^{-1} peak of perchlorate.)[23] Indeed, the LOD for perchlorate in concentrated fertilizer extracts is only slightly higher than that for DI water. The small increase is due to the Raman scatter and luminescence (and the associated shot noise) from various matrix components, which make it somewhat more difficult to discern the Raman peak from perchlorate. While this increase in LOD varies depending on the type of fertilizer, it is typically only about a factor of two to five. Also, for fertilizer extracts, the benefits of water subtraction are not as great (compared to perchlorate standards in water) because DI water no longer constitutes an ideal blank. For extracts of these hydroponic fertilizers, which contain highly water soluble nutrients but exhibit no appreciable fluorescence at this excitation wavelength, the LOD is about 50 ppm. Using our typical solid-to-water ratio of 1/4, this corresponds to a LOD of about 200 mg kg^{-1} for a fertilizer on a solid weight basis. Note that we have successfully detected perchlorate using a solid-to-water ratio as high as 1/1 (*i.e.*, for sample #1 using DD6 treatment of the extract), which sets the LOD at about 50 mg kg^{-1}. Given the high TDS tolerance of Raman spectroscopy, the w/w LOD for perchlorate in a solid (or liquid) fertilizer is no more than about one order of magnitude higher than that of IC and the other techniques described here.

As shown in Fig. 5, direct Raman analysis also allows some other fertilizer components (*e.g.*, nitrate, phosphate, sulfate, and urea) to be measured simultaneous, along with perchlorate. This capability, which is not present with methods that rely on selective complexation, is important in some situations. For example, the Raman spectrum can serve as a fertilizer brand signature because peak intensities from the various components are unique for a given formulation. This serves as a useful quality control feature when multiple products or multiple lots of a given product are analyzed comparatively.

In spite of the simultaneous presence of signal from multiple fertilizer components, Raman is adequately selective for perchlorate because Raman-active fertilizer nutrients (mostly inorganic ions) are relatively few, and each exhibits only one or two intense Raman bands that are well separated from those of the other components. On the other hand, direct Raman analysis without analyte separation is often not feasible for applications where numerous organic components are present, due to overlapping Raman bands and also to the presence of fluorescence. The Raman spectrometer described here relies on laser excitation at 785 nm, which avoids fluorescence from many organic compounds. In spite of this fact, we previously have observed significant fluorescence when analyzing for perchlorate in plant tissues and in a few fertilizer extracts.[23] However, significant fluorescence was not observed with any of the fertilizer solutions described here.

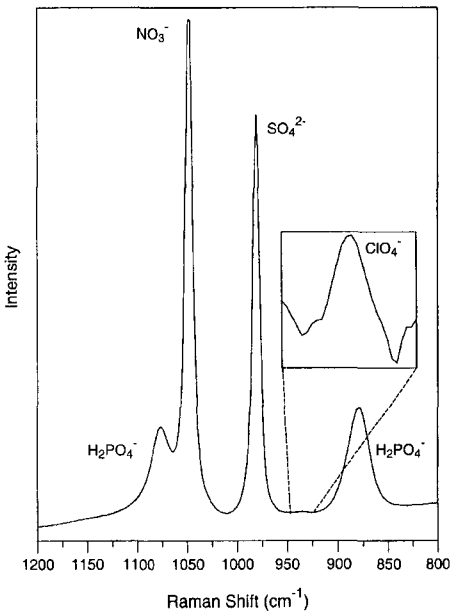

Fig. 5 Raman spectrum of a 0.2 g mL^{-1} solution of fertilizer sample #2 listed in Table 1. The spectrum was recorded at ~5 cm^{-1} resolution with an exposure time of 20 s with five accumulations co-added. Laser power at the sample was approximately 100 mW.

Perchlorate to nitrate ratios

Three of the five solid fertilizers listed in Table 1 were found to have detectable levels of perchlorate. Although none of these fertilizers have known links to caliche, we wondered whether their perchlorate concentrations were consistent with those in this mined ore. We have investigated this by comparing the perchlorate-to-nitrate concentration ratio (w/w) of the extracts of these fertilizers to that determined from published data[21] on the concentration of water-soluble saline components in mined Chilean caliche. The historical minimum and maximum ratios that we calculated, 3.7×10^{-4} and 9.0×10^{-2}, respectively, were based on eight samplings of large tonnages of ore mined by nitrate companies in northern Chile over a period of about 50 years.[21] Therefore, if the source of perchlorate in a solid fertilizer product originates solely from mined Chilean caliche, one would expect the perchlorate-to-nitrate concentration ratio in its aqueous extract to be within or near the range set by these limits. While this is clearly not a definitive test, it may be useful as a screening tool. For example, results from this test may influence a decision to investigate potential sources of perchlorate other than Chilean caliche.

Note that some of us previously have used Raman spectroscopy to conduct a perchlorate-to-nitrate concentration ratio test for a different set of fertilizers that were found to contain perchlorate.[23] Based on that test, we argued that it was not reasonable to attribute the source of perchlorate in those products solely to the presence of components derived from Chilean caliche, because, in many cases, the ratio significantly exceeded the upper limit set by the historical data. This earlier test was conducted by comparing directly the area of the Raman peak from perchlorate to that of nitrate in a single spectrum.[23] Here we have used a similar approach using Raman data, but have quantified independently the levels of nitrate and perchlorate in the solid fertilizers based on calibration curves and using two separate sets of extracts—one for nitrate analysis and one for perchlorate analysis. While less convenient, this new approach is probably more accurate, particularly when nitrate and perchlorate levels are vastly different and when very high solid-to-water ratios are needed to detect perchlorate by Raman analysis.

In addition, in this study we determined perchlorate-to-nitrate concentration ratios (w/w) with ATR-FTIR spectrscopy. As with the Raman work, both nitrate and perchlorate levels were measured using calibration curves based on the appropriate standards (as described in the Experimental section). The nitrate analyses were conducted with the uncoated ATR crystal, whereas the perchlorate analyses were conducted with the film-coated ATR crystal. Note that we could have determined perchlorate-to-nitrate concentration ratios with IC as well, but this would have been less convenient than the vibrational spectroscopic measurements because different IC columns and different IC methods are needed to measure nitrate and perchlorate. Given the agreement between Raman and ATR-FTIR measurements of perchlorate-to-nitrate concentration ratios, these IC measurements were not pursued.

Table 2 shows the results of perchlorate-to-nitrate concentration ratio determinations for the perchlorate-containing samples listed in Table 1 and for Bulldog Soda (SQM North America Corporation). Bulldog Soda is sodium nitrate derived solely from mined Chilean caliche and is sold as a single-component fertilizer product (N-P-K grade 16-0-0). The evaluation of Bulldog Soda serves as an independent assessment of the perchlorate-to-nitrate concentration ratio test. If this test is useful, then the ratio for Bulldog Soda (acquired ~January 2000) would fall between the minimum and maximum levels (3.7×10^{-4} and 9.0×10^{-2}, respectively) determined from the mined nitrate ores. Indeed, our measurements showed that the ratio for Bulldog Soda was within the expected range. (Note that our sample of Bulldog Soda, and all of these hydroponic fertilizers, were acquired before SQM modified its process to reduce the perchlorate concentration in its products.)

The concentration of nitrate in the fertilizer products is presented in Table 2 as '% nitrate nitrogen' so that our measurements can be compared to the concentration of nitrate as reported on the fertilizer product package. Note that our measurements, which reflect the nitrate level in small laboratory samples, are not to be taken as a challenge to the manufacturers' reported levels, which are representative of much larger amounts of product. Instead, we have presented our results in this manner to demonstrate their generally good agreement with the manufacturers' reported levels.

As shown in Tables 1 and 2, all of our hydroponic fertilizers list the majority, if not all, of their nitrogen content as nitrate; however, we do not know the original source of nitrate in these samples. Nonetheless, we note that all perchlorate-containing hydroponic products—three solid fertilizers—list potassium nitrate on the label as one of the chemicals from which the nutrients were derived. (As stated earlier, one industrial process for production of potassium nitrate involves Chilean caliche as a starting material.) Further, we note that the two solid fertilizers with no detectable perchlorate do not list potassium nitrate. However, there is no clear pattern here because potassium nitrate is listed for the 2 liquid fertilizers, neither of which contain detectable perchlorate.

For evaluating the perchlorate-to-nitrate concentration ratios, it is interesting to note that the range of this ratio for the historical mining data is quite large—the maximum level is about 243 times the minimum level. However, the range of this ratio for the products in Table 2, including Bulldog Soda, is considerably smaller—the maximum level is only about 15 times the minimum level. Additionally, it is interesting to note that all of the values for the fertilizers, including Bulldog Soda, are clustered near the lower level of the historical range for the mined ore. For these reasons, we argue that the perchlorate-to-nitrate concentration ratios are generally consistent with mined Chilean caliche even though the value for sample #1 falls just below the minimum level of the historical mining data. Further, we note that the ratios provide evidence of the resemblance of these samples to our sample of Bulldog Soda, all of which were likely manufactured near the same time. Based on these observations, we cannot eliminate mined Chilean caliche as the sole source of perchlorate in these three hydroponic products. In any event, it is important to point out that improvements in the refinement process for Chilean caliche are resulting in a substantial reduction of the amount of perchlorate in fertilizer products containing components derived from Chile saltpeter. However, it is not known how long after implementing the new process it will take before all old stocks of Chile saltpeter-derived materials (such as Bulldog Soda) are depleted and only new stocks, prepared by the modified process, find their way into commercial use. Also, it is important to recall that perchlorate-free synthetic sources of nitrogen overwhelmingly dominate the US fertilizer marketplace.

In conclusion, IC, cESI-MS, normal Raman spectroscopy, and FTIR spectroscopy with an extractant-coated ATR crystal have been used to determine perchlorate at relatively low levels (100–350 mg kg^{-1}) in some hydroponic fertilizer products. Our results are reported with a high level of confidence based on generally good agreement among the techniques. These spectroscopic methods provide much more definitive qualitative results than those obtained by the conventional perchlorate identification method of IC retention time matching. The cESI-MS and the extractant-coated ATR-FTIR method also exhibit high inherent sensitivity for perchlorate, but the w/w LODs and the convenience of application are limited, to some degree, by high TDS. The sensitivity of Raman spectroscopy is lower, but it exhibits inherently high TDS tolerance, and multiple fertilizer components often can be measured simultaneously along with perchlorate. Raman, and also the uncoated ATR-FTIR probe,

were useful in determining perchlorate-to-nitrate (w/w) ratios for the perchlorate-containing products. The techniques described here, when used in concert, offer a particularly powerful approach since all depend on a different property of perchlorate for identification.

An analytical approach such as ours, using multiple complementary spectroscopic techniques, may allow a better understanding of perchlorate in hydroponic fertilizers as they become more-and-more used worldwide. However, we caution that the products tested here may not be representative of those used in large scale hydroponic farming, but the matrixes appear to be representative of the macronutrients used in all hydroponics. Also, our results do not necessarily suggest a continuing or constant level of perchlorate, even in these tested products. Because fertilizer manufacturers vary the sources of their raw materials, it is likely that new lots of these same products will contain different levels of perchlorate, perhaps even be perchlorate-free. Finally, it is important to note that these hydroponic products are definitely not representative of those fertilizers used for production agriculture, which have recently been shown to be perchlorate-free.[25] Indeed, at the present, we are not aware of any perchlorate-contaminated site that has been linked to hydroponic fertilizers or to any fertilizers whatsoever.

Acknowledgements

Fruitful discussions with J. J. Ellington and A.W. Garrison, and some technical assistance from D. E. Norton, J. Washington, and J. Evans, in Athens are appreciated. The work at Colorado State University was funded by NSF grant CTS-0085892.

References

1 J. J. J. Clark, in *Perchlorate in the Environment*, ed. E. T. Urbansky, Kluwer/Plenum, New York, 2000, ch. 3.
2 US EPA, *Perchlorate environmental contamination: toxicological review and risk characterization based on emerging information. Second external review draft, NCEA-1-0503*, US Environmental Protection Agency, Office of Research and Development, National Center for Environmental Assessment, Washington, DC, 2002.
3 E. T. Urbansky, *Environ. Sci. Pollut. Res.*, 2002, **9**, 187.
4 *Fed. Regist.*, 1998, **63**, (40), p. 10274.
5 *Fed. Regist.*, 1999, **64**, (180), p. 50555.
6 P. E. Jackson, M. Laikhtman and J. S. Rohrer, *J. Chromatogr., A.*, 1999, **850**, 131.
7 P. E. Jackson, S. Gokhale, T. Streib, J. S. Rohrer and C. A. Pohl, *J. Chromatogr., A.*, 2000, **888**, 151.
8 P. E. Jackson, S. Gokhale and J. S. Rohrer, in *Perchlorate in the Environment*, ed. E. T. Urbansky, Kluwer/Plenum, New York, 2000, ch. 5.
9 M. L. Magnuson, E. T. Urbansky and C. A. Kelty, *Talanta*, 2000, **52**, 285.
10 M. L. Magnuson, E. T. Urbansky and C. A. Kelty, *Anal. Chem.*, 2000, **72**, 25.
11 E. T. Urbansky and M. R. Schock, *J. Environ. Manage.*, 1999, **56**, 79.
12 E. T. Urbansky, B. Gu, M. L. Magnuson, G. M. Brown and C. A. Kelty, *J. Sci. Food Agric.*, 2000, **80**, 1798.
13 R. Handy, D. A. Barnett, R. W. Purves, G. Horlick and R. Guevremont, *J. Anal. At. Spectrom.*, 2000, **15**, 907.
14 B. Ells, D. A. Barnet, R. W. Purves and R. Guevremont, *J. Environ. Monit.*, 2000, **2**, 393.
15 E. T. Urbansky, M. L. Magnuson, C. A. Kelty and S. K. Brown, *Sci. Total Environ.*, 2000, **256**, 227.
16 J. J. Ellington and J. J. Evans, *J. Chromatogr., A*, 2000, **898**, 193.
17 J. J. Ellington, N. L. Wolfe, A. W. Garrison, J. J. Evans, J. K. Avants and Q. Teng, *Environ. Sci. Technol.*, 2001, 3213.
18 E. T. Urbansky, *Biorem. J.*, 1998, **2**, 81.
19 A. A. Schilt, *Perchloric Acid and Perchlorates*, GFS Chemicals, Inc., Columbus, OH, 1979.
20 E. T. Urbansky, S. K. Brown, M. L. Magnuson and C. A. Kelty, *Environ. Pollut.*, 2001, **112**, 299.
21 G. E. Ericksen, *Geology and Origin of the Chilean Nitrate Deposits*, US Department of the Interior, Washington, DC, 1981.
22 G. E. Ericksen, *Am. Sci.*, 1983, **71**, 366.
23 T. L. Williams, R. B. Martin and T. W. Collette, *Appl. Spectrosc.*, 2001, **55**, 967.
24 A. R. Lauterbach, *ACS 222nd National Meeting, Chicago, USA*, 2001.
25 E. T. Urbansky, T. W. Collette, W. P. Robarge, W. L. Hall, J. M. Skillen and P. F. Kane, *Survey of Fertilizers and Related Materials for Perchlorate (ClO_4^-), EPA/6000/R-01/049*, 2001.
26 S. Susarla, T. W. Collette, A. W. Garrison, N. L. Wolfe and S. C. McCutcheon, *Environ. Sci. Technol.*, 1999, **33**, 3469.
27 S. Susarla, T. W. Collette, A. W. Garrison, N. L. Wolfe and S. C. McCutcheon, *Environ. Sci. Technol.*, 2000, **34**, 224.
28 E. T. Urbansky, M. L. Magnuson, C. A. Kelty, B. Gu and G. M. Brown, *Environ. Sci. Technol.*, 2000, **34**, 4452.
29 W. P. Robarge, M. Duffera and G. Ramirez, *ACS 220th National Meeting, Washington, DC, USA*, 2000.
30 H. A. P. Ltd, *Hydroponics as an Agricultural Production System', 01/141*, Rural Industries Research and Development Corporation, Sydney, NSW, Australia, 2001.
31 T. L. Giblin, D. C. Herman and W. T. Frankenberger, *J. Environ. Qual.*, 2000, **29**, 1057.
32 T. L. Giblin, D. C. Herman and W. T. Frankenberger, Jr, in *Perchlorate in the Environment*, ed. E. T. Urbansky, Kluwer/Plenum, New York, 2000, ch. 19.
33 J. D. Coates, U. Michaelidou, R. A. Bruce, S. M. O'Connor, J. N. Crespi and L. A. Achenbach, *Appl. Environ. Microbiol.*, 1999, **65**, 5234.
34 J. D. Coates, U. Michaelidou, S. M. O'Connor, R. A. Bruce and L. A. Achenbach, in *Perchlorate in the Environment*, ed. E. T. Urbansky, Kluwer/Plenum, New York, 2000, ch. 24.
35 B. E. Logan, *Biorem. J.*, 1998, **2**, 69.
36 V. A. Nzengung, C. Wang and G. Harvey, *Environ. Sci. Technol.*, 1999, **33**, 1470.
37 J. Mason, *Commercial Hydroponics*, Kangaroo Press, Kenthurst, Australia, 1990.
38 B. Van Aken and J. L. Schnoor, *Environ. Sci. Technol.*, 2002, **36**, 2783.
39 J. B. Jones, Jr, *Hydroponics—A Practical Guide for the Soilless Grower*, St. Lucie Press, Boca Raton, 1997.
40 H. M. Resh, *Hydroponic Food Production—A Definitive Guidebook of Soilless Food-Growing Methods*, Woodbridge Press Publishing Company, Santa Barbara, 1995.
41 H. Soffer, in *Hydroponics Worldwide: State of the Art in Soiless Crop Production*, ed. A. J. Savage, International Center for Special Studies, Inc., Honolulu, 1985, p. 123.
42 J. F. Clark, D. L. Clark, G. D. Whitener, N. C. Schroeder and S. H. Strauss, *Environ. Sci. Technol.*, 1996, **30**, 3124.
43 B. J. Clapsaddle, J. F. Clark, D. L. Clark, K. M. Gansle, A. E. Gash, C. K. Chambliss, M. A. Odom, S. M. Miller, O. P. Anderson, R. P. Hughes and S. H. Strauss, *Inorg. Chem.*, in preparation.
44 C. K. Chambliss, M. A. Odom, C. M. L. Morales, C. R. Martin and S. H. Strauss, *Anal. Chem.*, 1998, **70**, 757.
45 C. K. Chambliss, M. A. Odom, C. R. Martin, B. A. Moyer and S. H. Strauss, *Inorg. Chem. Commun.*, 1998, **1**, 435.
46 C. K. Chambliss, C. R. Martin, S. H. Strauss and B. A. Moyer, *Solvent Extr. Ion Exch.*, 1999, **177**, 553.
47 R. A. Nyquist, C. L. Putzig and M. A. Leugers, *The Handbook of Infrared and Raman Spectra of Inorganic Compounds and Organic Salts*, Academic Press, San Diego, 1997.
48 R. N. Wilhite and R. F. Ellis, *Appl. Spectrosc.*, 1963, **17**, 168.
49 S. H. Strauss, M. A. Odom, G. N. Hebert and B. J. Clapsaddle, *J. Am. Water Works Assoc.*, 2002, **94**, 109.
50 N. Everall, H. Owen and J. Slater, *Appl. Spectrosc.*, 1995, **49**, 610.
51 J. M. Tedesco and K. L. Davis, *Proc. SPIE-Int. Soc. Opt. Eng.*, 1998, 200.
52 T. W. Collette, W. P. Robarge and E. T. Urbansky, *Ion Chromatographic Determination of Perchlorate Ion: Analysis of Fertilizers and Related Materials*, EPA/600/R-01/026, US Environmental Protection Agency, Washington, DC, 2001.
53 E. T. Urbansky, M. L. Magnuson, D. Freeman and C. Jelks, *J. Anal. At. Spectrom.*, 1999, **14**, 1861.
54 M. L. Magnuson, C. A. Kelty and R. Cantú, *J. Am. Soc. Mass Spectrom.*, 2001, **12**, 1085.
55 M. L. Magnuson and C. A. Kelty, *Anal. Chem.*, 2000, **72**, 2308.

Anal. Chem. **2004,** *76,* 781−787

Attenuated Total Reflectance FTIR Detection and Quantification of Low Concentrations of Aqueous Polyatomic Anions

Gretchen N. Hebert, Matthew A. Odom, Stephanie C. Bowman, and Steven H. Strauss*

Department of Chemistry, Colorado State University, Fort Collins, Colorado 80523

Development of a new quantitative method for determining low concentrations of aqueous polyatomic anions using attenuated total reflectance (ATR) FTIR spectroscopy is described. Evaporated thin-film coatings of anion-selective tetraalkylated ferrocenium salts were applied to the surface of ATR crystals, which enabled anion detection limits to be lowered up to 23 000-fold below those achieved using the commercially available spectrometer with identical uncoated ATR crystals. Linear calibration curves based on d(absorbance)/dt, which is related to the rate of anion exchange in the thin film, were established in the 0.04−30 μM range. Limits of detection (10-min analyses) for perchlorate, chlorate, trifluoromethanesulfonate, perfluoro-*n*-butanesulfonate, perfluoro-*n*-octanesulfonate, tetrafluoroborate, hexafluorophosphate, and pinacolylmethylphosphonate in aqueous solution were 0.03, 0.2, 0.05, 0.07, 0.06, 0.06, 0.6, and 0.7 μM, respectively, using the thin-film coatings. This simple detection/quantification method afforded good reproducibility with relatively fast detection times.

Detection, identification, and quantification of aqueous anions, such as phosphonates, perchlorate, and perfluoroalkanesulfonates, are of interest given that they can cause problems to human health and persist in the environment. For example, the pinacolylmethylphosphonate anion ($C_7H_{16}O_3P^-$, PMPA$^-$) is a hydrolysis product of the G-type nerve agent Soman.[1] Although PMPA$^-$ itself is not toxic, identifying PMPA$^-$ in water would indicate the possible manufacture or release of Soman in the vicinity.

The perchlorate anion (ClO_4^-) interferes with thyroid gland function in infants.[2] Perchlorate is on the Contaminant Candidate List and the Unregulated Contaminant Monitoring Regulation List published by the U.S. Environmental Protection Agency (EPA), and in 2000 the EPA established a minimum reporting level for perchlorate in drinking water of 0.04 μM. In 2002, the EPA released a risk assessment draft that proposed a reference dose of 0.03 μg/kg day^{-1} for ClO_4^-.[3] Perchlorate has been detected at 0.18 μM or higher in a variety of lakes, rivers, and groundwater sources in the southwestern United States.[4]

The perfluoro-*n*-octanesulfonate anion ($C_8F_{17}SO_3^-$, PFOS$^-$) has been detected in surface waters, groundwater sources, human blood, and tissues of animals around the globe.[5] This is due in part to its ubiquitous presence as a component in many commercial products, including antistatic agents and fire-fighting aqueous film-forming foams (AFFFs). The widespread presence and persistence of PFOS$^-$ in the environment as well as the discovery of its toxicity[6,7] prompted the 3M Company to discontinue its production in 2000[8] and later for the EPA to regulate its production and use in the United States.[9]

In the past, Fourier transform infrared (FTIR) spectroscopy has not been viewed as a useful method for the detection of trace amounts of analytes in water matrixes.[10] This is due to the intense OH stretching and bending bands that extend over large regions of the IR spectrum. With the development of attenuated total internal reflectance (ATR) FTIR spectroscopy, this problem has been mitigated to some extent, and detection of aqueous analytes at millimolar concentrations is possible. The sensitivity of ATR-FTIR can be improved by applying a thin analyte-absorbing film to the surface of the ATR crystal.[11−16] Several reviews on the detection of analytes in aqueous solution using ATR crystals coated with polymeric or sol−gel materials have been published.[17,18] Sulfate and several carboxylates have been detected

* Phone: (970)-491-5104. Fax: (970)-491-1801. E-mail: strauss@lamar.colostate.edu.

(1) Epstein, J.; Bauer, V. E.; Saxe, M.; Demek, M. M. *J. Am. Chem. Soc.* **1956**, *78*, 4068−4071.
(2) Clark, J. J. J. In *Perchlorate in the Environment*; Urbansky, E. T., Ed.; Kluwer/Plenum: New York, 2000, pp 15−29.
(3) *Perchlorate environmental contamination: toxicological review and risk characterization*; Second external review draft, NCEA-1-0503; U.S. EPA, Office of Research and Development, National Center for Environmental Assessment, U.S. Government Printing Office: Washington, DC, 2002, and references therein.
(4) Urbansky, E. T. *Environ. Sci. Pollut. Res. Int.* **2002**, *9*, 187−192.
(5) Moody, C. A.; Hebert, G. N.; Strauss, S. H.; Field, J. A. *J. Environ. Monit.* **2003**, *5*, 341−345, and references therein.
(6) Case, M. T.; York, R. G.; Christian, M. S. *Int. J. Toxicol.* **2001**, *20*, 101−109.
(7) Seacat, A. M.; Thomford, P. J.; Hansen, K. J.; Olsen, G. W.; Case, M. T.; Butenhoff, J. L. *Toxicol. Sci.* **2002**, *68*, 249−264.
(8) Tullo, A. *Chem. Eng. News* **2000**, *May 22*, 9−10.
(9) *Federal Register* **2002**, *67*, 11008−11030.
(10) Griffiths, P. R.; de Haseth, J. *Fourier Transform Infrared Spectrometry*; John Wiley & Sons: New York, 1986.
(11) Rivera, D.; Poston, P. E.; Uibel, R. H.; Harris, J. M. *Anal. Chem.* **2000**, *72*, 1543−1554.
(12) Rivera, D.; Harris, J. M. *Anal. Chem.* **2001**, *73*, 411−423.
(13) Haibach, F. G.; Sanchez, A.; Floro, J. A.; Niemczyk, T. M. *Appl. Spectrosc.* **2002**, *56*, 398−400.
(14) Han, L.; Niemczyk, T. M.; Haaland, D. M.; Lopez, G. P. *Appl. Spectrosc.* **1999**, *53*, 381−389.
(15) Howley, R.; MacCraith, B. D.; O'Dwyer, K.; Masterson, H.; Kirwan, P.; McLoughlin, P. *Appl. Spectrosc.* **2003**, *57*, 400−406.
(16) Howley, R.; MacCraith, B. D.; O'Dwyer, K.; Kirwan, P.; McLoughlin, P. *Vib. Spectrosc.* **2003**, *31*, 271−278.

10.1021/ac034915i CCC: $27.50
Published on Web 12/19/2003

at concentrations as low as 1 μM using Fe_2O_3 and TiO_2 thin films, respectively, on zinc selenide (ZnSe) ATR crystals.[19,20] The lowest concentration of perchlorate reported by ATR-FTIR was 1 mM using a Cr_2O_3 film on a ZnSe ATR crystal.[21] See Supporting Information for more details.

We previously reported that coated ATR crystals could increase the sensitivity of a commercially available FTIR spectrometer by orders of magnitude for cyanide, perchlorate, and $PFOS^-$ in water.[22] For the perchlorate and $PFOS^-$ analyses, the ATR crystals were coated with thin-films of 1,1′,3,3′-tetrakis(2-methyl-2-nonyl)-ferrocenium nitrate ($DEC^+NO_3^-$), a homologue of the robust, selective, redox-recyclable anion extractant with 2-methyl-2-hexyl substituents previously developed in our laboratory for the efficient extraction and recovery of weakly hydrated anions from water.[23-25] We also quantified trace amounts of perchlorate in hydroponic nitrate fertilizers by the method of standard additions.[26]

In this report, we demonstrate the detection of $\leq$0.7 μM perchlorate, chlorate, three perfluoroalkanesulfonates, tetrafluoroborate, hexafluorophosphate, and pinacolylmethylphosphonate in water in 10 min using ATR crystals coated with thin films of salts of the organometallic ion-exchange cation DEC^+. Calibration curves based on d(absorbance)/dt (dA/dt) for three of the anions are linear over at least 1 order of magnitude of concentration starting at or near the quantification limit. We also present an analysis of ATR-FTIR-determined detection limits.

EXPERIMENTAL SECTION

Apparatus. IR spectra were recorded using an ATR-FTIR spectrometer (ReactIR-1000, Applied Systems Inc., Millersville, MD) equipped with a silicon (SiComp) or diamond (DiComp) ATR probe (Applied Systems Inc, Millersville, MD) and an MCT detector. The spectral window was 4000−650 cm^{-1} with a nominal spectral resolution of 8 cm^{-1}. The electronic gain was 1 (SiComp probe) or 2 (DiComp probe). Happ-Ganzel apodization was used with no postrun spectral smoothing. The SiComp probe consisted of a 30-bounce silicon ATR crystal mated to a ZnSe optical focusing element and was housed in a 5.2-cm-long × 2.5-cm-diameter cylindrical stainless steel conduit. The DiComp probe consisted of an 18-bounce diamond ATR crystal mated to a ZnSe optical focusing element and housed in a 1.3-cm-thick × 7.6-cm-diameter stainless steel DuraDisk (Applied Systems Inc., Millersville, MD). The wetted surface of both the silicon and diamond ATR crystals was a circular area 0.9 cm in diameter.

Reagents. The reagents sodium chlorate; potassium tetrafluoroborate; potassium hexafluorophosphate; lithium trifluoromethanesulfonate; pinacolylmethylphosphonic acid; sodium nitrate; dichloromethane; and the lithium, ammonium, sodium, and potassium salts of perchlorate were reagent grade or better and were used as received. The polyalkylated ferrocenium salts 1,1′,3,3′-tetrakis-(2-methyl-2-nonyl)ferrocenium nitrate ($DEC^+NO_3^-$) and DEC^+Cl^- were synthesized by literature methods.[23,25] Potassium perfluoro-*n*-octanesulfonate (K(PFOS)) was synthesized from perfluorooctanesulfonyl fluoride (3M Company, St. Paul, MN) by adding it to potassium hydroxide in water and recrystallizing the resultant salt five times from water to a final purity of >99%.[27] Potassium perfluoro-*n*-butanesulfonate (K(PFBS)) was synthesized from perfluorobutanesulfonyl fluoride (3M Company, St. Paul, MN) in the same manner. CAUTION: the preparation of K(PFOS) and K(PFBS) must be carried out in a fume hood by trained personnel because of the generation of hydrogen fluoride.

Procedure. All aqueous solutions, made from K^+, Li^+, or Na^+ salts of each anion except for $PMPA^-$, where H(PMPA) was used, were prepared in class A volumetric glassware using distilled deionized water (Barnstead NANOpure, Dubuque, IA) that had an initial resistivity of 18 MΩ cm. Experiments were performed at 24 ± 1 °C unless otherwise noted. Since the pKa of H(PMPA) is 2.4,[28] the concentration ratio $[PMPA^-]/[H(PMPA)]$ is ~400 when $[PMPA^-] + [H(PMPA)] = 10$ μM.

Uncoated-probe experiments involved contacting the unmodified silicon or diamond ATR crystal with 100 mL of water with stirring (silicon probe at ~200 rpm, diamond probe at ~60 rpm) and collecting a background spectrum (1660 co-added scans) over a 10-min time period. An aliquot of a stock solution was added to the water with stirring, and a 10-min sample spectrum was collected. Control experiments with colored dyes showed that mixing of the aliquot occurred within 10 s for both probes.

Coated-probe experiments involved treating the exposed surface of the ATR crystal with 20 ± 3 μL of a fresh (<1 week old) dichloromethane solution of either $DEC^+NO_3^-$ or DEC^+Cl^-. Evaporation of dichloromethane (~30 s) left a dry thin-film coating on the surface of the crystal. A nominal film thickness of 0.2 μm was calculated assuming a uniform cylinder of 0.9 cm diameter and using the density of $DEC^+NO_3^-$ from X-ray crystallography (1.1 g cm^{-3}).[25] Ellipsometry (WVASE32, J. A. Wollman Co., Lincoln, NE) was used to estimate the actual film thickness (~0.1 μm) and index of refraction for a silicon wafer coated with $DEC^+NO_3^-$. Using the experimentally determined index of refraction for the $DEC^+NO_3^-$ film, ~1.5, the evanescent wave extends 1.0, 0.4, or 0.2 μm beyond the surface of the ATR crystal at 650, 1555, or 4000 cm^{-1}, respectively (see Supporting Information for more details). Therefore, the entire thickness of the film was sensed by the evanescent wave below 1555 cm^{-1}.

The coated ATR probe was used for a single analysis, after which the thin-film coating was removed by washing with acetone. The ATR crystal was recoated with a thin film of extractant for each analysis. A spectrum of each film was collected prior to its use, and the absorbances of the observed IR bands were compared to previous films. For 46 films prepared from 20 μL of a 3 mM dichloromethane solution of $DEC^+NO_3^-$ on the silicon crystal, the absolute absorbance of the 2926 cm^{-1} ν(CH) band and the 1332

(17) Janotta, M.; Mizaikoff, B. *Proc. SPIE-Int. Soc. Opt. Eng.* **2002**, *4616*, 1−8, and references therein.
(18) Spichiger-Keller, U. E. *Sens. Actuators, B* **1997**, *38−39*, 68−77.
(19) Hug, S. J. *J. Colloid Interface Sci.* **1997**, *188*, 415−422.
(20) Weisz, A. D.; Rodenas, L. G.; Morando, P. J.; Regazzoni, A. E.; Blesa, M. A. *Catal. Today* **2002**, *76*, 103−112.
(21) Degenhardt, J.; McQuillan, A. J. *Langmuir* **1999**, *15*, 4595−4602.
(22) Strauss, S. H.; Odom, M. A.; Hebert, G. N.; Clapsaddle, B. J. *J. Am. Water Works Assoc.* **2002**, *94*, 109−115.
(23) Clark, J. F.; Clark, D. L.; Whitener, G. D.; Schroeder, N. C.; Strauss, S. H. *Environ. Sci. Technol.* **1996**, *30*, 3124−3127.
(24) Chambliss, C. K.; Martin, C. R.; Strauss, S. H.; Moyer, B. A. *Solvent Extr. Ion Exch.* **1999**, *17*, 553−584, and references therein.
(25) Clapsaddle, B. J.; Clark, J. F.; Clark, D. L.; Gansle, K. M.; Gash, A. E.; Chambliss, C. K.; Odom, M. A.; Miller, S. M.; Anderson, O. P.; Hughes, R. P.; Strauss, S. H. Unpublished work.
(26) Collette, T. W.; Williams, T. L.; Urbansky, E. T.; Magnuson, M. L.; Hebert, G. N.; Strauss, S. H. *Analyst* **2003**, *128*, 88−97.
(27) Hebert, G. N.; Odom, M. A.; Craig, P. S.; Dick, D. L.; Strauss, S. H. *J. Environ. Monit.* **2002**, *4*, 90−95.
(28) Mercier, J.-P.; Morin, P.; Dreux, M.; Tambute, A. *Chromatographia* **1998**, *48*, 529−534.

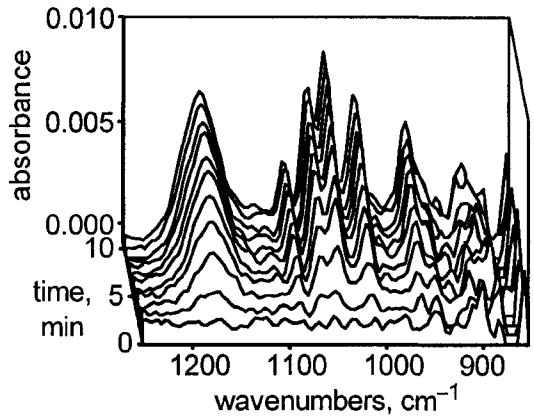

Figure 1. Detection of 10 μM $PMPA^-$ (100 mL water) using the diamond probe coated by evaporation of 20 μL of a 5 mM dichloromethane solution of DEC^+Cl^-. Spectra (64 co-added scans; 30-s collection time) were recorded every minute for 10 min. Six major bands assigned to the $PMPA^-$ anion in the mixed film DEC^+PMPA^-/DEC^+Cl^-(s) appear at 1170, 1089, 1065, 1046, 1015, and 961 cm^{-1}.

cm^{-1} ν(NO) band varied by only ±5 and ±6%, respectively. For nine $DEC^+NO_3^-$ films, the initial dA/dt rates (see below) for solutions of 5.0 μM ClO_4^- were reproducible to within ±11%.

Film thickness was optimized by coating the silicon probe with 20 μL of dichloromethane solutions of $DEC^+NO_3^-$ ranging in concentration from 0.1 to 10 mM. Concentrated extractant solutions resulted in more intense ν(CH) and ν(NO) bands due to the thicker ATR crystal coatings. The coated probe was immersed in 5.0 μM aqueous $LiClO_4$, and spectra were recorded every minute for 15 min. Films prepared from the 3 mM $DEC^+NO_3^-$ solution resulted in the largest initial dA/dt values. Therefore, unless otherwise noted, 3 mM solutions were used for all analyses using the $DEC^+NO_3^-$ extractant.

ATR crystals were coated with $DEC^+NO_3^-$ for all of the anion analyses except $PMPA^-$, which, because its hydration energy is larger than that of nitrate, was not extracted by $DEC^+NO_3^-$. Coating the diamond ATR crystal with DEC^+Cl^- enabled the extraction of $PMPA^-$ from aqueous solution as a result of the greater hydration energy of Cl^-. The film thickness of DEC^+Cl^- was not optimized.

In a typical analysis, the coated ATR probe was immersed in 100 mL of water stirred at 200 rpm for the silicon probe and at 75 rpm for the diamond probe. The film was equilibrated with water for 10 min, at which time a background spectrum was collected. An appropriate amount of an analyte stock solution was then added to the water with stirring to achieve the desired final analyte concentration, and FTIR spectra (64 co-added scans) of this solution were collected every minute for an appropriate amount of time (usually 10–60 min). The solution was stirred continuously during the entire experiment.

RESULTS

The ATR-FTIR analysis of 10 μM aqueous $PMPA^-$ anion is shown in Figure 1. Bands at 1170, 1089, 1065, 1046, 1015, and 961 cm^{-1} grew in over the 10-min experiment and are assigned to the $PMPA^-$ anion in the solid film, which had become a mixture of DEC^+PMPA^-(s) and DEC^+Cl^-(s) due to the $PMPA^-/Cl^-$ ion exchange. When the DEC^+Cl^- film was omitted from this experiment (i.e., when the uncoated diamond ATR probe was used), no bands were observed in this region of the IR spectrum, even when 1660 co-added scans were collected over a 10-min period. The corresponding bands for aqueous $PMPA^-$ at a much higher concentration (~1 mM) are 1162, 1085, 1061, 1042, 1015, and 973 cm^{-1}. Similar spectra were recorded for aqueous solutions of all of the anions studied in this work. Representative spectra for analyses of aqueous tetrafluoroborate (BF_4^-) and hexafluorophosphate (PF_6^-) after contact with $DEC^+NO_3^-$-coated probes are shown in the Supporting Information.

Limits of Detection (LODs). The standard definition of an LOD is the analyte concentration for which the signal-to-noise ratio (SNR) is equal to three. Since SNRs have experimental errors associated with them, the LOD can only be determined within certain error limits. In this work, we define an LOD as the analyte concentration for which SNR $\geq 3 \pm x$ and $x \leq 1$, where x is the estimated standard deviation of the SNR. All SNRs reported are averages of three or more trials at that concentration.

For any Fourier transform method, the SNR is dependent on the collection time (in principle, it is proportional to the square root of the number of scans that are averaged). Therefore, an LOD determined by FTIR is not a fixed quantity because it is time-dependent. LODs in this work are defined as SNR $\geq 3 \pm 1$ for a 10-min analysis. The choice of 10 min was arbitrary. In the case of perchlorate, a 30-min LOD was also determined for comparison. Spectral noise was the root-mean-square of the points in a blank spectrum over a wavenumber range centered at the peak absorbance maximum and extended to wavenumbers on either side of the peak where only 1% of the maximum peak absorbance remained. The peak position and maximum absorbance (i.e., signal intensity) were determined by least-squares fitting the experimental spectrum to a Gaussian function. See Supporting Information for more details.

For a given analyte, the most meaningful comparison of the LOD for a coated silicon or diamond probe with the LOD for the same probe without the extractant coating would be one that involved equal *total* analysis times, not equal numbers of co-added scans. For a coated-probe LOD, the coating underwent ion exchange with the aqueous analyte solution for 10 min, followed by the collection of only 64 co-added scans. For an uncoated-probe LOD, the probe was immersed in the analyte solution, and 1660 co-added scans were collected over the 10-min interval. The LODs are listed in Table 1.

Calibration Curves. In a typical spectroscopic experiment, one can use the Beer–Lambert law to construct a linear calibration curve of absorbance versus analyte concentration. For example, a plot of absorbance at 1347 cm^{-1} (ν_{asym}(NO) for nitrate in water) versus [NO_3^-] using the uncoated silicon probe, shown in Figure S-7 (Supporting Information), is linear from 10 to 400 mM. Such calibration curves were not possible with our extractant-coated probes. This is because $DEC^+NO_3^-$ and DEC^+Cl^- are so selective for weakly hydrated anions that the extractant films become saturated with the analyte at equilibrium. The result is the same final absorbance for a wide range of concentrations of a given analyte.

However, we found that a linear calibration curve based on ion-exchange kinetics could be constructed to determine unknown analyte concentrations. To our knowledge, this type of calibration

Table 1. 10-Min Limits of Detection (LODs) for Aqueous Anions Determined by ATR-FTIR[a]

	uncoated probe[b]				extractant coated probe[c]			
anion	ν, cm^{-1}	LOD, mM	SNR (σ)	ATR crystal	ν, cm^{-1}	LOD, μM	SNR (σ)	LOD ratio
ClO_4^-	1108	0.7	4 (1)	di[d]	1096	0.03	2.8 (6)	23 000
ClO_4^-	1108	0.8	4.0 (6)	Si[d]	1096	0.04	3.5 (8)	20 000
ClO_3^-	973	1.0	4 (1)	di[d]	973	0.2	3.2 (7)	5000
ClO_3^-	992	2.0	3.0 (7)	Si[d]	988	0.7	3.4 (6)	2860
BF_4^-	1073	0.3	4 (1)	di[d]	1057	0.06	4 (1)	5000
PF_6^-	861	1.7	4 (1)	di[d]	841	0.6	3.1 (8)	2830
$CF_3SO_3^-$	1258	0.3	3.7 (7)	Si[e]	1266	0.05	2.9 (5)	6000
$PFBS^-$	1254	0.5	3.5 (7)	Si[e]	1270	0.07	3.5 (8)	7140
$PFOS^-$	1243	0.01	4 (1)	Si[e]	1270	0.06	3 (1)	170
$PMPA^-$	1042	0.3	4 (1)	di[f]	1046	0.7	4 (1)	430

[a] Abbreviations: ν, IR spectral band monitored; SNR, signal-to-noise ratio; σ, estimated standard deviation; $PFBS^-$, perfluoro-*n*-butanesulfonate; $PFOS^-$, perfluoro-*n*-octanesulfonate; $PMPA^-$, pinacolylmethylphosphonate. [b] Each uncoated-probe LOD was determined from sample and background spectra (1660 co-added scans each) collected over 10-min intervals. [c] Each extractant-coated-probe LOD was determined from sample and background spectra (64 co-added scans each). The sample spectrum was collected after a 10-min period during which analyte/NO_3^- or analyte/Cl^- anion exchange took place. [d] The silicon (Si) or diamond (di) ATR crystal was coated by evaporation of 20 μL of a 3 mM dichloromethane solution of $DEC^+NO_3^-$. [e] The ATR crystal was coated by evaporation of 20 μL of a 1 mM dichloromethane solution of $DEC^+NO_3^-$. [f] The ATR crystal was coated by evaporation of 20 μL of a 5 mM dichloromethane solution of DEC^+Cl^-.

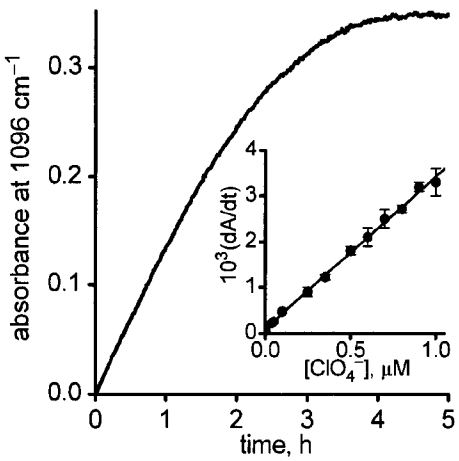

Figure 2. Absorbance of the ClO_4^- ATR-FTIR peak at 1096 cm^{-1} (due to $DEC^+ClO_4^-$(s)) versus time when the silicon probe coated by evaporation of 20 μL of a 3 mM dichloromethane solution of $DEC^+NO_3^-$ was immersed in a 1.0 μM aqueous solution of ClO_4^-. The inset is the initial dA/dt (min^{-1}) vs [ClO_4^-] calibration curve. The error bars represent $\pm 1\sigma$.

curve is unprecedented for quantitative IR analysis. Figure 2 shows a plot of absorbance at 1096 cm^{-1} (ν_{asym}(ClO) for perchlorate in $DEC^+ClO_4^-$(s)) versus time for the $DEC^+NO_3^-$-coated silicon probe immersed in 1.0 μM aqueous $LiClO_4$. The plot rises sharply at short times and exponentially approaches the final absorbance of 0.35 after several hours (there was a corresponding decrease in the ν_{asym}(NO) at 1347 cm^{-1}, and at equilibrium, this band had completely disappeared). In general, the sharp rise at short times (the *initial* slope of the A vs t curve, hereinafter referred to as dA/dt) was found to be constant for at least the first 10−30 min of the analysis for a given analyte concentration. More importantly, dA/dt was found to be directly proportional to analyte concentration up to a limiting concentration. For example, a plot of dA/dt versus [ClO_4^-], shown as the inset in Figure 2, was linear from 0.04 to 1.0 μM. (Recall that the LOD of aqueous ClO_4^- using the uncoated silicon probe is 800 μM.) Linear dA/dt-versus-analyte-concentration calibration curves, which consisted of at least seven concentrations (points), were also constructed for $PFOS^-$ and $PMPA^-$. For analytes with more than one band in their IR spectrum, the most intense peak that gave the smallest error (few interfering bands from water, the coating, and itself) was used for dA/dt analyses. Table 2 lists the concentration ranges over which the calibration curves are linear, the ranges in relative errors for the individual data points in each calibration curve, the linear least-squares fits for the data points, and the correlation coefficients. Three or more replicate analyses were averaged for each dA/dt value at a given analyte concentration for each of the three calibration curves.

DISCUSSION

The goal of this project was to demonstrate that IR spectroscopy is a suitable analytical method for the detection and quantification of aqueous anionic pollutants, such as perchlorate and perfluoro-*n*-octanesulfonate at submicromolar concentrations. The justification for the prejudice against analytical IR spectroscopy for trace analysis can be seen by examining the LODs listed in Table 1, which are all in the low millimolar concentration range when using the uncoated ATR probes. In a preliminary communication, we reported 60-min LODs for ClO_4^- and $PFOS^-$ using the silicon probe with and without a thin-film coating of $DEC^+NO_3^-$.[22] In that paper, we also noted that the time necessary to reach a particular SNR decreased as the analyte concentration increased when using a coated ATR crystal. This suggested that analyte quantification might be possible by monitoring dA/dt, the initial rate of absorbance increase for a particular analyte IR band, which itself is a function of the rate of anion exchange between the thin film and the aqueous sample. One advantage of analytical IR spectroscopy is the potential for simultaneous quantification and identification of a polyatomic analyte.

It was also our goal to develop a simple IR methodology, one that could be used by technicians in water quality laboratories (and possibly in the field), not only by skilled spectroscopists or materials scientists. This led to use of replaceable thin-film coatings of molecular anion exchangers that were insoluble in water but soluble in organic solvents. Thus, any laboratory with an FTIR spectrometer, an ATR attachment, and routine data

Table 2. Linear Calibration Curve Parameters for ClO_4^-, $PFOS^-$, and $PMPA^-$

anion[a] ν, cm^{-1}	extractant soln[b]	concn range, μM	error[c], %	$dA/dt = m$[analyte] + b		
				10^3 m, μM^{-1} min^{-1}	10^4 b min^{-1}	R^2
ClO_4^- 1096	3 mM $DEC^+NO_3^-$	0.04–1.0	3–15	3.3 (6)	1.1 (3)	0.99
$PFOS^-$ 1270	1 mM $DEC^+NO_3^-$	0.06–1.0	3–26	3.1 (1)	1.0 (8)	0.99
$PMPA^-$ 1046	5 mM DEC^+Cl^-	1–30	3–18	0.115 (2)	0.3 (2)	0.99

[a] All data were collected using the coated silicon ATR probe except for $PMPA^-$, for which the coated diamond ATR probe was used. [b] ATR crystals were coated by evaporation of 20 μL of the indicated extractant dissolved in dichloromethane. [c] The ranges of errors shown were calculated as the relative standard deviation from the average of the three or more initial dA/dt values at each concentration.

analysis software would be able to use the methodology. ATR probes with permanent, reusable anion-exchange coatings might improve reproducibility but would involve more sophisticated polymer-casting or sol–gel techniques for their preparation and could be subject to fouling over time. Although the focus of this work is on nonpermanent films, some initial experiments have been done exploring the possibility of recycling the ferrocene-based ion-exchange coating through a redox cycle which would allow a single film to be used multiple times. Our results demonstrate that evaporation of dichloromethane solutions of $DEC^+NO_3^-$ or DEC^+Cl^- can produce thin-film coatings that give reproducible LODs and dA/dt values to within ±11%.

10-Min Limits of Detection. One objective of this study was to show how the sensitivity of a commercially available ATR-FTIR spectrometer for weakly hydrated anions can be improved by applying a thin-film coating of an ion-exchange material to the surface of the ATR crystal. It was not our objective to design a method that would give LODs lower than all other analytical methods. We acknowledge that a lengthy, more elaborate method, such as solid-phase extraction coupled with HPLC/ESI-MS/MS, can achieve the orders-of-magnitude lower LOD of 0.01 nM for $PFOS^-$(aq) compared with the 0.06 μM 10-min LOD determined using the $DEC^+NO_3^-$-coated silicon ATR-FTIR probe.[29] On the other hand, our LOD for BF_4^-(aq), 0.06 μM, is lower than the lowest literature LOD of 0.1 μM determined by ion-pair extraction with spectrophotometric detection.[30] See Supporting Information for more details.

Using the unmodified ATR probes, the LODs for all of the anions listed in Table 1 are in the low millimolar range. Note that the 10-min LOD for $PFOS^-$ with the uncoated probe, 0.01 mM, is 30–50 times lower than the uncoated-probe LODs for the shorter-chain-length sulfonate anions $PFBS^-$ and $CF_3SO_3^-$. This could be due to the more intense ν(CF) bands of the longer perfluoroalkyl chain of $PFOS^-$, but this does not explain why the LODs for $PFBS^-$ and $CF_3SO_3^-$ are essentially the same. The LODs listed in Table 1 for the unmodified ATR probes could be improved somewhat by increasing the number of co-added scans that constitute a single spectrum. As the number of scans per spectrum is increased, the SNR increases with the square root of the number of scans being signal averaged.[10] Increasing the scanning time from 10 (1660 scans) to 30 min (5000 scans) should increase the SNR by a factor of 1.7. The 10- and 30-min LODs for ClO_4^- using the unmodified silicon probe are 0.8 and 0.4 mM, respectively. This 2-fold decrease in LOD agrees well with theory. Although there is some advantage to collecting more scans per spectrum in order to lower the LOD, this must be balanced with the increased amount of time required for the analysis. Furthermore, there is a point of diminishing returns: a 60-min LOD for ClO_4^- was not significantly different from the 30-min LOD.

The LODs of the ATR-FTIR instrument used in this study were greatly improved by coating the ATR crystals. For example, the 10-min LOD for ClO_4^- using the $DEC^+NO_3^-$-coated silicon probe was lowered by a factor of 20 000 to 0.04 μM (the uncoated-silicon-probe LOD is 0.8 mM). Using the $DEC^+NO_3^-$- or DEC^+Cl^--coated ATR probes, the LODs for all of the anions listed in Table 1 are in the submicromolar range. The increase in sensitivity of the coated ATR probes relative to the unmodified probes ranged from 170 for $PFOS^-$ to 23 000 for ClO_4^-.

The LOD for ClO_4^- using the $DEC^+NO_3^-$-coated diamond ATR probe, 0.03 μM, is 4 orders of magnitude lower than the 1 mM aqueous ClO_4^- detected using Cr_2O_3-coated ZnSe ATR crystals.[21] In fairness, we note that 1 mM was the concentration of perchlorate used for an experiment described in this reference; this concentration is not necessarily the LOD for the Cr_2O_3-coated ATR crystal. Only two studies have reported the detection of low micromolar concentrations of aqueous anions by ATR-FTIR using coated ATR crystals. In one study, 1 μM aqueous sulfate was detected using a ZnSe ATR crystal coated with Fe_2O_3.[19] In the other study, 1 μM aqueous carboxylate anions were detected with ZnSe ATR crystals coated with TiO_2.[20] These LODs are up to 2 orders of magnitude higher than the submicromolar LODs listed in Table 1.

The silicon and diamond LODs for ClO_4^- and chlorate (ClO_3^-) listed in Table 1 show that the detection limit of the anion can depend on the material of the ATR crystal. This is mainly because the IR throughput of the silicon ATR crystal decreases more significantly below 1000 cm^{-1} than the throughput of the diamond crystal. Other minor factors might be the difference in evanescent wave penetration depths due to the differences in refractive indexes of diamond and silicon and the possibility of different film morphologies on the different ATR crystals. The decreased throughput of the silicon ATR crystal results in an increase in noise below 1000 cm^{-1}. The SNRs for analytes that have IR bands below 1000 cm^{-1}, such as ClO_3^-, are ~4 times smaller with the 30-bounce silicon probe than with the 18-bounce diamond probe for the same analyte concentration, despite the greater number of internal reflections. Accordingly, the inherently lower noise level of the diamond probe below 1000 cm^{-1} led to a significantly lower LOD for ClO_3^- relative to the silicon probe. Even ClO_4^-, with

(29) Hansen, K. J.; Johnson, H. O.; Eldridge, J. S.; Butenhoff, J. L.; Dick, L. A. *Environ. Sci. Technol.* **2002**, *36*, 1681–1685.
(30) Kasahara, I.; Hosokawa, S.; Nata, N.; Taguchi, S.; Goto, K. *Analyst* **1993**, *118*, 1205–1208.

ν(ClO) centered at ~1100 cm^{-1}, has a slightly lower LOD with the diamond probe than with the silicon probe.

The LODs for anions using extractant-coated ATR probes can be lowered by allowing the anion exchange to proceed for a longer time. As shown in Figure 2, the absorbance of the T_2 ν(ClO) perchlorate peak increased linearly for more than 60 min once ion exchange was initiated. Since the absorbance of the analyte peaks increased with time but the noise remained the same (because 64 co-added scans were collected regardless of the length of the anion-exchange time interval), the SNR was higher at longer extraction times. This resulted in a 30-min LOD of 0.02 μM, which is 2 times lower than the 10-min LOD of 0.04 μM. Given the error limits of these determinations, the 2-fold lowering of the 30-min LOD is probably within error of the expected 3-fold decrease.

Lower LODs are possible at longer extraction times because the ion-exchange reaction is concentrating the analyte over time in the volume probed by the evanescent wave. The spectra in Figure 1 show the progress of the ion-exchange reaction of a film of DEC^+Cl^-(s) with aqueous $PMPA^-$, which is DEC^+Cl^-(film) + $PMPA^-$(aq) ⇌ DEC^+PMPA^-(film) + Cl^-(aq). The ion exchange is driven by the difference in hydration energies of the Cl^- and $PMPA^-$ anions, which is larger than the difference in lattice energies of DEC^+Cl^-(s) and DEC^+PMPA^-(s) because the DEC^+ cation is very large.[31] Ion-exchange reactions involving similar anions have been shown to be selective for the most weakly hydrated anion present in solution.[23,24] Therefore, given a mixture of anions present in solution, only the most weakly hydrated anion should generally be detected by the extractant-coated ATR probe *at equilibrium*. For example, in a study of hydroponic fertilizers, 12 μM ClO_4^- was detected even in the presence of an 8600 times mole excess NO_3^- (note that NO_3^- is a ubiquitous contaminant in surface and groundwater environments).[26] Furthermore, the ion exchange with DEC^+ salts is selective for monoanions; multiply charged anions such as sulfate and phosphate were not extracted using DEC^+Cl^- or $DEC^+NO_3^-$.

Linear Calibration Curves. Calibration curves of initial dA/dt values versus analyte concentration allow for quantification of the anions in aqueous solutions. The initial slope of absorbance versus time graphs (such as the one shown in Figure 2) was proportional to concentration, while the maximum or final absorbance achieved at long times was independent of concentration. Due to the very high selectivity of these ion-exchange compounds, the coatings undergo virtually complete anion exchange with the aqueous analyte at long times. This gives rise to a fixed maximum absorbance value for each analyte over a wide range of concentrations when there is an excess of analyte present. The use of initial dA/dt values instead of maximum absorbance values for quantification is a significant time advantage.

The errors listed in Table 2 for the three calibration curves correspond to the relative standard deviations of the average initial dA/dt values at each concentration. These errors were typically larger at higher concentrations, contrary to what is commonly seen, where large errors are generally associated with low concentrations near the detection limit. When using these ion-exchange films, high analyte concentrations saturate the film quickly, making the determination of the initial dA/dt value less precise.

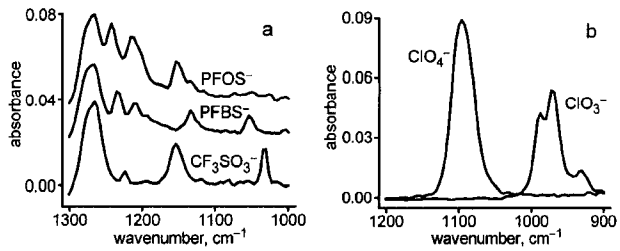

Figure 3. Comparison of the positions and relative intensities of IR bands for structurally similar anions. Part a shows ATR-FTIR spectra 10 min after the silicon ATR probe coated by evaporation of 20 μL of a 1 mM dichloromethane solution of $DEC^+NO_3^-$ was immersed in 1.0 μM aqueous K(PFOS), K(PFBS), and $LiCF_3SO_3$. Four major bands can be seen for DEC^+PFOS^-(s) at 1270, 1243, 1216, and 1154 cm^{-1}, while the four $DEC^+CF_3SO_3^-$(s) bands are located at 1266, 1224, 1154, and 1031 cm^{-1}. Five IR bands can be seen for DEC^+PFBS^-(s) at 1266, 1235, 1208, 1135, and 1054 cm^{-1}. Part b shows ATR-FTIR spectra 10 min after the diamond ATR probe coated by evaporation of 20 μL of a 3 mM dichloromethane solution of $DEC^+NO_3^-$ was immersed in 20 μM aqueous $LiClO_4$ or $NaClO_3$. The bands for $DEC^+ClO_4^-$(s) and $DEC^+ClO_3^-$(s) are at 1096 cm^{-1} and 973 cm^{-1}, respectively.

It was found that the initial dA/dt values and the 10-min SNRs for 1.0 μM aqueous solutions of $LiClO_4$, $NaClO_4$, $KClO_4$, and NH_4ClO_4 were the same within experimental error. In addition, preliminary experiments qualitatively demonstrated that initial dA/dt values for ClO_4^- depend on the temperature of the aqueous solution. This will be investigated quantitatively in a subsequent study.

Figure 3a displays spectra for thin films containing $PFOS^-$, perfluoro-*n*-butanesulfonate ($PFBS^-$, $C_4F_9SO_3^-$) and trifluoromethanesulfonate ($CF_3SO_3^-$). These anions differ only by the length of their perfluoroalkyl chains, yet they have distinguishable IR spectra. This highlights one of the advantages of using IR spectroscopy as a method of analysis. Nevertheless, the absorbance of the most intense peak in each spectrum is virtually the same because the initial dA/dt values for these three analytes were the same to within experimental error for a given concentration (this was true at 0.10, 1.0, and 10 μM). Since the extractant-coated probe LOD values for these three analytes are all 0.06 ± 0.01 μM, it appears that the initial dA/dt values are also the same at concentrations lower than 0.10 μM.

When the spectra shown in Figure 3b were analyzed, the integrated absorbance of the ν(ClO) band of the $DEC^+ClO_4^-$(s)-containing film was found to be 55% larger after 10 min of ion exchange than the integrated absorbance of the ν(ClO) bands of the $DEC^+ClO_3^-$(s)-containing film after 10 min (20 μM aqueous solutions were used for both analytes). In aqueous solution, using the uncoated probe, the two integrated absorbances were nearly equal. It is therefore reasonable to conclude that the ion-exchange rates of these two analytes do not differ by more than a factor of 2. Nevertheless, when a $DEC^+NO_3^-$-coated probe was immersed in an aqueous solution that was 20 μM in both ClO_4^- and ClO_3^-, only the perchlorate peak at 1096 cm^{-1} was observed. Therefore, the presence of ClO_4^- inhibited the uptake of ClO_3^- by the thin-film coating, not only at equilibrium but also at the beginning of

(31) Moyer, B. A.; Bonneson, P. V. In *Supramolecular Chemistry of Anions*; Bianchi, A., Bowman-James, K., Garcia Espana, E., Eds.; VCH Publishers: New York, 1997; pp 1–44.

the ion-exchange process. The investigation of the factors that affect the ATR-FTIR detection of analytes in the presence of a variety of interferants is an ongoing effort in our lab.

ACKNOWLEDGMENT

This work was supported by a grant from the National Science Foundation (CST-0085892) and by the U.S. Army Research Laboratory and the U.S. Army Research Office under Grant no. DAAD19-00-1-0417.

SUPPORTING INFORMATION AVAILABLE

References for the FTIR detection of anions using ATR crystals coated with polymers, sol–gels, etc.; evanescent wave penetration depth calculations; the method of determination of LODs in this work; a calibration curve for aqueous nitrate using the uncoated silicon ATR probe; the lowest concentrations reported in the literature by any analytical method for the anions studied in this work; and representative ATR-FTIR spectra of thin films containing $DEC^+BF_4^-$ and $DEC^+PF_6^-$. This information is available free of charge via the Internet at http://pubs.acs.org/ac.

Received for review August 5, 2003. Accepted November 13, 2003.

AC034915I

Appendix G

List of Abbreviations and Their Definitions

abbreviation	definition
AFFF	aqueous film-forming foam
ATR-FTIR	attenuated total reflectance Fourier transform infrared
d*A*/d*t*	initial d(absorbance)/d(time)
DDS^-	dodecylsulfate
$DEC^+NO_3^-$	1,1′,3,3′-tetrakis(2-methyl-2-nonyl)ferricenium nitrate
DI	distilled deionized (water)
ESIMS	electrospray ionization mass spectrometry
FTA-02	fire training area 2 at Wurtsmith Air Force Base
FT	fire training (well)
LOD	limit of detection
ML	multi-level (well)
$NiCl_2$(dppp)	1,3-bis(diphenylphosphino)propanedichloronickel(II)
$PFAS^-$	perfluoroalkanesulfonate
$PFBS^-$	perfluorobutanesulfonate
$PFHxS^-$	perfluorohexanesulfonate
$PFOS^-$	perfluorooctanesulfonate
$PMPA^-$	pinacolylmethylphosphonate
SNR	signal-to-noise ratio
WAFB	Wurtsmith Air Force Base